Title
Enantioselective Carbon-Carbon Bond Forming Reactions and Photochemistry Enabled by High-Valent Gold Catalysts

Author
Bohan, Patrick Thomas

Publication Date
2019

Peer reviewed|Thesis/dissertation

Enantioselective Carbon-Carbon Bond Forming Reactions and Photochemistry Enabled by High-Valent Gold Catalysts

by

Patrick Thomas Bohan

A dissertation submitted in partial satisfaction of the

Requirements for the degree of

Doctor of Philosophy

in

Chemistry

in the

Graduate Division

of the

University of California, Berkeley

Committee in charge:

Professor F. Dean Toste
Professor Richmond Sarpong
Professor James Bishop

Spring 2019

Abstract

Enantioselective Carbon-Carbon Bond Forming Reactions and Photochemistry Enabled by High-Valent Gold Catalysts

by

Patrick Thomas Bohan

Doctor of Philosophy in Chemistry

University of California, Berkeley

Professor F. Dean Toste, Chair

Chapter 1 – A brief introduction to enantioselective gold catalysis is presented in this chapter. The limitations of enantioselective gold catalysis and the various methods that have been exploited to overcome these barriers in gold-catalyzed reactions are discussed. The potential of gold(III) as a solution to problems associated with enantioselective gold(I) catalysis is also proposed.

Chapter 2 – The direct enantioconvergent 1,5-enyne cycloisomerization and kinetic resolution catalyzed by a gold(III) complex is described in this chapter. This represents the first highly enantioselective transformation catalyzed by a well-defined cationic gold(III) species and further corroborates our hypothesis that gold(III) can be used to induce chirality in situations where gold(I) is not successful. The transformation produces highly enantioenriched bicyclo[3.1.0]hexenes at all levels of conversion while simultaneously resulting in enantioenriched 1,5-enynes. Additionally, the nature of the direct enantioconvergent kinetic resolution is further explored along with the substrate scope of the transformation.

Chapter 3 – A highly enantioselective Mukaiyama-Michael addition controlled by chiral phosphoramidite gold(III) catalysts is described in this chapter. To the best of our knowledge, this is the first report of a highly enantioselective Mukaiyama-Michael addition wherein silyl ketene acetals are suitable nucleophiles for the transformation, as well as the first report exploiting chiral phosphoramidite gold(III) catalysts as the source of chirality. The transformation was optimal with TADDOL-based phosphoramidite ligands on gold(III), resulting in high regio- and enantioselectivity. Additional studies are underway with prochiral silylketene acetals to also explore potential control of diastereoselectivity.

Chapter 4 – The photophysical properties of several gold(III) complexes and their use as dual Lewis acid-photocatalysts are described in this chapter. With triplet state energies in excess of 50 kcal/mol, the gold(III) complexes have been successfully used as photosensitizers for the generation of singlet oxygen used for the oxidation of benzylic amines. Preliminary results are promising for the development of a chemoselective oxidation of amines with potential use as a late stage functionalization technique.

Enantioselective Carbon-Carbon Bond Forming Reactions and Photochemistry Enabled by High-Valent Gold Catalysts

Table of Contents

List of Figures

List of Schemes

List of Tables

List of Equations

Acknowledgements

I would first and foremost like to thank my parents, Judy and Michael Bohan, for fostering my interest in science through their boundless love and constant support in all things that I have done. My brother, Rankin, has always been an excellent friend and is always there for me when I need him. My extended family has also been wholly supportive of my academic adventures westward and I owe them a debt of gratitude.

Without the mentorship of Professor Erik Alexanian and Dr. Kayla Bloome during my time as an undergraduate at UNC, I certainly would not be where I am now. Under their tutelage I was able to learn to conduct independent research and grew to understand what it means to be a chemist, and more importantly, what it takes to become a chemist. Thanks to them I will always look back fondly on my time at UNC.

I can't imagine surviving graduate school without the guidance of my advisor, Professor Dean Toste. He has always instilled a spirit for hypothesis-driven research, and was more than willing to let me take on any project that gave me inspiration, no matter how far-fetched it was. This freedom has allowed me to pursue intellectually challenging ideas that have kept me engaged my entire time at Berkeley. One constant I will certainly miss is walking down the hallway and hearing Dean's classic line of "How's the ee?"

The friendly, collaborative, group environment that Dean has created has also helped me to foster a number of friendships and collaborations that have helped immensely during my time a Berkeley. In particular, as a young graduate student trying to find my place in the lab, I would like to thank Dr. Rake Wu and Dr. Susumu Ito for helping get my research underway, as well as the senior lab members at the time for their guidance and constant willingness to help out, Dr. Andrew Neel, Dr. Jigar Patel, Dr. Willie Wolf, Dr. Dillon Miles, Dr. Dimitri Khrakovsky, Dr. Mark Levin, Dr. Drew Samant, Dr. Rebecca Triano, Dr. Dave Kaphan, Dr. Richard Thornbury, and Dr. Cindy Hong. I also would like to thank the visiting scholars that I had the pleasure to work with, Dr. Melissa Van Overtveldt and Lukas Zeisel.

Prof. Jonathan Brantley, Dr. Steve Jacob, Dr. Christine Le, and Dr. Mario Ellwart have all left a profound impact on who I am as a person and a scientist through our shared time together in Latimer 605. I also want to thank my fellow classmates, John Lee, Suhong Kim, and Alec Christian for their friendship, advice, and general tomfoolery as we became back-to-back-to-back-to-back College of Chemistry softball champions.

I would like to thank my collaborators Dr. Heinz Frei, Dr. Georgios Katsoukis, and Trevor Roberts for their helpful discussions and expertise with photophysical measurements.

Finally, Sarah. I could not have survived the trials and tribulations of graduate school without your endless love and support. You always know how to bring a smile to my face, and challenge me to grow to be the best person I can be. I am so lucky to have you in my life and I am so excited for us to begin the next chapter of our lives together.

Chapter 1

A Brief Introduction to Enantioselective Gold Catalysis

1.1 Introduction

The field of homogeneous gold catalysis has been the subject of intense investigation during the past decade due to its unique and powerful mode of reactivity. The mechanistic sequence of π-activation, nucleophilic attack, and protodeauration has allowed chemists to rapidly construct complex molecular structures under mild reaction conditions. While there have been numerous developments in the field, difficulties associated with further development of enantioselective gold catalysis can generally be traced back to the linear coordination geometry of gold(I).[1] This geometry forces the substrate and the chiral ligand to be on opposing sides of the gold center, thereby limiting the possibility of enantioinduction. This issue has largely been addressed by taking advantage of chiral bisphosphine ligands resulting in bimetallic gold(I) complexes.[2,3] More recently, phosphoramidite ligands have also been successfully employed for enantioselective gold(I) catalysis.[1] Another method that was developed to combat this challenge was the introduction of a chiral counterion to the reaction manifold.[4] By introducing a different source of chiral information to the reaction landscape it was possible to overcome some of the shortcomings associated with the linear geometry of gold(I). Although this has been successful at addressing some of the problems associated with enantioselective gold catalysis, there still remains numerous reactions that do not achieve high enantioselectivities when using gold(I) catalysts with chiral ligands and chiral counterions.[4]

Another way to address the steric limitations of having a linear gold(I) catalyst would be to use a gold(III) catalyst which would exhibit square-planar geometry. However, the majority of gold(III) catalyzed reactions employ simple gold halide salts or have ligands that produce unstable or unreactive complexes, making introduction of a chiral ligand problematic.[5,6] Fortunately, the Toste group recently reported on an oxidative addition strategy that allows access to well-defined and stable gold(III) catalysts that, as a result of their square-planar geometry, place an ancillary ligand much closer to the active site.[7] This new class of organometallic gold(III) complexes takes advantage of a cyclometallated C−C ligand framework to stabilize the catalytically active cationic species, and offers the possibility to leverage an L-type ligand to introduce chiral information.

1.2 Discussion

The earliest report of an asymmetric gold-catalyzed reaction was published by Hayashi and coworkers in 1986.[8] The transformation took advantage of a chiral ferrocenylphosphine ligand with a gold(I) catalytic species to form enantioenriched oxazolines. The reaction was found to be largely selective for the formation of the *trans* product which exhibited enantioselectivities up to 97% ee (Scheme 1.1). While this early report was promising, further developments in the field were not made until almost 15 years later following renewed interest in homogeneous gold catalysis largely in part due to the ease of handling under atmospheric conditions while still resulting in powerful transformations acting as a carbophilic Lewis acid.

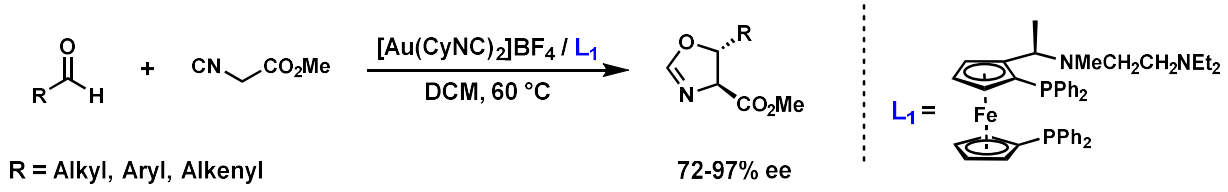

Scheme 1.1 Seminal report on enantioselective homogeneous gold catalysis.

With this renewed interest came a plethora of reports on enantioselective homogeneous gold catalysis. These reports focused on the use of bimetallic gold(I) complexes with chiral bisphopshine ligands. Initial studies from Echavarren and coworkers reported the enantioselective methoxycyclization of 1,6-enynes where although most enantioselectivities remained low (30-49% ee) they were able to obtain 94% ee for one substrate (Scheme 1.2).[9]

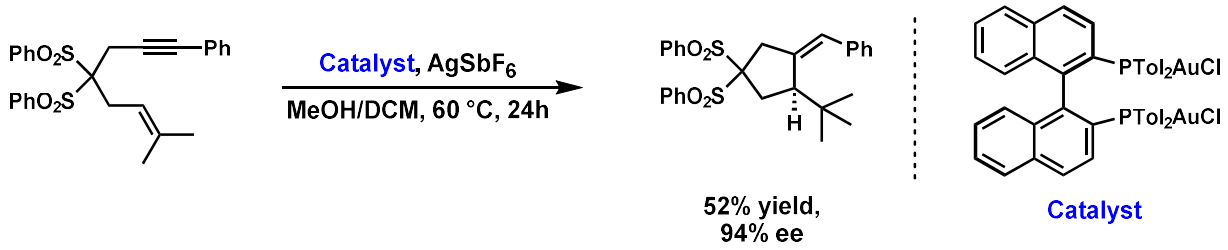

Scheme 1.2 Representative example of enantioselective bimetallic gold(I) catalysis.

In 2007 the Toste group reported on an exciting new methodology to the field of enantioselective homogeneous gold catalysis through the introduction of chiral counterions. Taking advantage of chiral BINOL derived phosphate anions they generated the desired products ranging from 90 to 99% enantiomeric excess (Scheme 1.3).[4] Additionally, they demonstrated that the chiral counterion strategy could be combined with more traditional chiral ligands to achieve high enantioselectivities in cases where employing only one method was not selective enough.

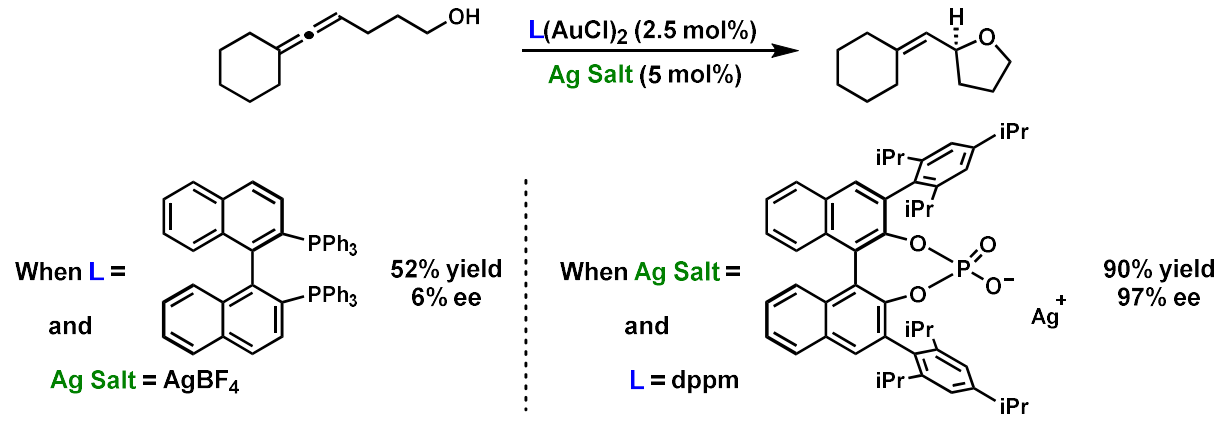

Scheme 1.3 Enantioselective catalysis promoted by a chiral counterion.

When N-heterocyclic carbenes (NHCs) are used in homogeneous gold catalysis they can exhibit widely varying selectivity and reactivity when compared to phosphine-based ligands, in part due to their strong σ-donating ability. While there are limited examples of transformations catalyzed by chiral gold(I)-carbene complexes with high enantioselectivities, as a whole the class of NHC ligands has lagged behind phosphine-based ligands when it comes to enantioselective gold catalysis.[10] The main difficulty associated with NHC ligands is that their structure projects the chiral information out and away from the gold center rather than toward the central active site. This problem has been approached the same way it was with phosphine ligands; through synthesizing bimetallic species to build steric walls around the gold centers.[11,12] Taking advantage of this method, Toste and coworkers showed the enantioselective synthesis of 2-substituted chromenyl pivalates from racemic phenol-substituted propargyl pivalates (Scheme 1.4).[13] The

reaction mechanism proceeds through a dynamic kinetic asymmetric transformation and results in excellent enantioselectivities ranging from 90 to >99% ee.

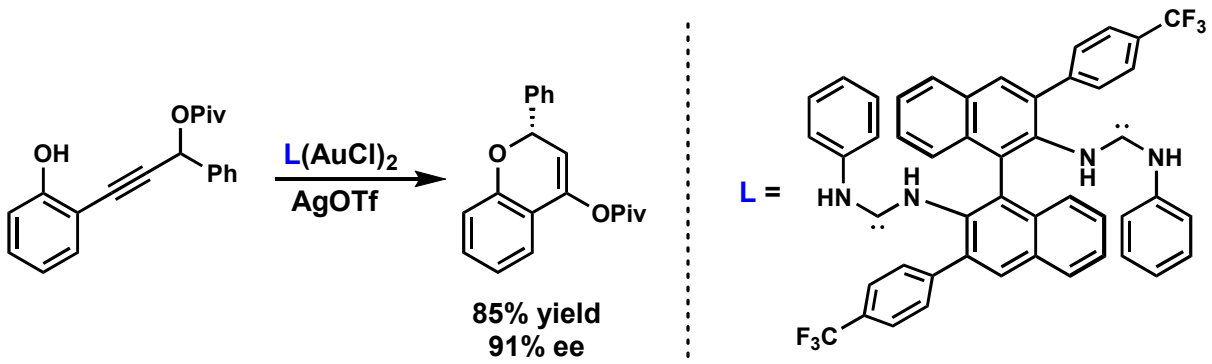

Scheme 1.4 Chiral gold-carbene catalyzed dynamic kinetic asymmetric transformation.

The linear nature of gold(I) complexes has played a large role in limiting the development of enantioselective transformations, but there remains another accessible oxidation state of gold that can be utilized, gold(III). Unfortunately, the majority of gold(III) catalyzed reactions employ simple gold halide salts as catalysts or ligands that produce unstable or unreactive complexes.[5,14–16] Despite these difficulties, access to new class of gold(III) complexes that are both catalytically active and stable was recently disclosed by Toste and coworkers.[7] This class of gold(III) complexes has introduced the possibility of locating chiral information significantly closer to the active site due to the square planar geometry they exhibit (Scheme 1.5).

Scheme 1.5 Ligand environment of gold(I) and gold(III) complexes.

1.3 Conclusion

Although there has been a significant investment of time and resources in to the development of enantioselective gold catalysis, there still remains much room for improvement. With the recent development of our new class of stable gold(III) complexes, a door has been opened for the development of enantioselective catalysis promoted by chiral gold(III) complexes. The advancements in enantioselective gold catalysis outlined in this chapter help to set the scene for the development of the first highly enantioselective reaction catalyzed by a gold(III) complex which will be presented in Chapter 2.

1.4 Notes and References

(1) Zi, W.; Toste, F. D. *Chem. Soc. Rev.* **2016**, *45*, 4567–4589.
(2) Wang, Y.-M.; Lackner, A. D.; Toste, F. D. *Acc. Chem. Res.* **2014**, *47*, 889–901.
(3) López, F.; Mascareñas, J. L. *Beilstein J. Org. Chem.* **2013**, *9*, 2250–2264.
(4) Hamilton, G. L.; Kang, E. J.; Mba, M.; Toste, F. D. *Science* **2007**, *317*, 496–499.
(5) Johnson, M. W.; Dipasquale, A. G.; Bergman, R. G.; Toste, F. D. *Organometallics* **2014**, *33*, 4169–4172.

(6) Kumar, R.; Nevado, C. *Angew. Chem. Int. Ed.* **2017**, *56*, 1994–2015.
(7) Wu, C.; Horibe, T.; Jacobsen, C. B.; Toste, F. D. *Nature* **2015**, *517*, 449–454.
(8) Ito, Y.; Sawamura, M.; Hayashi, T. *J. Am. Chem. Soc.* **1986**, *108*, 6405–6406.
(9) Paz Muñoz, M.; Adrio, J.; Carretero, J. C.; Echavarren, A. M. *Organometallics* **2005**, *24*, 1293–1300.
(10) Widenhoefer, R. A. *Chem. - A Eur. J.* **2008**, *14*, 5382–5391.
(11) Ramiro, Z.; Espinet, P.; Garcı, D. *Inorg. Chem.* **2010**, *49*, 9758–9764.
(12) Juan, A.; Villaverde, G.; Arnanz, A.; Gonza, C. *Chem. Commun.* **2010**, *46*, 3001–3003.
(13) Wang, Y. M.; Kuzniewski, C. N.; Rauniyar, V.; Hoong, C.; Toste, F. D. *J. Am. Chem. Soc.* **2011**, *133*, 12972–12975.
(14) Hashmi, A. S. K.; Weyrauch, J. P.; Rudolph, M.; Kurpejovic, E. *Angew. Chem. Int. Ed.* **2004**, *43*, 6545–6547.
(15) Lo, V. K.; Liu, Y.; Wong, M.; Che, C. *Org. Lett.* **2006**, *8*, 1529–1532.
(16) Hashmi, A. S. K.; Blanco, M. C.; Fischer, D.; Bats, J. W. *Eur. J. Org. Chem.* **2006**, No. 6, 1387–1389.

Chapter 2

Well-Defined Chiral Gold(III) Complex Catalyzed Direct Enantioconvergent Kinetic Resolution of 1,5-Enynes

2.1 Introduction

Cycloisomerization reactions are generally classified as rearrangements in which polyunsaturated substrates form new carbon-carbon bonds with consumption of at least one degree of saturation to form a cyclic product.[17] As a whole, this class of reactions has been extensively studied due to their ability to rapidly and efficiently build molecular complexity.[18–23] In particular, transition metal-mediated cycloisomerizations allow access to structural motifs that are not accessible through more traditional thermal means.[24] There are numerous examples of Alder-ene type cycloisomerizations of 1,6- and 1,7-enynes catalyzed by transition metals, but significantly fewer examples of transition metal mediated 1,5-enyne cycloisomerizations exist.[25–32]

The 1,5-enyne cycloisomerization was first reported by Toste and coworkers in 2004, but an enantioselective variant was never developed.[33–35] A challenge inherent to this reaction is that the (R) and (S) enantiomer of the 1,5-enyne can transform to either the (R,R) or the (S,S) enantiomer of the bicyclo[3.1.0]hexene, and transfer of chirality has been observed for certain classes of substrates with achiral catalysts (Scheme 2.1).[36] Therefore in order to develop an enantioselective variant of this cycloisomerization, the inherent bias of the substrates will have to be overcome with our chiral gold(III) catalysts.

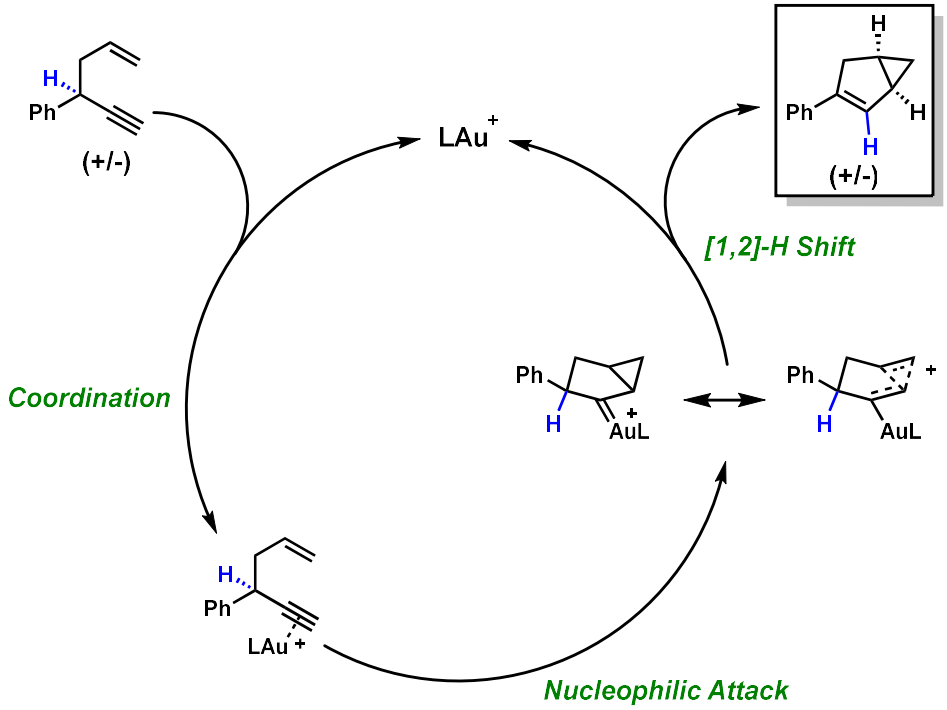

Scheme 2.1 Proposed mechanism of the 1,5-enyne cycloisomerization.

With access to the new gold(III) scaffold described in Chapter 1, we imagined that this reaction would be an ideal proof of concept for the development of enantioselective gold(III) catalysis. We hypothesized that the hydrocarbon structure of the starting materials that would minimize any reactivity differences due to utilizing the more oxophilic, hard Lewis-acidic gold(III), relative to gold(I). Traditionally, the mechanism of the majority of enantioselective gold-catalyzed reactions has involved the gold acting simply as a π-Lewis acid for hydrofunctionalization reactions.[37] However, the other typical intermediate invoked is a gold carbenoid, and enantioselective variants of these reactions are limited.[38] Previously, it has been

shown that phosphine-ligated gold complexes exhibit less carbenoid character when compared to *N*-heterocyclic carbene (NHC)-ligated gold complexes.[9] We hypothesized that our new gold(III) complexes would promote this gold carbenoid reactivity with their supporting NHC ligand that will also be used as the source of chiral information.

The development of a gold(III) catalyzed direct enantioconvergent 1,5-enyne cycloisomerization and kinetic resolution is described in depth within this chapter.[39] The transformation results in highly enantioenriched bicyclo[3.1.0]hexenes at all levels of conversion, with no racemization or symmetrization taking place during the course of the reaction, and simultaneously affords optically enriched 1,5-enynes. This chapter details the first highly enantioselective transformation catalyzed by a well-defined cationic gold(III) catalyst and further demonstrates the unique potential of gold(III) complexes in enantioselective catalysis.

Portions of this chapter were adapted with permission from: Bohan, P.T.; Toste, F.D. *J. Am. Chem. Soc.* **2017**, *139*, 11016-11019.

2.2 Results and Discussion

2.2.1 Synthesis of NHC Gold(III) Complexes

In order to test our hypothesis that the newfound gold(III) scaffold would be more effective for enantioinduction than traditional gold(I) species, we first synthesized a library of chiral gold(III) complexes. During the course of our studies we quickly discovered that the identity of the NHC ligand greatly impacted the success of the oxidative addition of biphenylene to the cationic gold(I) species. While we attempted to determine the reasons behind why the oxidative addition was only successful when certain NHCs were used, no clear correlation was exposed. As a result of this inconsistency, synthesizing each chiral gold(I) complex and then testing the oxidative addition and subsequent re-optimization would lead to significant amounts of waste and inefficiency. To avoid this issue, we instead approached the synthesis of the library *via* a gold(III) phosphine intermediate (Scheme 2.2). This pathway is preferential because a large amount of the gold(III) phosphine can be prepared at once beforehand and the NHC addition is the final step of the synthesis, allowing for a large number of chiral gold(III) complexes to be accessed in an expedient, divergent manner.

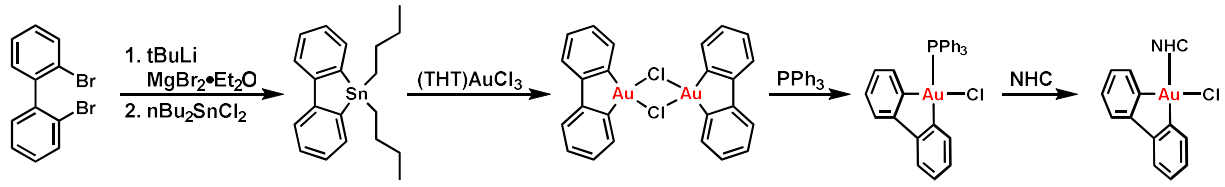

Scheme 2.2 Original synthesis of gold(III) complexes.

While this method was helpful to synthesize the desired gold complexes, we also wanted to improve on the previous route because there are several drawbacks. The first being a safety hazard with the use of *t*-BuLi to generate the Grignard, which then needs to be isolated before transmetalation with the dibutyltin dichloride.[40] The second main drawback is the inefficient atom economy from the addition of triphenylphosphine which is then replaced by the NHC. In testing whether *t*-BuLi was necessary for lithium halogen exchange with 2,2'-dibromobiphenyl we discovered that double lithiation could instead be achieved using the a significantly safer reagent,

n-BuLi. It was also discovered that direct transmetalation from the dilithiate to the dibutyltin dichloride could be achieved, thereby removing a step from the sequence. Originally triphenylphosphine was added to the break the gold(III) dimer before addition of 1,3-bis(2,6-diisopropylphenyl)imidazol-2-ylidene (IPr) to displace the ligand. However, we found that addition of the pre-formed free carbene was sufficient to break the gold(III) dimer and give the desired product. Overall these factors resulted in a significantly safer, cheaper, and more efficient route to our desired library of chiral gold(III) complexes (Scheme 2.3).

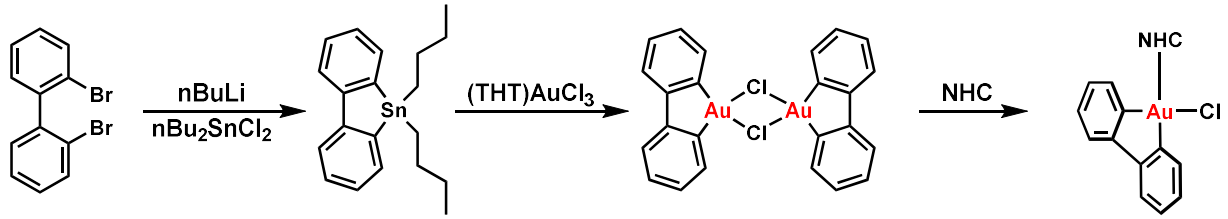

Scheme 2.3 Updated synthesis of gold(III) complexes.

2.2.2 Synthesis of Chiral NHCs

With the updated route to access the desired library of gold(III) complexes, it was now necessary to prepare the chiral NHC precursors. For the first class of ligands explored we wanted to maintain the 2,6-diisopropylphenyl substitution on one side of the NHC because this pattern appeared to be important for the reactivity in the initial report of the gold(III) complex. Following this rationale, we synthesized several imidazolium salts following the method reported by Fürstner and coworkers (Scheme 2.4).[41] The route began with an N-alkylation of 2,6-diisopropylaniline followed by an N-formylation and deprotection to give the corresponding formamide. The subsequent cyclization was followed by the addition of a chiral amine to afford chiral imidazolium salts. This synthetic route allowed for simple late-stage diversification due to the chiral amine addition taking place in the final step.

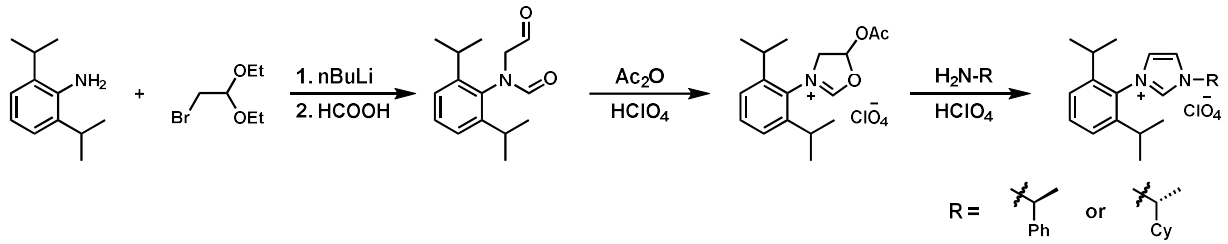

Scheme 2.4 Synthesis of imidazolium salts containing 2,6-diisopropylphenyl substitution.

After addition of potassium bis(trimethylsilyl)amide (KHMDS) to generate the free carbene, both NHCs were successfully added to the gold(III) dimer to generate **2.1** and **2.2**. Analysis of the gold(III) complexes by ^{1}H NMR indicated that there were two isomers corresponding to the two possible configurations of the NHC relative to the biphenyl substituent (Scheme 2.5). These isomers were determined to atropisomers using variable temperature NMR experiments in toluene-d_8 and DMSO-d_6. From these experiments it was determined that the barrier of rotation for **2.1** was in excess of 19.7 kcal/mol (see Supporting Information for details). In order to avoid potential complications that could arise from multiple catalyst isomers we also looked to synthesize C_2-symmetric NHCs where the orientation of the NHC would not result in the formation of atropisomers.

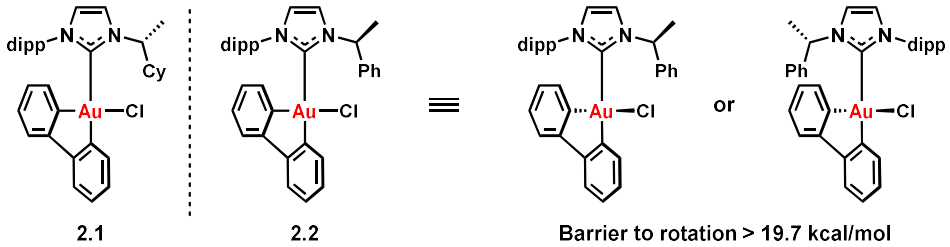

Scheme 2.5 Isolable atropisomers of complex **1.1**.

C_2-symmetric NHCs can have their chirality displayed in two main categories. First, the chirality can be projected off of the back of the saturated ring structure when starting from an imidazolinium salt. The second category is when the chirality is instead displayed off of the nitrogen substituents of the NHC. When the chirality is on the backbone of the NHC, it is projected away from the cationic gold center, while the chirality off of the nitrogen substituents could be closer to the active site. The first class was synthesized beginning with a condensation of the desired aldehyde with the chiral diamine, followed by a reduction to the corresponding secondary amine. The addition of triethyl orthoformate and ammonium tetrafluoroborate results in ring closure gave the desired imidazolinium salt where chirality is displayed off the saturated backbone (Scheme 2.6).

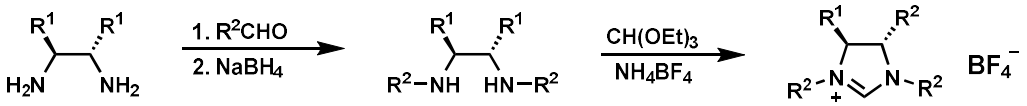

Scheme 2.6 Synthesis of imidazolinium salts with chirality on the backbone.

For the NHCs where the chiral information is displayed off of the nitrogen substituents it is possible to have either a saturated or unsaturated backbone, derived from the imidazolium or imidazolinium salts respectively. Synthesis of the saturated backbone variant began with S_N2 of dibromoethane with the chiral primary amine, followed by triethyl orthoformate and ammonium tetrafluoroborate to give the imidazolinium salt (Scheme 2.7). The unsaturated variant was synthesized by simply reacting the chiral primary amine with paraformaldehyde and glyoxal under acidic conditions (Scheme 2.8).

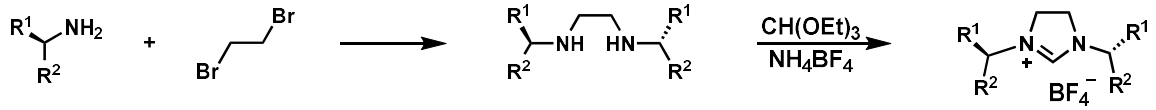

Scheme 2.7 Synthesis of imidazolinium salts with chirality on the nitrogen substituents.

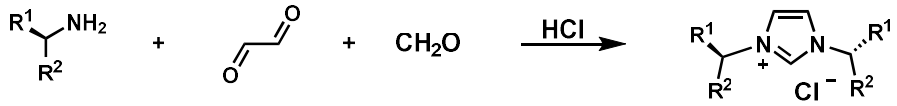

Scheme 2.8 Synthesis of imidazolium salts with chirality on the nitrogen substituents.

2.2.3 Optimization of the 1,5-Enyne Cycloisomerization

Using these methods we synthesized a number of chiral NHC precursors that were utilized to generate a library of chiral gold(III) complexes. With this library in hand we next looked to test

them as chiral catalysts. As previously mentioned, our efforts towards developing an enantioselective transformation with our new gold(III) complexes began with the 1,5-enyne cycloisomerization.

Initial investigations began by testing a number of chiral gold(III) complexes for competency in this transformation (Table 2.1). The catalysts bearing non-C_2-symmetric ligands (entries 1-2) were found to be competent at promoting the transformation, but enantioselectivity was almost non-existent. Similar results were seen when using C_2-symmetric ligands where the chiral information is found on the saturated backbone of the NHC (entry 3). Swapping to the C_2-symmetric ligands where the chirality is displayed off of the nitrogen substituents saw an increase in enantioselectivity of the bicyclo[3.1.0]hexene product. The gold(III) complex bearing a saturated NHC ligand catalyzed the formation of the desired product in higher enantioselectivity when compared to the unsaturated analog (entries 4-5). Among the saturated NHC ligands, the more sterically encumbered napthyl-substituted ligand resulted in higher enantioselectivity than the phenyl-substituted ligand (entry 6). Increasing the steric bulk of the NHC ligand by changing the methyl substitution to *t*-butyl resulted in a large drop in enantioselectivity as well as catalytic activity (entry 7). To confirm that *in situ* reductive elimination of biphenylene from the gold(III) species to form an active gold(I) species was not the operative mechanism, **2.8** was synthesized and tested and resulted in no enantioselectivity as well as decreased catalytic activity (entry 8). A range of gold(I) complexes bearing chiral phosphine ligands were also tested and showed complete conversion to product as expected based on the original report; however, the enantioselectivity was significantly lower than that obtained with the gold(III) complexes as catalysts (entries 9-11).

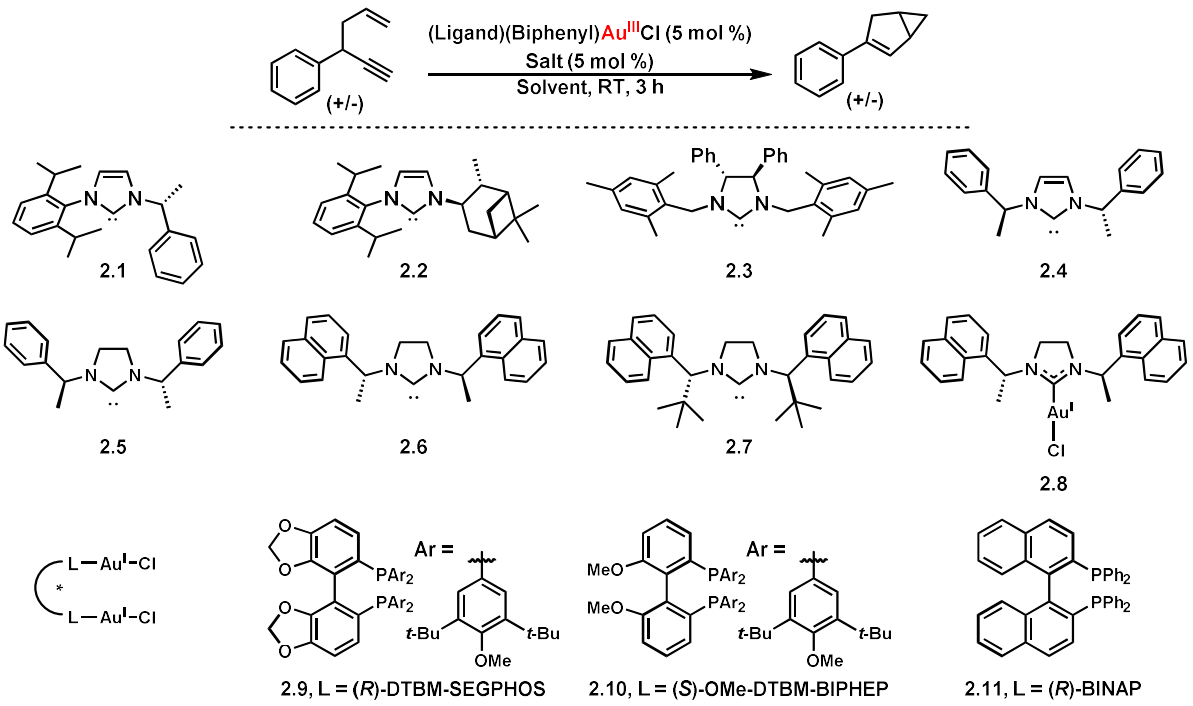

Entry	Catalyst	Salt	Solvent	Conversion (%)	ee (%)
1	2.1	$AgSbF_6$	DCM	100	2
2	2.2	$AgSbF_6$	DCM	100	4
3	2.3	$AgSbF_6$	DCM	100	5
4	2.4	$AgSbF_6$	DCM	100	-24
5	2.5	$AgSbF_6$	DCM	100	-34
6	2.6	$AgSbF_6$	DCM	100	37
7	2.7	$AgSbF_6$	DCM	4	2
8	2.8	$AgSbF_6$	DCM	23	0
9	2.9	$AgSbF_6$	DCM	100	9
10	2.10	$AgSbF_6$	DCM	100	6
11	2.11	$AgSbF_6$	DCM	100	2

Table 2.1 Ligand optimization for the enantioselective 1,5-enyne cycloisomerization.

Additionally, the gold(III) catalyst was re-isolated from the reaction mixture with no observable reductive elimination to gold(I), and it showed the same catalytic activity when re-subjected to the reaction conditions (see Supporting Information for details). Moving forward with catalyst **2.6** bearing the imidazolinium based NHC, we next probed the effect of the counterion on the reaction.

It has been frequently reported that the identity of the counterion in homogeneous gold catalysis can have a significant impact on the outcome of a reaction.[42,43] A prime example is the gold-catalyzed cycloisomerization of bromoallenyl ketones reported by Li and coworkers (Scheme 2.9)[44] When triflate was used as the counterion the transformation resulted in complete conversion to the 2-bromofuran product; but simply changing the counterion to hexafluoroantimonate resulted in a complete reversion of selectivity to give only the 3-bromofuran product.

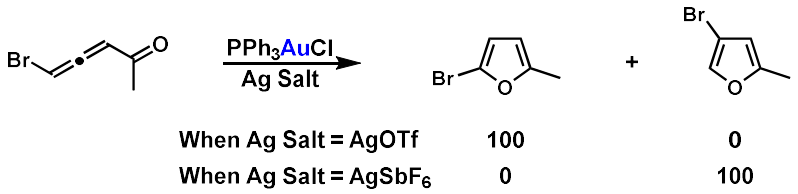

Scheme 2.9 Regiodivergent gold(I)-catalyzed synthesis of bromofurans.

Similarly, when Toste and coworkers reported on the gold(I) catalyzed hydroamination of allenes, they observed that tetrafluoroborate as a counterion resulted in high yield but low enantioselectivity, but when switching to *para*-nitrobenzoate as the counterion, both high yield and enantioselectivity were obtained (Scheme 2.10).[45] As a consequence of these studies we therefore found it important to determine what effects, if any, the counterion might have on the enantioselective 1,5-enyne cycloisomerization.

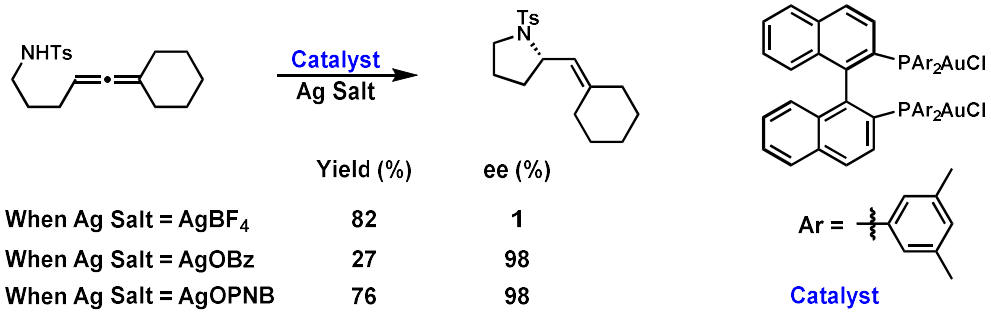

Scheme 2.10 Counterion modulated enantioselective hydroamination of allenes.

Screening of possible counterions in our gold(III) system revealed that a number of counterions were incompatible with the reaction (Table 2.2). Presumably, the decrease in catalytic activity results from tight binding of the counterion to the cationic gold(III) center, which has been shown to exhibit hard Lewis acidity and high oxophilicity (entries 1-4). Accordingly, we hypothesized that less coordinating counterions would be better candidates for our gold(III)-catalyzed variant of the 1,5-enyne cycloisomerization (entries 5-10). This indeed turned out to be the case with a number of less coordinating counterions, resulting in good to high levels of conversion. Ultimately tetrafluoroborate proved to be the optimal counterion, retaining catalytic activity and further increasing enantioselectivity (entry 8).

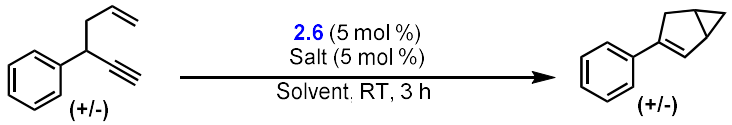

Entry	Salt	Solvent	Conversion (%)	ee (%)
1	AgOMs	DCM	0	-
2	AgONs	DCM	0	-
3	AgTFA	DCM	0	-
4	AgTRIP	DCM	0	-
5	AgOTf	DCM	31	48
6	$AgNTf_2$	DCM	100	21
7	$AgPF_6$	DCM	68	44
8	$AgBF_4$	DCM	91	53
9	$AgSbF_6$	DCM	100	37
10	$NaBArF_{24}$	DCM	72	19

Table 2.2 Counterion optimization for the enantioselective 1,5-enyne cycloisomerization.

In an effort to increase the enantioselectivity beyond our obtained 53% ee, we next looked towards optimizing the solvent conditions (Table 2.3). Solvents that were capable of strong coordination to the cationic gold(III) center were found to give no- to low reactivity (entries 1-3). When switching from DCM to toluene, a significant increase in enantioselectivity was observed, albeit with a decrease in reactivity (entries 5-6). Running the reaction for 16 h instead of 3 h resulted in increased conversion, but also a significant decrease in enantioselectivity (entry 7). This decrease in product enantioselectivity with increased conversion suggested that there was potentially a kinetic resolution taking place.

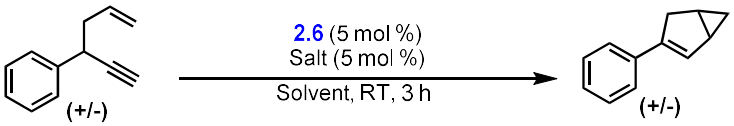

Entry	Salt	Solvent	Conversion (%)	ee (%)
1	$AgBF_4$	Pyridine	0	-
2	$AgBF_4$	DMF	0	-
3	$AgBF_4$	MeCN	8	58
4	$AgBF_4$	THF	68	29
5	$AgBF_4$	DCM	91	53
6	$AgBF_4$	Toluene	41	73
7	$AgBF_4$	Toluene	61	54

Table 2.3 Solvent optimization for the enantioselective 1,5-enyne cycloisomerization.

2.2.4 Discovery of an Enantioconvergent Kinetic Resolution

A kinetic resolution is when the two enantiomers of a starting material react with a chiral catalyst or substrate at different rates (Figure 2.1).[46] This results in an enantioenriched sample of the slower reacting enantiomer of starting material. In a standard catalytic kinetic resolution, the relative rates of reaction for each enantiomer of starting material is referred to as the selectivity, or s factor (Equation 2.1). The s factor is therefore controlled by the magnitude of $\Delta\Delta G^{\ddagger}$, which corresponds to the energy difference in the diastereomeric transition states of the selectivity determining step of the reaction. While this is also true for a standard enantioselective transformation using a prochiral substrate, there is a critical difference between the two types of reactions. Normal enantioselective reactions generate product of constant enantiomeric excess

over the course of the reaction, while the overall enantiomeric excess of the product in a kinetic resolution changes with conversion. Practically, this means that extremely high enantiomeric excess of recovered starting material can be consistently obtained by modulating to what extent a reaction goes towards complete conversion based on the s factor of the transformation. On the other hand, high enantiomeric excess of the product can only be obtained when the reaction has a reasonably large s factor and the reaction is stopped close to 50% conversion.

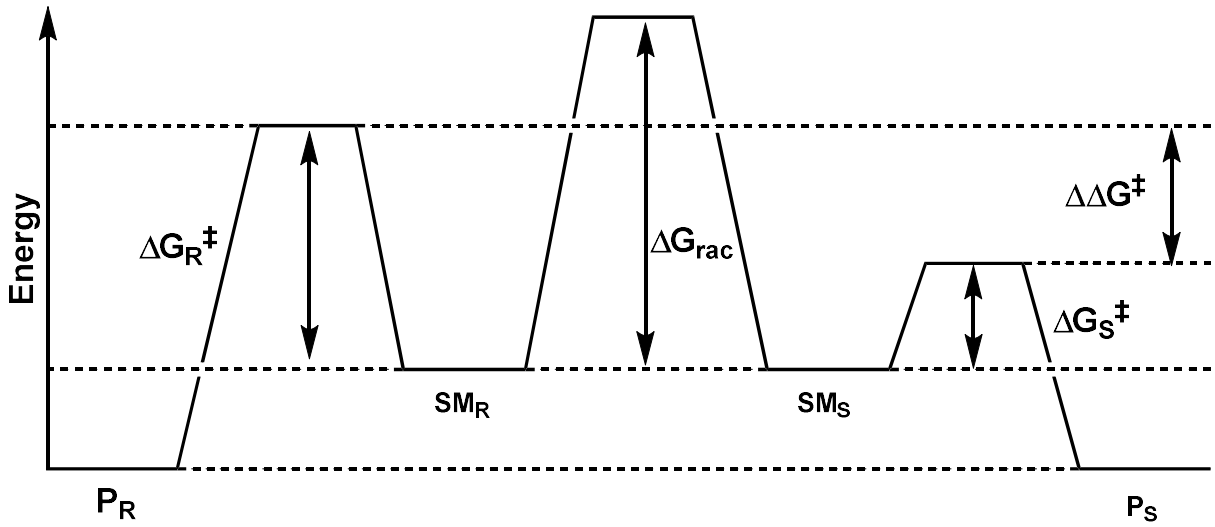

Figure 2.1 Reaction coordinate diagram for a standard kinetic resolution.

$$s = k_{rel} = k_{fast}/k_{slow} = e^{\Delta\Delta G^{\ddagger}/RT}$$

Equation 2.1 Selectivity of a kinetic resolution.

Isolation of the starting 1,5-enyne and subsequent analysis by chiral high-performance liquid chromatography (HPLC) showed that the enyne was highly enantioenriched in addition to the bicyclo[3.1.0]hexene. Additional optimization of the kinetic resolution was done focusing on solvent and temperature, with the optimal temperature found to be −40 °C; any colder and the catalyst would simply crash out of solution and halt reactivity (entries 1-6) (Table 2.4). Another brief solvent screen at −40 °C showed that chloroform gave the highest s factor with a value of 23 (entries 7-10).

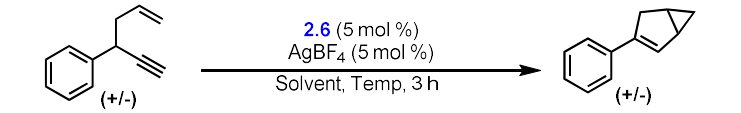

Entry	Solvent	Temperature (°C)	Conversion (%)	s factor
1	DCM	RT	30	6
2	DCM	0	31	9
3	DCM	–20	46	12
4	DCM	–30	55	14
5	DCM	–40	51	21
6	DCM	–50	0	-
7	DCM	–40	51	21
8	PhCl	–40	14	18
9	DCE	–40	44	16
10	$CHCl_3$	–40	44	23

Table 2.4 Kinetic resolution optimization of temperature and solvent.

In order to further explore the interplay between the kinetic resolution and the enantioselective product formation, we first isolated enantioenriched starting material and subjected it to the reaction conditions with an achiral gold(I) and gold(III) catalyst. The bicyclo[3.1.0]hexene product was isolated with 44% and 43% enantiomeric excess respectively, indicating that the reaction proceeded with some, but not complete, chirality transfer (Scheme 2.11). Additionally, when the racemic starting material was reacted under our conditions to complete conversion, the product was enantioenriched. This observation stands in contrast to a standard kinetic resolution where there would be no enantioenrichment at complete conversion.

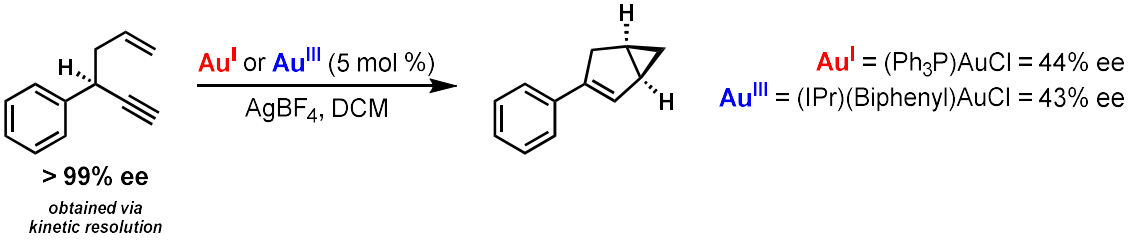

Scheme 2.11 Transfer of chirality using an achiral catalyst with the model substrate.

These result indicate that instead of just a simple kinetic resolution, the transformation might be operating via dynamic kinetic resolution (DKR) or dynamic kinetic asymmetric transformation (DYKAT).[47–49] In a DYKAT the reaction proceeds through a common, generally achiral, intermediate that is then transformed selectively to one product. Considering the reaction mechanism of our 1,5-enyne cycloisomerization, there is no common achiral intermediate for each enantiomer to converge to, ruling out the possibility of a DYKAT taking place. However, a DKR is operative when the barrier for racemization of starting material (ΔG_{rac}) is lower than the barrier to product formation (Figure 2.2). To test if this might be the operative mechanism in our reaction, we synthesized deuterated versions of our model substrate and subjected them to the reaction condition to see if there was any scrambling of the location of the deuterium. The plausible racemization pathway would proceed through an allene intermediate, allowing for the formation of two distinct deuterated products from a single deuterated starting material. In testing both of the deuterated starting materials we observed no mixing of deuterium location in either the starting material or the product (Scheme 2.12).

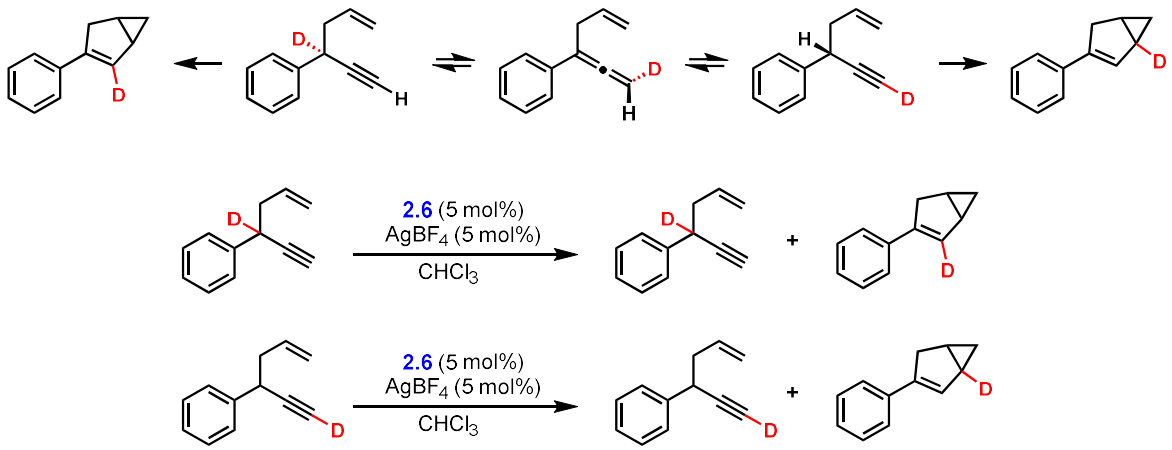

Scheme 2.12 Deuterium experiments to test for racemization.

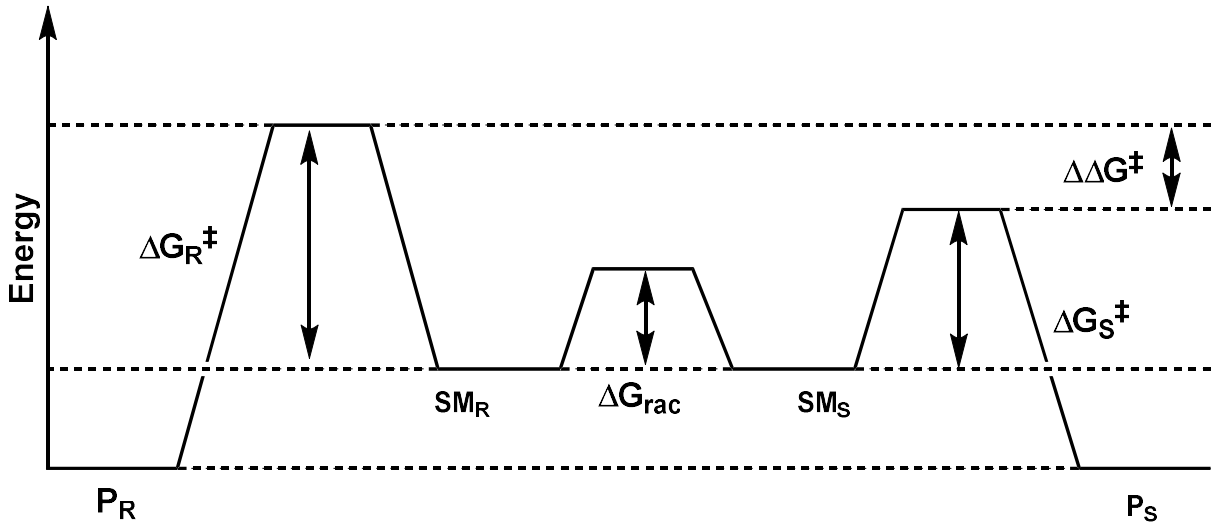

Figure 2.2 Reaction coordinate diagram for a dynamic kinetic resolution.

After ruling out both a DYKAT and DKR, we next considered whether the reaction was proceeding through an enantioconvergent kinetic resolution.[50] In this case each enantiomer converts directly to product at different rates and enantiomeric ratios. In order to further explore this phenomenon, we aimed to derive an equation that would determine our product enantioselectivity at any conversion. Beginning with data obtainable from a chiral HPLC trace we first obtained the consumed amount of each enantiomer of enyne (Equation 2.2, Equation 2.3). Multiplying this value by the enantiomeric ratio of the (R) or (S) enantiomer of starting material as it converts to one enantiomer of product results in the mole fraction of one enantiomer of product that comes from the consumed given enantiomer of starting material (Equation 2.4, Equation 2.5). Finally, these two equations can be combined to give an overall equation where given the enantiomeric excess data from at least two different values of conversion, it becomes possible to solve for the enantiomeric ratios that each starting material is converting to product (Equation 2.6).

$$\left[0.5\left[(1-C)\left(X_{R,SM}\right)\right]\right] = X_{R,SM-consumed}$$

Equation 2.2 Mol fraction of consumed (*R*) starting material at conversion C.

$$\left[0.5\left[(1-C)\left(X_{S,SM}\right)\right]\right] = X_{S,SM-consumed}$$

Equation 2.3 Mol fraction of consumed (*S*) starting material at conversion C.

$$\left[0.5\left[(1-C)\left(X_{R,SM}\right)\right]\right]\left(er_{R,SM\rightarrow RP}\right) = X_{R,P-from-R,SM}$$

Equation 2.4 Mol fraction of (*R*) product from consumed (*R*) starting material.

$$\left[0.5\left[(1-C)\left(X_{S,SM}\right)\right]\right]\left(er_{S,SM\rightarrow RP}\right) = X_{R,P-from-S,SM}$$

Equation 2.5 Mol fraction of (*R*) product from consumed (*S*) starting material.

$$\left[0.5\left[(1-C)\left(X_{S,SM}\right)\right]\right]\left(er_{S,SM\rightarrow RP}\right) + \left[0.5\left[(1-C)\left(X_{R,SM}\right)\right]\right]\left(er_{R,SM\rightarrow RP}\right) = X_{R,P}$$

Equation 2.6 Mol fraction of (*R*) product from combined equations.

Using this method determined that the (R)-enyne starting material transformed to the bicyclo[3.1.0]hexene product with 89% ee catalyzed by **2.6**, whereas the (S)-enyne converted to the same product with 42% ee under our optimized reaction conditions. Wanting to experimentally verify the calculated values, we isolated enantiopure (*R*) and (*S*) 1,5-enyne and subjected them to the reaction conditions and found the experimental values to be in close agreement with the predicted values (Scheme 2.13).

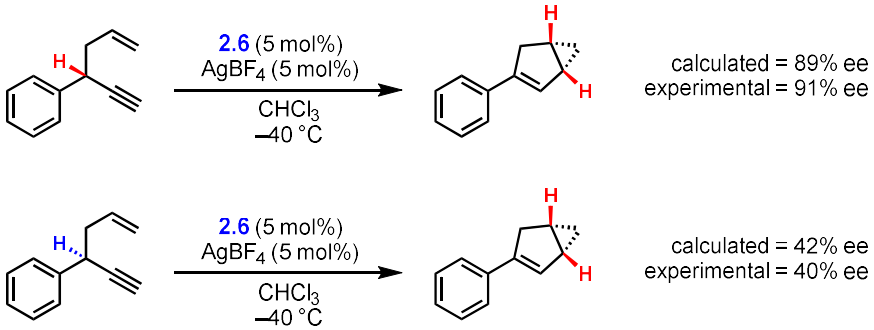

Scheme 2.13 Calculated versus experimental values of enantiomeric excess.

Employing this equation, we created a model to determine product enantioenrichment at any conversion, which can then be compared to a similar plot for a standard kinetic resolution (Figure 2.3). From the comparison it is immediately clear that the enantioconvergent kinetic resolution results in more highly enantioenriched product at synthetically useful conversions (above 40%) when s factors are identical, while simultaneously maintaining the high levels of starting material enantioenrichment seen in a standard kinetic resolution.

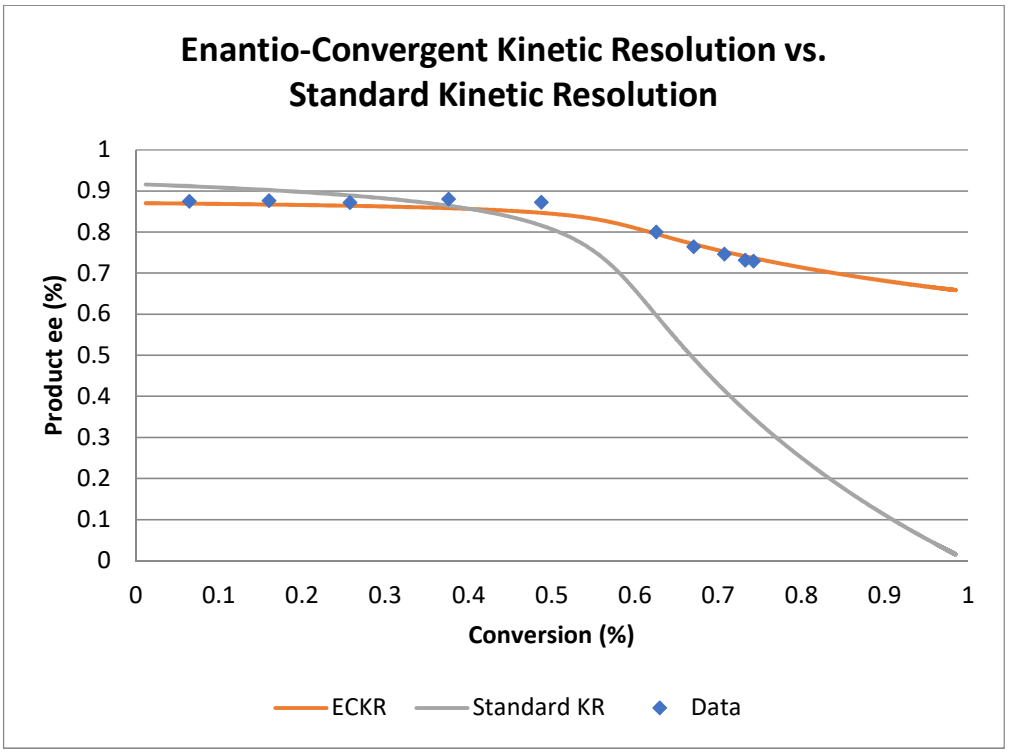

Figure 2.3 Product enantioselectivity of a kinetic resolution and enantioconvergent kinetic resolution where $s = 23$.

The previously proposed mechanism for this reaction accounts for the chirality transfer of the reaction if we consider the half-chair transition states (Scheme 2.14). In the matched case the (*R*)-enyne preferentially forms the (*S*,*S*)-bicyclo[3.1.0]hexene, and this preference is reinforced when the transformation is performed with **2.6** as the catalyst. In the mismatched case the (*S*)-enyne preferentially forms the (*R*,*R*)-bicyclo[3.1.0]hexene. However, the chiral gold(III) catalyst overrides this preference and the major product becomes the (*S*,*S*)-bicyclo[3.1.0]hexene. These observations can be best explained by examining the selectivity determining transition state and noticing that chiral catalyst either induces the large phenyl substituent to be in the axial position of the half-chair, or it induces the cyclopropane ring to fold in to a half-boat conformation. Because both enantiomers of starting material convert to the same enantiomer of product without any racemization or symmetrization processes, this gold(III)-catalyzed cycloisomerization reaction therefore falls under the rare class of direct enantioconvergent transformations.[50–55]

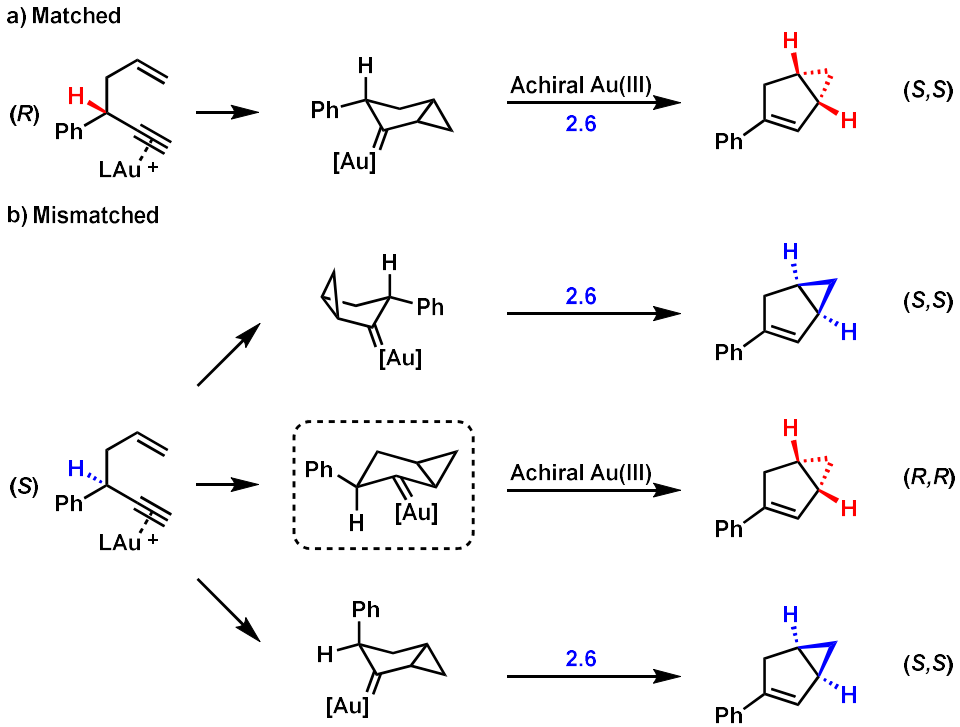

Scheme 2.14 Direct enantioconvergence of the 1,5-enyne cycloisomerization under chiral gold(III) catalyst control.

2.2.5 Scope of the 1,5-Enyne Cycloisomerization

With the optimized reaction conditions in hand we next looked to explore the scope of the transformation (Table 2.5). Substrates with more sterically hindered *ortho* substitution on the arene required higher temperatures but maintained similarly high levels of enantioselectivity and s factor (enynes **2.14** and **2.15**). Despite the potential for nonproductive coordination to the hard Lewis-acidic cationic gold(III), we found that heteroarene substrates were tolerated and in one case exceeded the selectivity of the model substrate (enynes **2.19**-**2.21**). Substrates in which the propargyl substitution was changed from aryl to alkyl were compatible with the reaction but with a decreased selectivity (enyne **2.22**). On the other hand, the use of a silyl-substituted alkyne dramatically slowed the rate of the reaction resulting in no kinetic resolution or product enantioselectivity, even for an extended period of time at an elevated temperature (enyne **2.23**). Phenyl substitution on the alkyne was also found to be deleterious to both the kinetic resolution and enantioselective product formation (enyne **2.24**). When the substitution was changed from the propargyl position to the allyl position, neither kinetic resolution nor enantioselective product formation was observed (enyne **2.25**). Substitution of the alkene also resulted in no desired product formation (enyne **2.26**).

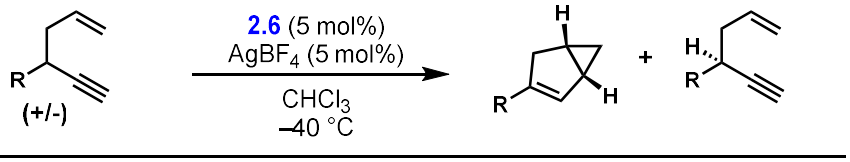

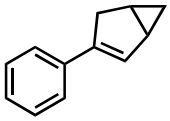

2.12
s factor = 23
conversion = 44%
pdt ee = 85%

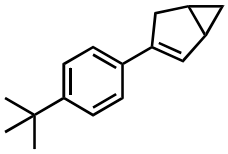

2.13
s factor = 12
conversion = 28%
pdt ee = 88%

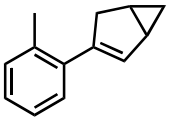

2.14[a]
s factor = 19
conversion = 14%
pdt ee = 90%

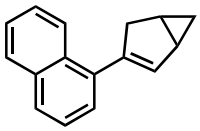

2.15[a]
s factor = 29
conversion = 33%
pdt ee = 84%

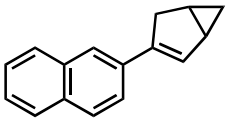

2.16
s factor = 48
conversion = 24%
pdt ee = 89%

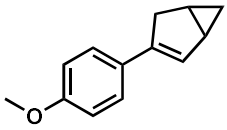

2.17
s factor = 23
conversion = 22%
pdt ee = 85%

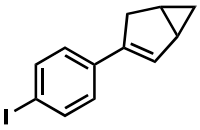

2.18[b]
s factor = 25
conversion = 40%
pdt ee = 88%

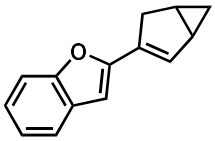

2.19
s factor = 6
conversion = 35%
pdt ee = 68%

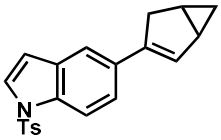

2.20
s factor = 48
conversion = 38%
pdt ee = 88%

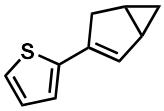

2.21[a]
s factor = 9
conversion = 36%
pdt ee = 61%

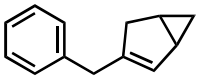

2.22[a]
s factor = 1.5
conversion = 64%
pdt ee = nd

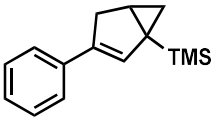

2.23[c]
s factor = --
conversion = 0%
pdt ee = --

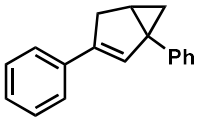

2.24
s factor = 1
conversion = 8%
pdt ee = nd%

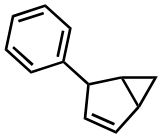

2.25
s factor = 1
conversion = 20%
pdt ee = 0%

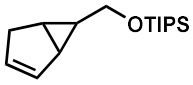

2.26
s factor = --
conversion = 0%
pdt ee = --%

Table 2.5 Substrate scope for the enantioselective 1,5-enyne cycloisomerization. [a]–20 °C for 3h, [b] –30 °C for 3h, [c] 60 °C for 24h.

2.3 Conclusion

In summary, we have developed an enantioconvergent kinetic resolution that allows access to enantioenriched 1,5-enynes and bicyclo[3.1.0]hexenes that has not been shown to be possible with gold(I). This transformation represents a rare mode of direct enantioconvergent kinetic resolution wherein product enantioenrichment is increased at synthetically useful conversions and starting material enantioenrichment is maintained when compared to a standard kinetic resolution.

More importantly, these transformations mark the first highly enantioselective reactions catalyzed by a well-defined gold(III) complex and set the stage for further exploration and development.

2.4 Supporting Information

2.4.1 General Methods

Unless stated otherwise, all reactions were performed in oven-dried glassware sealed with rubber septa under a nitrogen atmosphere and were stirred with Teflon-coated magnetic stir bars. Dry tetrahydrofuran (THF), acetonitrile (MeCN), dichloromethane (DCM), methanol (MeOH), and toluene (Tol) were obtained by passing these previously degassed solvents through activated alumina columns. All other reagents were used as received. Reactions were monitored by thin layer chromatography (TLC) on Silicycle Siliaplate^{TM} glass backed TLC plates (250 μm thickness, 60 Å porosity, F-254 indicator) and visualized by UV irradiation and iodine stain. Volatile solvents were removed under reduced pressure with a rotary evaporator and dried on high vacuum on a Schlenk line. ^{1}H-NMR and ^{13}C-NMR spectra were taken with Bruker AV-300, AVQ-400, AVB-400, AV-500, DRX-500, and AV-600 spectrometers. Chemical shifts are reported relative to the residual solvent signal. NMR data are reported as follows: chemical shift (multiplicity, coupling constants where applicable, number of hydrogens). Splitting is reported with the following symbols: s = singlet, d = doublet, t = triplet, dd = doublet of doublets, dt = doublet of triplets, m = multiplet, dq = doublet of quartets, ddd = doublet of doublets of doublets, ddt = doublet of doublets of triplets. Chiral phase high performance liquid chromatography (HPLC) was performed on Shimadzu VP and Shimadzu prominence series instruments using the specified column (5μm, 4.6 mm x 250 mm). Racemic traces were obtained by substituting IPr(Biphenyl)Au(III)Cl in place of the chiral Au(III) catalyst (**2.6**). Chiral supercritical fluid chromatography (SFC) was performed on a JASCO SF-2000 integrated analytical system. High-resolution mass spectra (HRMS) were obtained from the Micro-Mass/Analytical Facility operated by the College of Chemistry, University of California, Berkeley. Previously reported compounds were synthesized according to literature procedures. The following compounds were prepared according to previously published procedures and their spectra match those reported in literature: 5,5-dibutyl-5H-dibenzo[b,d]stannole,[40] 1,3-bis((R)-1-phenylethyl)-1H-imidazol-3-ium tetrafluoroborate,[56] 1,3-bis((R)-1-phenylethyl)-4,5-dihydro-1H-imidazol-3-ium tetrafluoroborate,[57] 1,3-bis((S)-1-(naphthalen-1-yl)ethyl)-4,5-dihydro-1H-imidazol-3-ium tetrafluoroborate,[58] 1,3-bis((S)-2,2-dimethyl-1-(naphthalen-1-yl)propyl)-4,5-dihydro-1H-imidazol-3-ium iodide.[59]

2.4.2 Preparation and Characterization of 1,5-Enynes

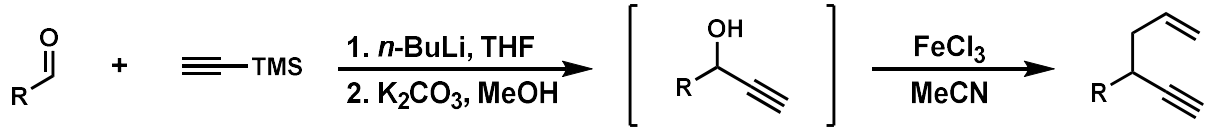

Scheme 2.15 General 1,5-enyne synthesis.

1,5-Enynes were prepared according to the reaction sequence depicted in Scheme 2.15, adapted from a published procedure.[60] To a 250 mL round bottom flask was added THF (40 mL, 0.5 M) and trimethylsilylacetylene (3.11 mL, 22 mmol, 1.1 equiv). The reaction mixture was cooled to −78 °C and *n*-BuLi (8.4 mL, 21 mmol, 1.05 equiv) was added dropwise and stirred for 30 min. To the reaction mixture was added the corresponding aldehyde (20 mmol, 1 equiv) in a

dropwise manner. After addition of the aldehyde, the reaction mixture was allowed to warm to room temperature and stir for 3 h. The reaction mixture was then quenched with the slow addition of water. The reaction mixture was extracted with Et_2O (3 x 35 mL). The combined organic phases were dried over Na_2SO_4, filtered, and concentrated under reduced pressure. The resultant oil was taken up in MeOH (33 mL, 0.6 M) and K_2CO_3 (2.76 g, 20 mmol, 1 equiv) was added. After stirring for 2 h the reaction mixture was filtered through celite, and the celite pad was washed with DCM. The filtrate was then washed with $NH_4Cl_{(sat.,aq)}$, $NaCl_{(sat.,\ aq)}$, dried over Na_2SO_4, and concentrated under reduced pressure. The crude alcohol was taken up in MeCN (40 mL, 0.5 M) and allyltrimethylsilane (9.5 mL, 60 mmol, 3 equiv) was added. To the reaction mixture was added $FeCl_3$ (0.162 g, 1 mmol, 0.05 equiv) dissolved in MeCN (5 mL) in a dropwise fashion. The reaction mixture was stirred for 2 h and then $FeCl_3$(0.162 g, 1 mmol, 0.05 equiv) dissolved in MeCN (5 mL) was added again dropwise. The reaction mixture was allowed to stir for 16 h before being concentrated under reduced pressure. The crude product was purified by column chromatography (100% pentane) to afford the desired product, unless otherwise specified. Enantioenriched HPLC traces were obtained from the resolved starting materials.

hex-5-en-1-yn-3-ylbenzene (SI 1)

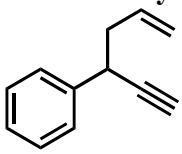

Prepared according to literature procedure. Characterization matches previously reported data.[60] 1H NMR (500 MHz, CDCl3) δ 7.39 – 7.31 (m, 4H), 7.27 – 7.23 (m, 1H), 5.86 (ddt, J = 17.1, 10.2, 7.0 Hz, 1H), 5.13 – 5.03 (m, 2H), 3.71 (td, J = 7.2, 2.5 Hz, 1H), 2.57 – 2.47 (m, 2H), 2.31 (d, J = 2.5 Hz, 1H); HPLC Chiralpak OD-H column (100:0 hexanes:isopropanol, 0.25 mL/min, 215 nm); first enantiomer tr = 30.3 min, second enantiomer tr = 33.3 min.

(S)-hex-5-en-1-yn-3-ylbenzene (SI 1a)

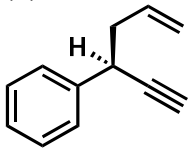

Prepared according to the general procedure using (*R*,*R*)-**2.6**. Isolated via column chromatography (100% hexanes). Characterization matches previously reported data.[61] $[\alpha]^{22}_D$ = 29.34 (*c* = 1.06, $CHCl_3$). **HPLC** Chiralpak OD-H column (100:0 hexanes:isopropanol, 0.25 mL/min, 215 nm); (*R*) enantiomer t_r = 30.3 min, (*S*) enantiomer t_r = 33.3 min.

(R)-hex-5-en-1-yn-3-ylbenzene (SI 1b)

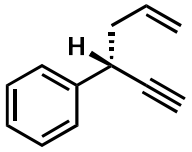

Prepared according to the general procedure using (*S*,*S*)-**2.6**. Isolated via column chromatography (100% hexanes). Characterization matches previously reported data.[62] $[\alpha]^{22}_D$ = -28.65 (*c* = 1.00, $CHCl_3$). **HPLC** Chiralpak OD-H column (100:0 hexanes:isopropanol, 0.25 mL/min, 215 nm); (*R*) enantiomer t_r = 30.3 min, (*S*) enantiomer t_r = 33.3 min.

1-(tert-butyl)-4-(hex-5-en-1-yn-3-yl)benzene (SI 2)

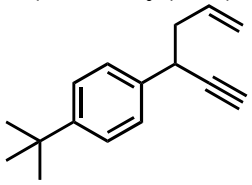

Prepared according to the general procedure. **^{1}H NMR** NMR (500 MHz, $CDCl_3$) δ 7.43 – 7.37 (m, 2H), 7.37 – 7.32 (m, 2H), 5.92 (ddt, *J* = 17.2, 10.1, 7.0 Hz, 1H), 5.19 – 5.08 (m, 2H), 3.72 (td, *J* = 7.2, 2.5 Hz, 1H), 2.59 – 2.52 (m, 2H), 2.33 (d, *J* = 2.5 Hz, 1H), 1.36 (d, *J* = 1.4 Hz, 8H); **^{13}C NMR** (101 MHz, $CDCl_3$) δ 149.71, 137.71, 135.38, 127.01, 125.40, 116.98, 85.59, 71.16, 42.30, 37.22, 34.42, 31.36; **HRMS** (EI): found 212.1567 $C_{16}H_{20}$ requires 212.1565. **SFC** OJ-H column (1% isopropanol, 2.5 mL/min, 215 nm); first enantiomer t_r = 1.7 min, second enantiomer t_r = 1.9 min.

1-(hex-5-en-1-yn-3-yl)-2-methylbenzene (SI 3)

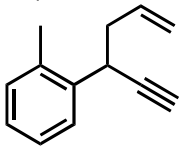

Prepared according to the general procedure. **^{1}H NMR** (500 MHz, Chloroform-*d*) δ 7.54 (d, *J* = 7.3 Hz, 1H), 7.27 – 7.14 (m, 3H), 6.00 – 5.86 (m, 1H), 5.13 (m, 2H), 3.92 (m, 1H), 2.49 (m, 2H), 2.38 (s, 3H), 2.29 – 2.25 (m, 1H); **^{13}C NMR** (126 MHz, $CDCl_3$) δ 139.02, 135.40, 134.84, 130.48, 127.35, 126.90, 126.36, 117.09, 85.73, 70.70, 40.93, 34.06, 19.29; **HRMS** (EI): found 170.1098 $C_{13}H_{14}$ requires 170.1096; **HPLC** Chiralpak OD-H column (100:0 hexanes:isopropanol, 0.25 mL/min, 215 nm); first enantiomer t_r = 29.8 min, second enantiomer t_r = 34.1 min.

1-(hex-5-en-1-yn-3-yl)naphthalene (SI 4)

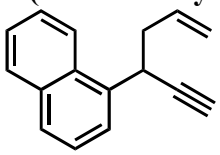

Prepared according to the general procedure. **^{1}H NMR** (400 MHz, $CDCl_3$) δ 8.08 (d, *J* = 8.4 Hz, 1H), 7.90 (d, *J* = 8.0, 1.5 Hz, 1H), 7.78 (t, *J* = 7.9 Hz, 2H), 7.61 – 7.44 (m, 3H), 5.99 (ddt, *J* = 17.1, 10.2, 6.9 Hz, 1H), 5.20 – 5.08 (m, 2H), 4.51 (ddd, *J* = 8.2, 5.1, 2.5 Hz, 1H), 2.80 – 2.58 (m, 2H), 2.38 (d, *J* = 2.5 Hz, 1H); **^{13}C NMR** (101 MHz, $CDCl_3$) δ 136.30, 135.34, 133.96, 130.47, 129.04, 127.70, 126.12, 125.51, 125.45, 125.15, 122.78, 117.06, 85.43, 71.67, 41.02, 34.06; **HRMS** (EI): found 206.1098 $C_{16}H_{14}$ requires 206.1096; **HPLC** Chiralpak AD-H column (99.9:0.1 hexanes:isopropanol, 0.25 mL/min, 270 nm); first enantiomer t_r = 25.6 min, second enantiomer t_r = 36.3 min.

2-(hex-5-en-1-yn-3-yl)naphthalene (SI 5)

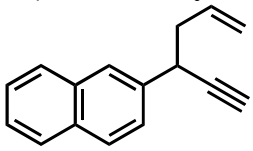

Prepared according to the general procedure. **^{1}H NMR** (400 MHz, $CDCl_3$) δ 7.87 – 7.80 (m, 4H), 7.49 (m, 3H), 5.89 (ddt, *J* = 17.1, 10.2, 7.0 Hz, 1H), 5.15 – 5.05 (m, 2H), 3.89 (td, *J* = 7.1, 2.5 Hz, 1H), 2.62 (tt, *J* = 7.1, 1.3 Hz, 2H), 2.38 (d, *J* = 2.5 Hz, 1H).; **^{13}C NMR** (151 MHz, $CDCl_3$) δ 138.05, 135.02, 133.37, 132.48, 128.21, 127.75, 127.58, 126.07, 126.00, 125.67, 117.24, 85.27, 71.62, 42.15, 37.79; **HRMS** (EI): found 206.1096 $C_{16}H_{14}$ requires 206.1096; **HPLC** Chiralpak AD-H column (99.9:0.1 hexanes:isopropanol, 0.25 mL/min, 270 nm); first enantiomer t_r = 26.3 min, second enantiomer t_r = 28.0 min.

1-(hex-5-en-1-yn-3-yl)-4-methoxybenzene (SI 6)

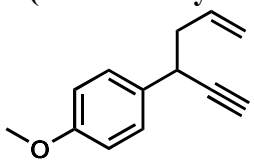

Prepared according to the general procedure. Characterization matches previously reported data.[61] **^{1}H NMR** (500 MHz, $CDCl_3$) δ 7.28 (d, *J* = 8.6 Hz, 2H), 6.87 (d, *J* = 8.6 Hz, 2H), 5.84 (ddt, *J* = 17.2, 10.1, 7.0 Hz, 1H), 5.13 – 5.01 (m, 2H), 3.80 (s, 3H), 3.66 (td, *J* = 7.2, 2.6 Hz, 1H), 2.56 – 2.45 (m, 2H), 2.29 (d, *J* = 2.5 Hz, 1H); **HPLC** Chiralpak AD-H column (99.9:0.1 hexanes:isopropanol, 0.25 mL/min, 225 nm); first enantiomer t_r = 26.5 min, second enantiomer t_r = 29.5 min.

1-(hex-5-en-1-yn-3-yl)-4-iodobenzene (SI 7)

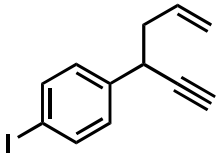

Prepared according to the general procedure. **^{1}H NMR** (600 MHz, $CDCl_3$) δ 7.65 (d, *J* = 8.3 Hz, 2H), 7.11 (d, *J* = 8.3 Hz, 2H), 5.81 (ddt, *J* = 18.5, 9.6, 7.0 Hz, 1H), 5.09 – 5.02 (m, 2H), 3.65 (td, *J* = 7.1, 2.5 Hz, 1H), 2.48 (t, *J* = 6.8 Hz, 2H), 2.30 (d, *J* = 2.5 Hz, 1H); **^{13}C NMR** (151 MHz, $CDCl_3$) δ 140.39, 137.49, 134.57, 129.49, 117.51, 92.16, 84.60, 71.72, 42.08, 37.22; **HRMS** (EI): found 281.9907 $C_{12}H_{11}I$ requires 281.9906; **HPLC** Chiralpak OD-H column (100:0 hexanes:isopropanol, 0.25 mL/min, 270 nm); first enantiomer t_r = 27.9 min, second enantiomer t_r = 30.2 min.

2-(hex-5-en-1-yn-3-yl)benzofuran (SI 8)

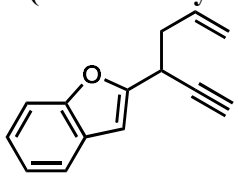

Prepared according to the general procedure. **^{1}H NMR** (400 MHz, $CDCl_3$) δ 7.56 – 7.50 (m, 1H), 7.48 – 7.43 (m, 1H), 7.28 – 7.18 (m, 2H), 6.66 (s, 1H), 5.90 (ddt, *J* = 17.1, 10.1, 7.0 Hz, 1H), 5.16 (dd, *J* = 17.1, 1.7 Hz, 1H), 5.11 (dd, *J* = 10.2, 1.6 Hz, 1H), 3.96 (ddd, *J* = 8.1, 5.5, 2.5 Hz, 1H), 2.83 – 2.60 (m, 2H), 2.33 (d, *J* = 2.5 Hz, 1H); **^{13}C NMR** (126 MHz, $CDCl_3$) δ 156.25, 154.96, 134.17, 128.34, 123.84, 122.74, 120.80, 117.90, 111.06, 103.33, 82.04, 71.49, 38.30, 31.89; **HRMS** (EI): found 196.0889 $C_{14}H_{12}O$ requires 196.0888; **HPLC** Chiralpak OD-H column (100:0

hexanes:isopropanol, 0.25 mL/min, 270 nm); first enantiomer t_r = 21.0 min, second enantiomer t_r = 22.3 min.

5-(hex-5-en-1-yn-3-yl)-1-tosyl-1H-indole (SI 9)

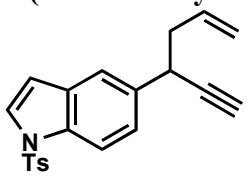

Prepared according to the general procedure. Purified by column chromatography (15:1 hexanes:ethyl acetate). **^{1}H NMR** (400 MHz, $CDCl_3$) δ 7.93 (d, *J* = 8.6 Hz, 1H), 7.76 (d, *J* = 8.3 Hz, 2H), 7.55 (d, *J* = 3.7 Hz, 1H), 7.53 (d, *J* = 1.7 Hz, 1H), 7.29 (dd, *J* = 8.6, 1.8 Hz, 1H), 7.22 (d, *J* = 8.1 Hz, 2H), 5.83 (ddt, *J* = 17.2, 10.2, 7.0 Hz, 1H), 5.11 – 5.00 (m, 2H), 3.76 (td, *J* = 7.2, 2.5 Hz, 1H), 2.55 – 2.48 (m, 2H), 2.34 (s, 3H), 2.31 (d, *J* = 2.5 Hz, 1H); **^{13}C NMR** (126 MHz, $CDCl_3$) δ 144.96, 135.95, 135.28, 135.10, 133.84, 130.98, 129.90, 126.84, 126.76, 124.24, 120.05, 117.26, 113.52, 109.00, 85.59, 71.47, 42.68, 37.58, 21.60; **HRMS** (EI): found 349.1138 $C_{21}H_{19}NO_2S$ requires 349.1137 ; **HPLC** Chiralpak IA column (95:5 hexanes:isopropanol, 1 mL/min, 230 nm); first enantiomer t_r = 12.1 min, second enantiomer t_r = 13.5 min.

2-(hex-5-en-1-yn-3-yl)thiophene (SI 10)

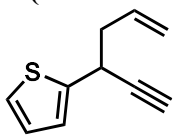

Prepared according to the general procedure. **^{1}H NMR** (500 MHz, $CDCl_3$) δ 7.23 – 7.21 (m, 1H), 7.03 (s, 1H), 6.98 (s, 1H), 5.91 (app dt, *J* = 17.2, 8.7 Hz, 1H), 5.20 – 5.11 (m, 2H), 4.05 – 4.02 (m, 1H), 2.67 – 2.62 (m, 2H), 2.37 (d, *J* = 2.1 Hz, 1H); **^{13}C NMR** (126 MHz, $CDCl_3$) δ 144.05, 134.59, 126.68, 124.69, 124.13, 117.76, 84.56, 71.34, 42.42, 32.87; **HRMS** (EI): found 162.0503 $C_{10}H_{10}S$ requires 162.0503; **HPLC** Chiralpak OD-H column (100:0 hexanes:isopropanol, 0.25 mL/min, 270 nm); first enantiomer t_r = 32.0 min, second enantiomer t_r = 36.0 min.

(2-ethynylpent-4-en-1-yl)benzene (SI 11)

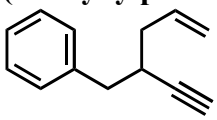

Prepared according to literature procedure. Characterization matches previously reported data.[61] **^{1}H NMR** (300 MHz, $CDCl_3$) δ 7.37 – 7.17 (m, 5H), 5.92 (ddt, *J* = 16.8, 9.8, 7.0 Hz, 1H), 5.20 – 5.03 (m, 2H), 2.83 – 2.75 (m, 2H), 2.75 – 2.64 (m, 1H), 2.35 – 2.14 (m, 2H), 2.10 (d, *J* = 2.3 Hz, 1H); **HPLC** Chiralpak OD-H column (100:0 hexanes:isopropanol, 0.25 mL/min, 210 nm); first enantiomer t_r = 30.1 min, second enantiomer t_r = 33.1 min.

2.4.3 Preparation and Characterization of Bicyclo[3.1.0]hexene products

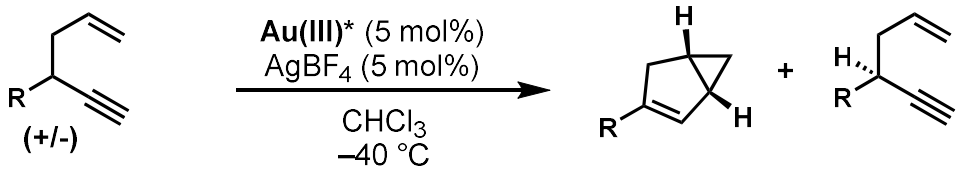

Scheme 2.16 General gold(III) catalyzed enantioconvergent kinetic resolution.

To a 1 dram vial was added the Au(III) catalyst (0.05 equiv), $AgBF_4$ (0.05 equiv), and $CHCl_3$ (0.3 M). The vial was capped and sonicated for 5 minutes. The reaction mixture was passed through a glass fiber filter and collected in a 1 dram vial. The vial was then cooled to −40 °C and the 1,5-enyne (1 equiv) was added. The reaction mixture was allowed to stir for 3 h and quenched with the addition of NH_4Cl. S factor was determined via NMR of the quenched reaction mixture. The starting material and product were then isolated by column chromatography (100% pentane) unless otherwise noted.

3-phenylbicyclo[3.1.0]hex-2-ene (SI 12)

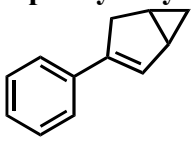

Prepared according to the general procedure. Characterization matches previously reported data.[33] **^{1}H NMR** (300 MHz, $CDCl_3$) δ 7.48 – 7.41 (m, 2H), 7.35 (m, 2H), 7.26 (m, 1H), 6.48 (dd, *J* = 2.1, 1.8 Hz, 1H), 3.08 (ddd, *J* = 16.8, 7.3, 1.8 Hz, 1H), 2.80 (dt, *J* = 17.0, 2.5 Hz, 1H), 2.01 (m, 1H), 1.78 (ddd, *J* = 11.2, 9.1, 5.8 Hz, 1H), 1.01 (td, *J* = 7.6, 3.8 Hz, 1H), 0.19 (q, *J* = 3.7 Hz, 1H); **HPLC** Chiralpak OD-H column (100:0 hexanes:isopropanol, 0.25 mL/min, 270 nm); first enantiomer t_r = 49.9 min, second enantiomer t_r = 58.1 min.

3-(4-(tert-butyl)phenyl)bicyclo[3.1.0]hex-2-ene (SI 13)

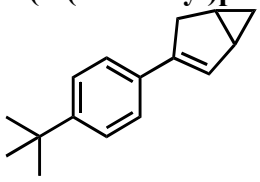

Prepared according to the general procedure. The compound was isolated in pentane due to rapid decomposition when dried. **^{1}H NMR** (500 MHz, $CDCl_3$) δ 7.33 (s, 4H), 6.37 (q, *J* = 2.0 Hz, 1H), 3.01 (ddd, *J* = 16.8, 7.3, 1.8 Hz, 1H), 2.77 – 2.68 (m, 1H), 1.96 – 1.90 (m, 1H), 1.75 – 1.68 (m, 1H), 1.33 (s, 9H), 0.96 – 0.92 (m, 1H), 0.06 (q, *J* = 3.7 Hz, 1H); **^{13}C NMR** (126 MHz, $CDCl_3$) δ 149.76, 139.46, 133.88, 128.89, 125.22, 124.90, 36.35, 34.52, 31.34, 24.15, 17.63, 15.39; **HRMS** (EI): found 212.1566 $C_{16}H_{20}$ requires 212.1565; **SFC** OJ-H column (5% isopropanol, 2.5 mL/min, 210 nm); first enantiomer t_r = 3.4 min, second enantiomer t_r = 3.6 min.

3-(o-tolyl)bicyclo[3.1.0]hex-2-ene (SI 14)

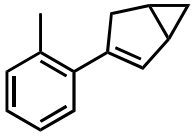

Prepared according to the general procedure. **^{1}H NMR** (600 MHz, Chloroform-*d*) δ 7.17 – 7.09 (m, 4H), 5.98 (q, *J* = 2.1 Hz, 1H), 3.00 (dd, *J* = 18.1, 7.4 Hz, 1H), 2.66 (dt, *J* = 17.2, 2.6 Hz, 1H),

2.34 (s, 3H), 1.99 – 1.93 (m, 1H), 1.71 – 1.65 (m, 1H), 0.92 (td, *J* = 7.6, 3.8 Hz, 1H), 0.10 (q, *J* = 3.7 Hz, 1H); **^{13}C NMR** (151 MHz, $CDCl_3$) δ 140.09, 137.42, 135.56, 133.13, 130.45, 128.13, 126.49, 125.46, 39.64, 24.30, 21.37, 16.97, 14.97; **HRMS** (EI): found 170.1098 $C_{13}H_{14}$ requires 170.1096; **HPLC** Chiralpak OD-H column (100:0 hexanes:isopropanol, 0.25 mL/min, 270 nm); first enantiomer t_r = 32.8 min, second enantiomer t_r = 36.0 min.

1-(bicyclo[3.1.0]hex-2-en-3-yl)naphthalene (SI 15)

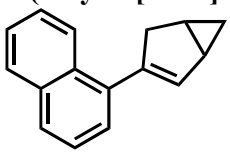

Prepared according to the general procedure. **^{1}H NMR** (600 MHz, Chloroform-*d*) δ 8.17 – 8.12 (m, 1H), 7.86 – 7.83 (m, 1H), 7.73 (d, *J* = 8.1 Hz, 1H), 7.49 – 7.45 (m, 2H), 7.44 – 7.38 (m, 1H), 7.31 – 7.30 (m, 1H), 6.14 (s, 1H), 3.15 (ddd, *J* = 17.4, 7.2, 1.9 Hz, 1H), 2.83 – 2.77 (m, 1H), 2.10 – 2.04 (m, 1H), 1.82 – 1.74 (m, 1H), 1.01 (td, *J* = 7.6, 3.9 Hz, 1H), 0.28 (q, *J* = 3.8 Hz, 1H) ; **^{13}C NMR** (151 MHz, $CDCl_3$) δ 139.11, 136.30, 134.32, 133.80, 131.55, 128.29, 127.01, 125.75, 125.66, 125.54, 125.18, 124.98, 40.68, 24.50, 16.97, 15.27; **HRMS** (EI): found 206.1093 $C_{16}H_{14}$ requires 206.1096; **HPLC** Chiralpak IB column (99.9:0.1 hexanes:isopropanol, 0.5 mL/min, 322 nm); first enantiomer t_r = 14.7min, second enantiomer t_r = 15.5 min.

2-(bicyclo[3.1.0]hex-2-en-3-yl)naphthalene (SI 16)

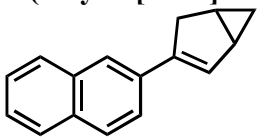

Prepared according to the general procedure. **^{1}H NMR** (600 MHz, Chloroform-*d*) δ 7.79 – 7.75 (m, 2H), 7.73 (d, *J* = 8.6 Hz, 1H), 7.64 – 7.59 (m, 2H), 7.46 – 7.38 (m, 2H), 6.54 (d, *J* = 2.1 Hz, 1H), 3.12 (ddd, *J* = 16.6, 7.2, 1.7 Hz, 1H), 2.89 – 2.83 (m, 1H), 2.01 – 1.96 (m, 1H), 1.81 – 1.75 (m, 1H), 0.97 (td, *J* = 7.7, 3.8 Hz, 1H), 0.14 (q, *J* = 3.7 Hz, 1H).; **^{13}C NMR** (151 MHz, $CDCl_3$) δ 139.76, 134.01, 133.54, 132.45, 130.52, 127.90, 127.62, 127.50, 126.04, 125.40, 123.84, 123.42, 36.31, 24.27, 17.84, 15.62; **HRMS** (EI): found 206.1097 $C_{16}H_{14}$ requires 206.1096; **HPLC** Chiralpak AD-H column (99.9:0.1 hexanes:isopropanol, 0.25 mL/min, 320 nm); first enantiomer t_r = 24.3 min, second enantiomer t_r = 26.1 min.

3-(4-methoxyphenyl)bicyclo[3.1.0]hex-2-ene (SI 17)

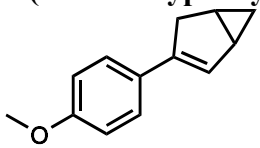

Prepared according to the general procedure. The compound was isolated in pentane due to rapid decomposition when dried. **^{1}H NMR** (500 MHz, $CDCl_3$) δ 7.29 (d, *J* = 8.8 Hz, 2H), 6.82 (d, *J* = 8.9 Hz, 2H), 6.25 (q, *J* = 2.1 Hz, 1H), 3.80 (s, 3H), 2.97 (ddd, *J* = 16.9, 7.3, 1.9 Hz, 1H), 2.71 – 2.63 (m, 1H), 1.94 – 1.86 (m, 1H), 1.72 – 1.65 (m, 1H), 0.92 – 0.89 (m, 1H), 0.05 (q, *J* = 3.6 Hz, 1H); **^{13}C NMR** (126 MHz, $CDCl_3$) δ 158.54, 139.20, 129.54, 127.47, 126.29, 113.67, 55.30, 36.48, 24.10, 17.63, 15.30; **HRMS** (EI): found 186.1043 $C_{13}H_{14}O$ requires 186.1045; **HPLC** Chiralpak OJ column (99.5:0.5 hexanes:isopropanol, 1 mL/min, 300 nm); first enantiomer t_r = 12.4 min, second enantiomer t_r = 15.8 min.

3-(4-iodophenyl)bicyclo[3.1.0]hex-2-ene (SI 18)

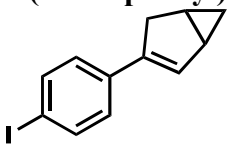

Prepared according to the general procedure. The compound was isolated in pentane due to rapid decomposition when dried. **^{1}H NMR** (500 MHz, $CDCl_3$) δ 7.58 (d, *J* = 8.5 Hz, 1H), 7.08 (d, *J* = 8.4 Hz, 1H), 6.41 (q, *J* = 2.1 Hz, 1H), 2.95 (ddd, *J* = 16.8, 7.3, 1.8 Hz, 1H), 2.66 (dt, *J* = 17.0, 2.5 Hz, 1H), 1.96 – 1.89 (m, 1H), 1.76 – 1.68 (m, 1H), 0.93 (td, *J* = 7.6, 3.8 Hz, 1H), 0.07 (q, *J* = 3.7 Hz, 1H); **^{13}C NMR** (126 MHz, $CDCl_3$) δ 138.69, 137.28, 136.09, 130.81, 126.99, 91.73, 36.18, 24.29, 17.64, 15.62; **HRMS** (EI): found 281.9908 $C_{12}H_{11}I$ requires 281.9906; **HPLC** Chiralpak OJ column (99.5:0.5 hexanes:isopropanol, 1 mL/min, 270 nm); first enantiomer t_r = 16.8 min, second enantiomer t_r = 18.1 min.

2-(bicyclo[3.1.0]hex-2-en-3-yl)benzofuran (SI 19)

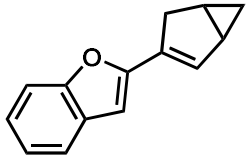

Prepared according to the general procedure. **^{1}H NMR** (600 MHz, $CDCl_3$) δ 7.48 (d, *J* = 6.9 Hz, 1H), 7.40 (d, *J* = 8.2 Hz, 1H), 7.23 – 7.20 (m, 1H), 7.16 (t, *J* = 7.4 Hz, 1H), 6.55 (q, *J* = 2.1 Hz, 1H), 6.41 (s, 1H), 2.99 (dd, *J* = 16.6, 7.3 Hz, 1H), 2.73 – 2.68 (m, 1H), 2.01 – 1.95 (m, 1H), 1.79 – 1.73 (m, 1H), 1.00 (td, *J* = 7.7, 3.9 Hz, 1H), 0.14 (q, *J* = 3.8 Hz, 1H); **^{13}C NMR** (126 MHz, $CDCl_3$) δ 154.61, 154.10, 132.73, 130.15, 129.06, 124.01, 122.61, 120.57, 110.75, 101.60, 35.53, 24.42, 17.93, 15.83; **HRMS** (EI): found 196.0887 $C_{14}H_{12}O$ requires 196.0888; **HPLC** Chiralpak OD-H column (100:0 hexanes:isopropanol, 0.25 mL/min, 315 nm); first enantiomer t_r = 12.5 min, second enantiomer t_r = 14.6 min.

5-(bicyclo[3.1.0]hex-2-en-3-yl)-1-tosyl-1H-indole (SI 20)

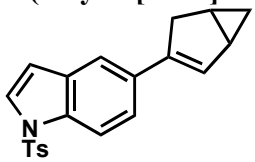

Prepared according to the general procedure. Purified by column chromatography (15:1 hexanes:ethyl acetate). **^{1}H NMR** (600 MHz, $CDCl_3$) δ 7.87 (d, *J* = 8.7 Hz, 1H), 7.73 (d, *J* = 8.4 Hz, 2H), 7.51 (d, *J* = 3.7 Hz, 1H), 7.44 – 7.41 (m, 1H), 7.38 (dd, *J* = 8.7, 1.7 Hz, 1H), 7.20 (d, *J* = 8.2 Hz, 2H), 6.60 (d, *J* = 3.6 Hz, 1H), 6.36 (q, *J* = 2.1 Hz, 1H), 3.01 (ddd, *J* = 16.6, 7.3, 1.8 Hz, 1H), 2.75 – 2.69 (m, 1H), 2.32 (s, 3H), 1.95 – 1.88 (m, 1H), 1.74 – 1.66 (m, 1H), 0.91 (td, *J* = 7.6, 3.8 Hz, 1H), 0.05 (q, *J* = 3.7 Hz, 1H); **^{13}C NMR** (151 MHz, $CDCl_3$) δ 144.81, 139.49, 135.26, 133.75, 132.22, 130.88, 129.78, 129.11, 126.71, 126.60, 122.22, 117.61, 113.27, 109.25, 36.57, 24.13, 21.49, 17.63, 15.36; **HRMS** (EI): found 349.1137 $C_{21}H_{19}NO_2S$ requires 349.1137; **HPLC** Chiralpak IA column (95:5 hexanes:isopropanol, 1 mL/min, 230 nm); first enantiomer t_r = 15.6 min, second enantiomer t_r = 20.9 min.

2-(bicyclo[3.1.0]hex-2-en-3-yl)thiophene (SI 21)

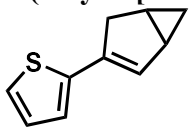

Prepared according to the general procedure. The compound was isolated in pentane due to rapid decomposition when dried. **^{1}H NMR** (500 MHz, $CDCl_3$) δ 7.09 (dd, *J* = 5.1, 1.2 Hz, 1H), 6.93 (dd, *J* = 5.1, 3.6 Hz, 1H), 6.84 (dd, *J* = 3.6, 1.1 Hz, 1H), 6.20 (q, *J* = 2.0 Hz, 1H), 2.99 (ddd, *J* = 16.7, 7.3, 1.8 Hz, 1H), 2.70 (dt, *J* = 16.7, 2.5 Hz, 1H), 1.93 – 1.87 (m, 1H), 1.73 – 1.66 (m, 1H), 0.93 (td, *J* = 7.6, 3.9 Hz, 1H), 0.12 (q, *J* = 3.8 Hz, 1H); **^{13}C NMR** (126 MHz, $CDCl_3$) δ 141.10, 134.14, 129.44, 127.18, 123.26, 122.80, 37.39, 24.19, 17.77, 15.53; **HRMS** (EI): found 162.0502 $C_{10}H_{10}S$ requires 162.0503; **HPLC** Chiralpak OD-H column (100:0 hexanes:isopropanol, 0.25 mL/min, 210 nm); first enantiomer t_r = 42.1 min, second enantiomer t_r = 44.3 min.

3-benzylbicyclo[3.1.0]hex-2-ene (SI 22)

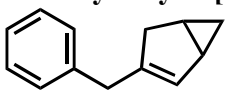

Prepared according to the general procedure. **^{1}H NMR** (400 MHz, $CDCl_3$) δ 7.33 – 7.25 (m, 2H), 7.24 – 7.13 (m, 3H), 5.62 – 5.56 (m, 1H), 3.31 (s, 2H), 2.49 (dd, *J* = 17.3, 7.2 Hz, 1H), 2.17 (d, *J* = 17.3, 2.3 Hz, 1H), 1.79 – 1.68 (m, 1H), 1.59 – 1.47 (m, 1H), 0.78 (td, *J* = 7.5, 3.7 Hz, 1H), -0.06 (q, *J* = 3.7 Hz, 1H); ^{13}C NMR (101 MHz, $CDCl_3$) δ 141.57, 140.23, 129.48, 128.85, 128.36, 125.99, 37.97, 37.63, 23.10, 17.12, 15.26; **HRMS** (EI): found 170.1096 $C_{13}H_{14}$ requires 170.1096.

2.4.4 Preparation and Characterization of NHC Gold(III) Complexes

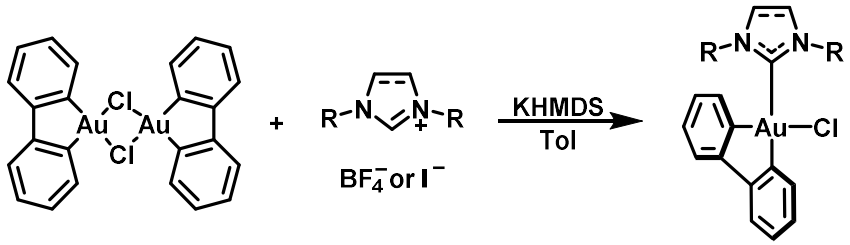

Scheme 2.17 Synthesis of gold(III)-NHC complexes.

In a glovebox, to the corresponding imidazolium salt (2 equiv) in toluene (0.1 M) was added KHMDS (2.4 equiv) in one portion at 22 °C. The reaction mixture was stirred for 5 h and then [Au(III)(biphenyl) chloride]$_2$ (1 equiv) was added in one portion. The reaction mixture was stirred for 16 h and then the reaction vessel was removed from the glovebox. The reaction mixture was then passed through Celite and dried under vacuum to give the crude product. The pure product was isolated by column chromatography (DCM:hexanes 1:1).

Catalyst 2.1 (SI 23)

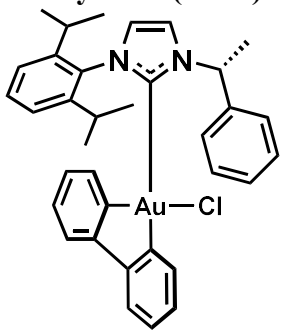

Prepared according to the general procedure with (R)-3-(2,6-diisopropylphenyl)-1-(1-phenylethyl)-1H-imidazol-3-ium tetrafluoroborate. **^{1}H NMR** (400 MHz, $CDCl_3$, mixture of atropisomers)) δ 8.12 (ddd, J = 7.5, 5.9, 1.5 Hz, 1H), 7.68 – 7.60 (m, 1H), 7.55 – 7.49 (m, 1H), 7.46 – 7.30 (m, 6H), 7.22 – 6.99 (m, 7H), 6.89 – 6.76 (m, 1H), 6.72 (dd, J = 6.8, 1.6 Hz, 1H), 6.30 (dq, J = 56.3, 7.0 Hz, 1H), 2.92 – 2.62 (m, 2H), 2.03 (dd, J = 36.9, 7.0 Hz, 3H), 1.43 (dd, J = 6.6, 2.4 Hz, 3H), 1.00 (ddd, J = 30.7, 20.9, 6.8 Hz, 6H), 0.67 (dd, J = 28.8, 6.7 Hz, 3H). **^{13}C NMR** (151 MHz, CDCl3, mixture of atropisomers): δ 185.20, 184.89, 159.83, 159.69, 154.79, 152.96, 152.92, 151.85, 151.64, 147.20, 147.12, 145.15, 145.08, 139.08, 138.05, 133.66, 133.64, 133.54, 133.41, 133.09, 133.07, 130.58, 130.56, 129.08, 129.02, 128.86, 128.49, 128.12, 127.28, 127.24, 127.17, 127.08, 127.04, 126.84, 126.49, 126.35, 126.30, 125.72, 124.39, 124.37, 123.96, 121.76, 121.61, 120.43, 118.42, 118.36, 60.34, 58.81, 29.65, 28.67, 28.33, 28.22, 26.82, 26.77, 25.96, 25.93, 23.07, 23.03, 22.34, 22.31, 22.17, 19.54.; **HRMS** (ESI+): found 681.2543 $C_{35}H_{36}AuN_2$ $[M]^+$ requires 681.2539.

Catalyst 2.2 (SI 24)

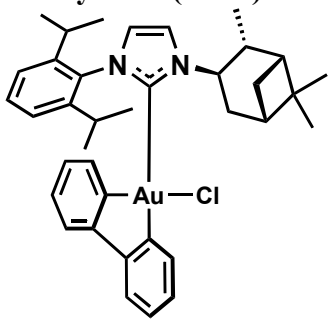

Prepared according to the general procedure with 3-(2,6-diisopropylphenyl)-1-((1R,2R,3R,5S)-2,6,6-trimethylbicyclo[3.1.1]heptan-3-yl)-1H-imidazol-3-ium tetrafluoroborate. **^{1}H NMR** (400 MHz, CD_2Cl_2, mixture of atropisomers) δ 7.97 (ddd, *J* = 15.2, 7.6, 1.4 Hz, 1H), 7.57 (dd, *J* = 7.1, 2.0 Hz, 1H), 7.45 – 7.36 (m, 2H), 7.34 – 7.26 (m, 2H), 7.24 (dd, *J* = 6.1, 1.9 Hz, 1H), 7.19 – 7.04 (m, 3H), 7.03 – 6.96 (m, 1H), 6.90 – 6.81 (m, 1H), 6.80 – 6.67 (m, 1H), 5.23 (dt, *J* = 10.3, 7.1 Hz, 1H), 2.91 – 2.53 (m, 4H), 2.39 – 2.19 (m, 1H), 2.14 – 2.04 (m, 1H), 2.01 – 1.86 (m, 1H), 1.42 (d, *J* = 6.6 Hz, 2H), 1.38 – 1.32 (m, 3H), 1.28 – 1.18 (m, 5H), 1.13 (dd, *J* = 10.4, 7.0 Hz, 3H), 1.04 (dd, *J* = 6.8, 2.7 Hz, 2H), 0.97 – 0.91 (m, 3H), 0.84 (s, 2H), 0.74 (d, *J* = 6.7 Hz, 1H), 0.59 (d, *J* = 6.7 Hz, 2H).; **^{13}C NMR** (101 MHz, CD_2Cl_2, mixture of atropisomers) δ 185.79, 184.75, 160.20, 159.96, 154.87, 154.79, 153.67, 153.56, 151.85, 151.78, 147.65, 145.85, 145.69, 134.76, 134.29, 134.23, 134.16, 133.39, 133.33, 130.89, 130.79, 127.76, 127.67, 127.60, 127.40, 127.28, 127.14, 126.92, 126.85, 126.77, 124.75, 124.59, 124.44, 124.36, 121.92, 121.76, 120.78, 120.74, 118.77,

118.42, 61.53, 61.23, 48.45, 48.09, 46.98, 43.59, 41.98, 41.93, 39.24, 39.06, 36.65, 35.13, 35.02, 29.32, 28.99, 28.85, 28.60, 27.93, 27.88, 27.12, 26.97, 26.50, 25.88, 23.81, 23.54, 23.29, 23.19, 22.44, 22.16, 21.37, 20.78.; **HRMS** (ESI+): found 713.3152 $C_{37}H_{44}AuN_2$ $[M]^+$ requires 713.3170.

Catalyst 2.4 (SI 25)

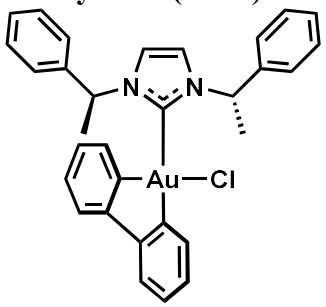

Prepared according to the general procedure with 1,3-bis((R)-1-phenylethyl)-1H-imidazol-3-ium tetrafluoroborate. **^{1}H NMR** (600 MHz, CD_2Cl_2) δ 8.14 (dd, *J* = 7.5, 1.4 Hz, 1H), 7.58 – 7.53 (m, 2H), 7.45 (dd, *J* = 7.6, 1.5 Hz, 1H), 7.43 – 7.36 (m, 3H), 7.35 – 7.31 (m, 3H), 7.30 – 7.25 (m, 3H), 7.17 (dtd, *J* = 8.8, 7.4, 1.3 Hz, 2H), 7.13 (td, *J* = 7.4, 1.5 Hz, 1H), 7.02 (d, *J* = 2.1 Hz, 1H), 6.94 (d, *J* = 2.1 Hz, 1H), 6.75 (td, *J* = 7.5, 1.5 Hz, 1H), 6.50 (dd, *J* = 7.6, 1.2 Hz, 1H), 6.11 (q, *J* = 7.0 Hz, 1H), 6.07 (q, *J* = 7.1 Hz, 1H), 1.95 (d, *J* = 7.1 Hz, 3H), 1.77 (d, *J* = 7.1 Hz, 3H); **^{13}C NMR** (151 MHz, CD_2Cl_2) δ 182.06, 160.05, 154.39, 153.13, 151.08, 138.95, 138.80, 134.01, 132.99, 128.75, 128.71, 128.48, 128.45, 127.48, 127.39, 127.33, 127.19, 126.84, 126.77, 121.73, 120.51, 119.52, 119.15, 59.66, 58.81, 20.83, 19.90; **HRMS** (ESI+): found 683.1505 $C_{31}H_{28}AuClN_2Na$ $[M+Na]^+$ requires 683.1504.

Catalyst 2.5 (SI 26)

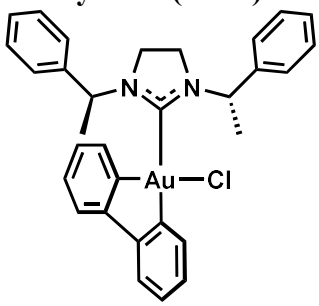

Prepared according to the general procedure with imidazolium 1,3-bis((R)-1-phenylethyl)-4,5-dihydro-1H-imidazol-3-ium tetrafluoroborate. **^{1}H NMR** (600 MHz, CD_2Cl_2) δ 8.13 (dd, *J* = 7.5, 1.4 Hz, 1H), 7.65 – 7.63 (m, 2H), 7.51 (dd, *J* = 7.6, 1.5 Hz, 1H), 7.45 – 7.39 (m, 3H), 7.37 – 7.33 (m, 1H), 7.32 – 7.28 (m, 5H), 7.27 – 7.23 (m, 2H), 7.19 (td, *J* = 7.4, 1.4 Hz, 1H), 7.14 (td, *J* = 7.4, 1.5 Hz, 1H), 6.95 (td, *J* = 7.5, 1.5 Hz, 1H), 5.77 (dq, *J* = 23.9, 7.0 Hz, 2H), 3.67 – 3.51 (m, 2H), 3.34 – 3.18 (m, 2H), 1.78 (d, *J* = 7.0 Hz, 3H), 1.56 (d, *J* = 5.8 Hz, 3H); **^{13}C NMR** (151 MHz, CD_2Cl_2) δ 204.57, 160.20, 154.52, 152.99, 150.29, 138.34, 138.03, 134.40, 132.88, 128.52, 128.51, 128.08, 127.71, 127.68, 127.63, 127.16, 126.84, 126.83, 121.83, 120.52, 57.82, 56.87, 44.01, 43.69, 16.45, 16.08; **HRMS** (ESI+): found 685.1663 $C_{31}H_{30}AuClN_2Na$ $[M+Na]^+$ requires 685.1661.

Catalyst 2.6 (SI 27)

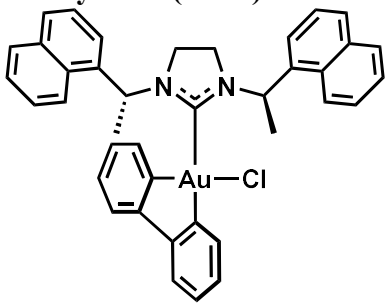

Prepared according to the general procedure with 1,3-bis((S)-1-(naphthalen-1-yl)ethyl)-4,5-dihydro-1H-imidazol-3-ium tetrafluoroborate. **^{1}H NMR** (500 MHz, $CDCl_3$) δ 8.90 (d, *J* = 8.6 Hz, 1H), 8.41 – 8.37 (m, 1H), 8.04 (d, *J* = 8.5 Hz, 1H), 7.83 (d, *J* = 8.2 Hz, 1H), 7.81 – 7.75 (m, 3H), 7.73 (ddd, *J* = 8.5, 6.8, 1.4 Hz, 1H), 7.58 – 7.50 (m, 4H), 7.48 (dd, *J* = 7.0, 2.0 Hz, 1H), 7.45 – 7.32 (m, 3H), 7.25 – 7.17 (m, 3H), 6.96 (d, *J* = 7.6 Hz, 1H), 6.89 – 6.83 (m, 1H), 6.67 (td, *J* = 7.5, 1.5 Hz, 1H), 6.38 (q, *J* = 6.9 Hz, 1H), 6.24 (q, *J* = 6.9 Hz, 1H), 3.49 – 3.33 (m, 2H), 3.05 – 2.86 (m, 2H), 2.04 (d, *J* = 6.9 Hz, 3H), 1.77 (d, *J* = 6.9 Hz, 3H); **^{13}C NMR** (126 MHz, $CDCl_3$) δ 207.45, 160.49, 154.73, 153.11, 151.12, 135.70, 134.25, 133.86, 133.69, 133.07, 132.18, 132.12, 131.58, 130.85, 129.47, 129.19, 128.48, 128.42, 127.53, 127.42, 127.36, 127.13, 126.69, 126.37, 126.01, 124.98, 124.92, 124.89, 124.73, 124.48, 121.75, 120.76, 53.77, 53.76, 45.76, 44.95, 29.74, 18.63, 18.29; **HRMS** (ESI+): found 785.1979 $C_{39}H_{34}AuClN_2Na$ $[M+Na]^+$ requires 785.1976.

Catalyst 2.7 (SI 28)

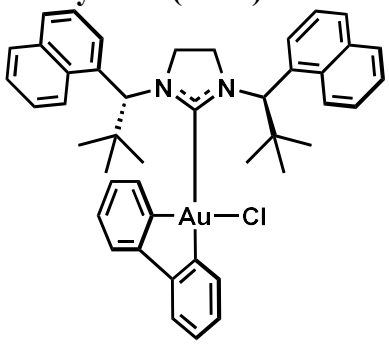

Prepared according to the general procedure with 1,3-bis((S)-2,2-dimethyl-1-(naphthalen-1-yl)propyl)-4,5-dihydro-1H-imidazol-3-ium iodide. **^{1}H NMR** (600 MHz, $CDCl_3$) δ 8.06 (d, *J* = 8.7 Hz, 1H), 7.96 (d, *J* = 8.6 Hz, 1H), 7.84 (d, *J* = 7.8 Hz, 1H), 7.78 (d, *J* = 8.0 Hz, 1H), 7.57 (t, *J* = 7.4 Hz, 2H), 7.53 – 7.46 (m, 3H), 7.38 (t, *J* = 7.6 Hz, 1H), 7.33 (d, *J* = 8.1 Hz, 1H), 7.27 – 7.23 (m, 1H), 7.20 – 7.16 (m, 1H), 7.10 (t, *J* = 7.4 Hz, 1H), 7.00 – 6.92 (m, 3H), 6.82 (ddd, *J* = 8.3, 6.7, 1.3 Hz, 1H), 6.70 (ddd, *J* = 8.3, 6.8, 1.3 Hz, 1H), 6.64 (td, *J* = 7.1, 1.9 Hz, 1H), 6.35 (s, 1H), 6.07 (s, 1H), 5.94 – 5.85 (m, 2H), 4.53 – 4.35 (m, 4H), 1.14 (s, 9H), 0.98 (s, 9H); **^{13}C NMR** (101 MHz, $CDCl_3$) δ 214.86, 161.16, 153.30, 152.55, 151.50, 135.92, 135.17, 133.89, 133.42, 132.72, 132.34, 132.24, 132.06, 128.66, 128.46, 128.43, 128.04, 126.28, 126.22, 126.20, 126.07, 125.99, 125.51, 125.33, 125.29, 124.90, 124.86, 124.02, 123.45, 120.42, 119.81, 65.13, 64.49, 50.32, 50.08, 36.61, 36.20, 28.85, 28.69; **HRMS** (ESI+): $C_{45}H_{46}AuClN_2Na$ $[M+Na]^+$ found 869.2910**,** requires 869.2913.

2.4.5 Catalyst Recycling Procedure

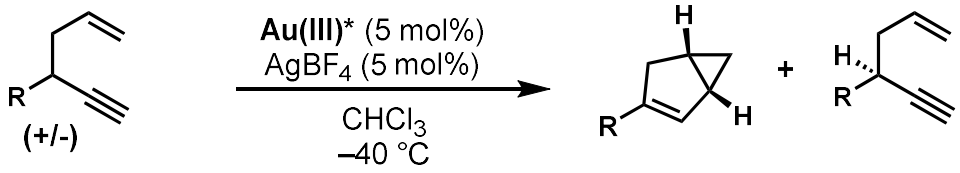

Scheme 2.18 Catalyst recycling procedure.

To a 1 dram vial was added the gold(III) catalyst (0.05 equiv), $AgBF_4$ (0.05 equiv), and $CHCl_3$ (0.3 M). The vial was capped and sonicated for 5 minutes. The reaction mixture was passed through a glass fiber filter and collected in a 1 dram vial. The vial was then cooled to −40 °C and the 1,5-enyne (1 equiv) was added. The reaction mixture was allowed to stir for 3 h and quenched with the addition of NH_4Cl. S factor was determined via NMR of the quenched reaction mixture. The starting material and product were then isolated by column chromatography using 100% hexanes. Catalyst was then isolated by switching the solvent to 100% DCM. The fractions containing catalyst were concentrated under reduced pressure to give pure catalyst. This isolated catalyst was then re-subjected to the procedure described here.

Run	Catalyst Used (mg)	s factor	Catalyst Recovered (mg)
1	24.4	22	22.6
2	22.6	24	22.0
3	22.0	23	21.0

Table 2.6 Results from catalyst recycling.

2.4.6 NMR Spectra

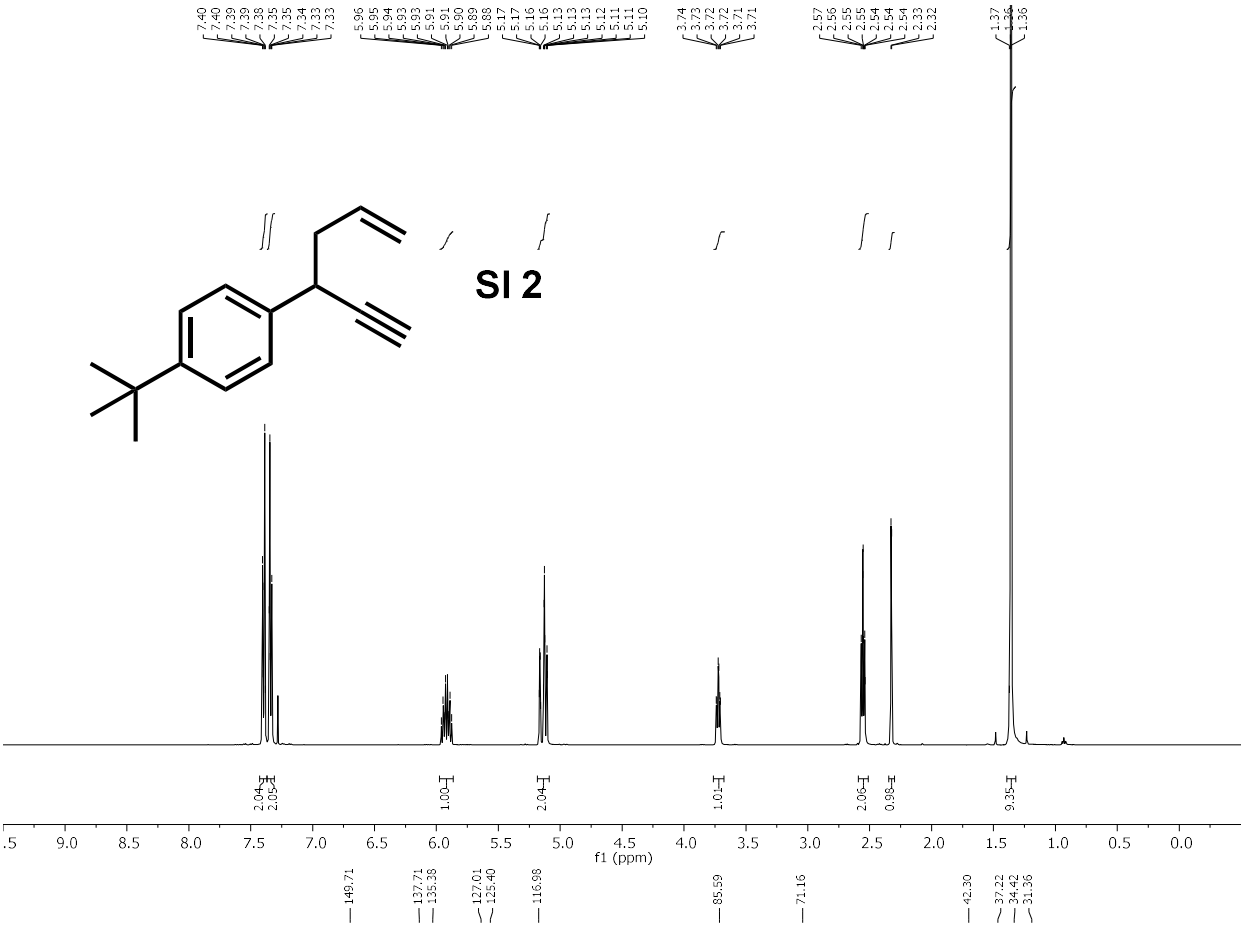
SI 2
f1 (ppm)

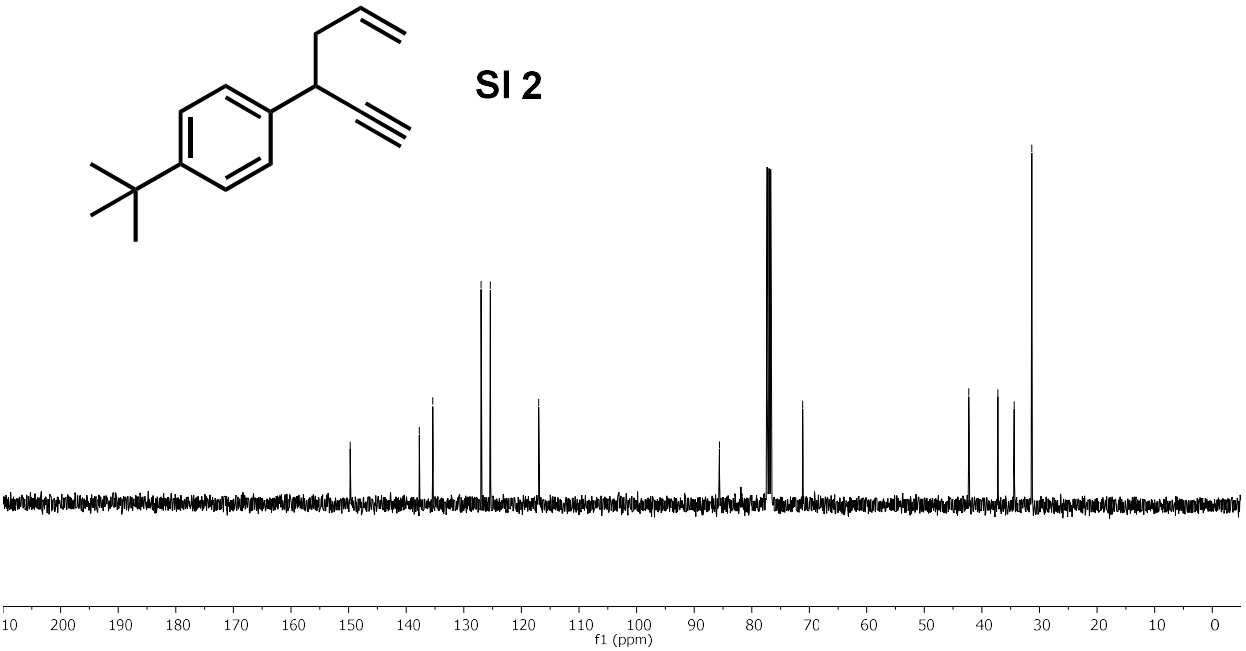
SI 2
f1 (ppm)

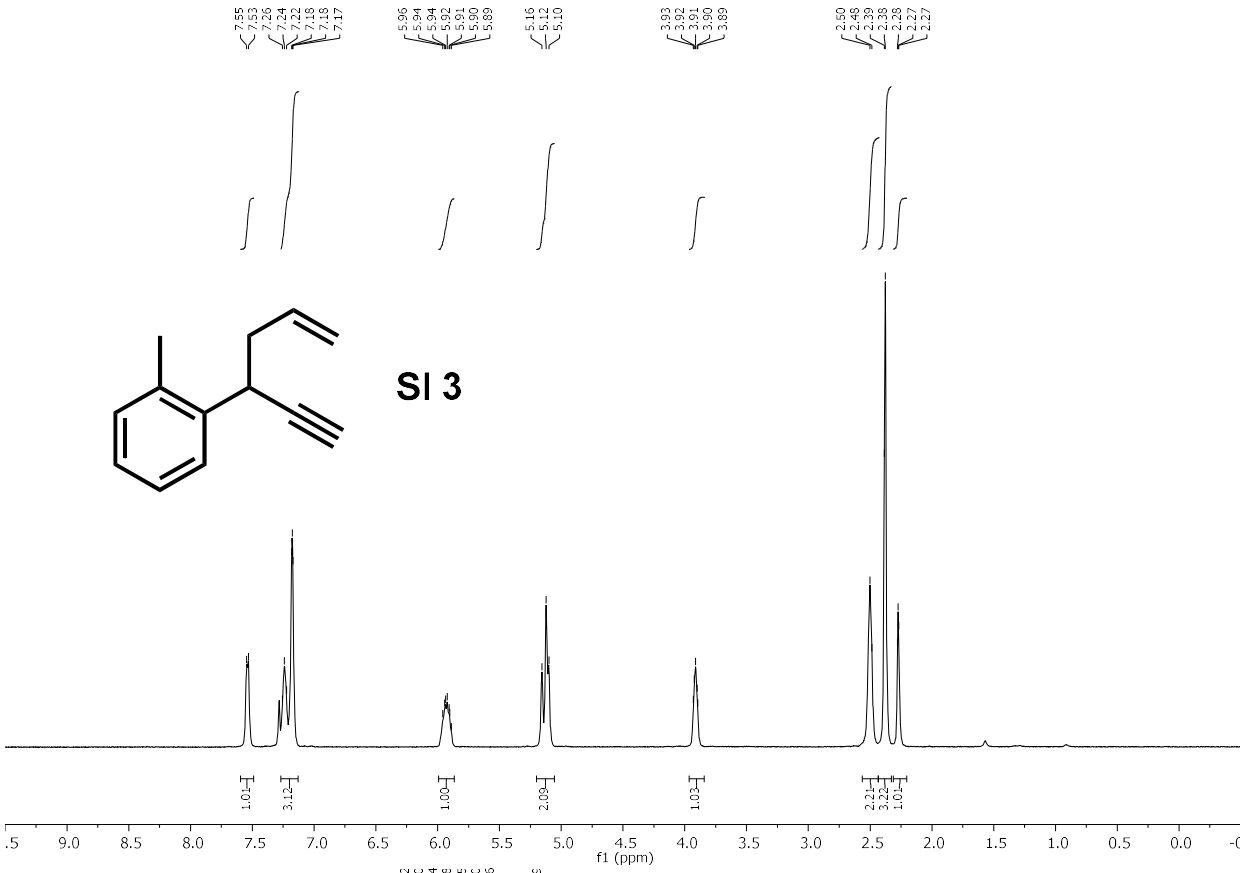
7.55
7.53
7.26
7.24
7.22
7.18
7.18
7.17
5.96
5.94
5.94
5.92
5.91
5.90
5.89
5.16
5.12
5.10
3.93
3.92
3.91
3.90
3.89
2.50
2.48
2.39
2.38
2.28
2.27
2.27
SI 3
1.01
3.12
1.00
2.09
1.03
2.21
3.22
1.01
f1 (ppm)

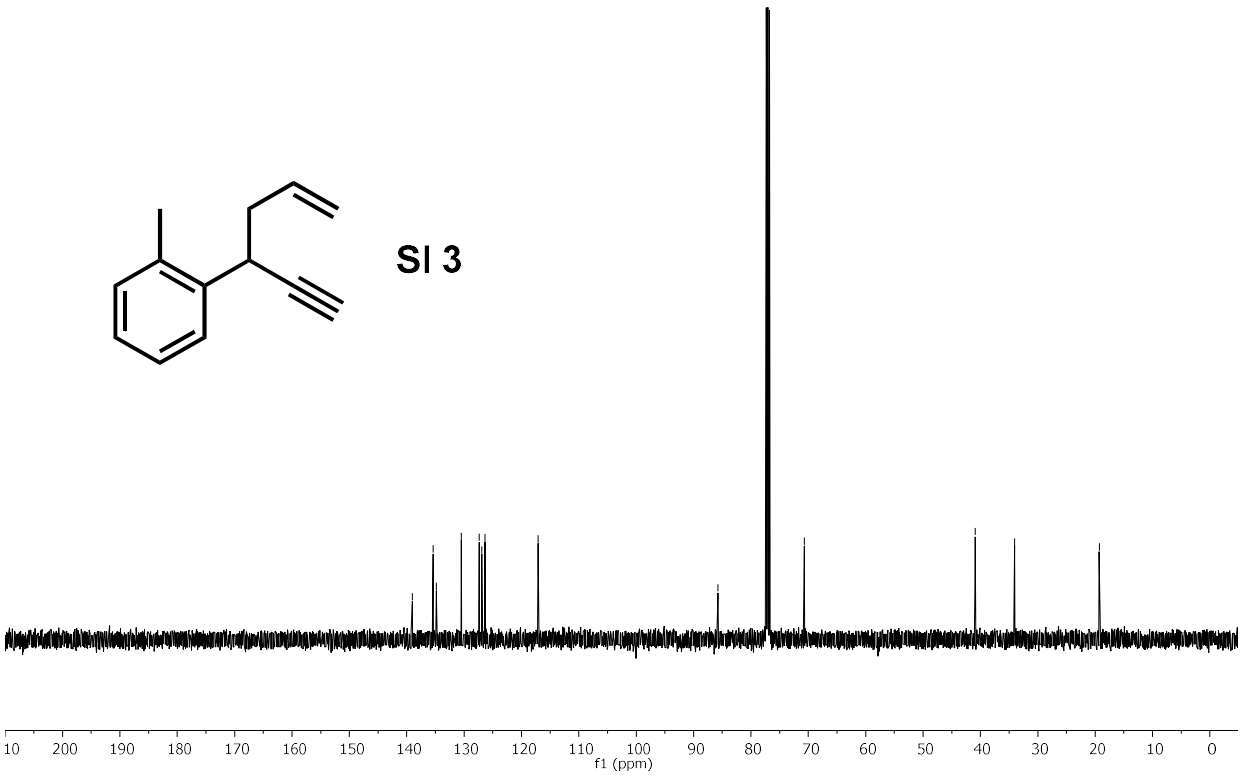
139.02
135.46
134.84
130.48
127.35
126.90
126.36
117.08
85.73
70.70
40.93
34.06
19.29
SI 3
f1 (ppm)

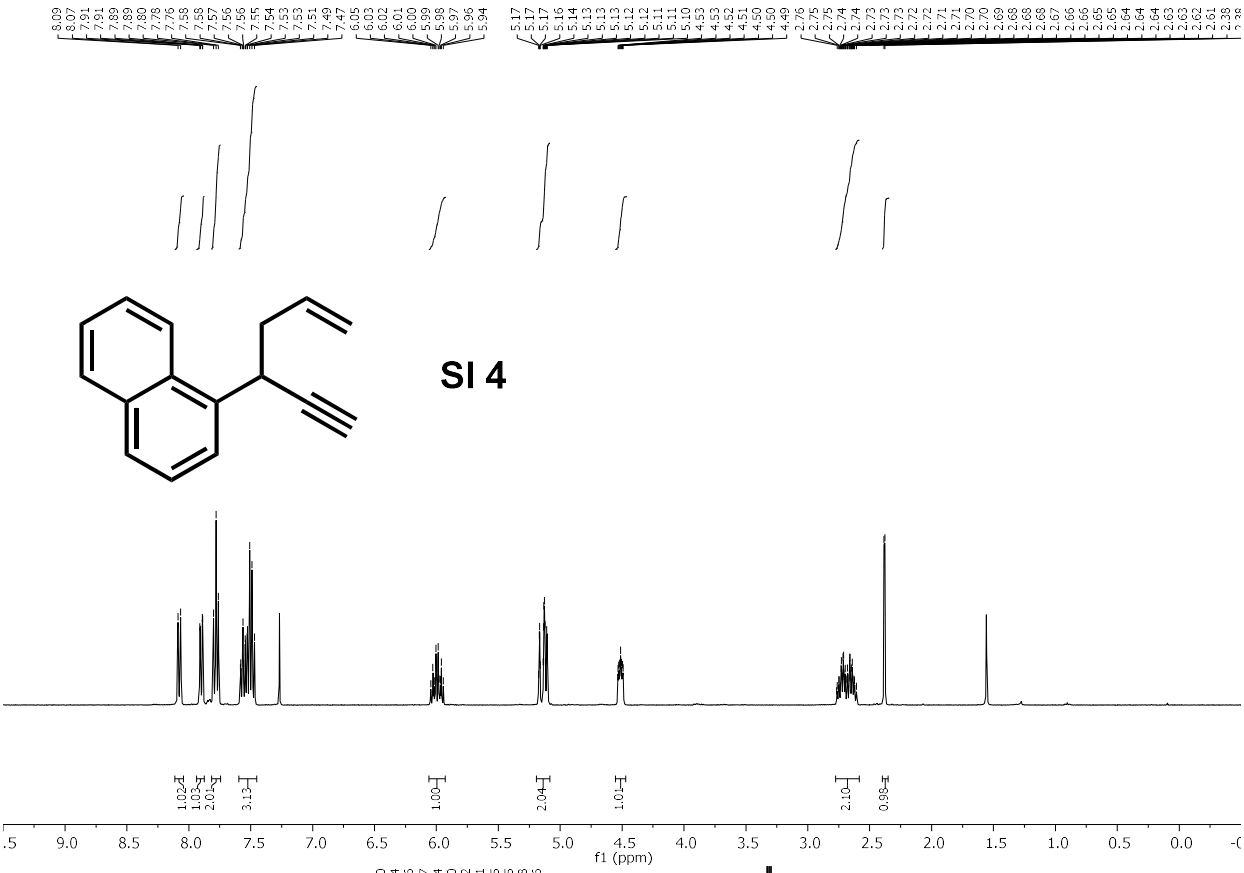
SI 4
f1 (ppm)

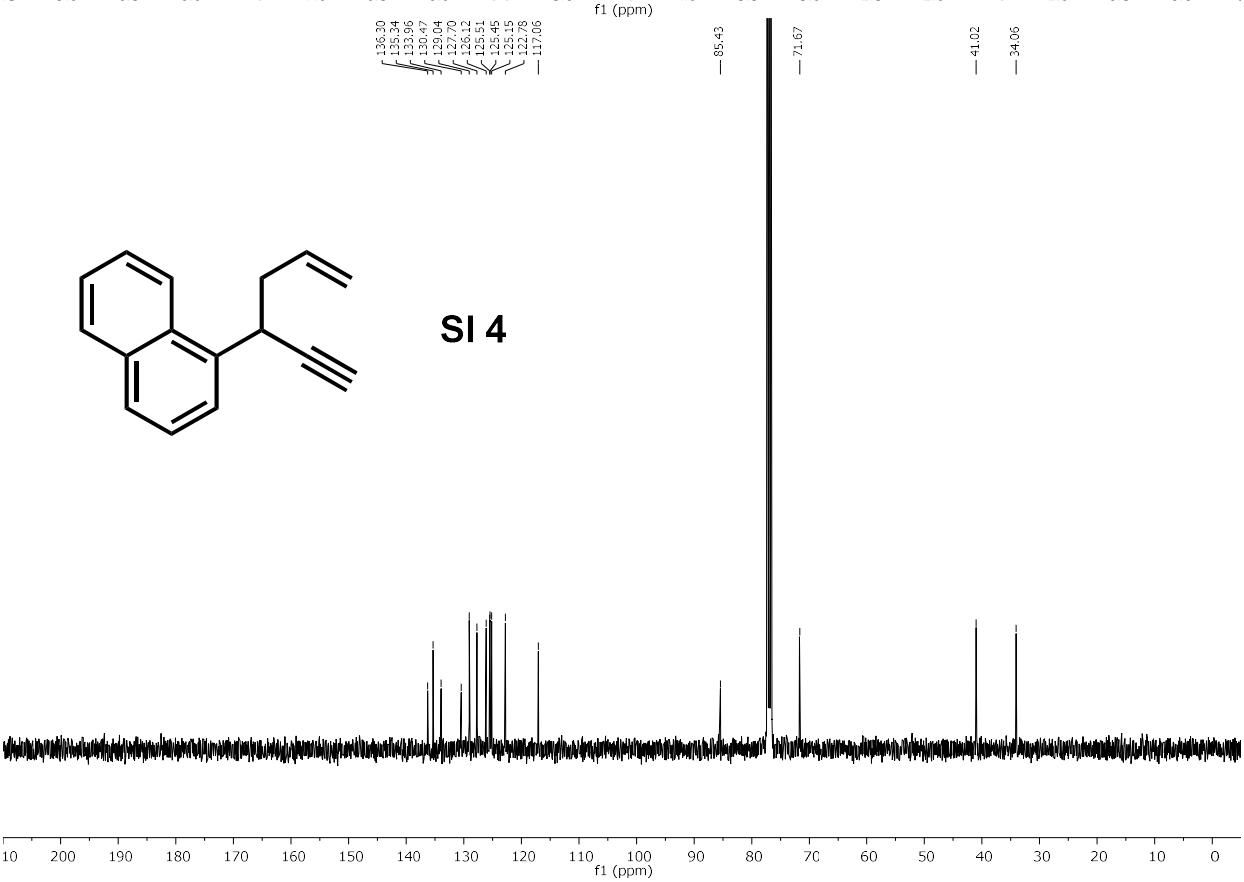
SI 4
f1 (ppm)

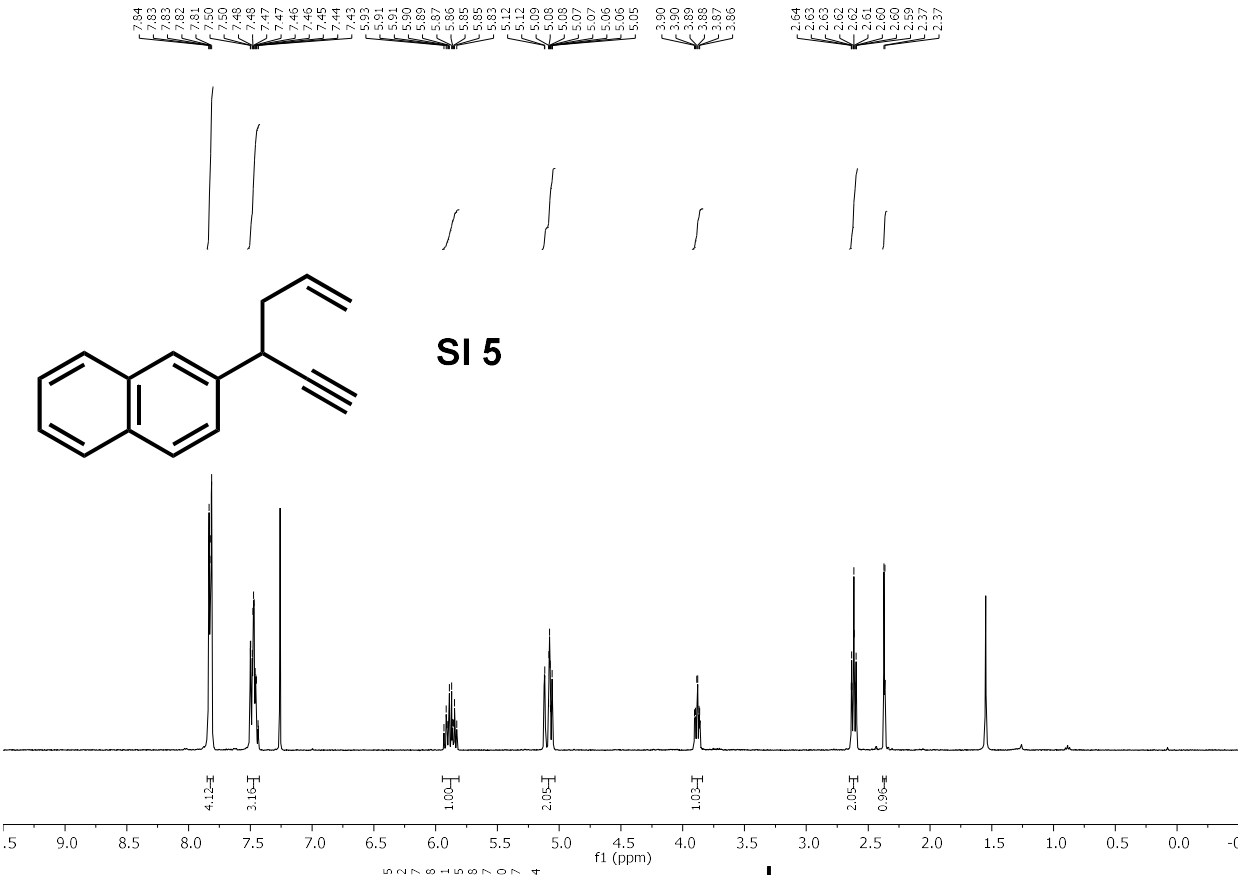
SI 5
f1 (ppm)

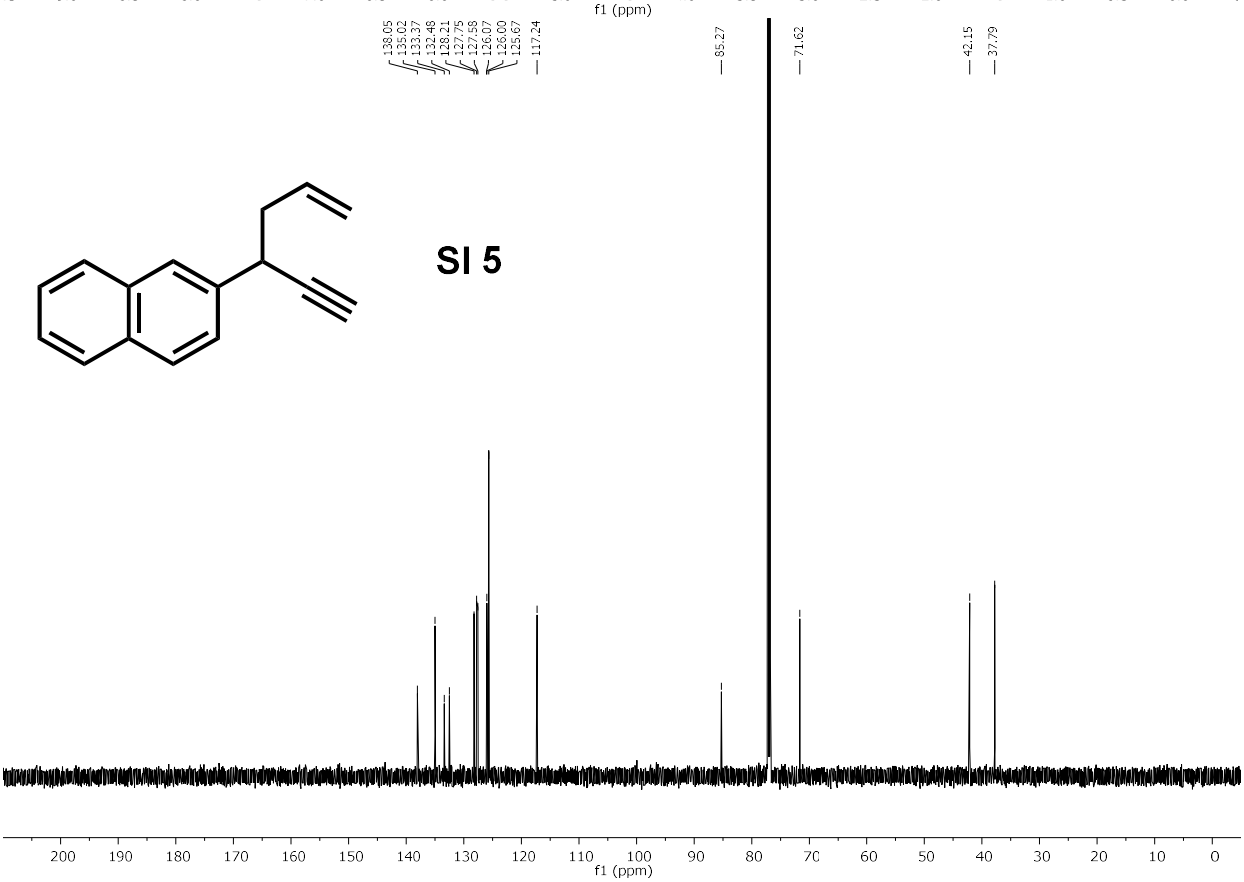
SI 5
f1 (ppm)

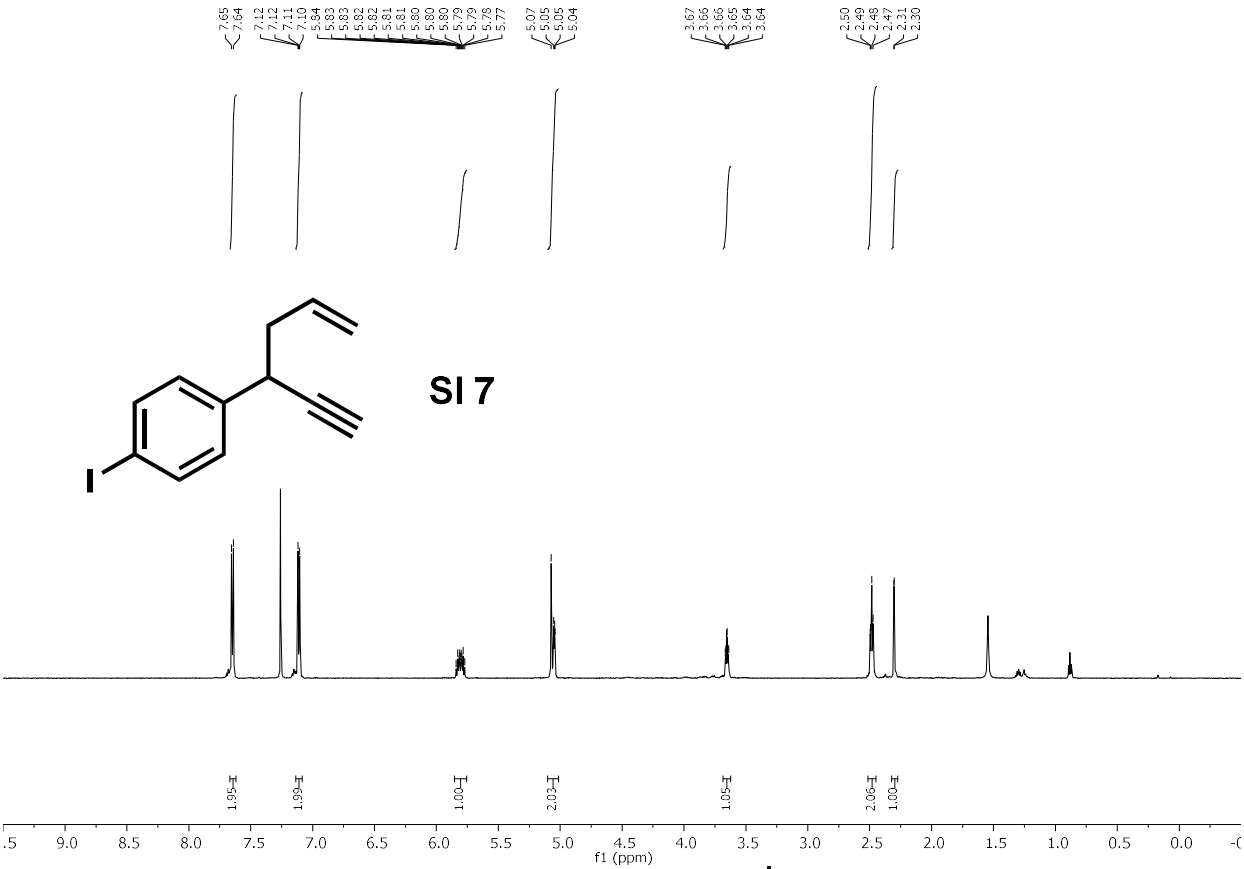
7.65
7.64
7.12
7.12
7.11
7.10
5.84
5.83
5.82
5.82
5.81
5.81
5.80
5.80
5.80
5.79
5.79
5.78
5.77
5.07
5.05
5.05
5.04
3.67
3.66
3.66
3.65
3.64
3.64
2.50
2.49
2.48
2.47
2.31
2.30
SI 7
I
1.95
1.99
1.00
2.03
1.05
2.06
1.00
f1 (ppm)

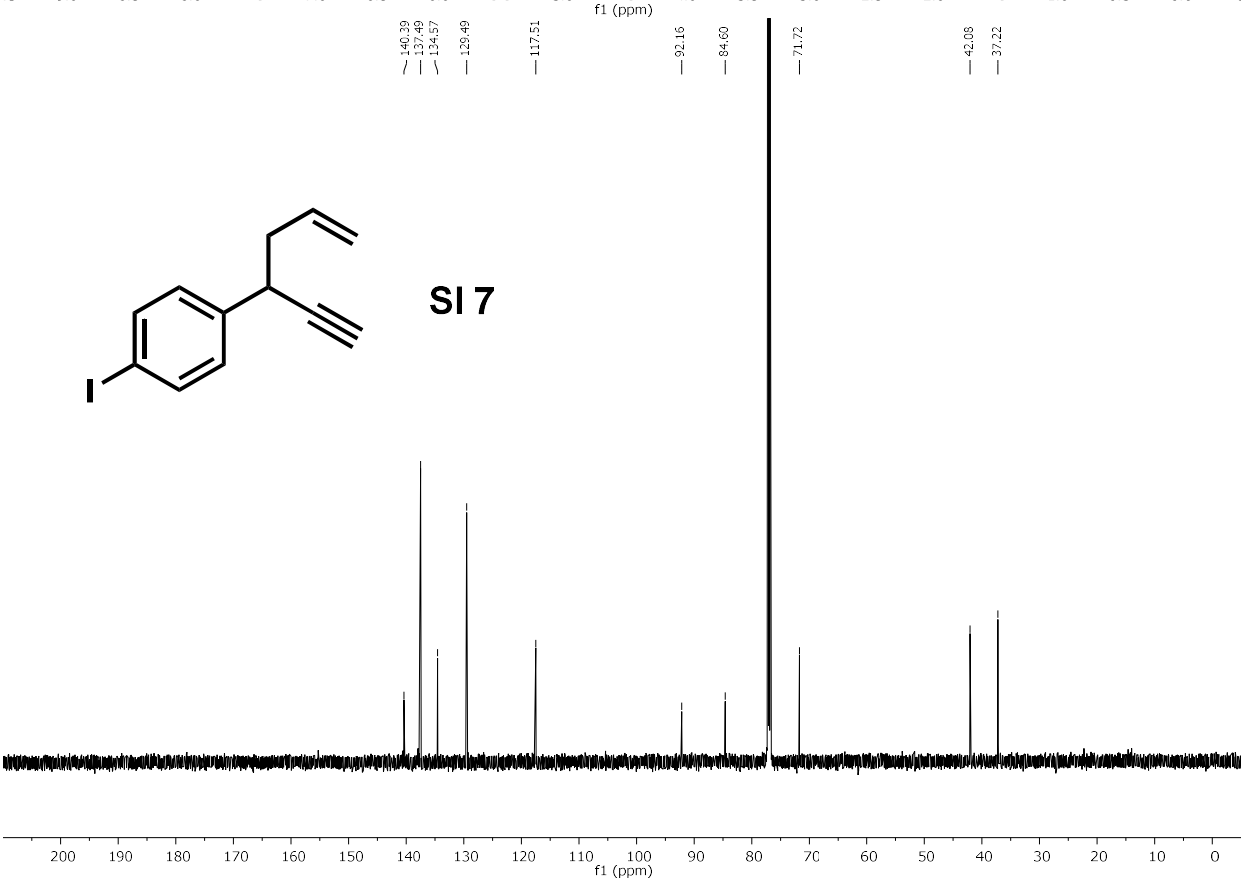
140.39
137.49
134.57
129.49
117.51
92.16
84.60
71.72
42.08
37.22
SI 7
I
f1 (ppm)

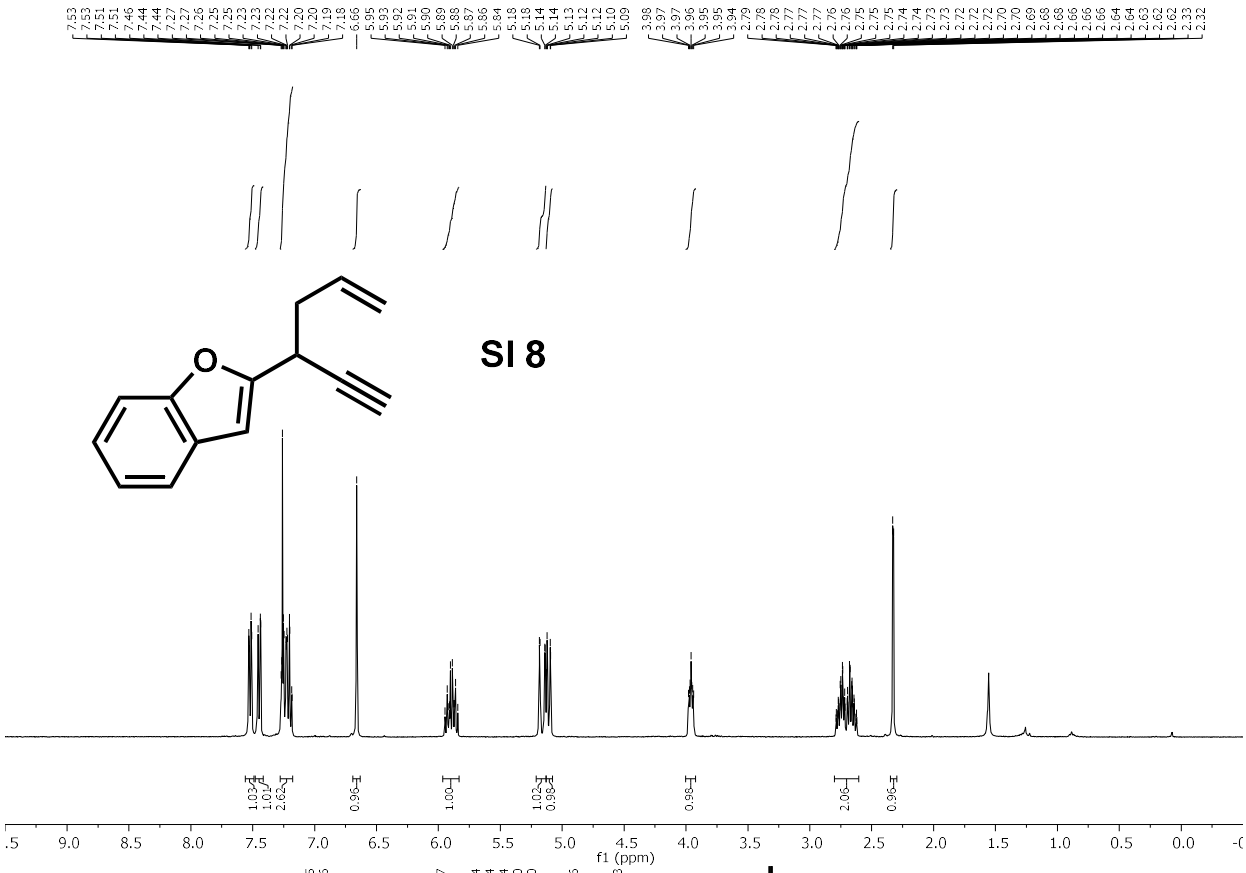
SI 8
f1 (ppm)

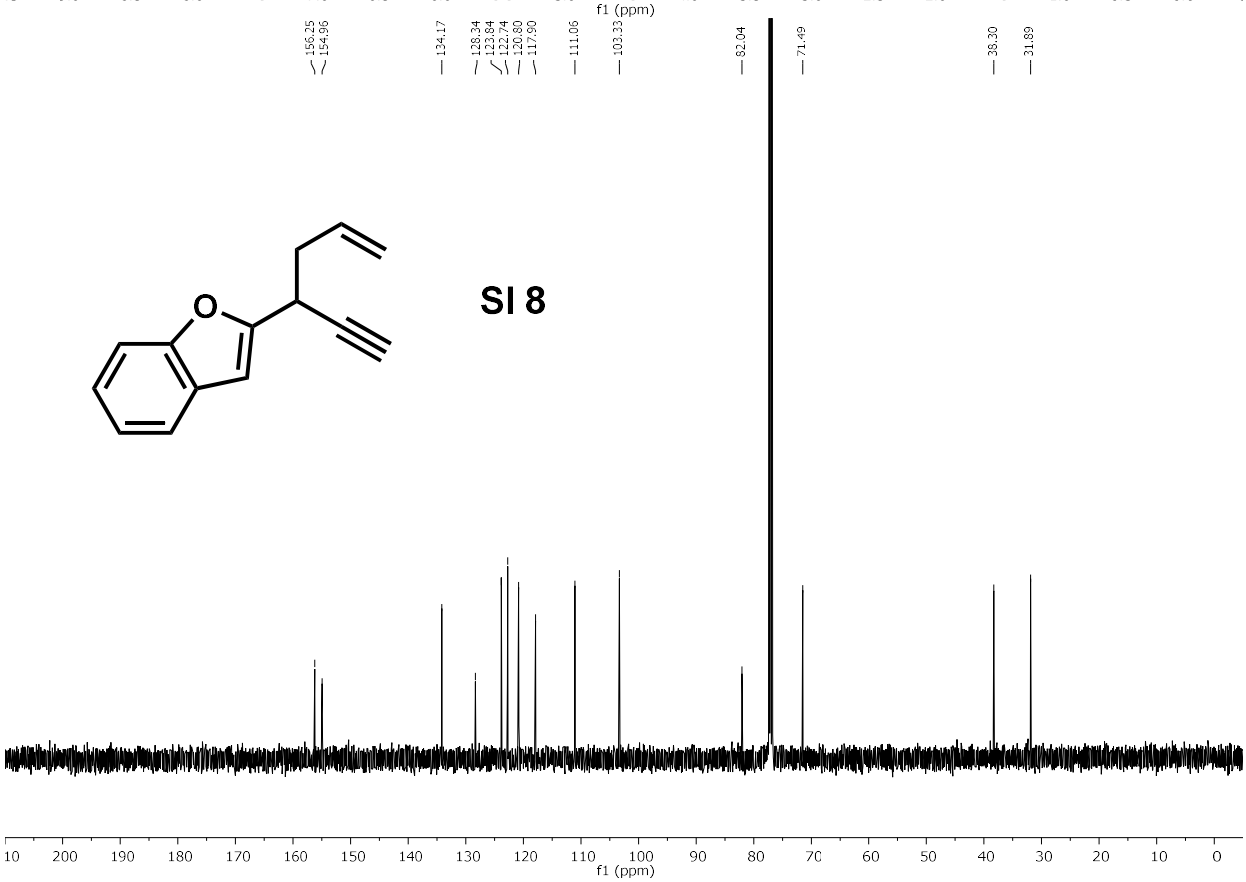
SI 8
f1 (ppm)

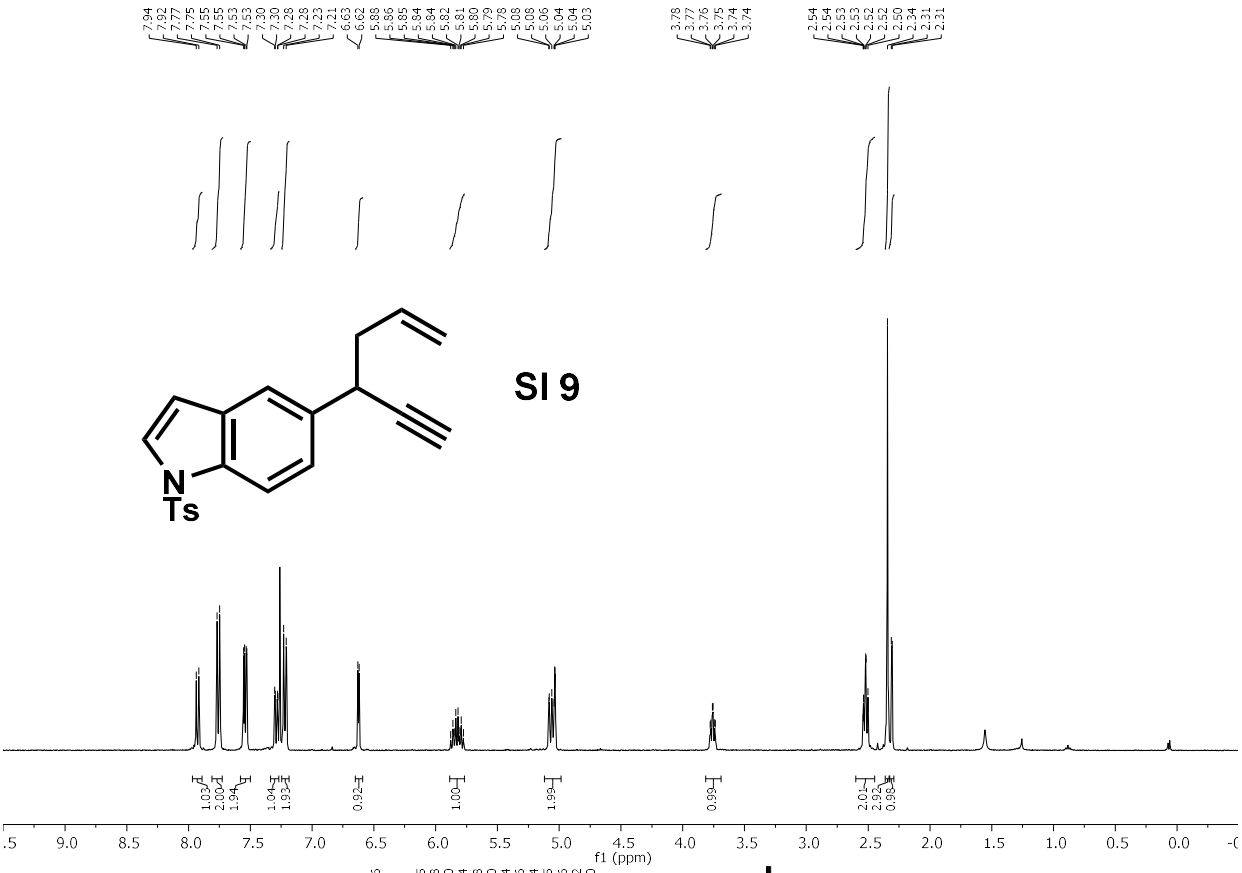
SI 9
N
Ts
f1 (ppm)

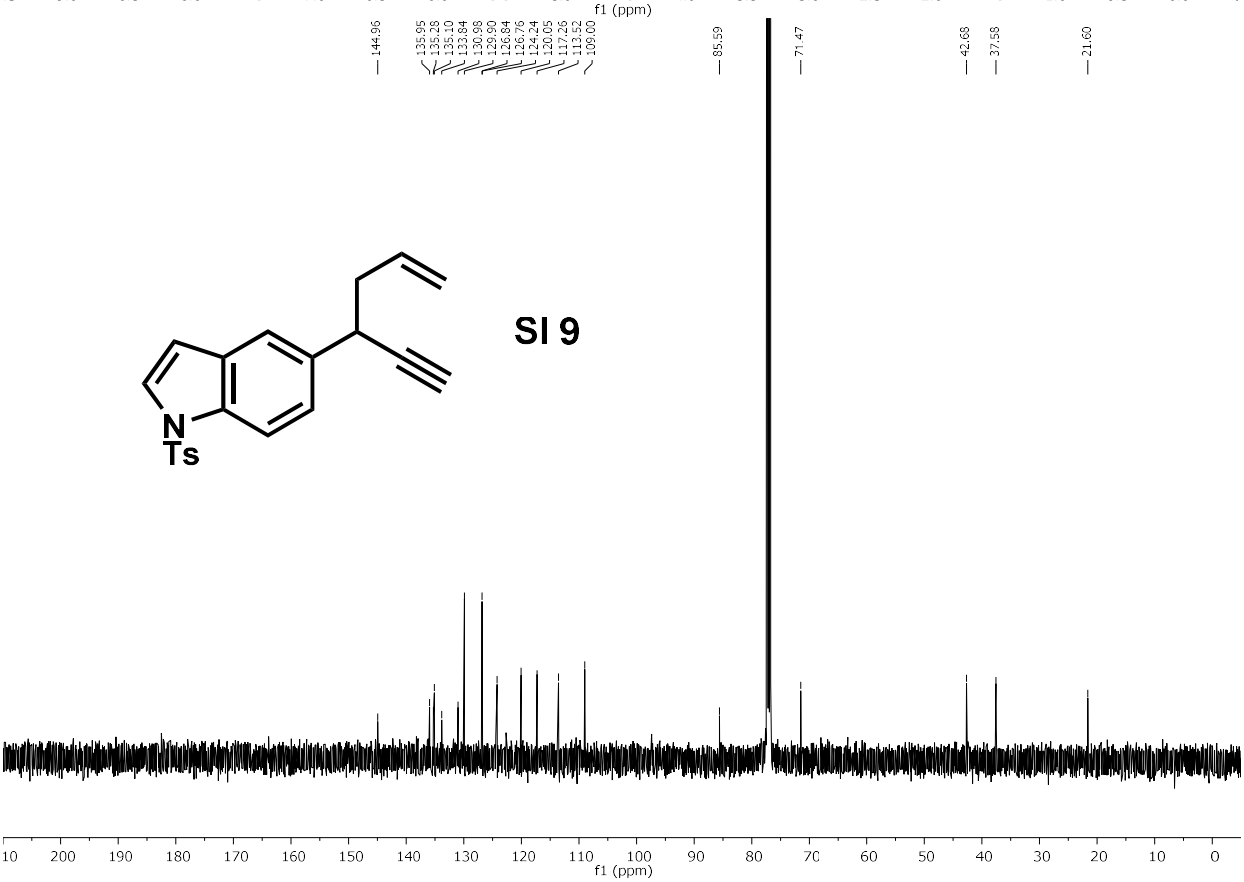
SI 9
N
Ts
f1 (ppm)

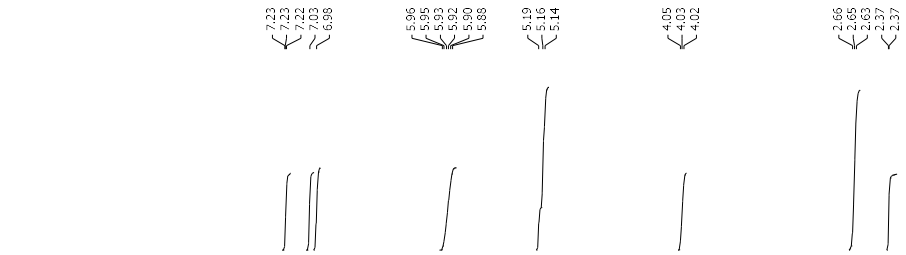
7.23
7.23
7.22
7.03
6.98
5.96
5.95
5.93
5.92
5.90
5.88
5.19
5.16
5.14
4.05
4.03
4.02
2.66
2.65
2.63
2.37
2.37

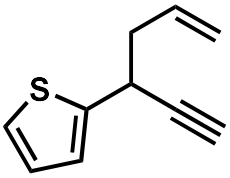

SI 10

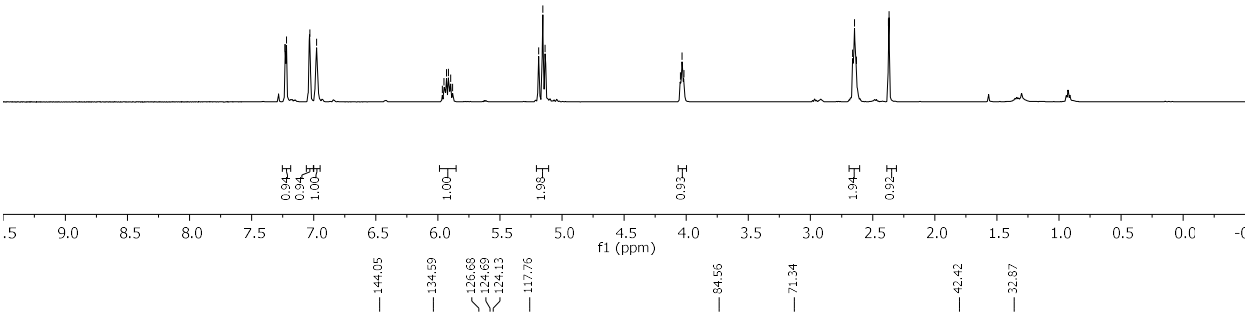
0.94
0.94
1.00
1.00
1.98
0.93
1.94
0.92
f1 (ppm)
144.05
134.59
126.68
124.69
124.13
117.76
64.56
71.34
42.42
32.87

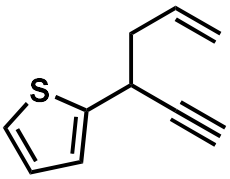

SI 10

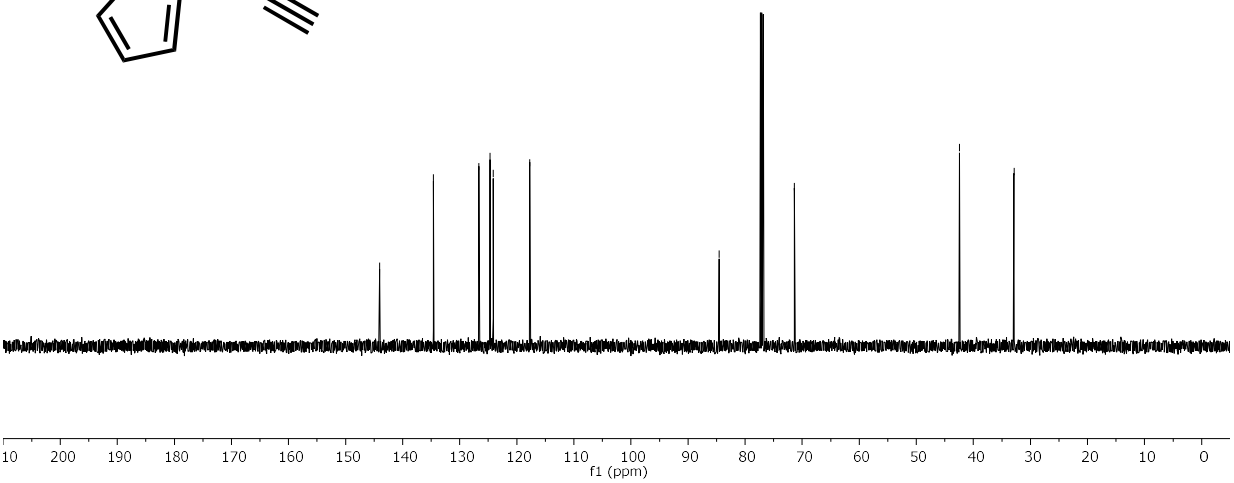
f1 (ppm)

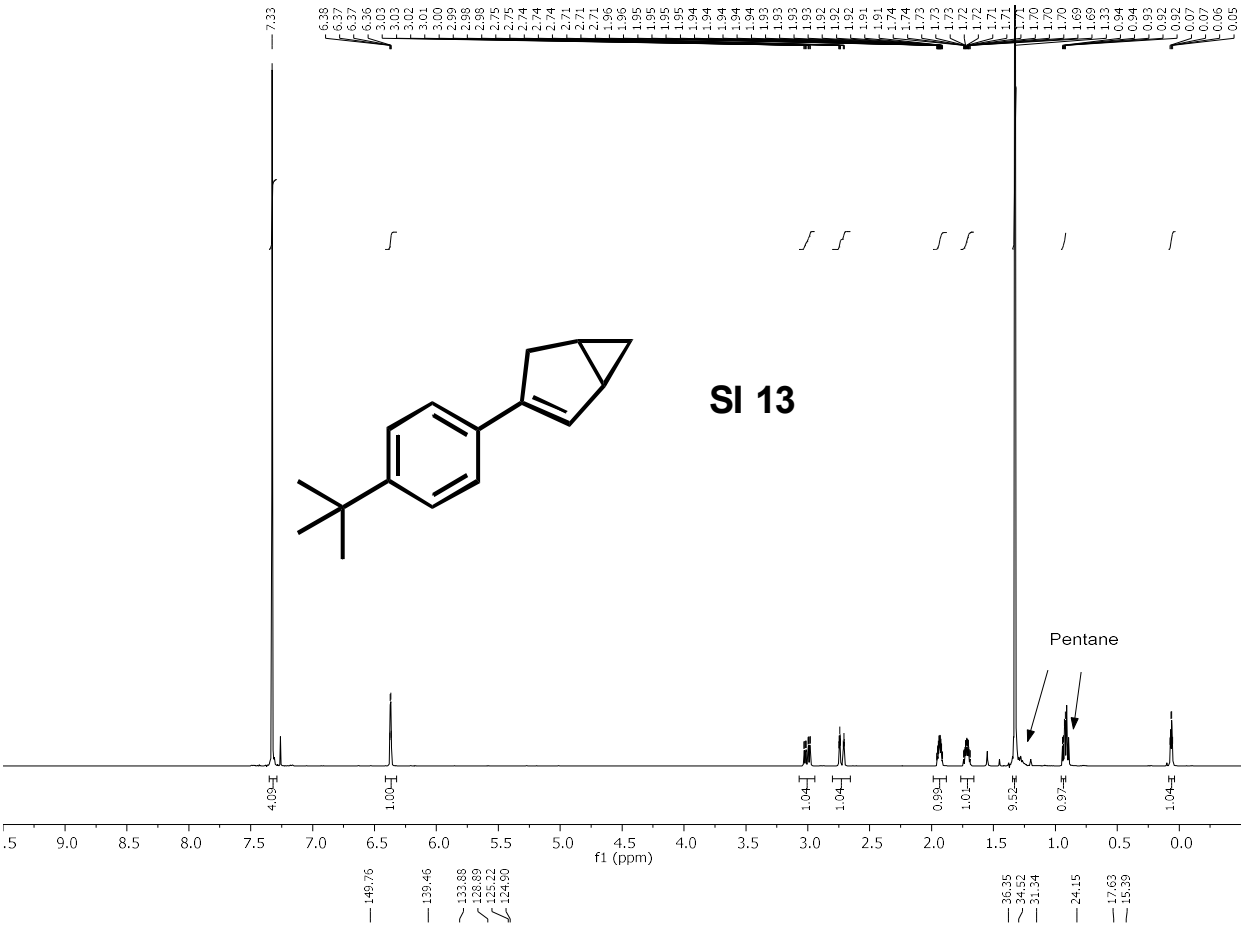
SI 13
Pentane
f1 (ppm)

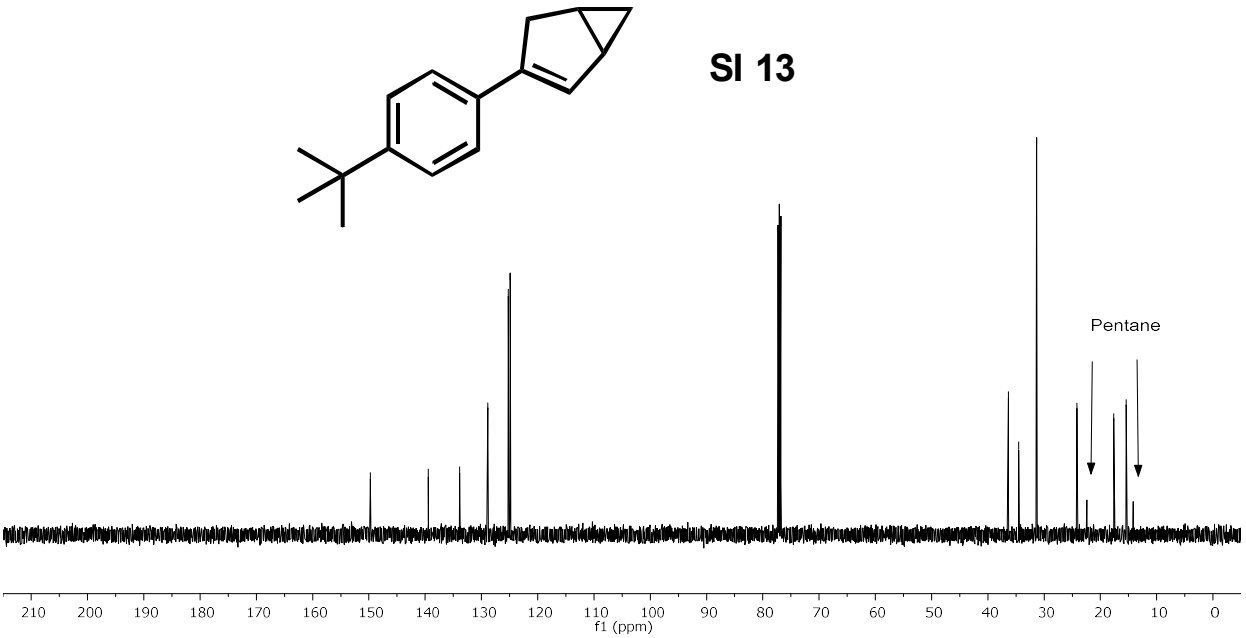
SI 13
Pentane
f1 (ppm)

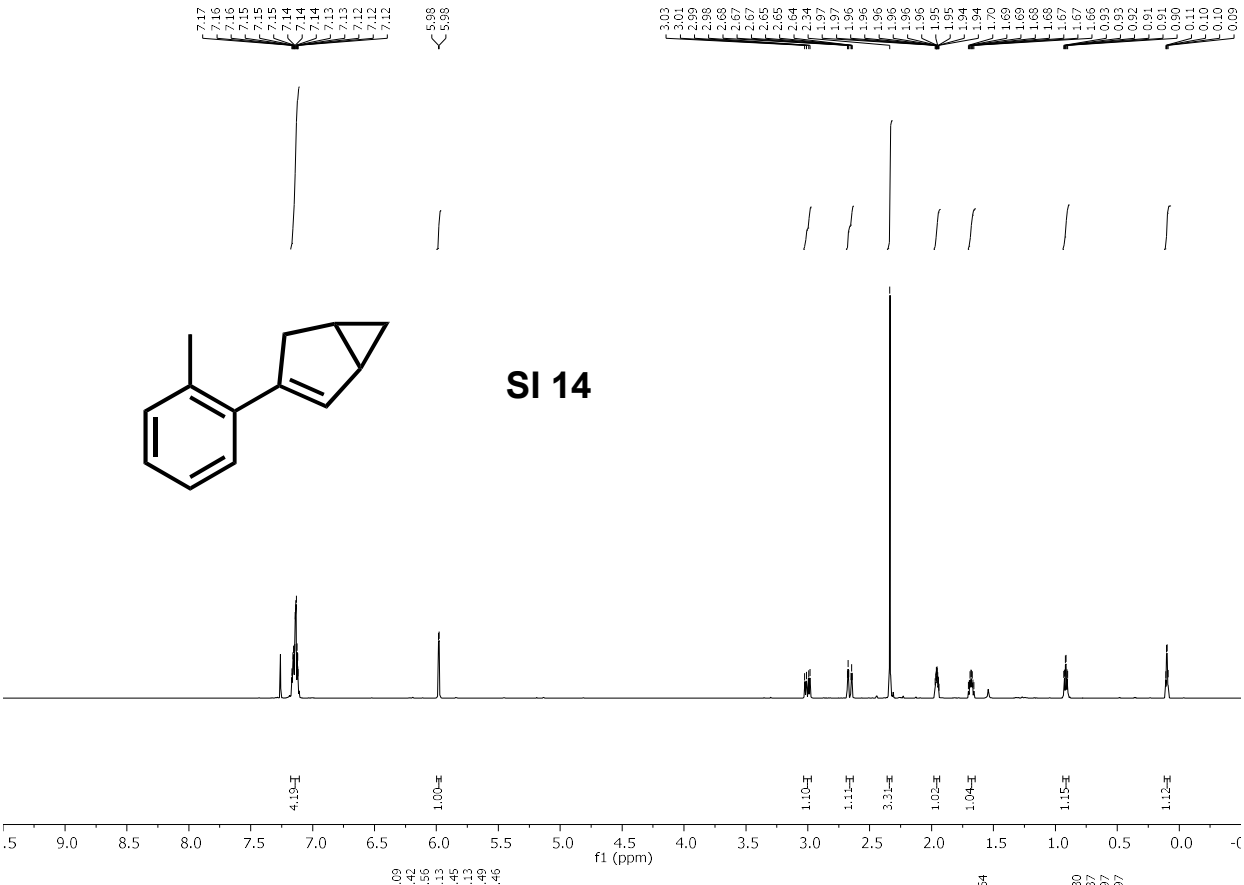
SI 14
f1 (ppm)

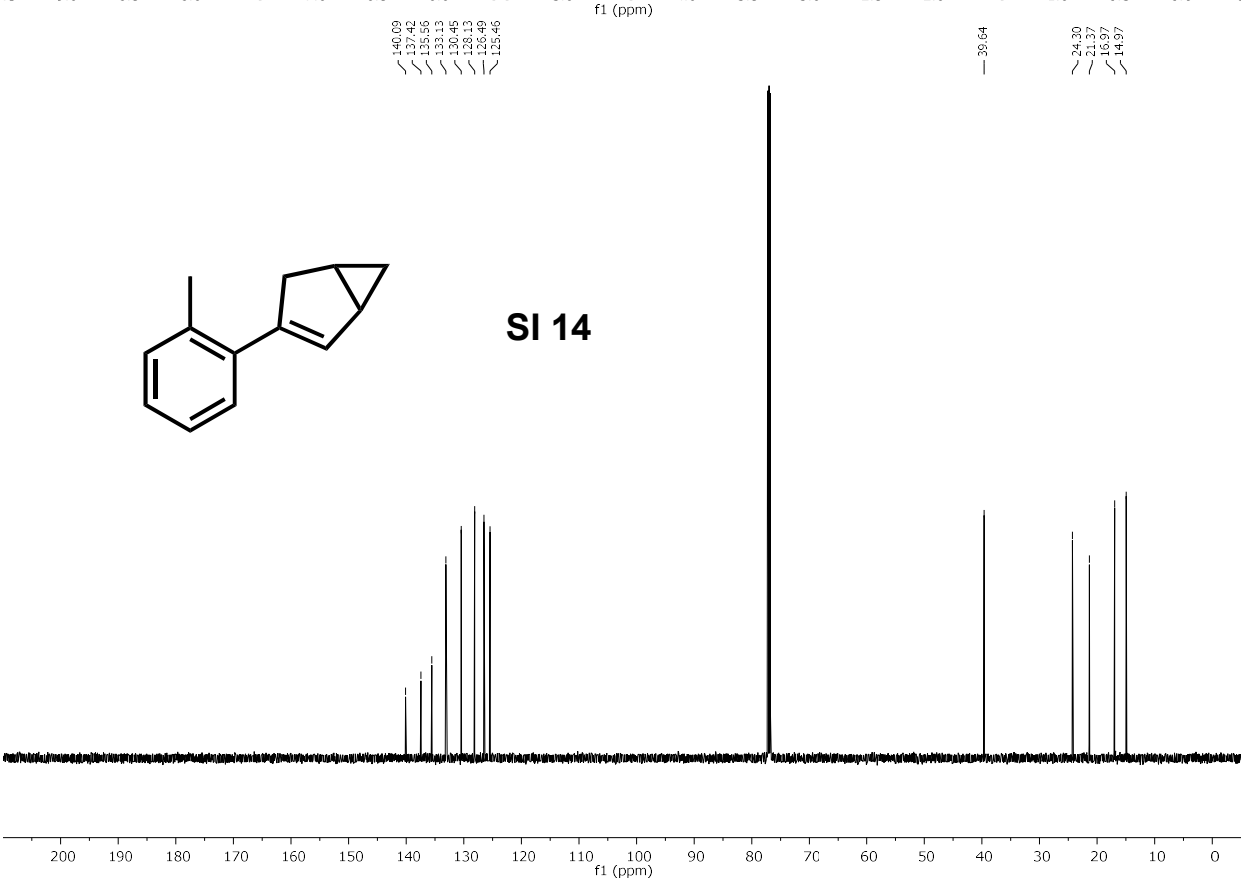
SI 14
f1 (ppm)

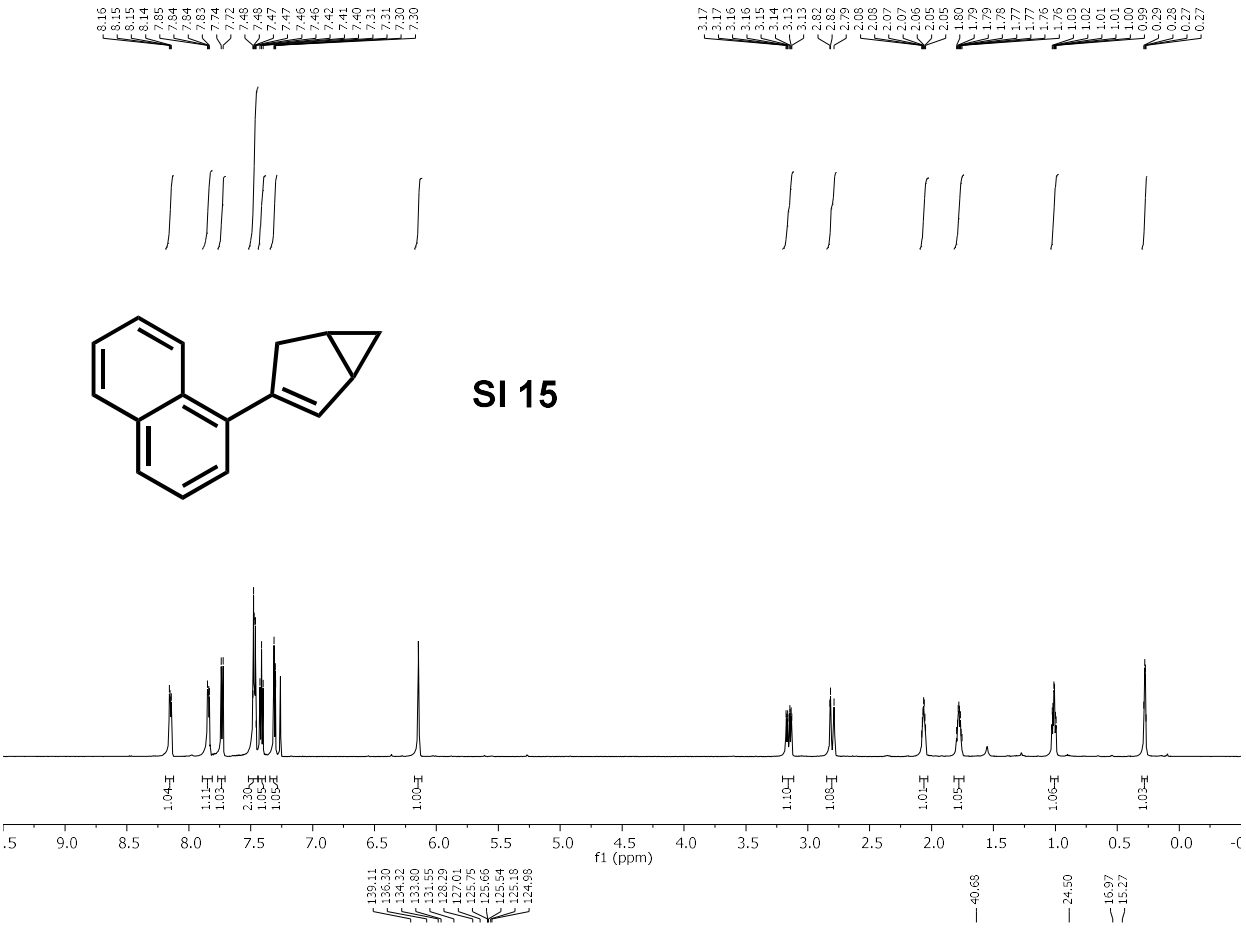
SI 15
f1 (ppm)

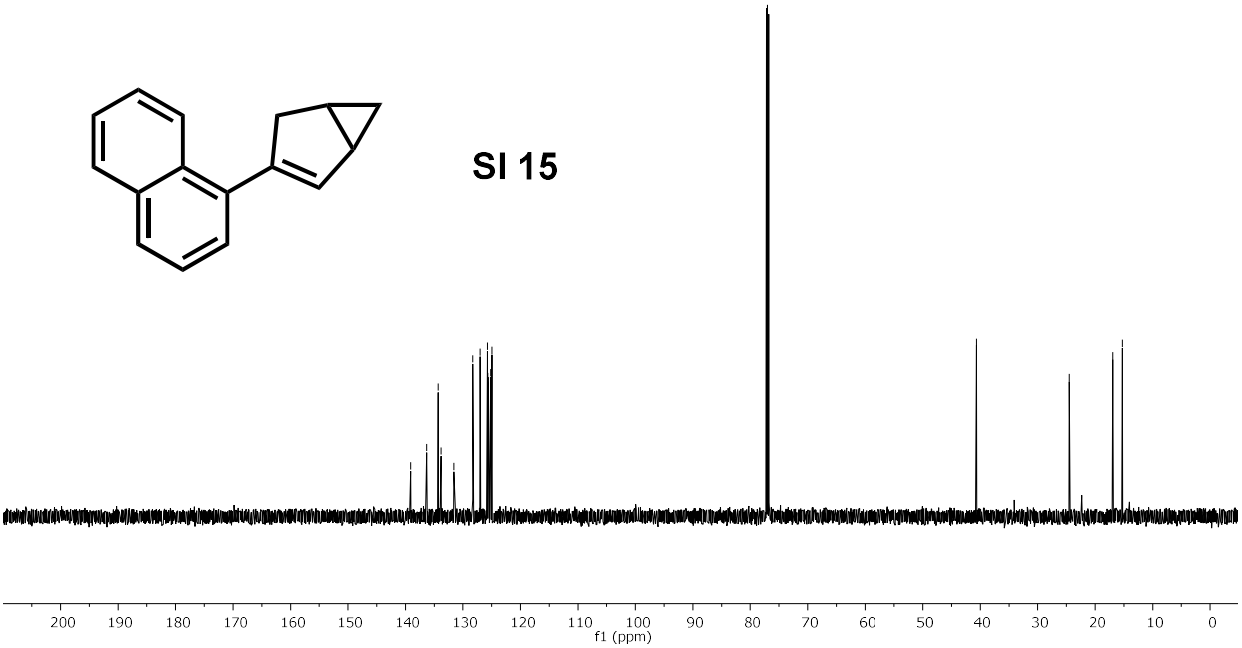
SI 15
f1 (ppm)

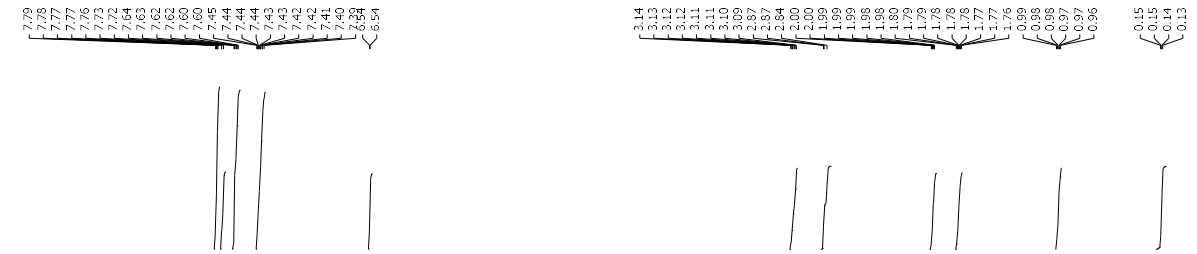

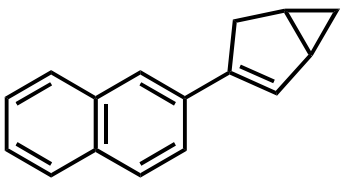

SI 16

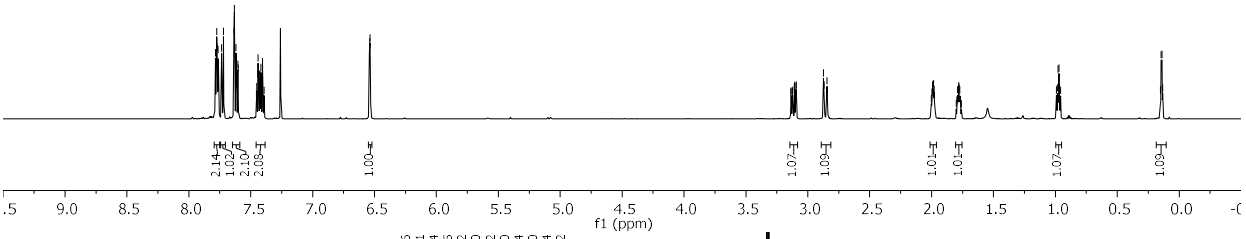

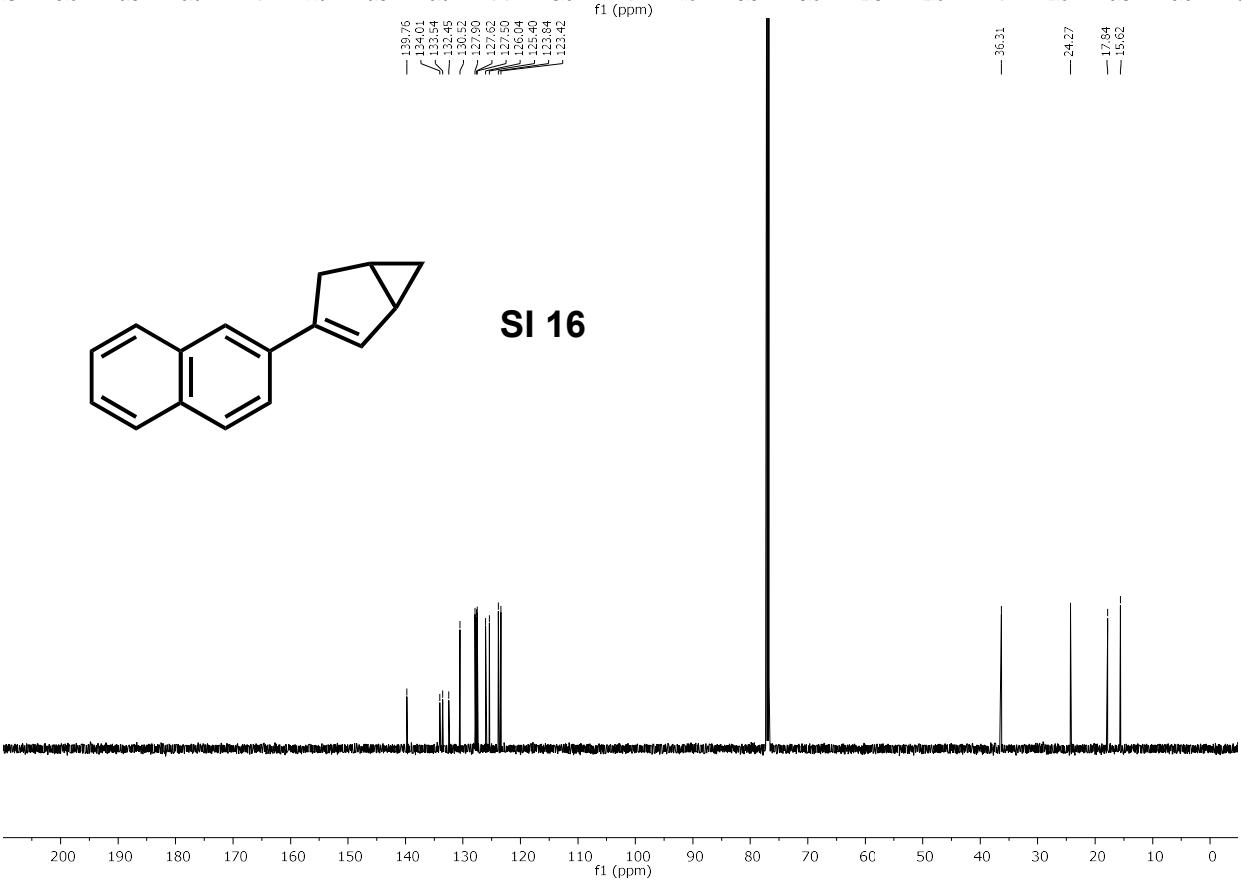

SI 16

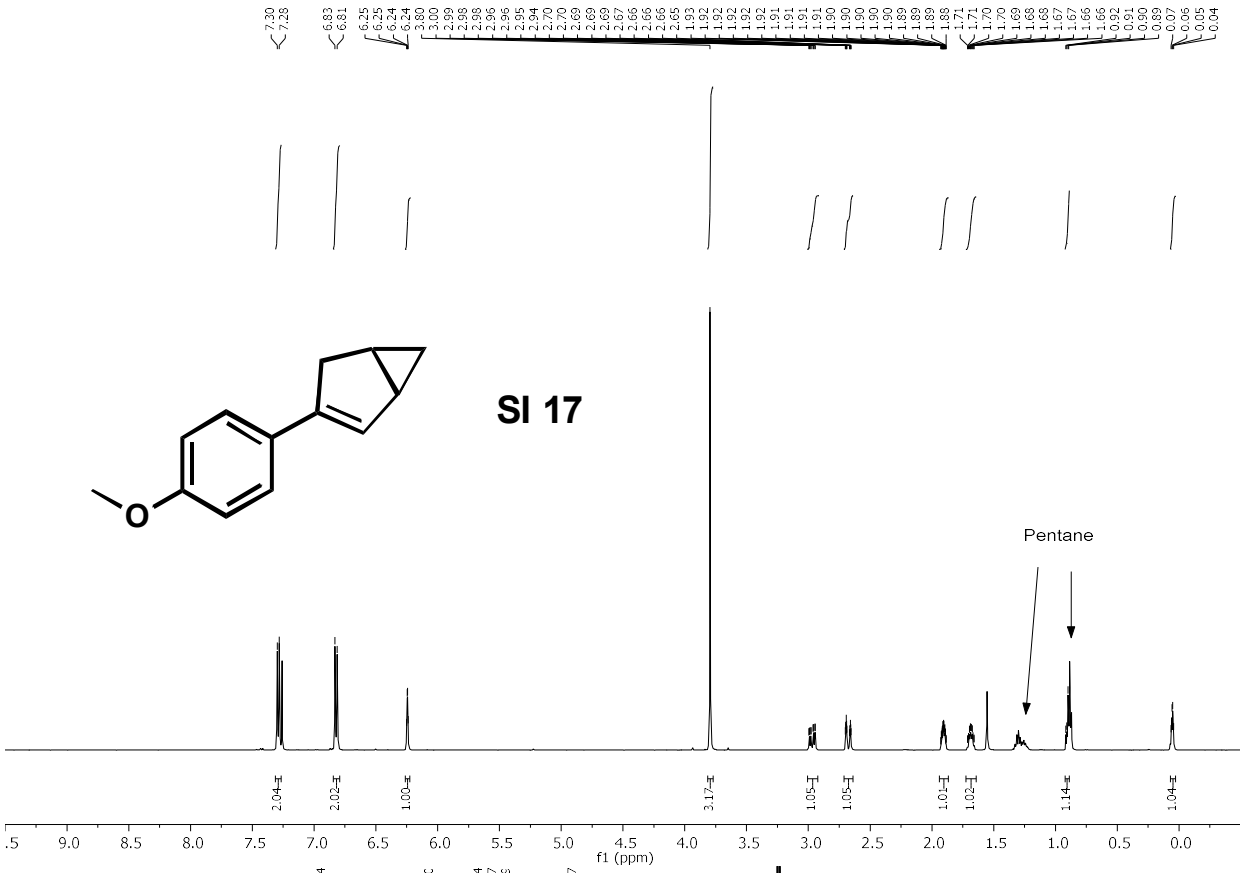
SI 17
Pentane
f1 (ppm)

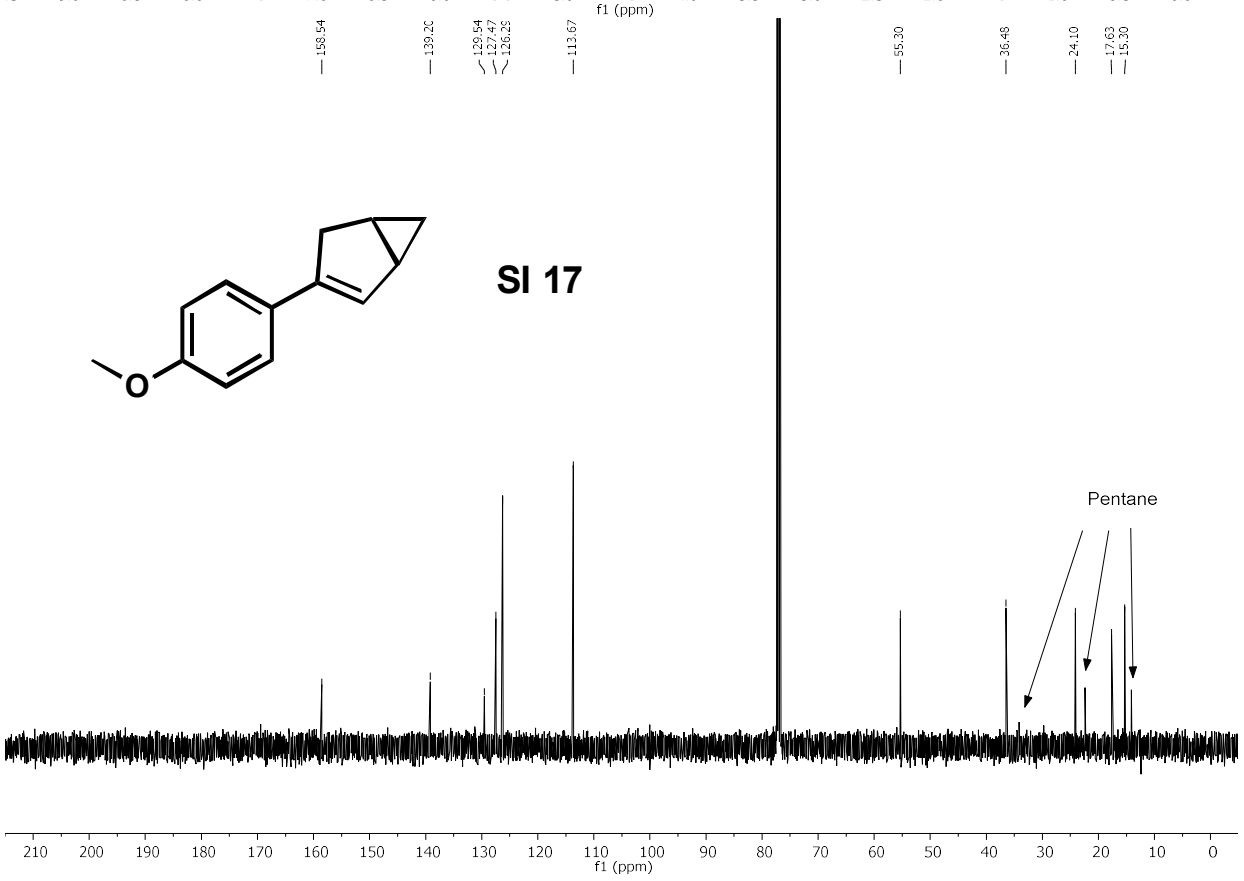
SI 17
Pentane
f1 (ppm)

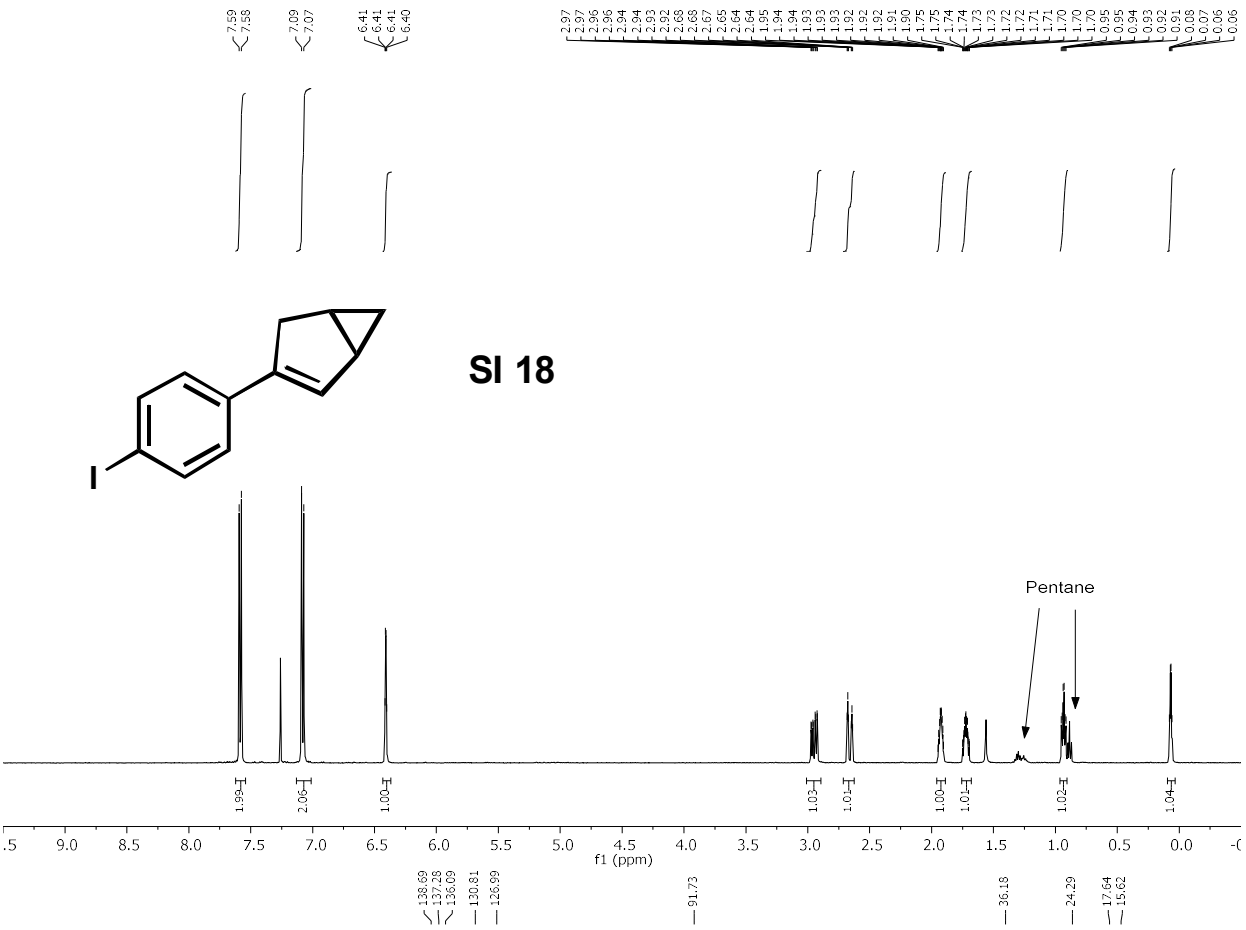
SI 18
Pentane
f1 (ppm)

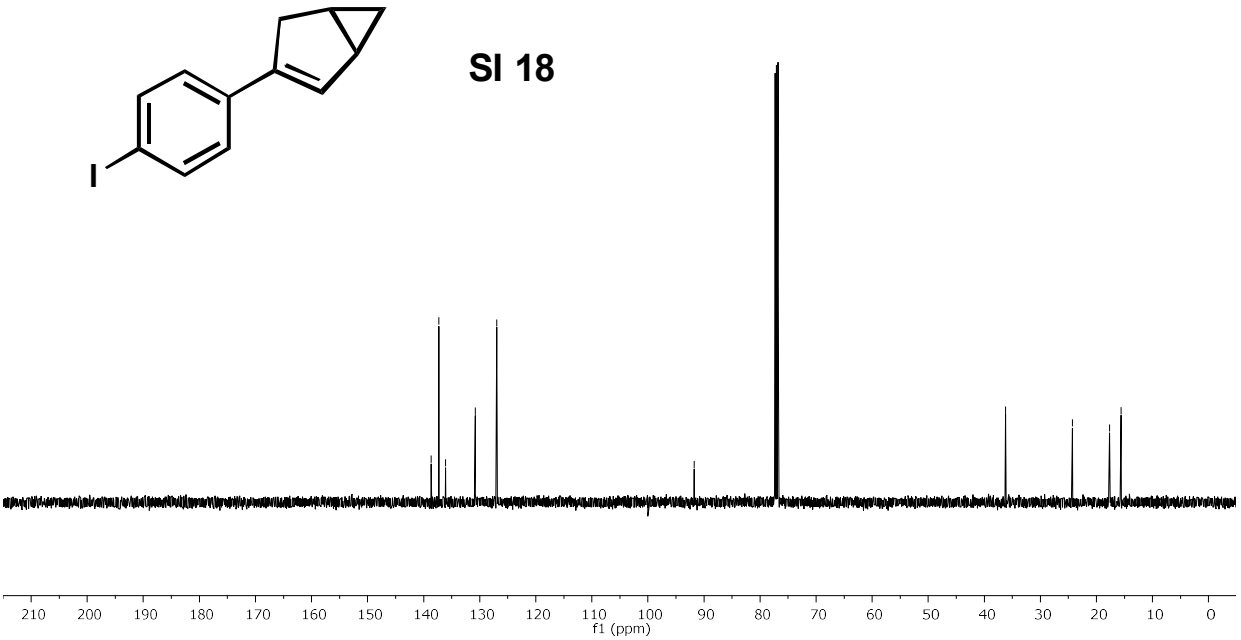
SI 18
f1 (ppm)

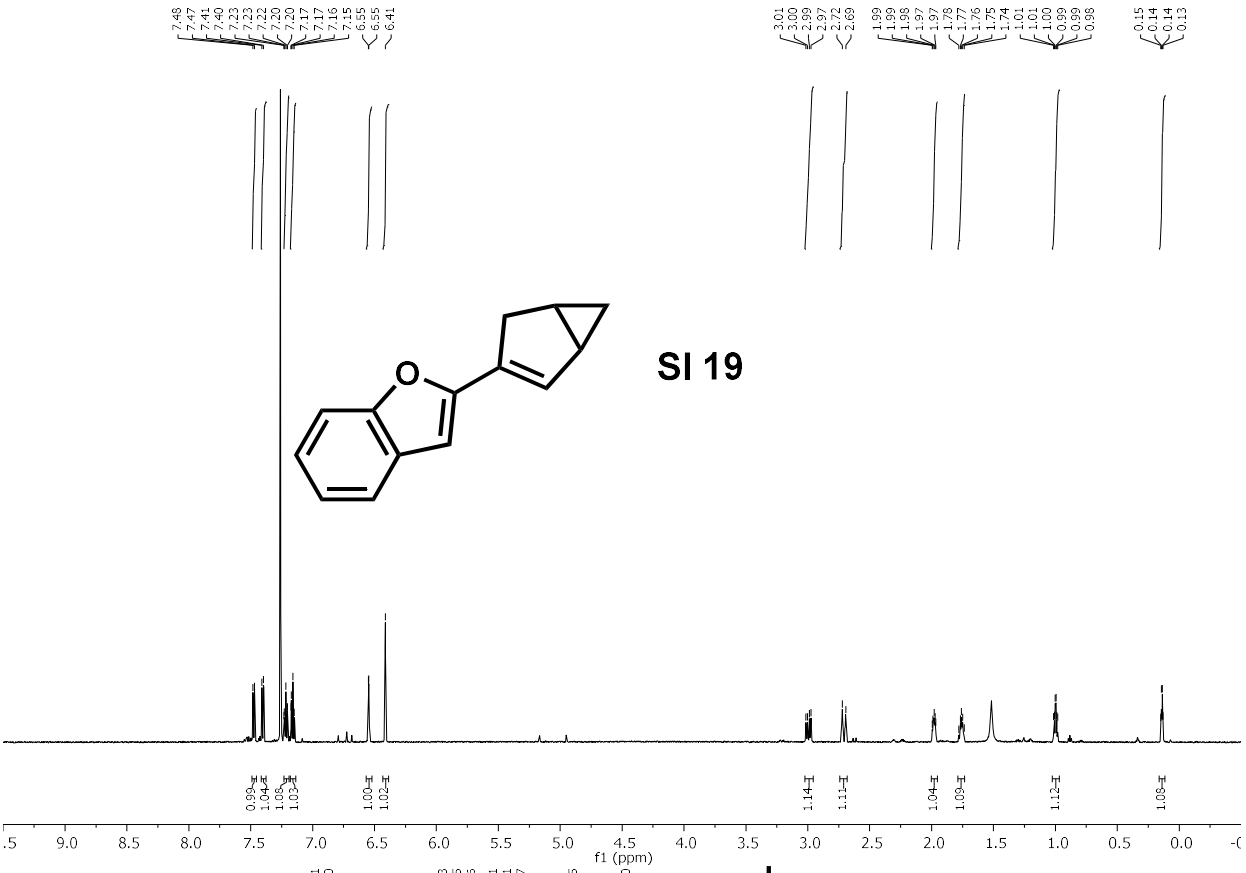
SI 19
f1 (ppm)

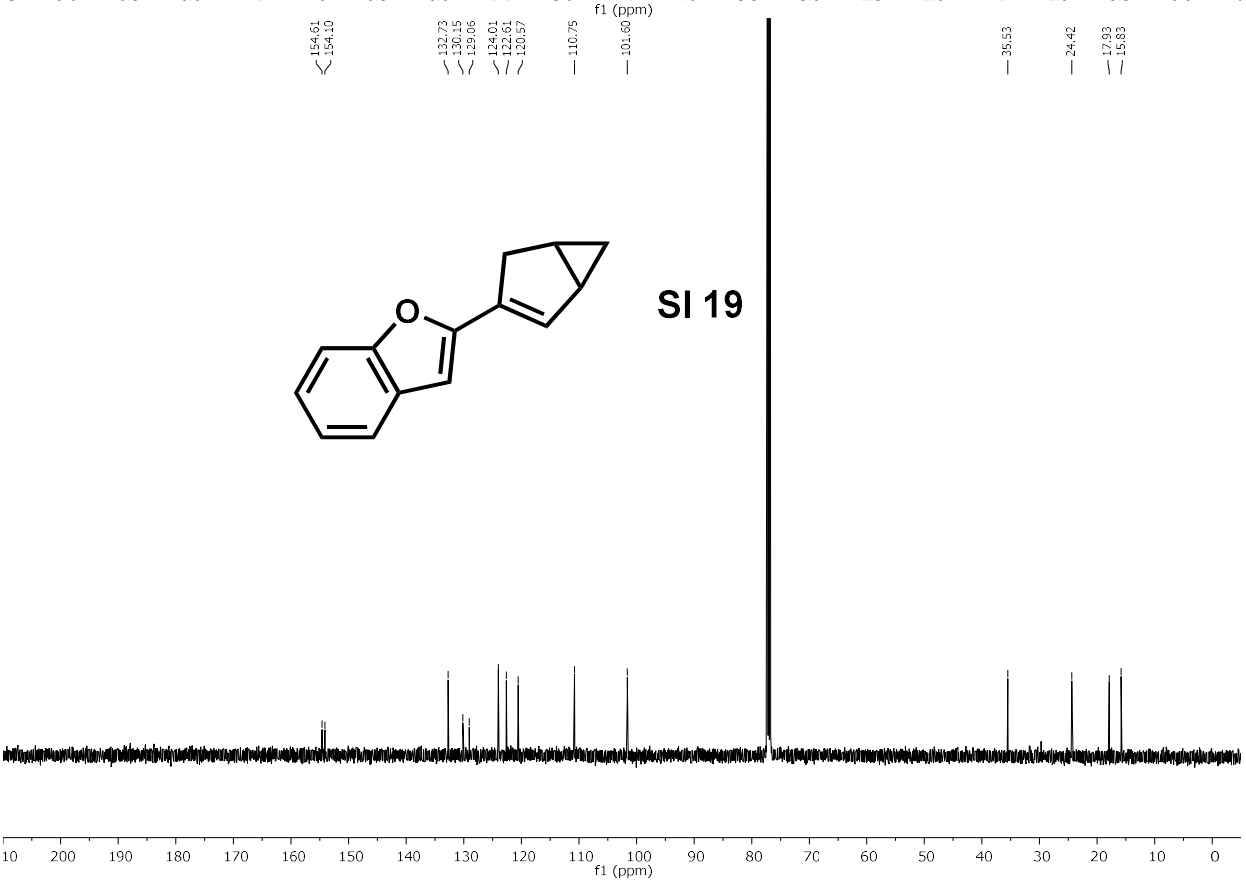
SI 19
f1 (ppm)

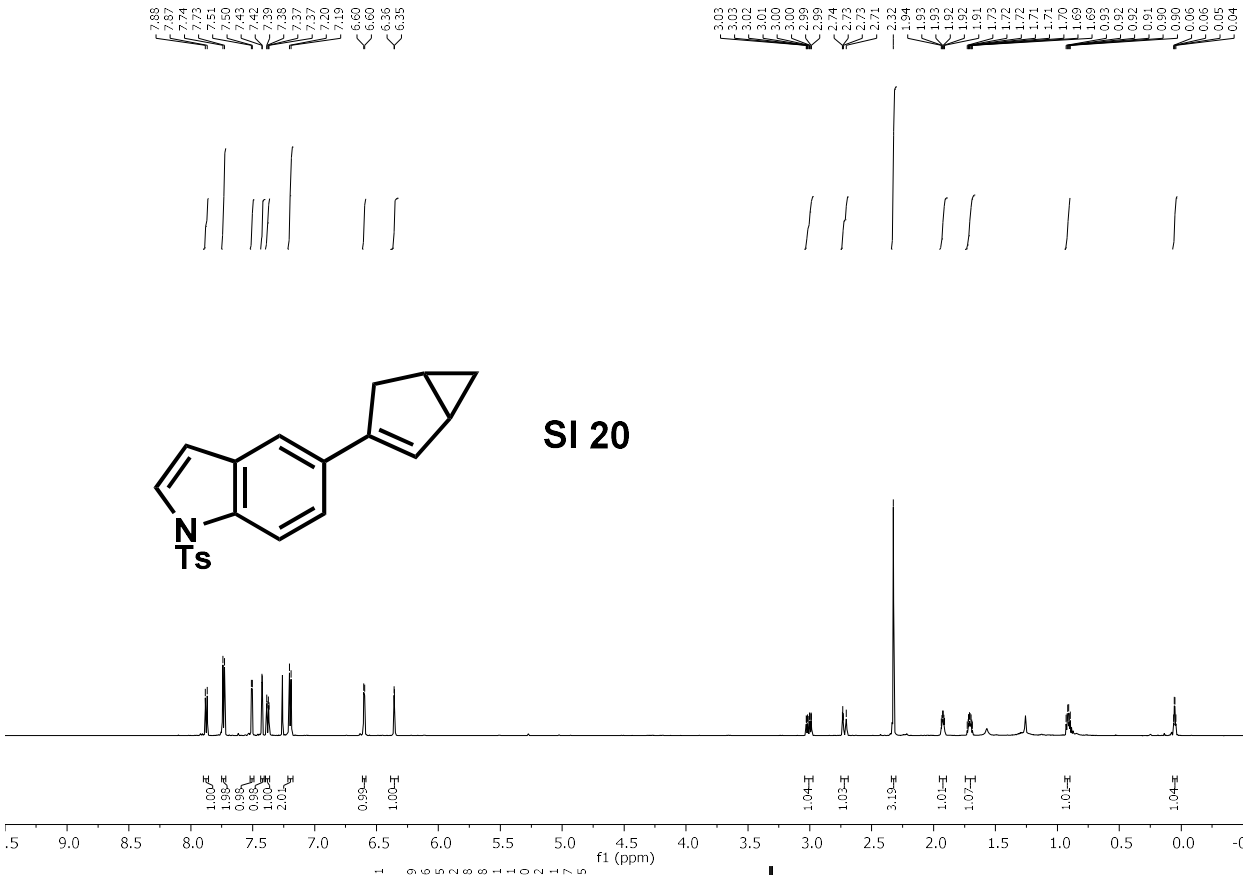
7.88
7.87
7.74
7.73
7.51
7.50
7.43
7.42
7.39
7.38
7.37
7.37
7.37
7.20
7.19
6.60
6.60
6.36
6.35
3.03
3.03
3.02
3.01
3.00
3.00
2.99
2.99
2.74
2.73
2.73
2.71
2.32
1.94
1.93
1.93
1.92
1.91
1.73
1.72
1.72
1.71
1.71
1.70
1.69
1.69
1.69
0.93
0.92
0.92
0.91
0.90
0.90
0.06
0.06
0.05
0.04
N
Ts
SI 20
1.00
1.98
0.98
0.98
1.00
2.01
0.99
1.00
1.04
1.03
3.19
1.01
1.07
1.01
1.04
f1 (ppm)

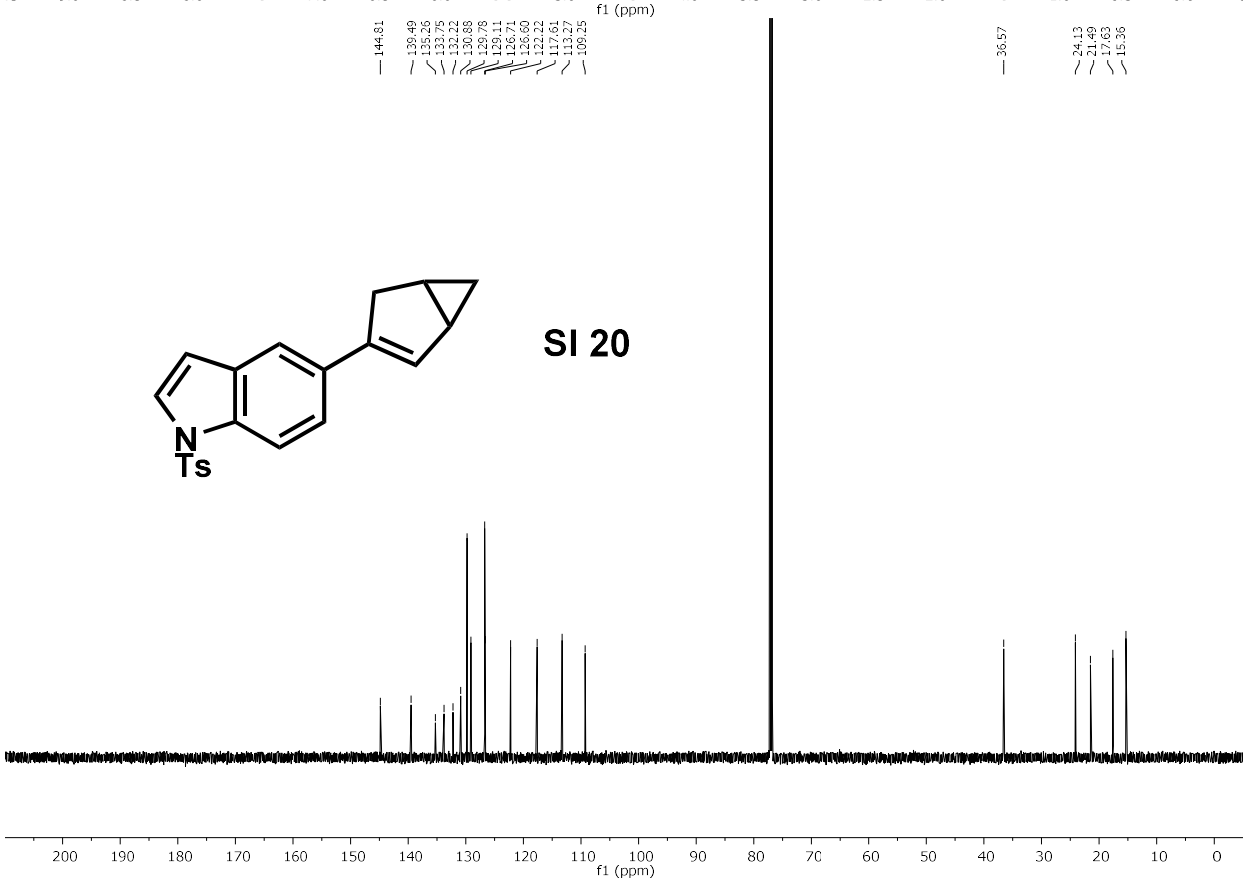
144.81
139.49
135.26
133.75
132.22
130.88
129.78
129.11
126.71
126.60
123.22
117.61
113.27
109.25
36.57
24.13
21.49
17.63
15.36
N
Ts
SI 20
f1 (ppm)

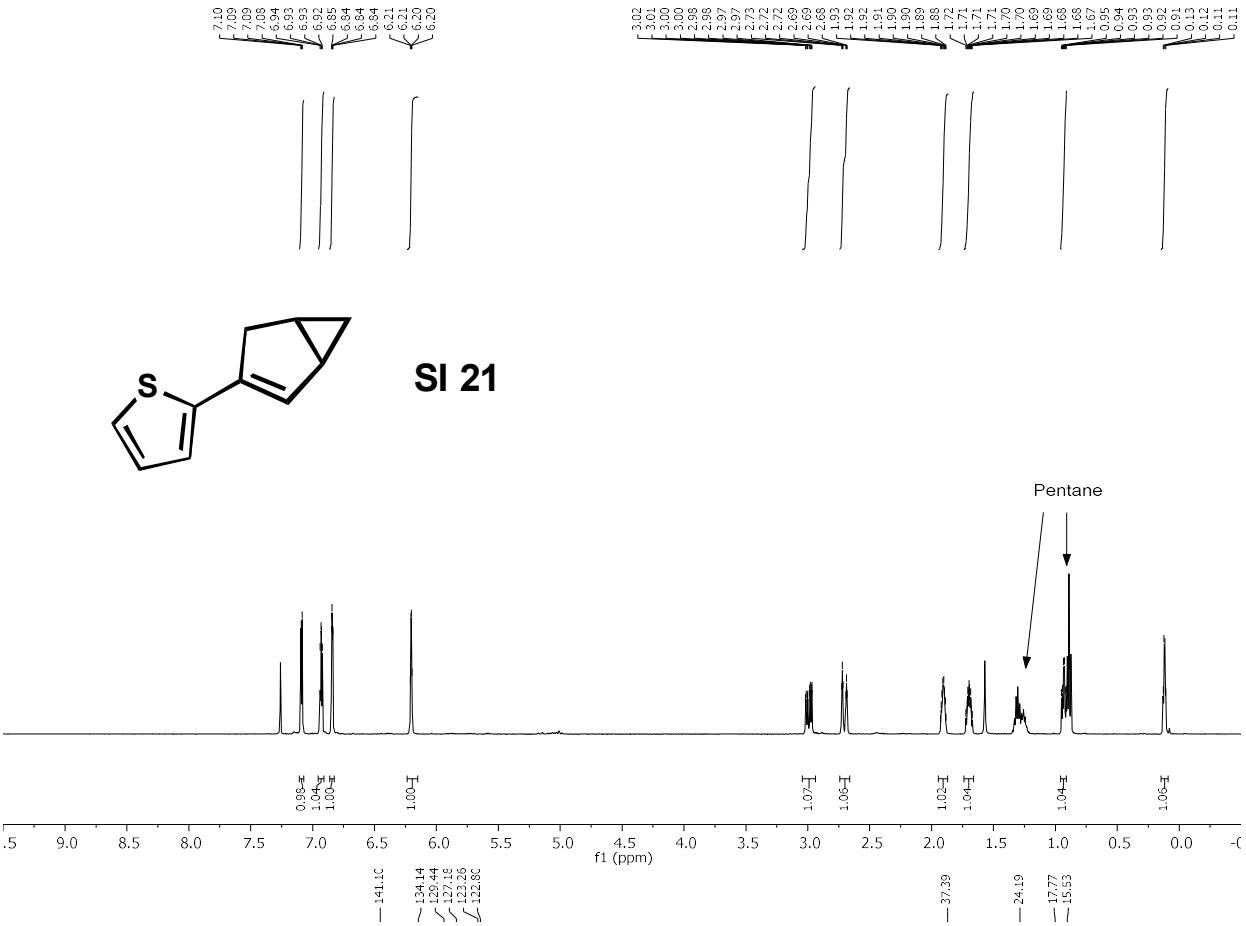
SI 21
Pentane
f1 (ppm)

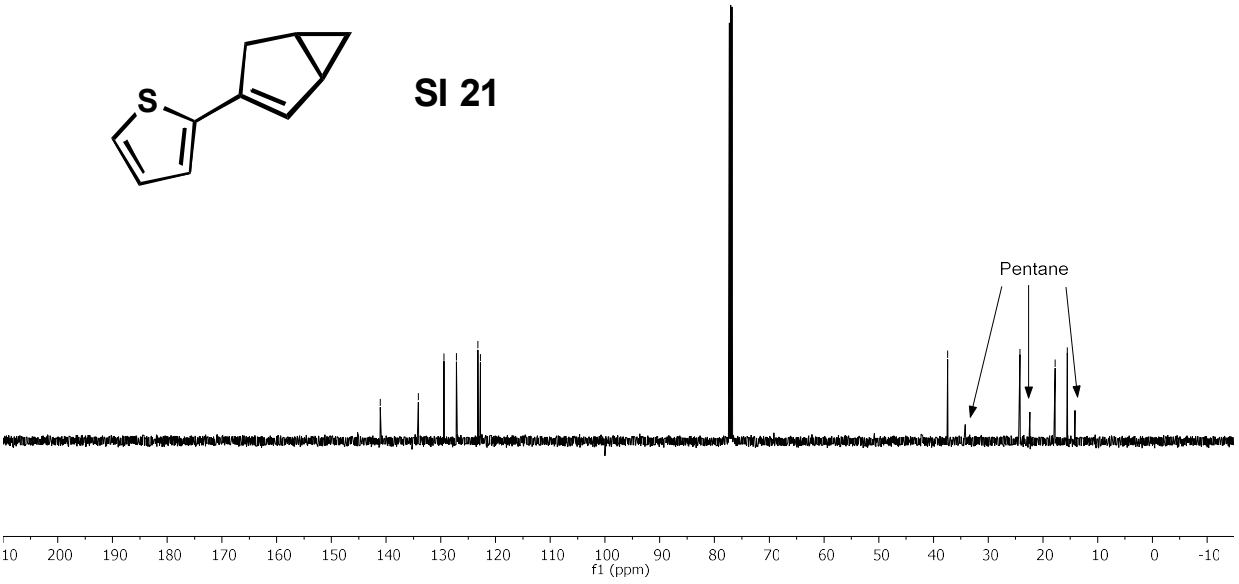
SI 21
Pentane
f1 (ppm)

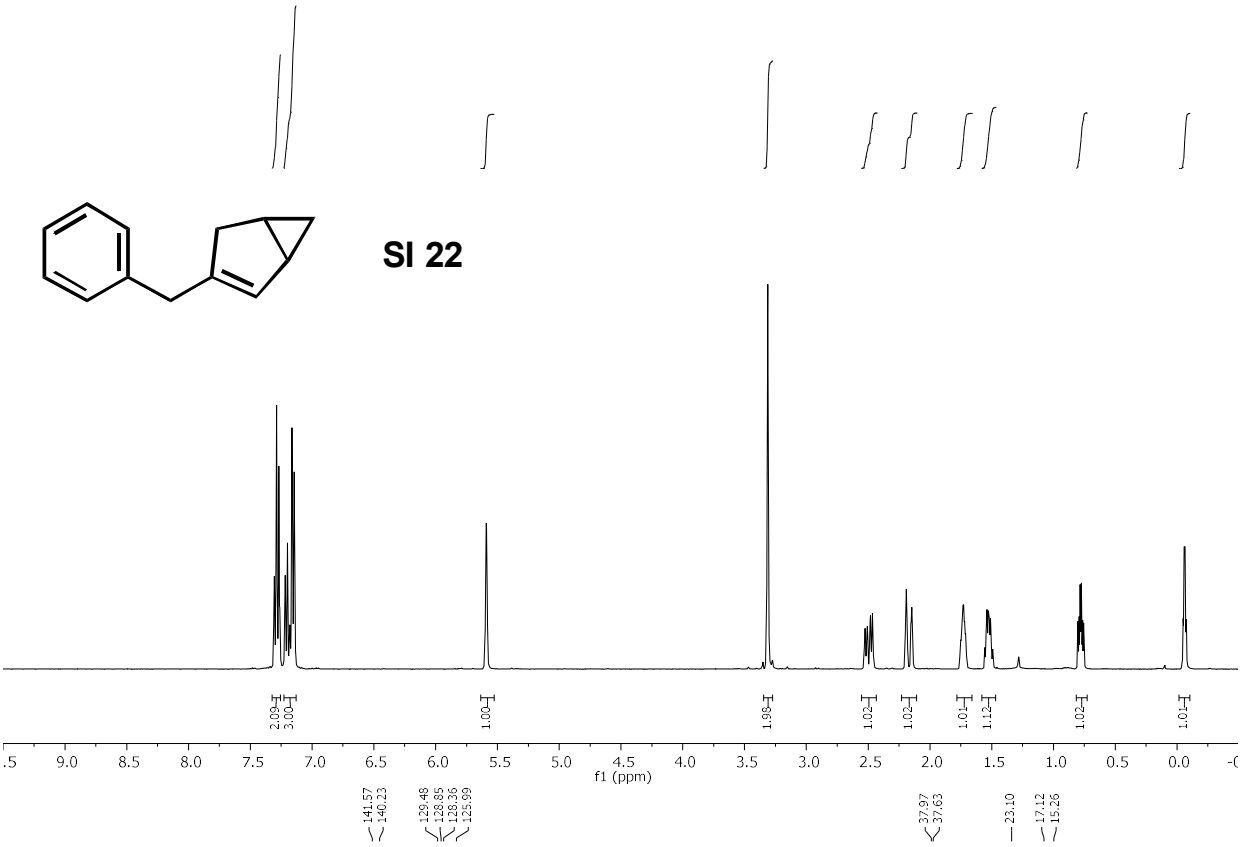
SI 22
2.09
3.00
1.00
1.98
1.02
1.02
1.01
1.12
1.02
1.01
f1 (ppm)
141.57
140.23
129.48
128.85
128.36
125.99
37.97
37.63
23.10
17.12
15.26

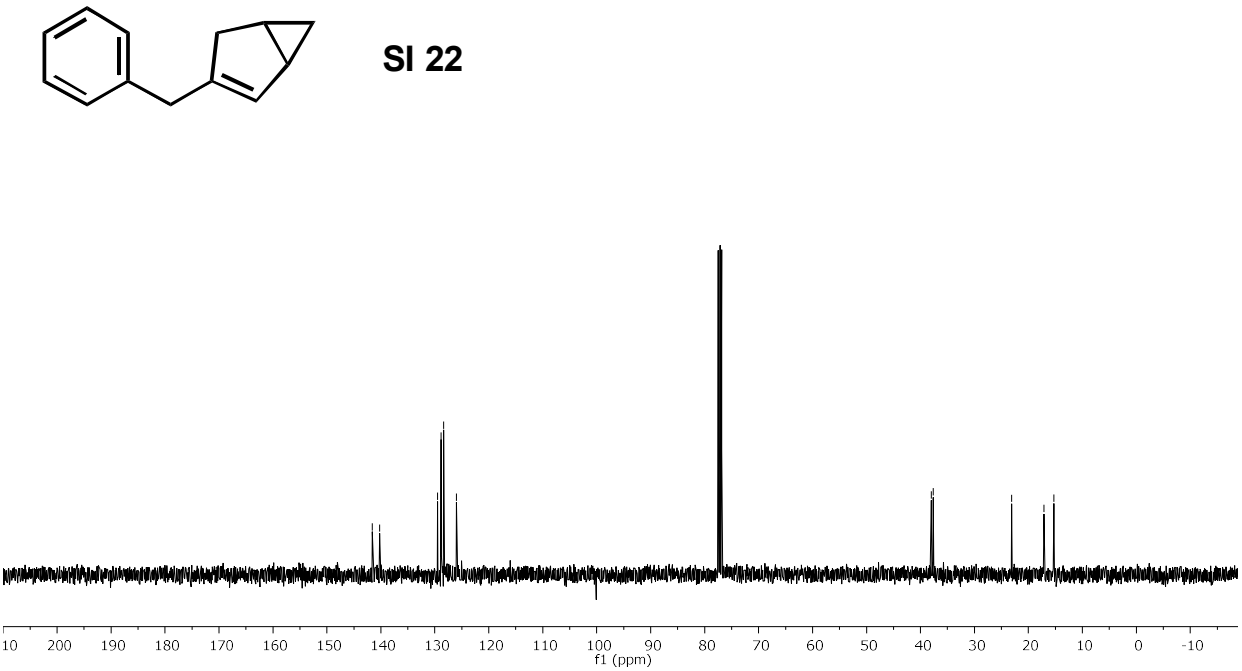
SI 22
f1 (ppm)

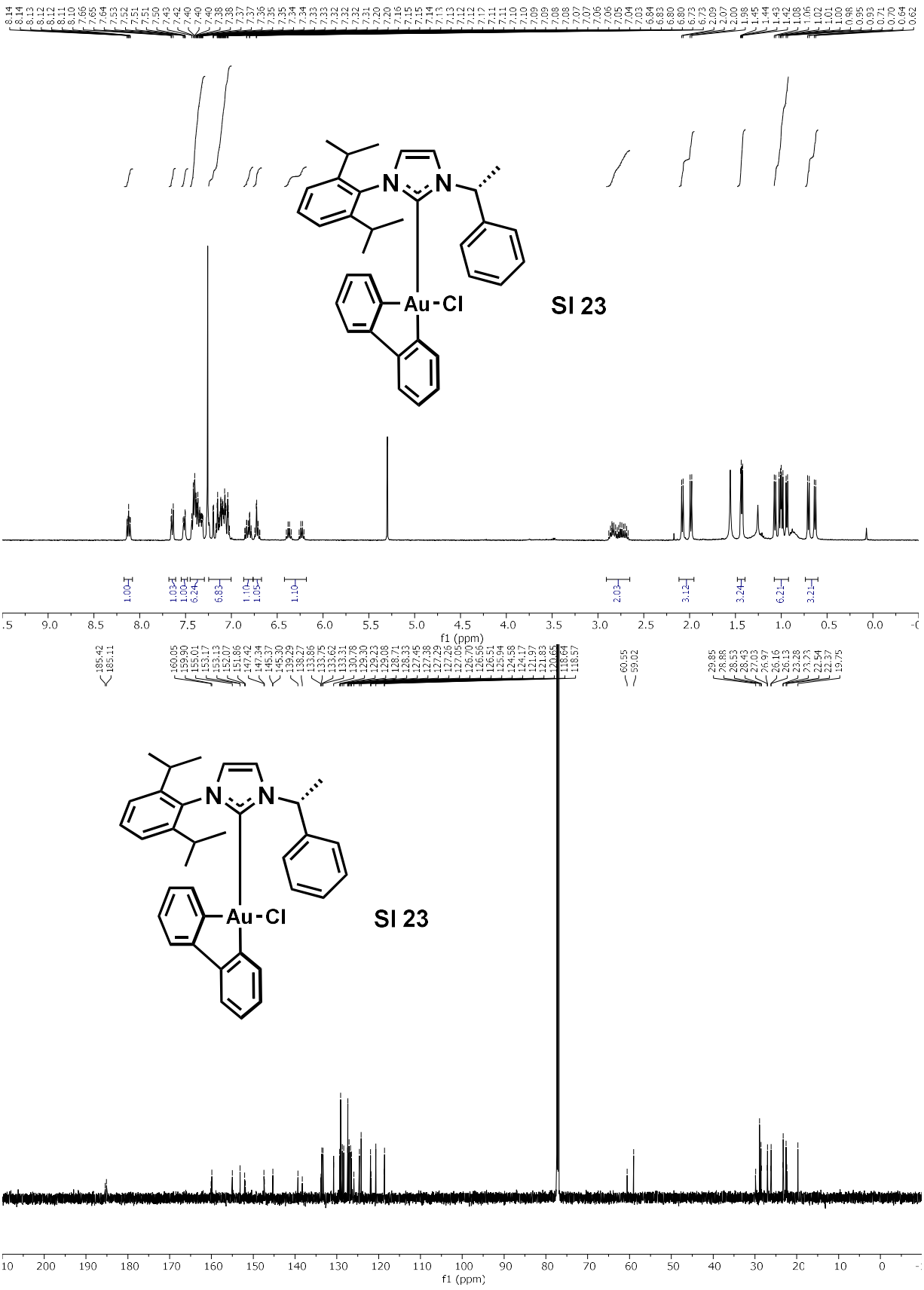
Au-Cl
SI 23
f1 (ppm)
Au-Cl
SI 23
f1 (ppm)

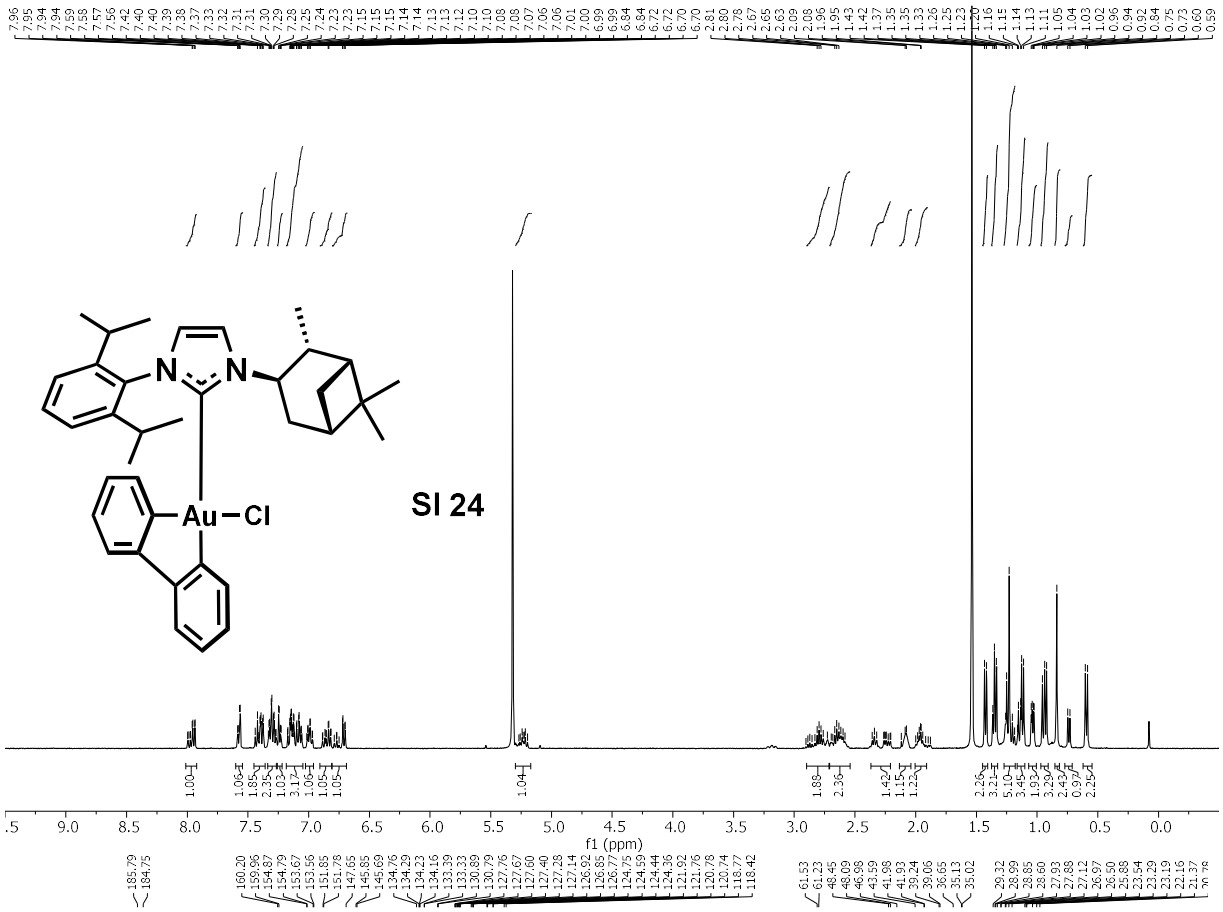
Au–Cl
SI 24
f1 (ppm)

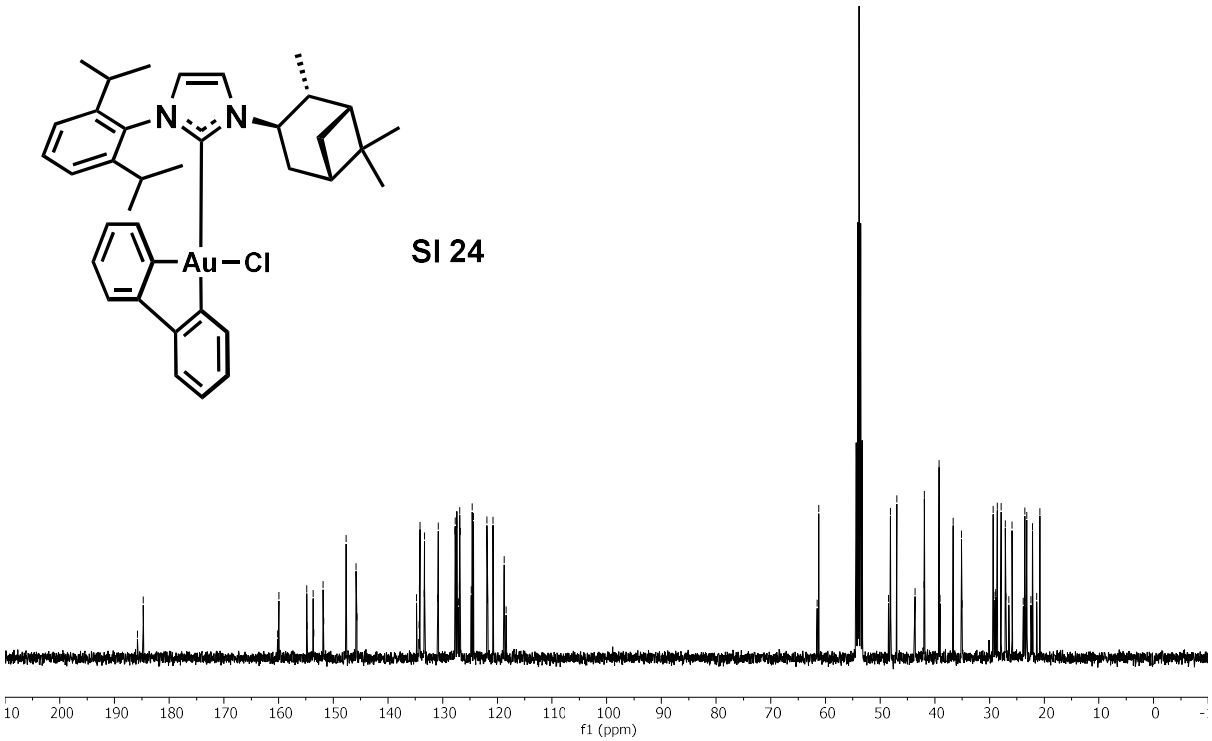
Au–Cl
SI 24
f1 (ppm)

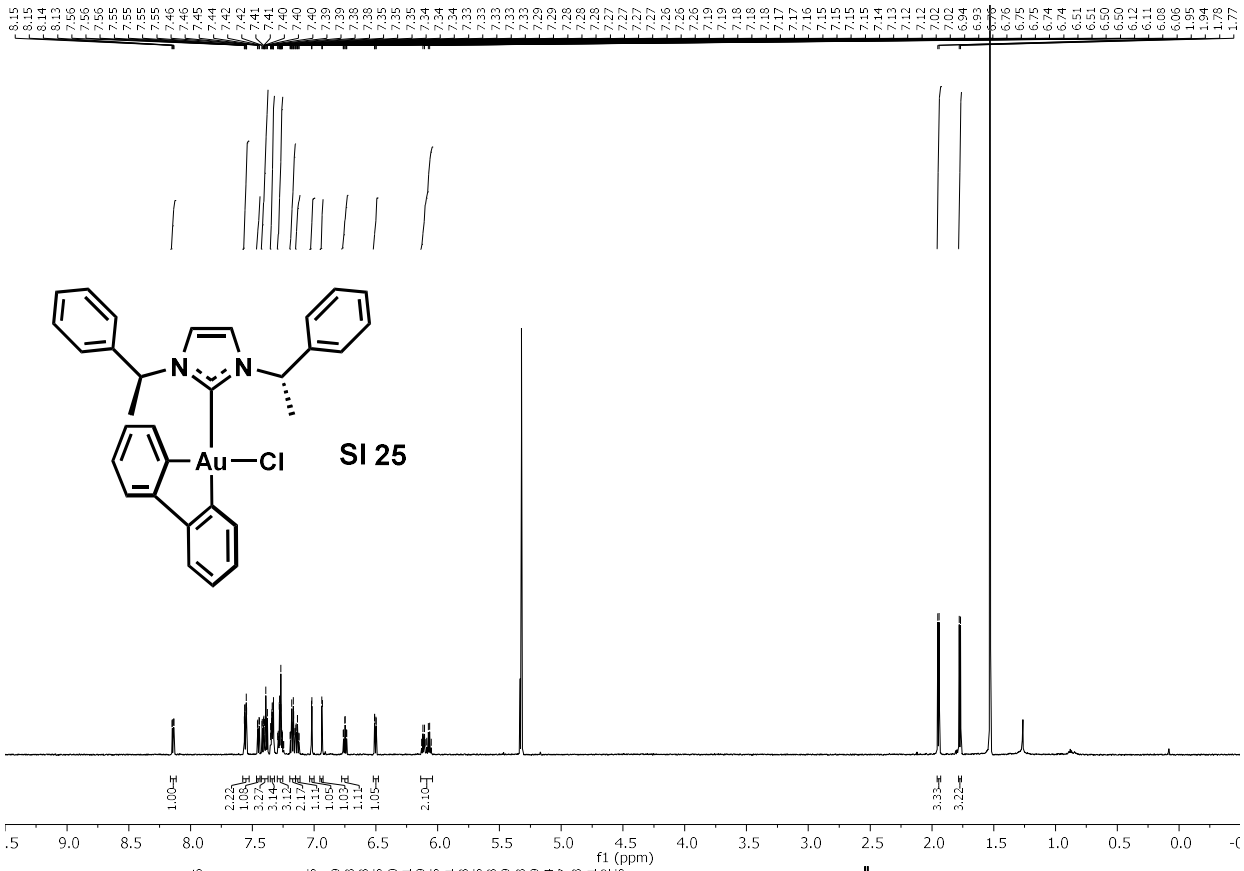
Au—Cl
SI 25
f1 (ppm)

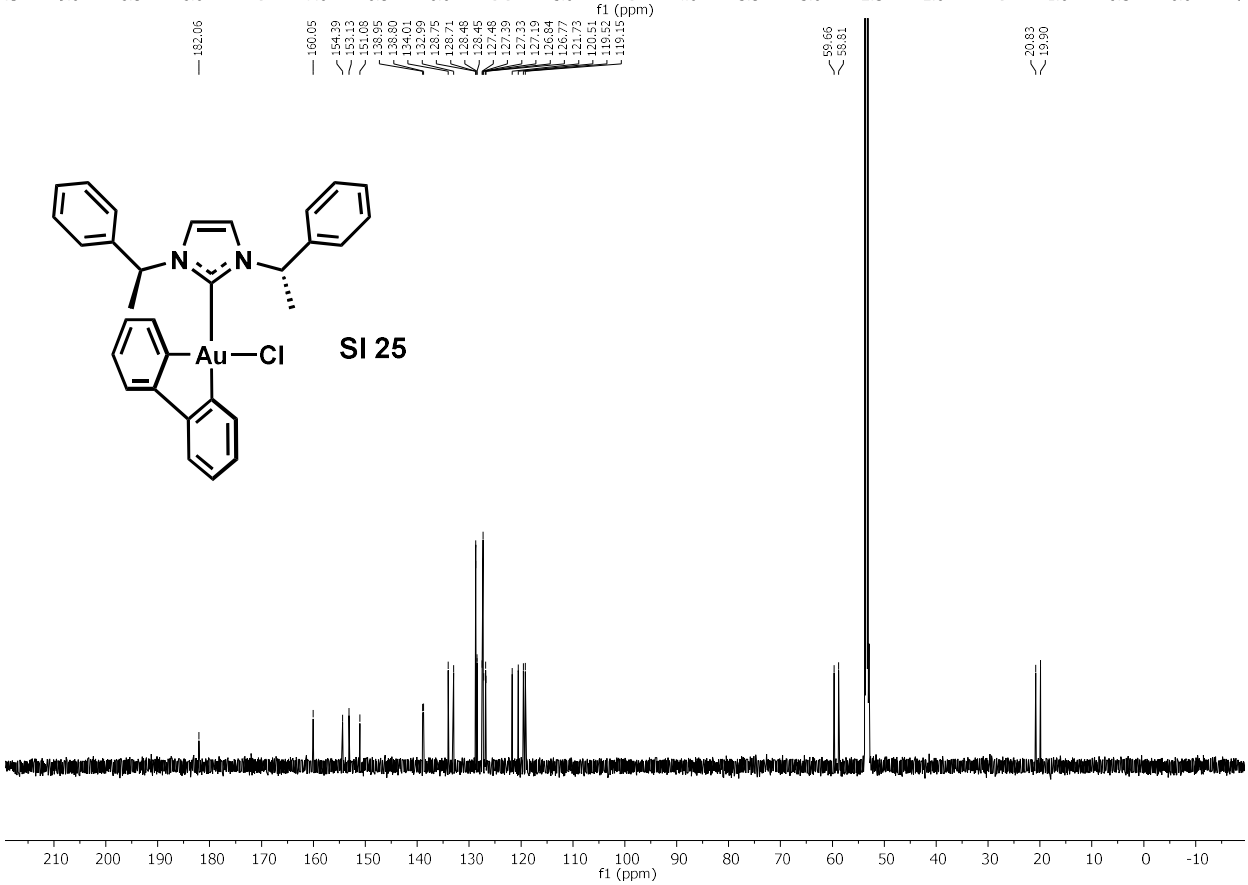
Au—Cl
SI 25
f1 (ppm)

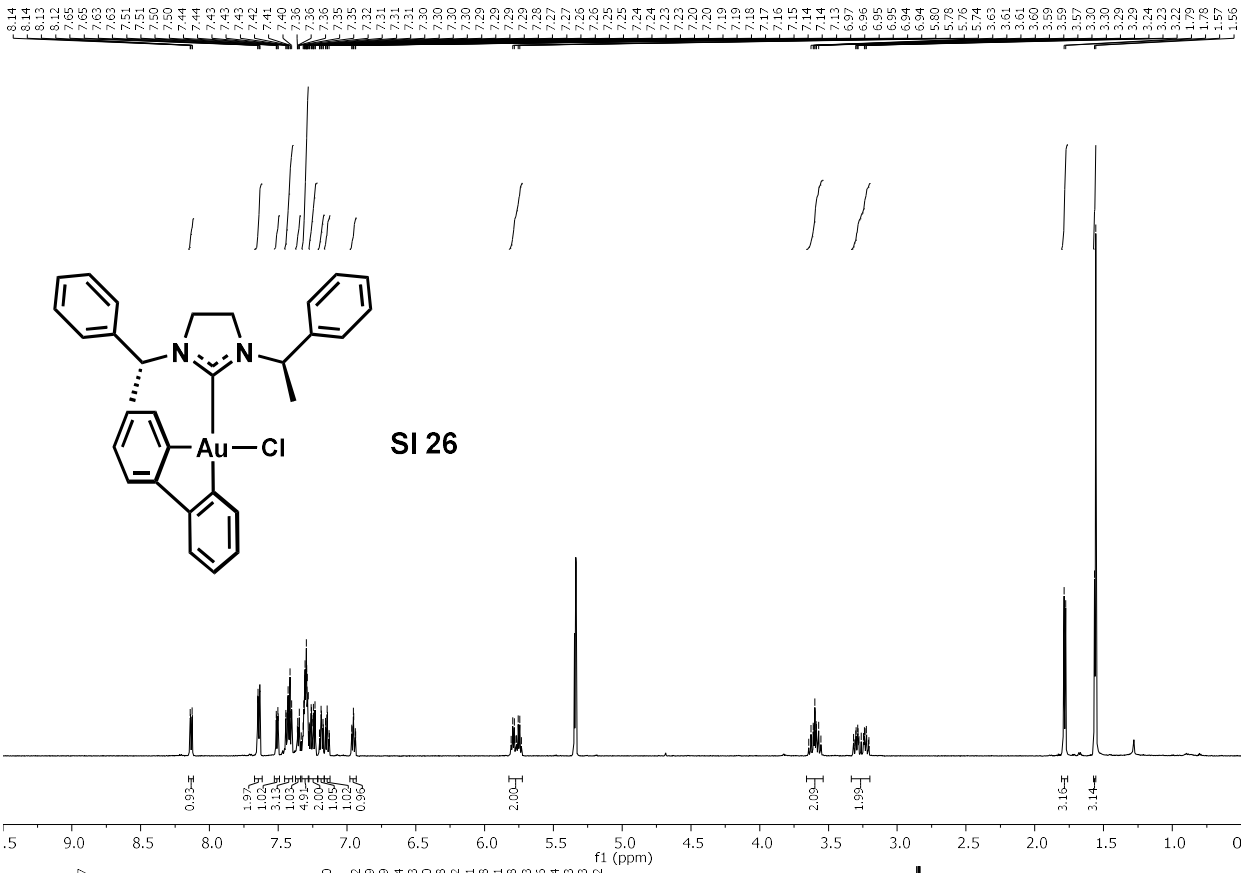
Au—Cl
SI 26
f1 (ppm)

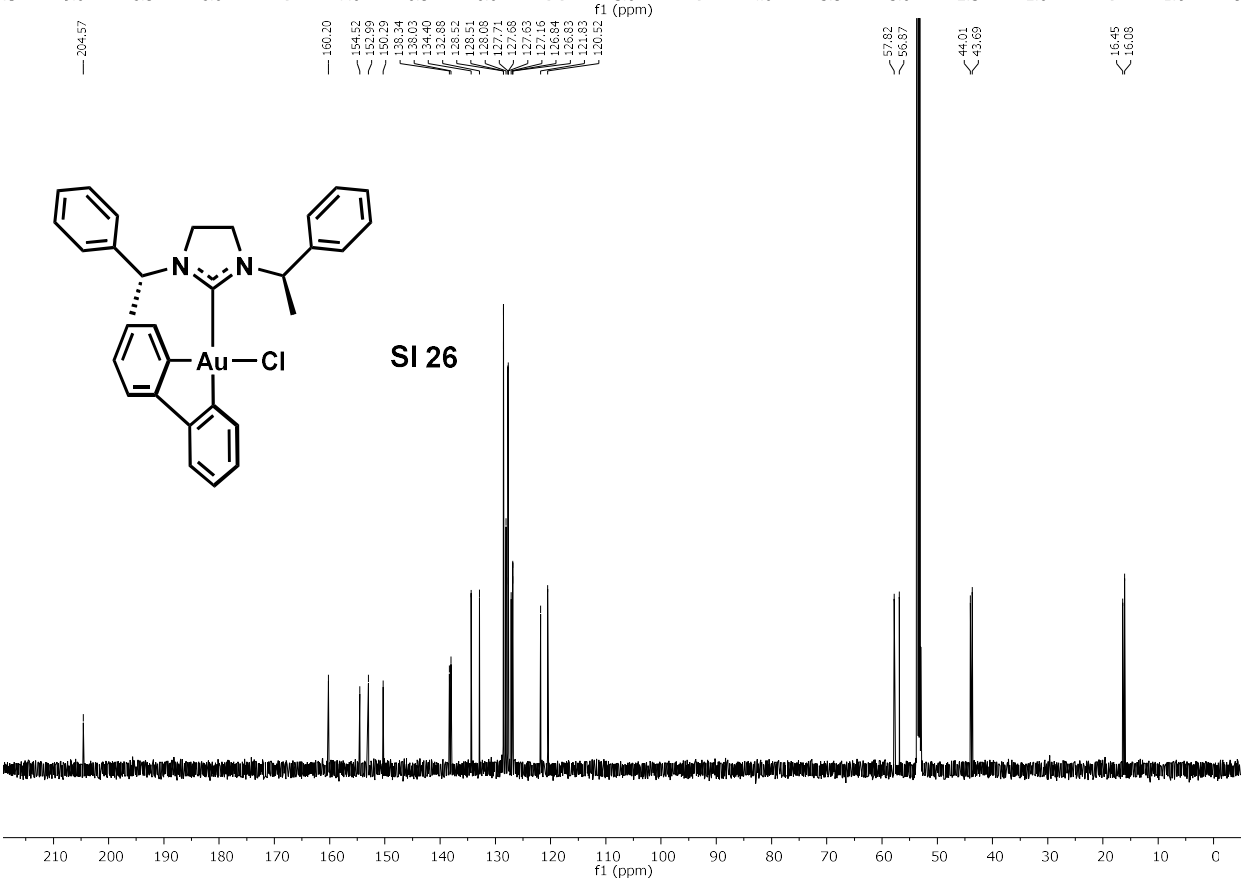
Au—Cl
SI 26
f1 (ppm)

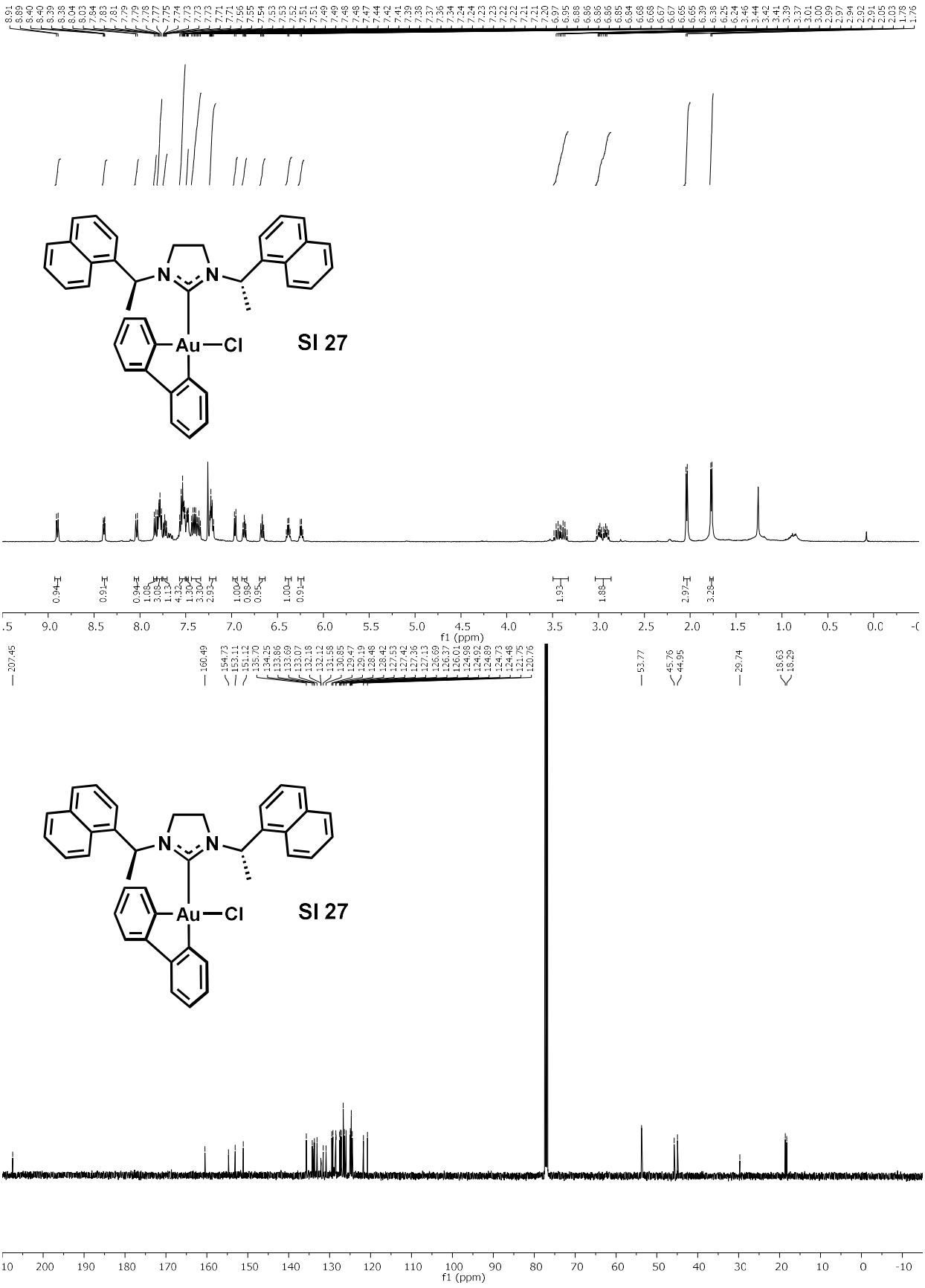
Au—Cl
SI 27
f1 (ppm)
Au—Cl
SI 27
f1 (ppm)

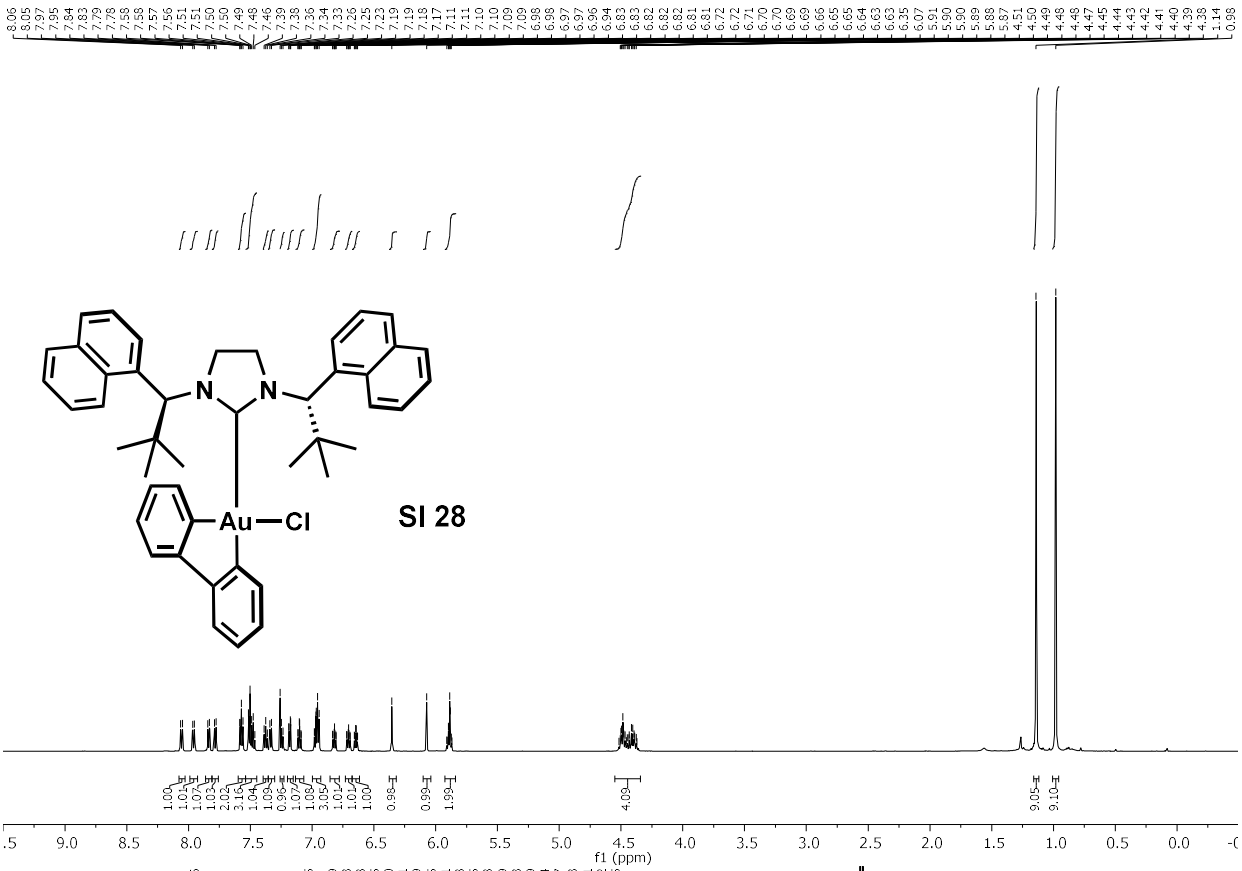
Au—Cl
SI 28
f1 (ppm)

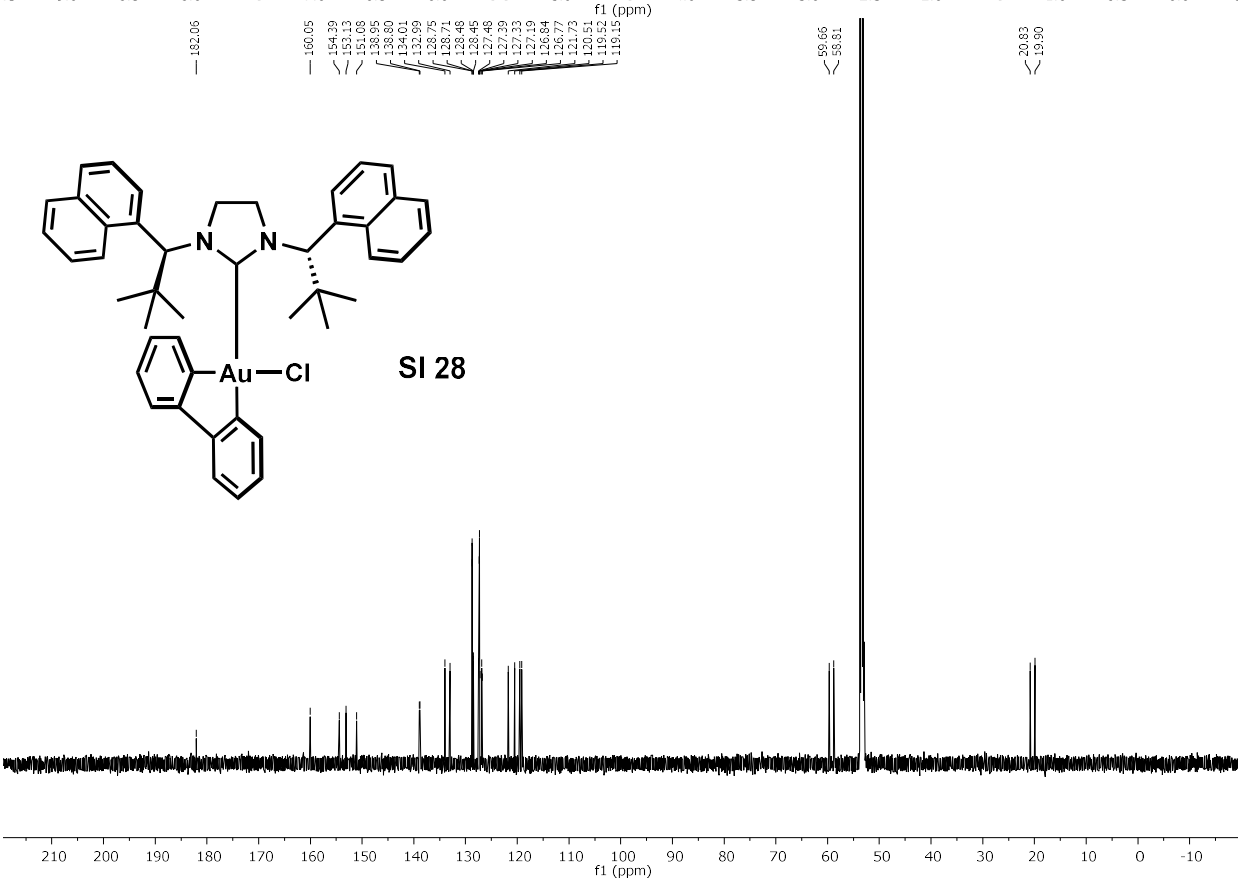
Au—Cl
SI 28
f1 (ppm)

2.4.7 HPLC Traces

hex-5-en-1-yn-3-ylbenzene (SI 1)

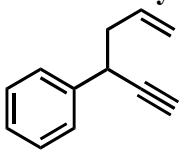

HPLC Chiralpak OD-H column (100:0 hexanes:isopropanol, 0.25 mL/min, 215 nm); first enantiomer t_r = 30.3 min, second enantiomer t_r = 33.3 min.

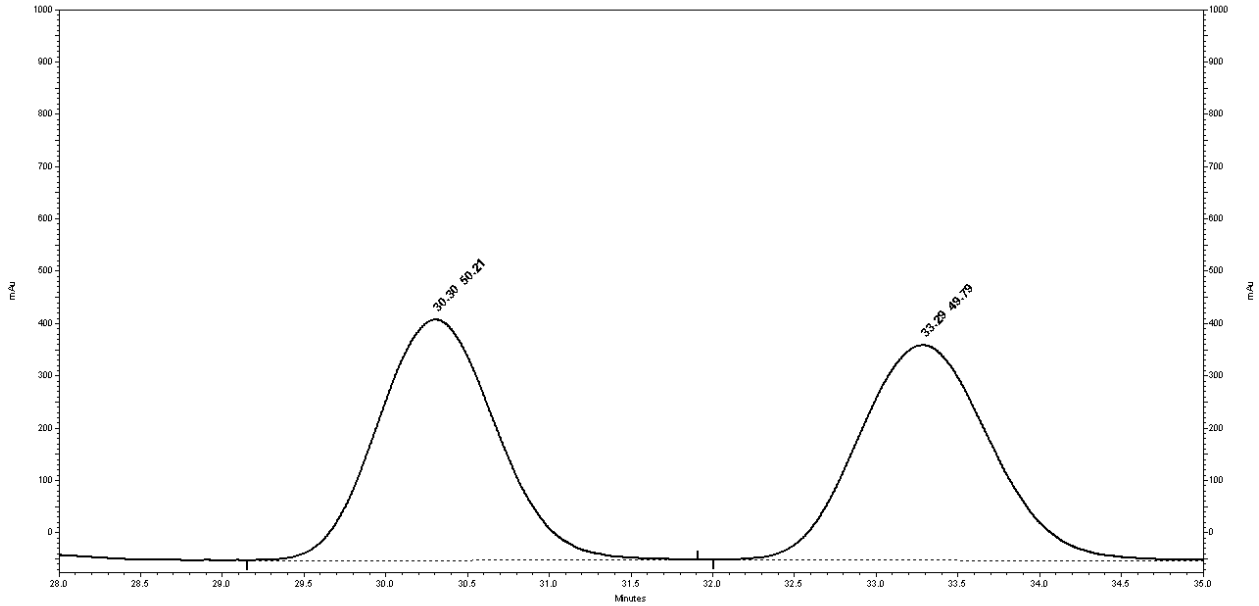

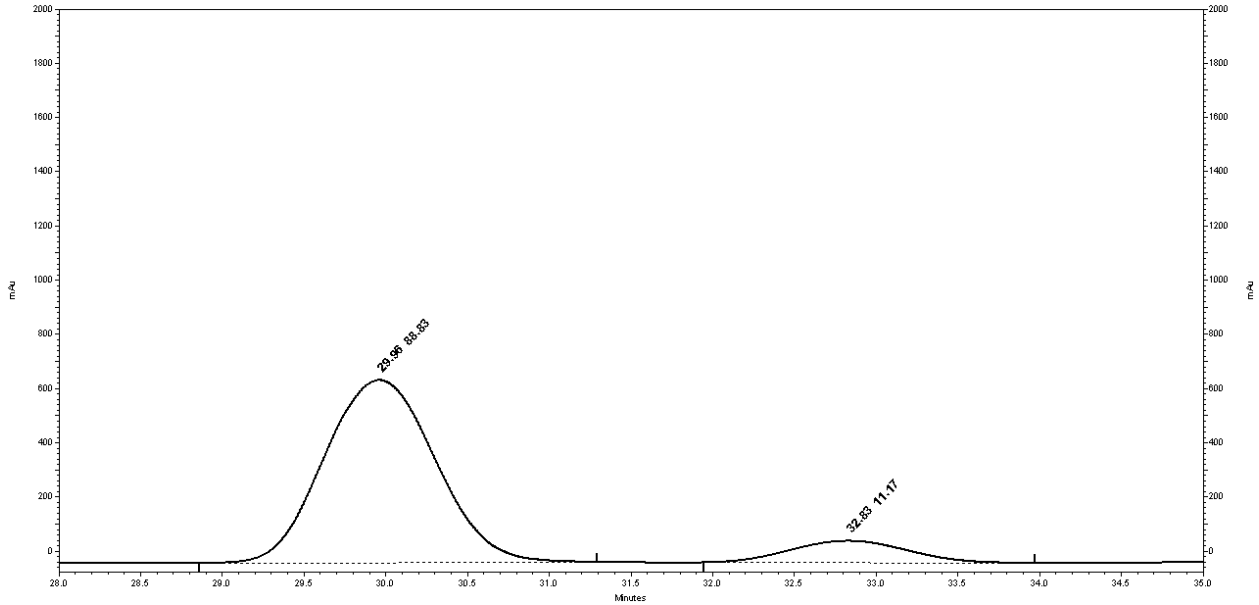

1-(tert-butyl)-4-(hex-5-en-1-yn-3-yl)benzene (SI 2)

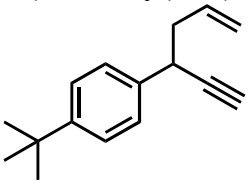

SFC OJ-H column (1% isopropanol, 2.5 mL/min, 215 nm); first enantiomer t_r = 1.7 min, second enantiomer t_r = 1.9 min.

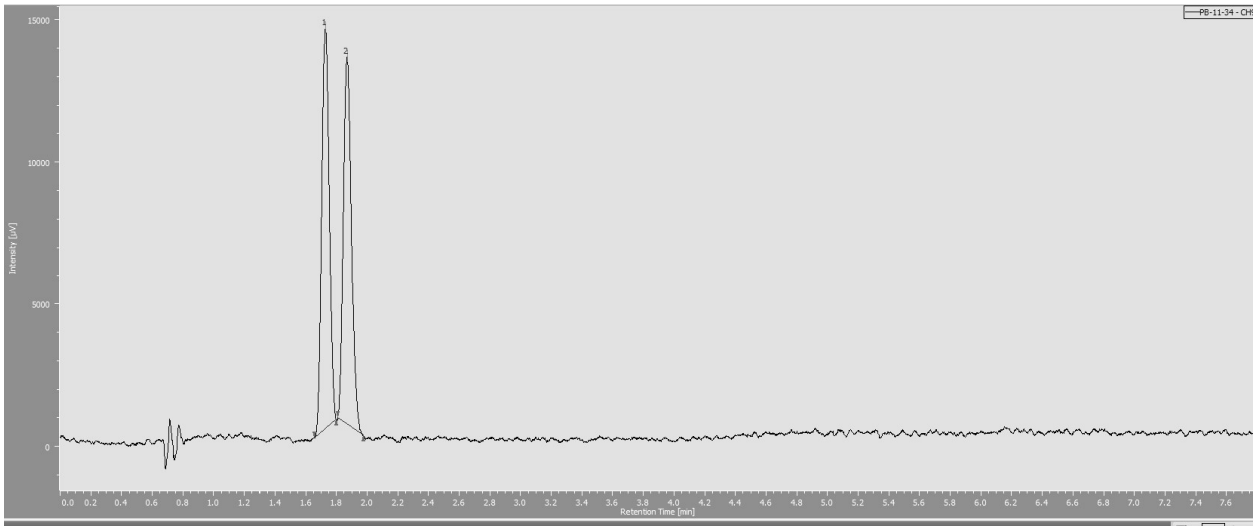

Peak Info. Table: PB-11-34

#	Peak Name	CH	tR	Area	Height	Area%	Height%	Quantity	NTP	Resolution	Symmetry Factor	Warning
1	Unknown	9	1.728	47643	14041	50.120	52.121	N/A	5721	1.504	1.050	
2	Unknown	9	1.870	47415	12898	49.880	47.879	N/A	5889	N/A	1.147	

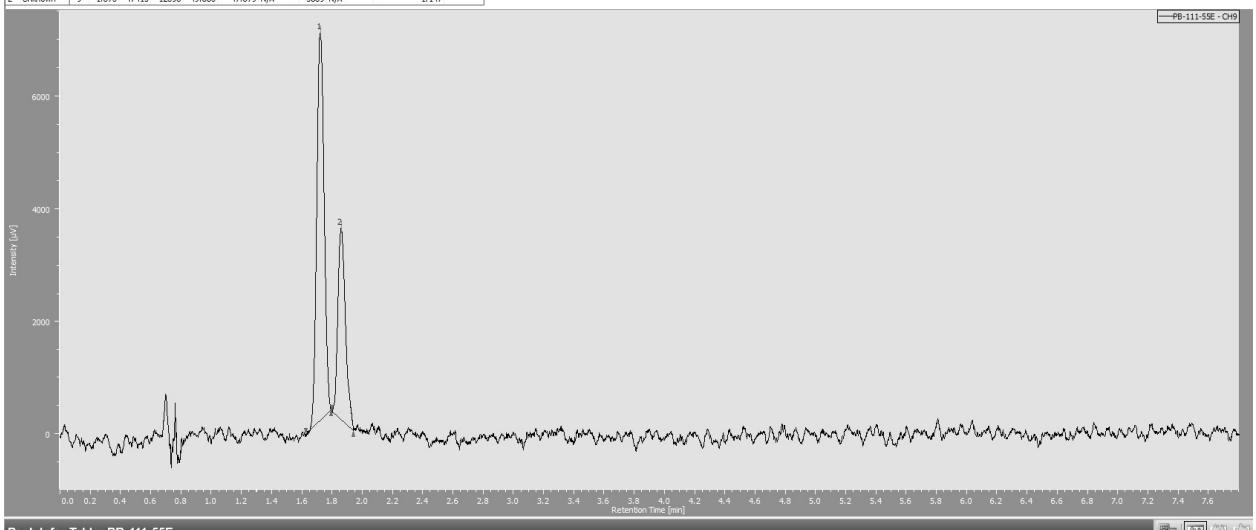

Peak Info. Table: PB-111-55E

#	Peak Name	CH	tR	Area	Height	Area%	Height%	Quantity	NTP	Resolution	Symmetry Factor	Warning
1	Unknown	9	1.722	23062	6882	65.618	66.771	N/A	5861	1.523	1.061	
2	Unknown	9	1.860	12084	3425	34.382	33.229	N/A	6505	N/A	1.261	

1-(hex-5-en-1-yn-3-yl)-2-methylbenzene (SI 3)

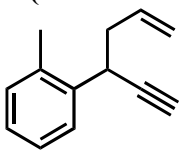

HPLC Chiralpak OD-H column (100:0 hexanes:isopropanol, 0.25 mL/min, 215 nm); first enantiomer t_r = 29.8 min, second enantiomer t_r = 34.1 min.

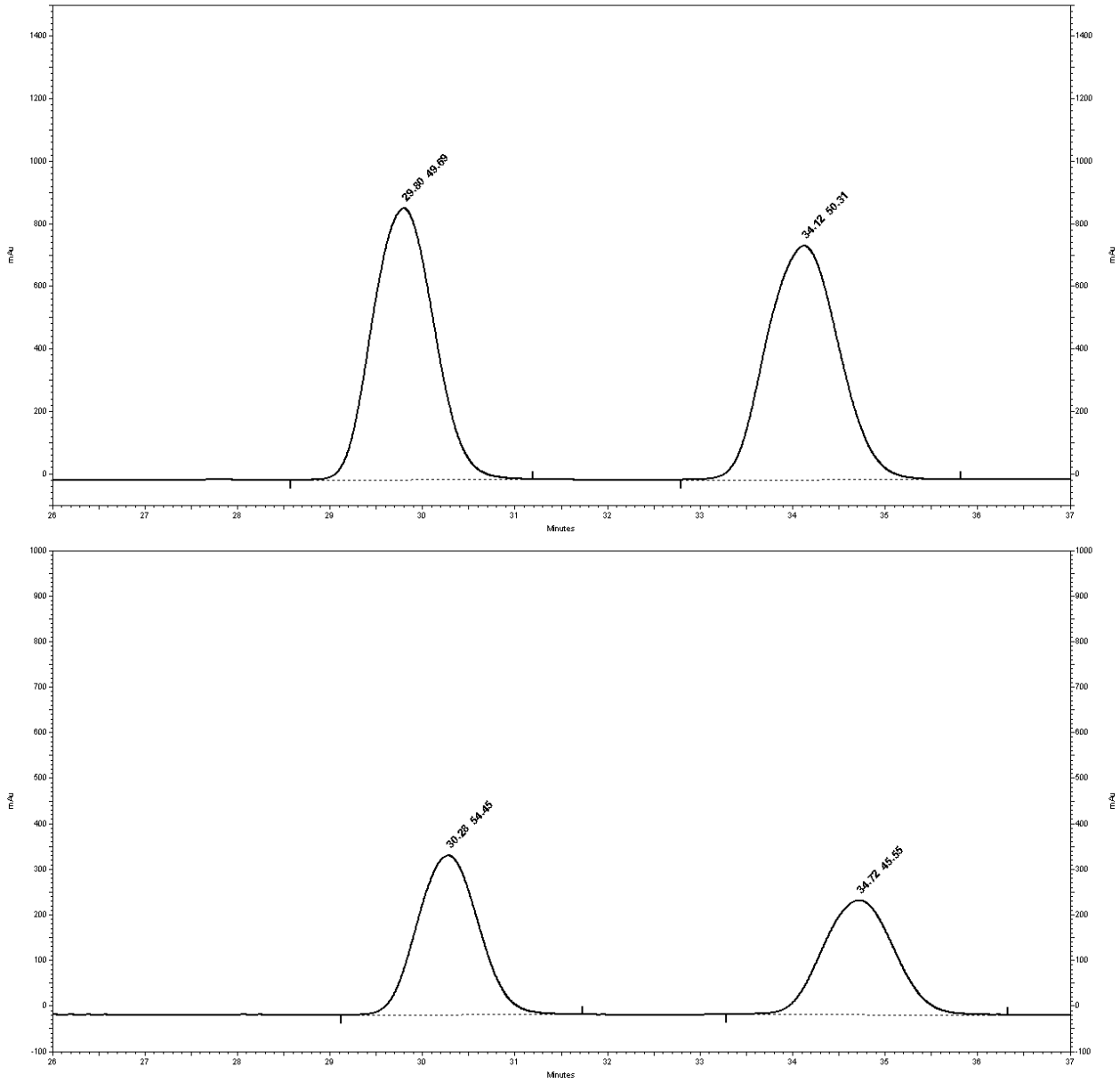

1-(hex-5-en-1-yn-3-yl)naphthalene (SI 4)

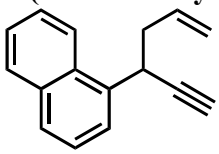

HPLC Chiralpak AD-H column (99.9:0.1 hexanes:isopropanol, 0.25 mL/min, 270 nm); first enantiomer t_r = 25.6 min, second enantiomer t_r = 36.3 min.

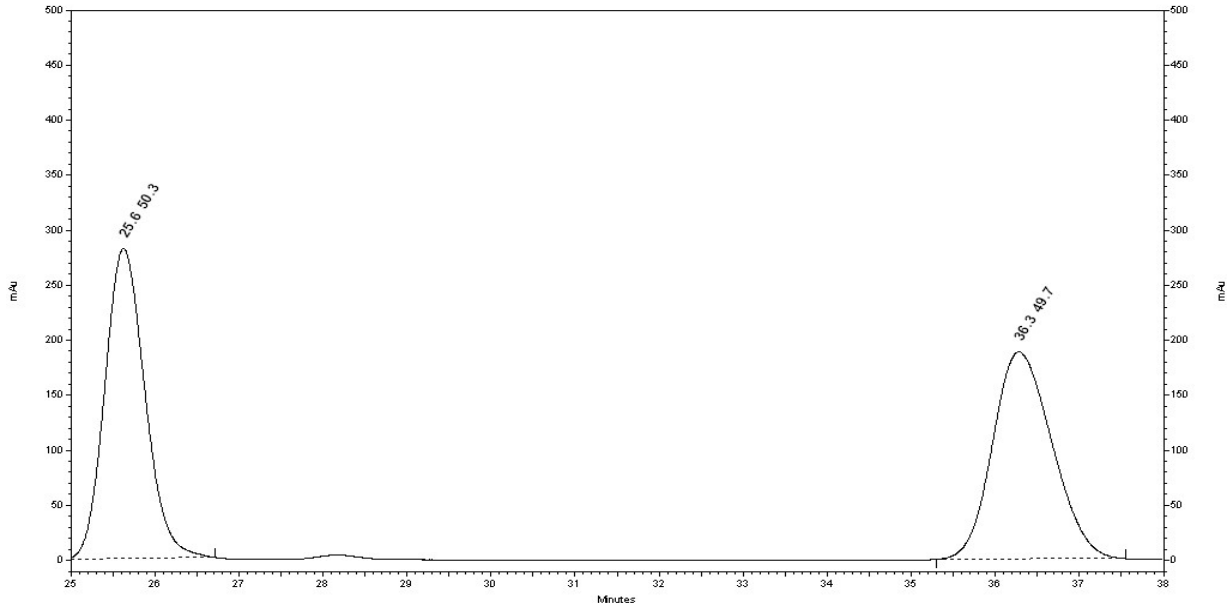

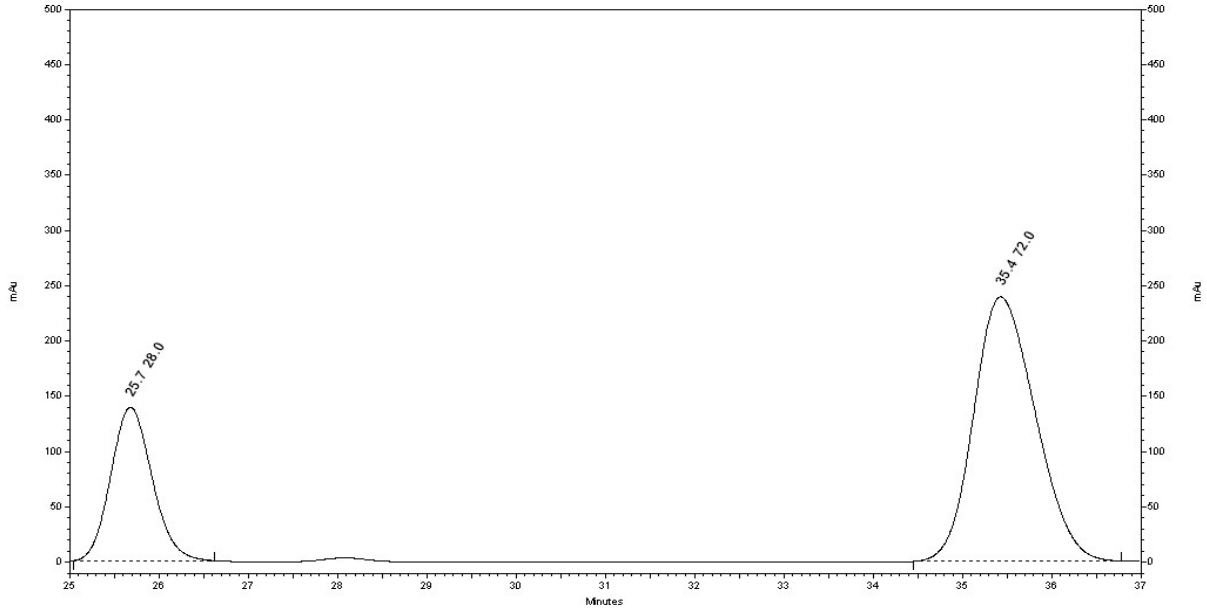

2-(hex-5-en-1-yn-3-yl)naphthalene (SI 5)

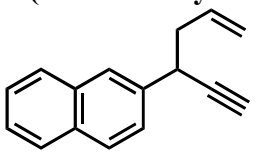

HPLC Chiralpak AD-H column (99.9:0.1 hexanes:isopropanol, 0.25 mL/min, 270 nm); first enantiomer t_r = 26.3 min, second enantiomer t_r = 28.0 min.

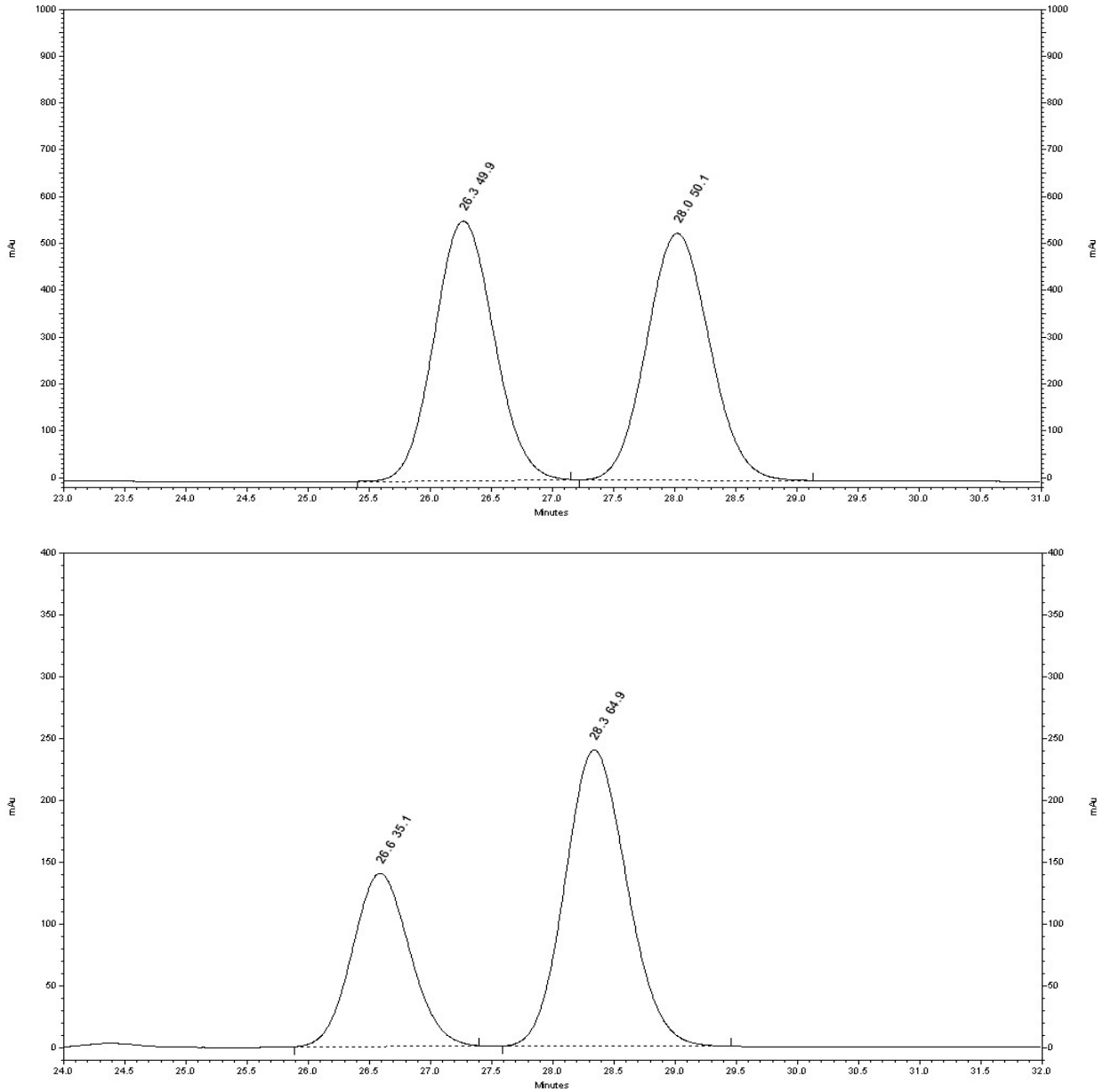

1-(hex-5-en-1-yn-3-yl)-4-methoxybenzene (SI 6)

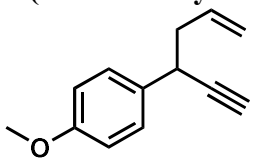

HPLC Chiralpak AD-H column (99.9:0.1 hexanes:isopropanol, 0.25 mL/min, 225 nm); first enantiomer t_r = 26.5 min, second enantiomer t_r = 29.5 min.

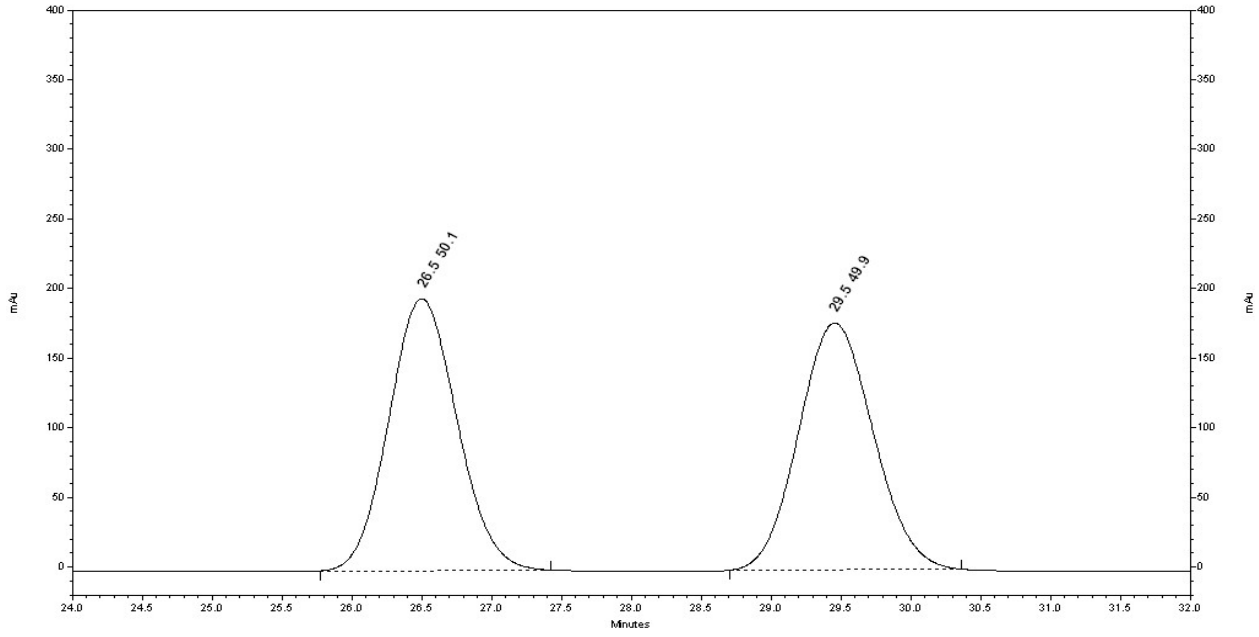

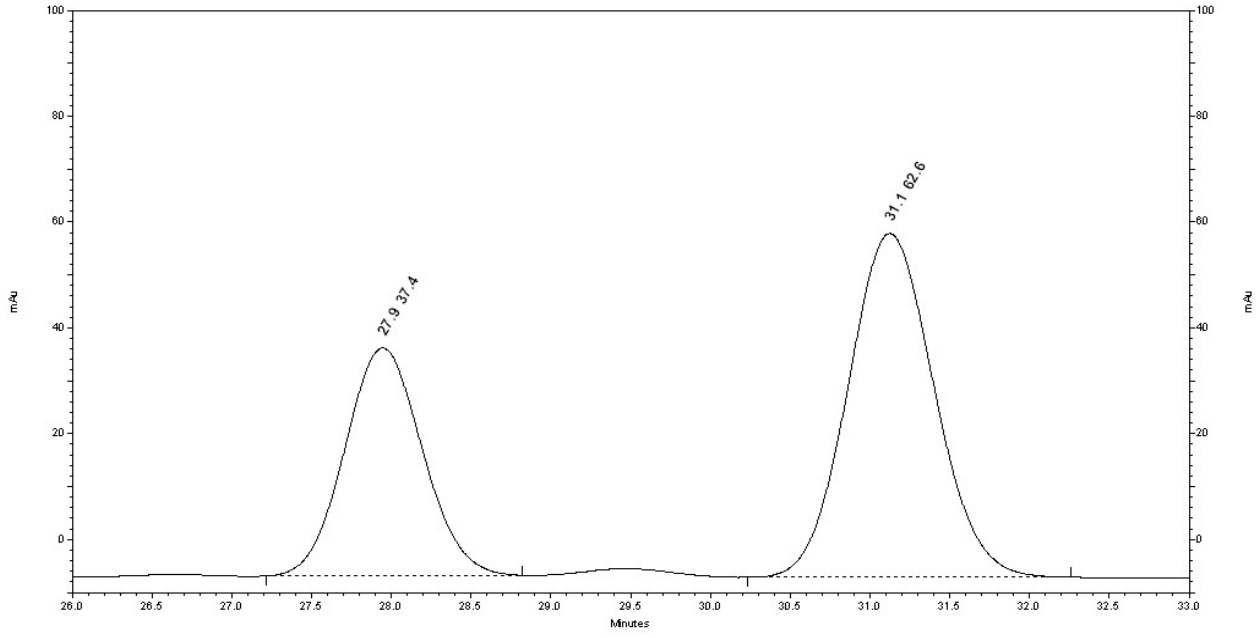

1-(hex-5-en-1-yn-3-yl)-4-iodobenzene (SI 7)

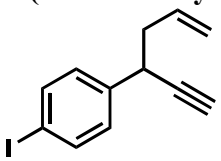

HPLC Chiralpak OD-H column (100:0 hexanes:isopropanol, 0.25 mL/min, 270 nm); first enantiomer t_r = 27.9 min, second enantiomer t_r = 30.2 min.

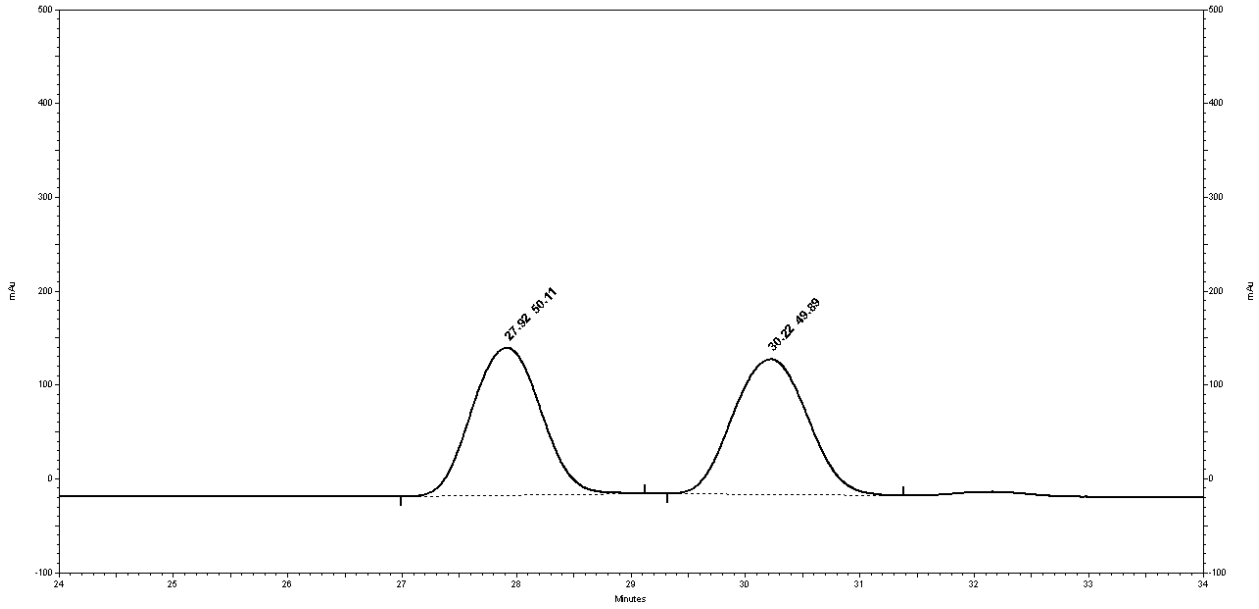

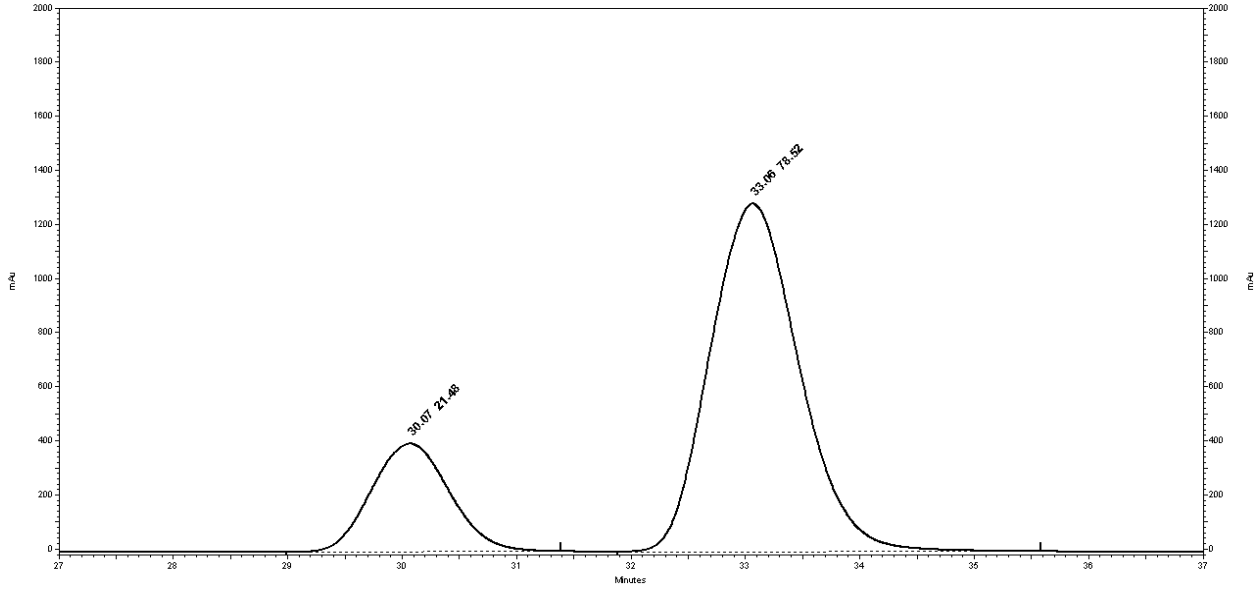

2-(hex-5-en-1-yn-3-yl)benzofuran (SI 8)

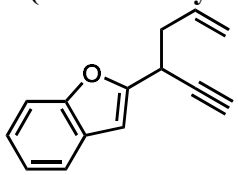

HPLC Chiralpak OD-H column (100:0 hexanes:isopropanol, 0.25 mL/min, 270 nm); first enantiomer t_r = 21.0 min, second enantiomer t_r = 22.3 min.

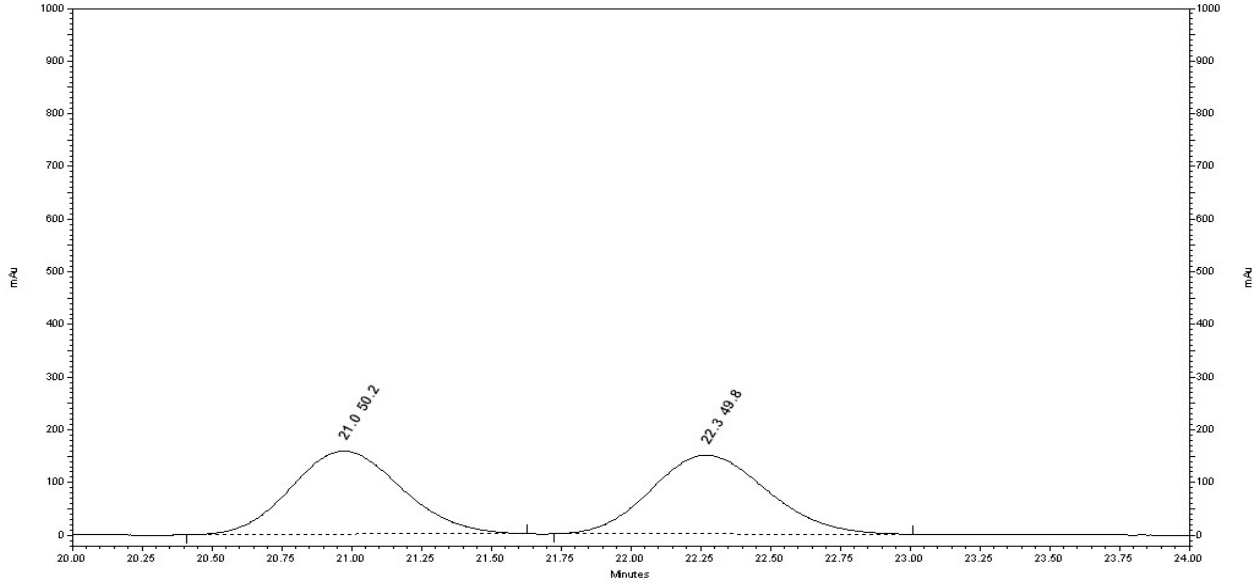

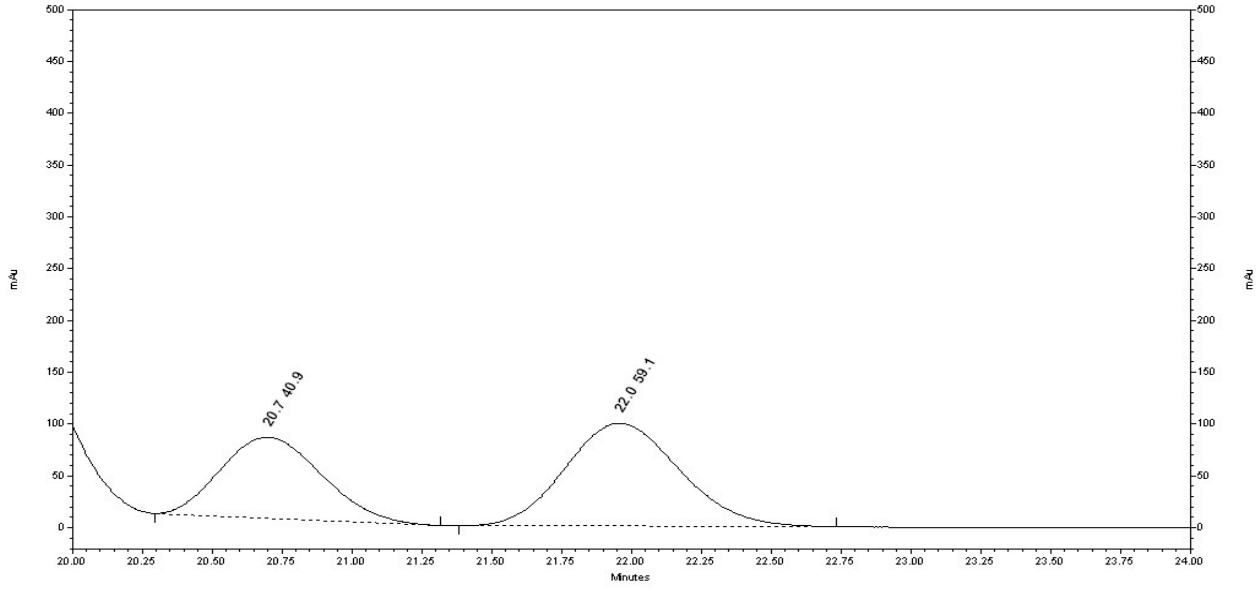

5-(hex-5-en-1-yn-3-yl)-1-tosyl-1H-indole (SI 9)

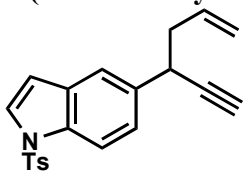

HPLC Chiralpak IA column (95:5 hexanes:isopropanol, 1 mL/min, 230 nm); first enantiomer t_r = 12.1 min, second enantiomer t_r = 13.5 min.

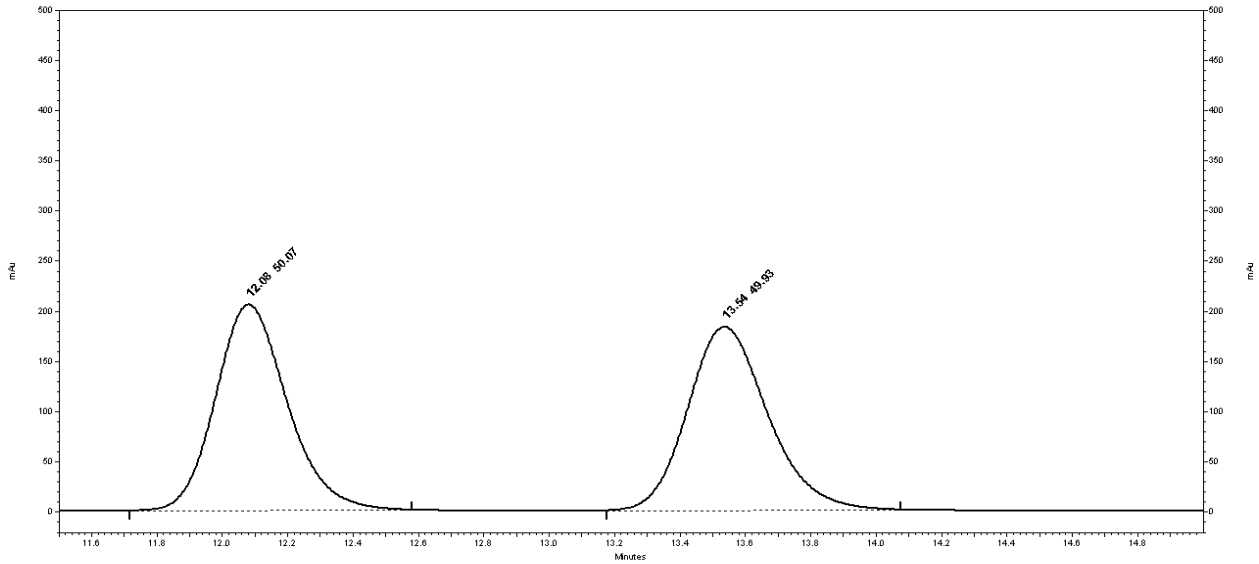

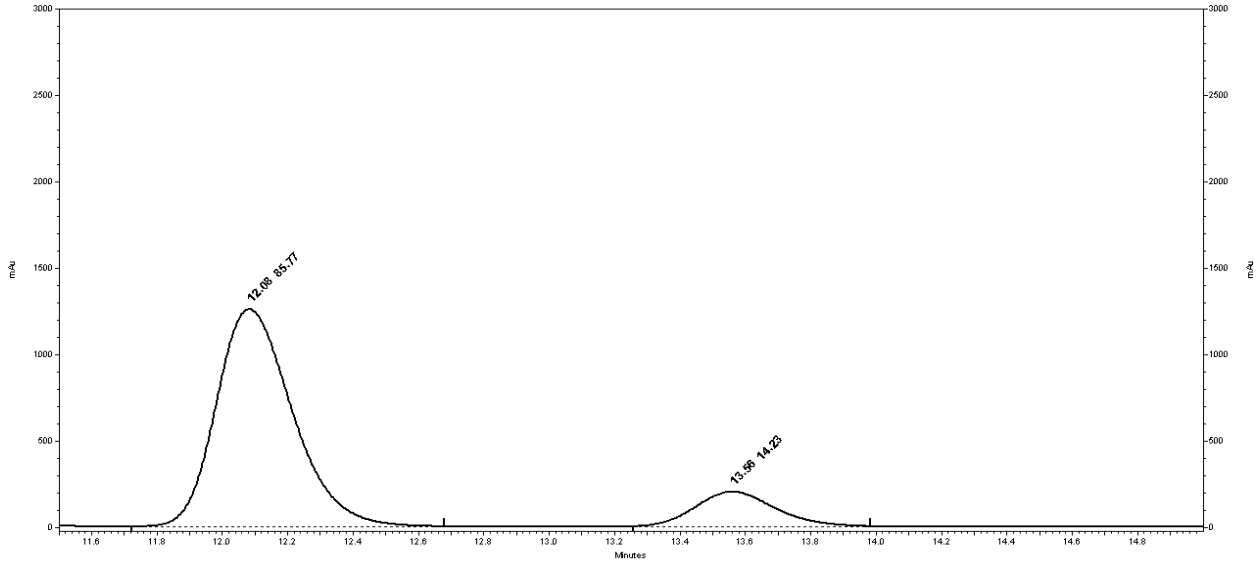

2-(hex-5-en-1-yn-3-yl)thiophene (SI 10)

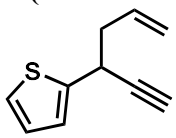

HPLC Chiralpak OD-H column (100:0 hexanes:isopropanol, 0.25 mL/min, 270 nm); first enantiomer t_r = 32.0 min, second enantiomer t_r = 36.0 min.

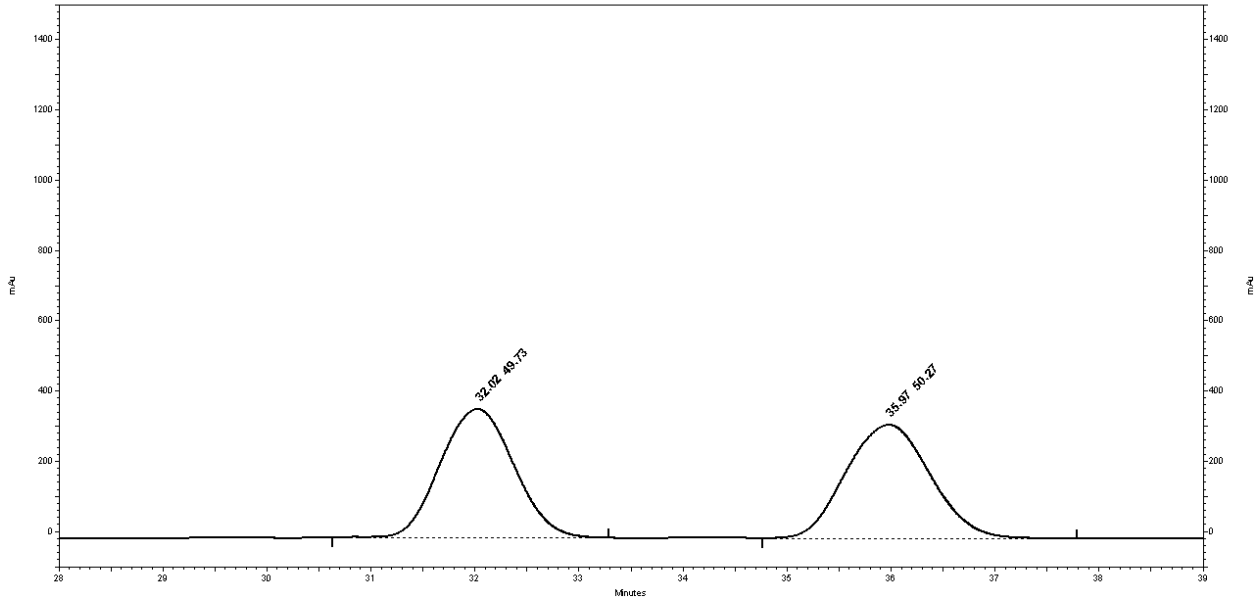

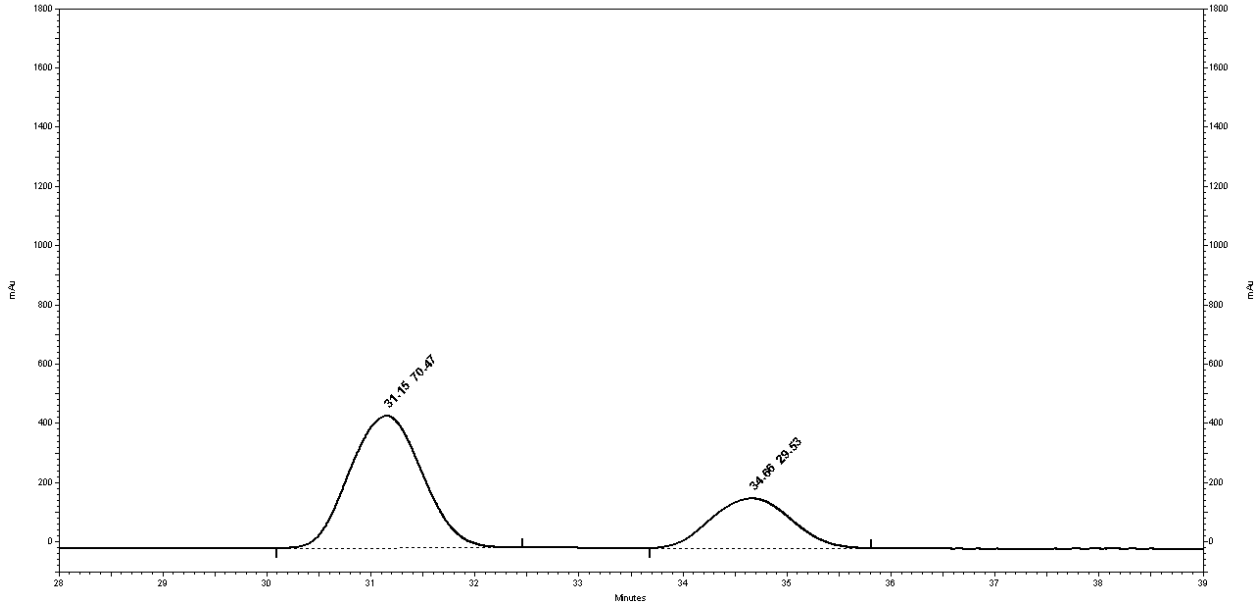

(2-ethynylpent-4-en-1-yl)benzene (SI 11)

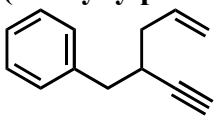

HPLC Chiralpak OD-H column (100:0 hexanes:isopropanol, 0.25 mL/min, 210 nm); first enantiomer t_r = 30.1 min, second enantiomer t_r = 33.1 min.

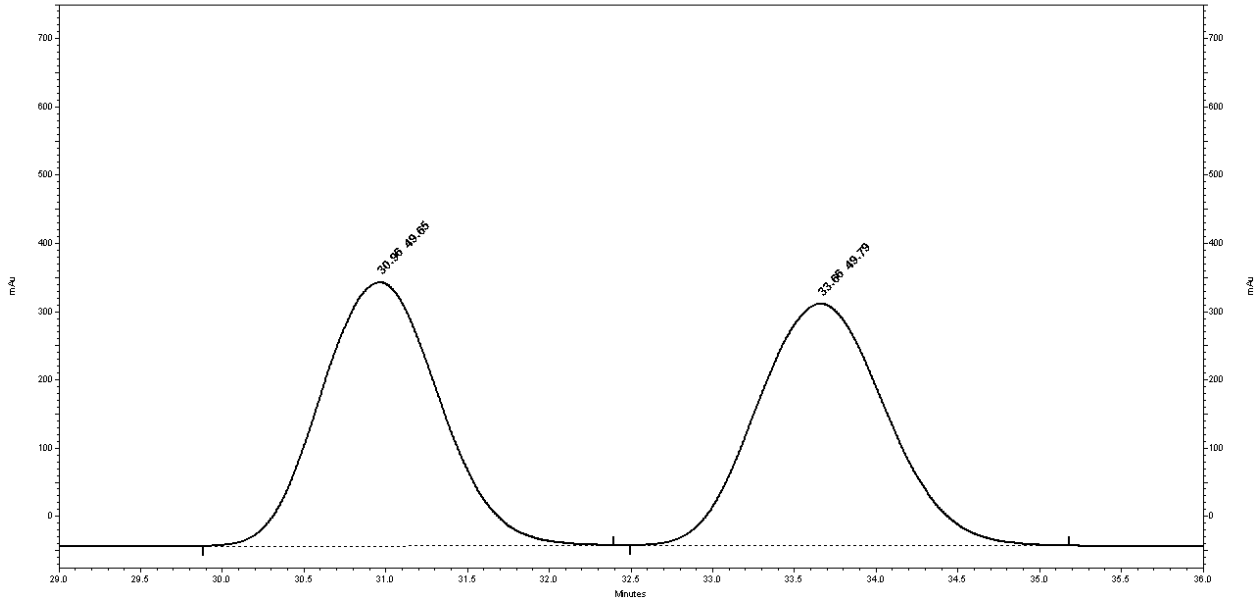

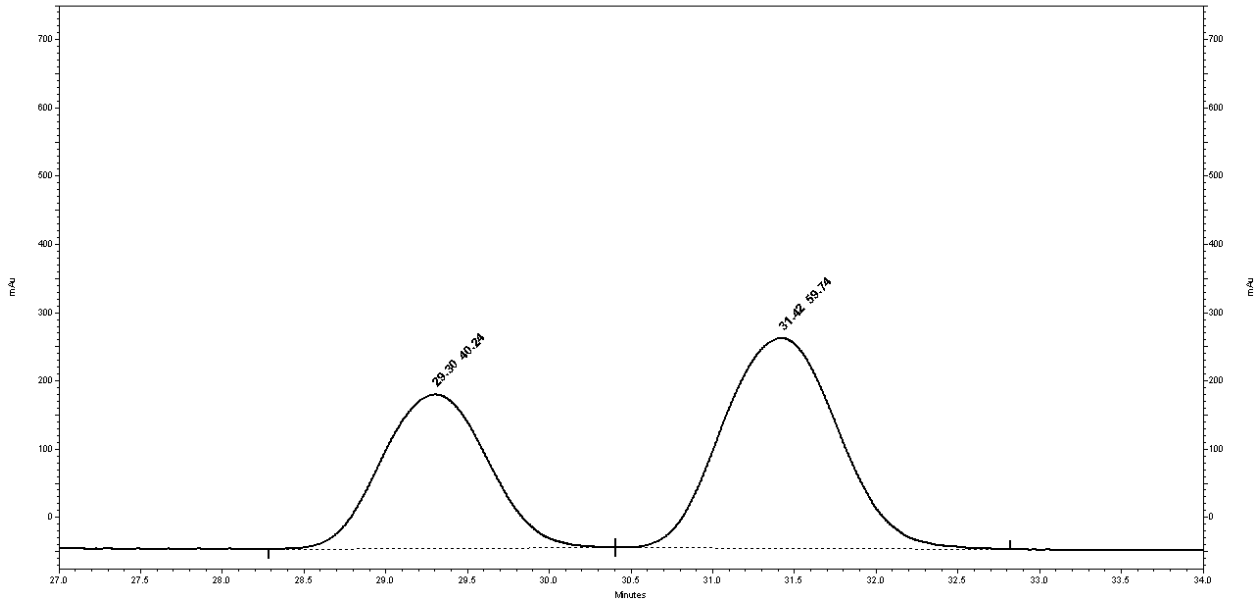

3-phenylbicyclo[3.1.0]hex-2-ene (SI 12)

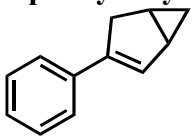

HPLC Chiralpak OD-H column (100:0 hexanes:isopropanol, 0.25 mL/min, 270 nm); first enantiomer t_r = 49.9 min, second enantiomer t_r = 58.1 min.

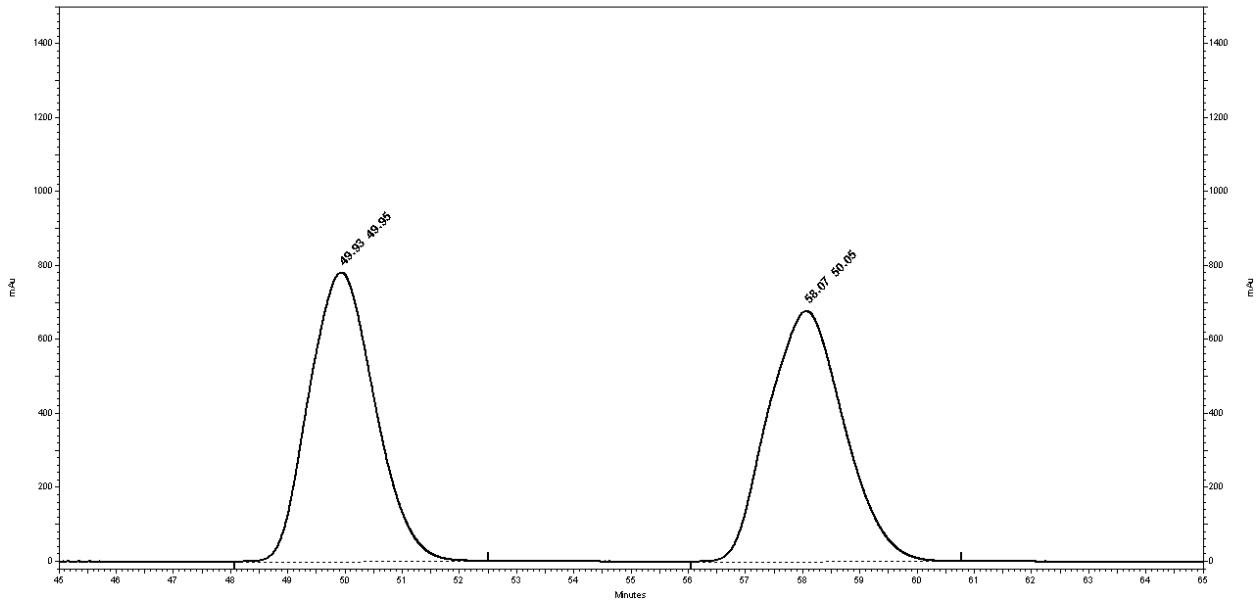

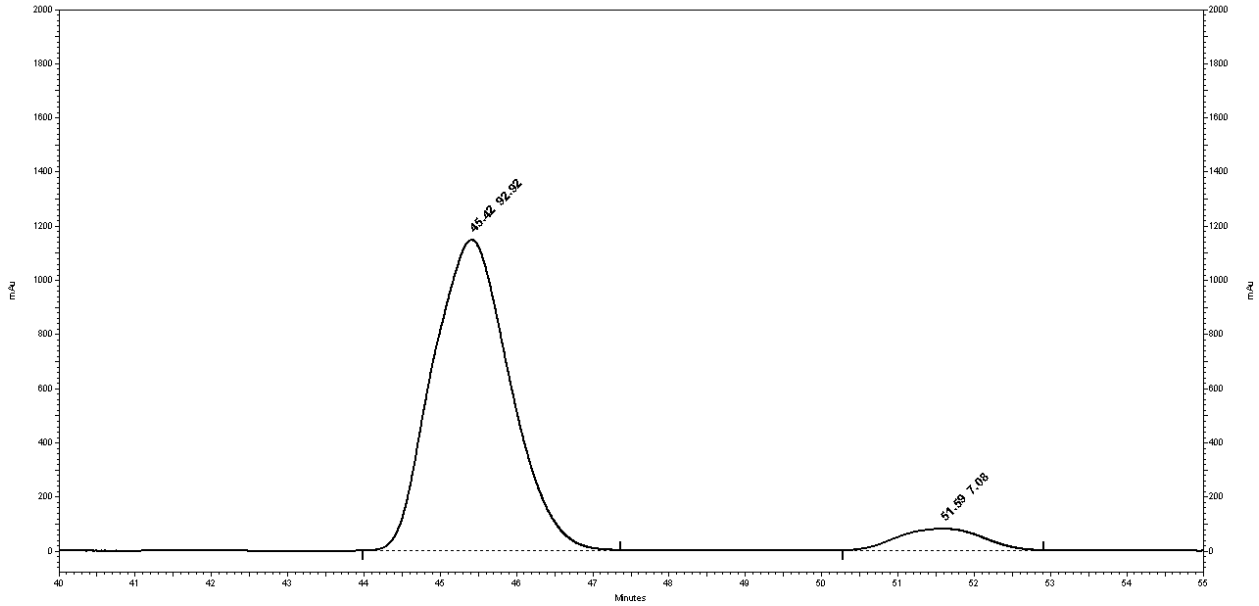

3-(4-(tert-butyl)phenyl)bicyclo[3.1.0]hex-2-ene (SI 13)

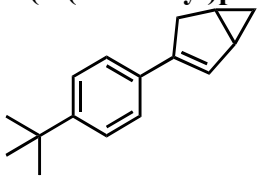

SFC OJ-H column (5% isopropanol, 2.5 mL/min, 210 nm); first enantiomer t_r = 3.4 min, second enantiomer t_r = 3.6 min.

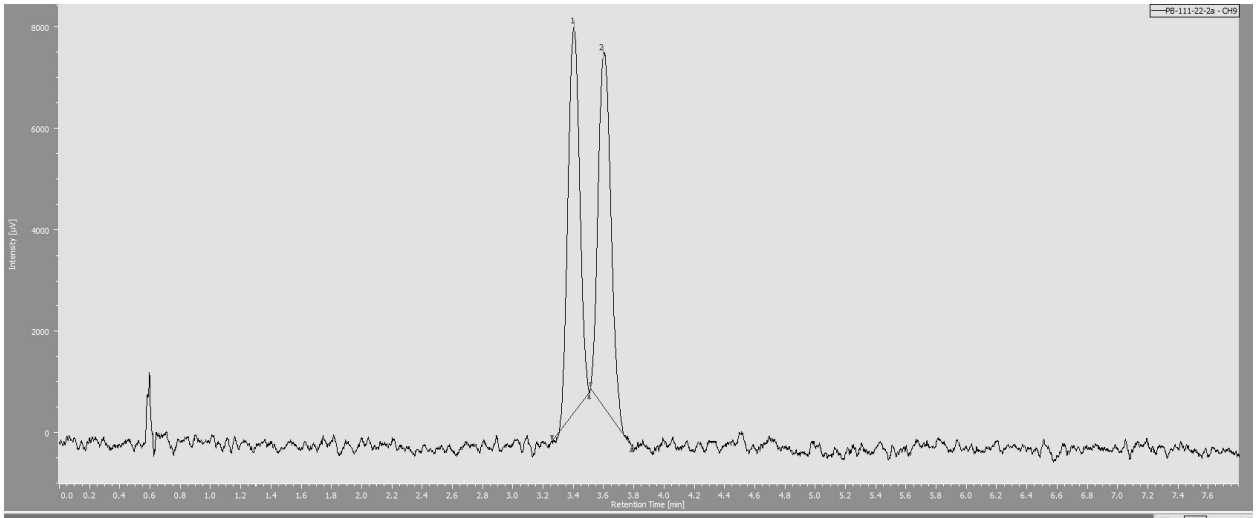

Peak Info. Table: PB-111-22-2a

#	Peak Name	CH	tR	Area	Height	Area%	Height%	Quantity	NTP	Resolution	Symmetry Factor	Warning
1	Unknown	9	3.402	40786	7600	49.678	52.212	N/A	8649	1.278	1.030	
2	Unknown	9	3.597	41314	6956	50.322	47.788	N/A	8115	N/A	1.237	

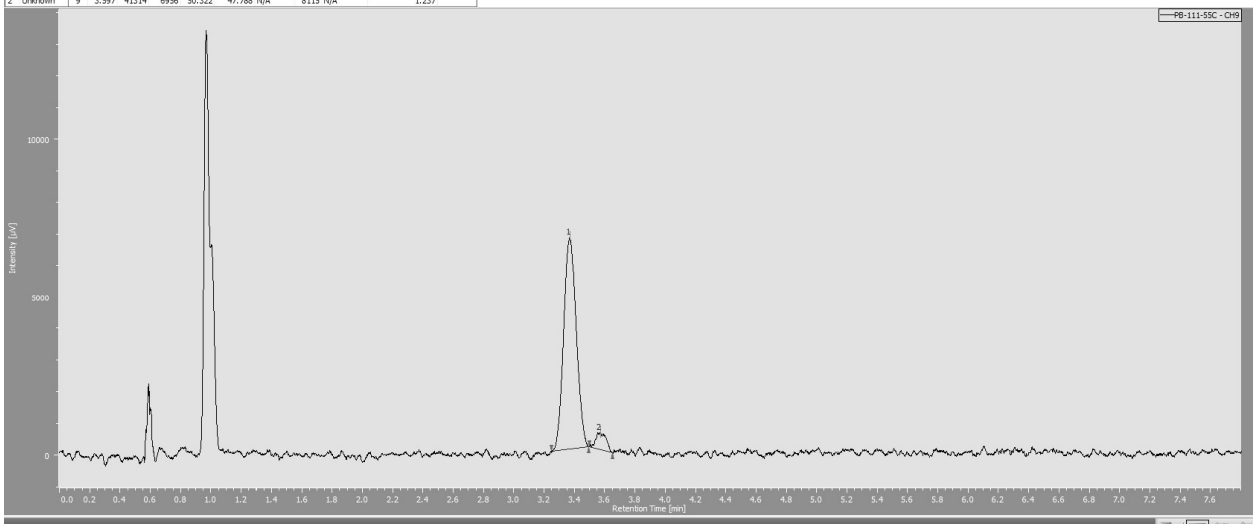

Peak Info. Table: PB-111-55C

#	Peak Name	CH	tR	Area	Height	Area%	Height%	Quantity	NTP	Resolution	Symmetry Factor	Warning
1	Unknown	9	3.368	38574	6685	93.919	92.530	N/A	7666	1.402	1.067	
2	Unknown	9	3.570	2498	540	6.081	7.470	N/A	11250	N/A	0.981	

3-(o-tolyl)bicyclo[3.1.0]hex-2-ene (SI 14)

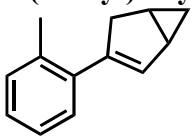

HPLC Chiralpak OD-H column (100:0 hexanes:isopropanol, 0.25 mL/min, 270 nm); first enantiomer t_r = 32.8 min, second enantiomer t_r = 36.0 min.

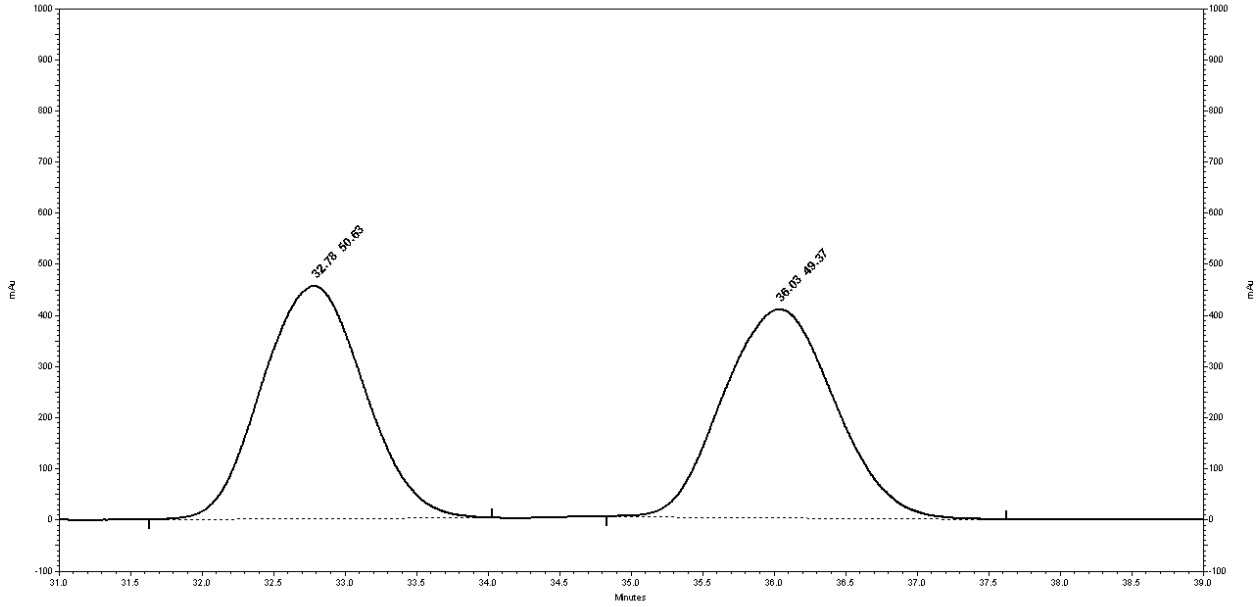

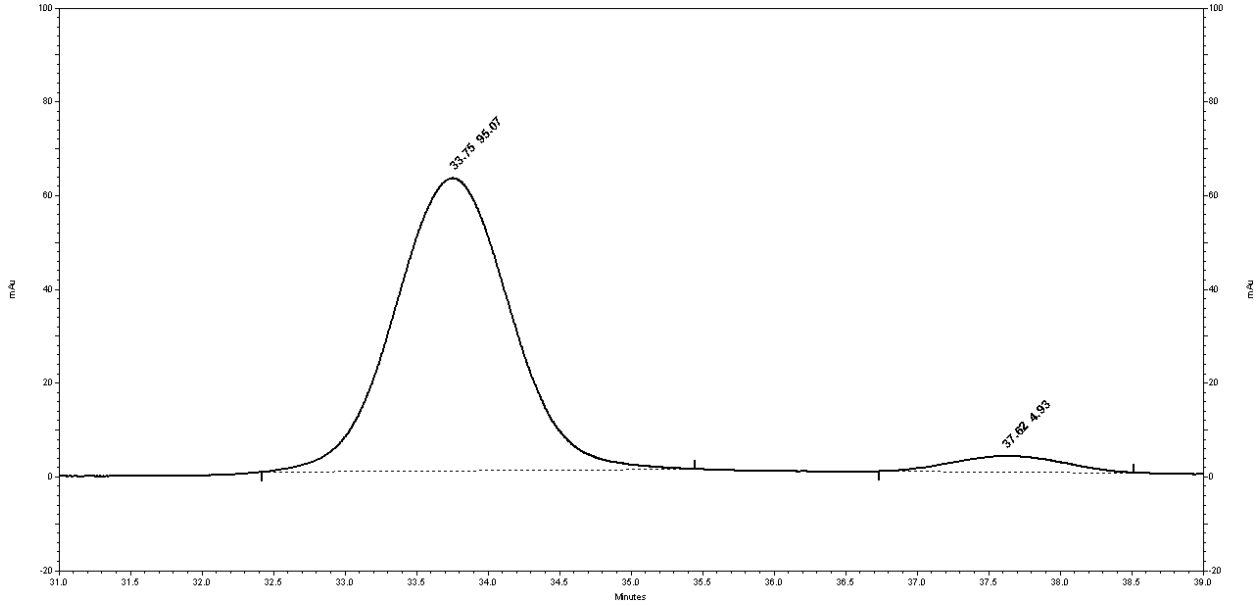

1-(bicyclo[3.1.0]hex-2-en-3-yl)naphthalene (SI 15)

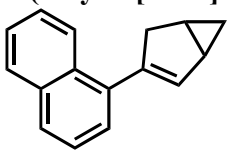

HPLC Chiralpak IB column (99.9:0.1 hexanes:isopropanol, 0.5 mL/min, 322 nm); first enantiomer t_r = 14.7min, second enantiomer t_r = 15.5 min.

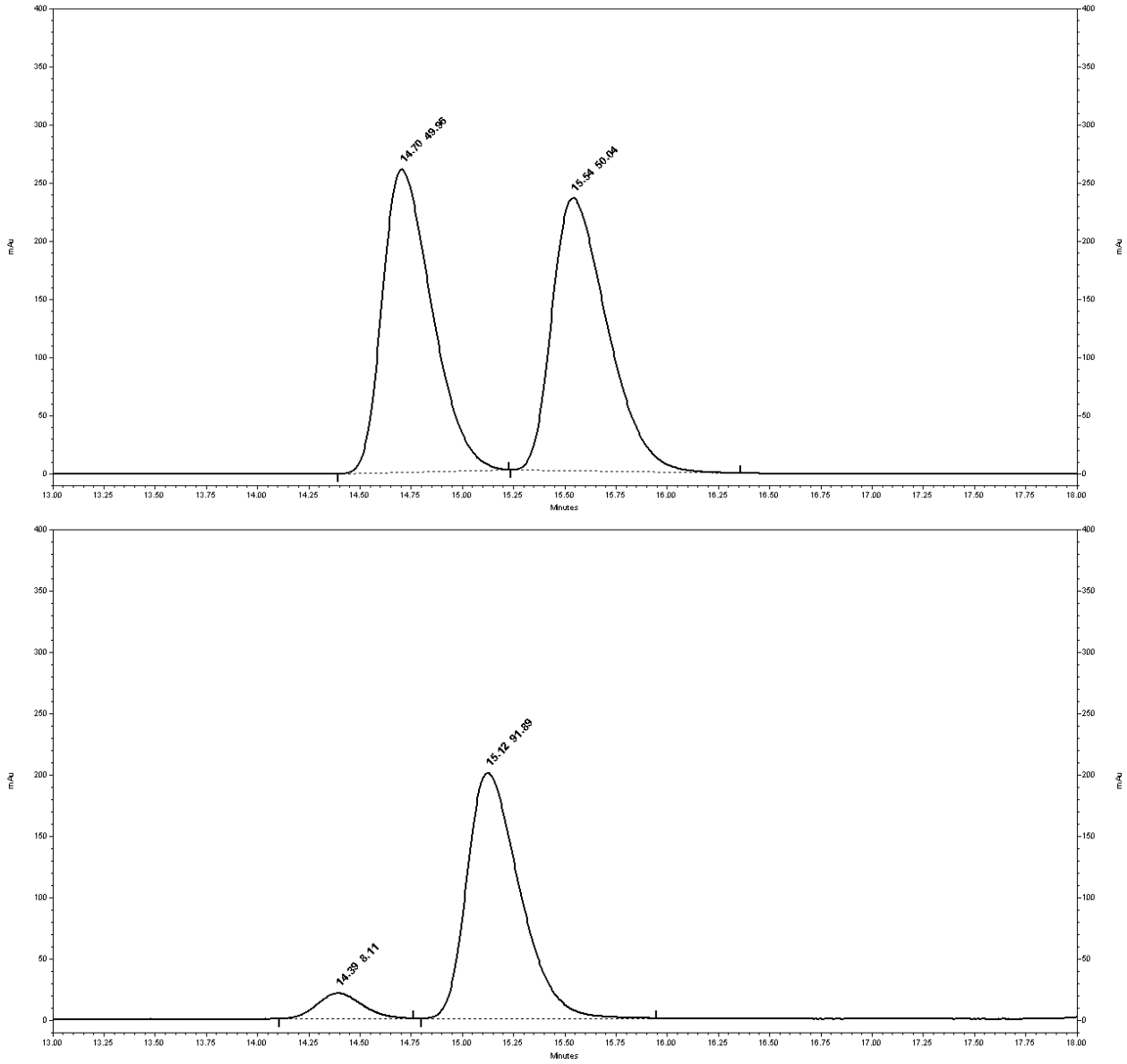

2-(bicyclo[3.1.0]hex-2-en-3-yl)naphthalene (SI 16)

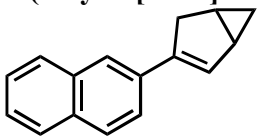

HPLC Chiralpak AD-H column (99.9:0.1 hexanes:isopropanol, 0.25 mL/min, 320 nm); first enantiomer t_r = 24.3 min, second enantiomer t_r = 26.1 min.

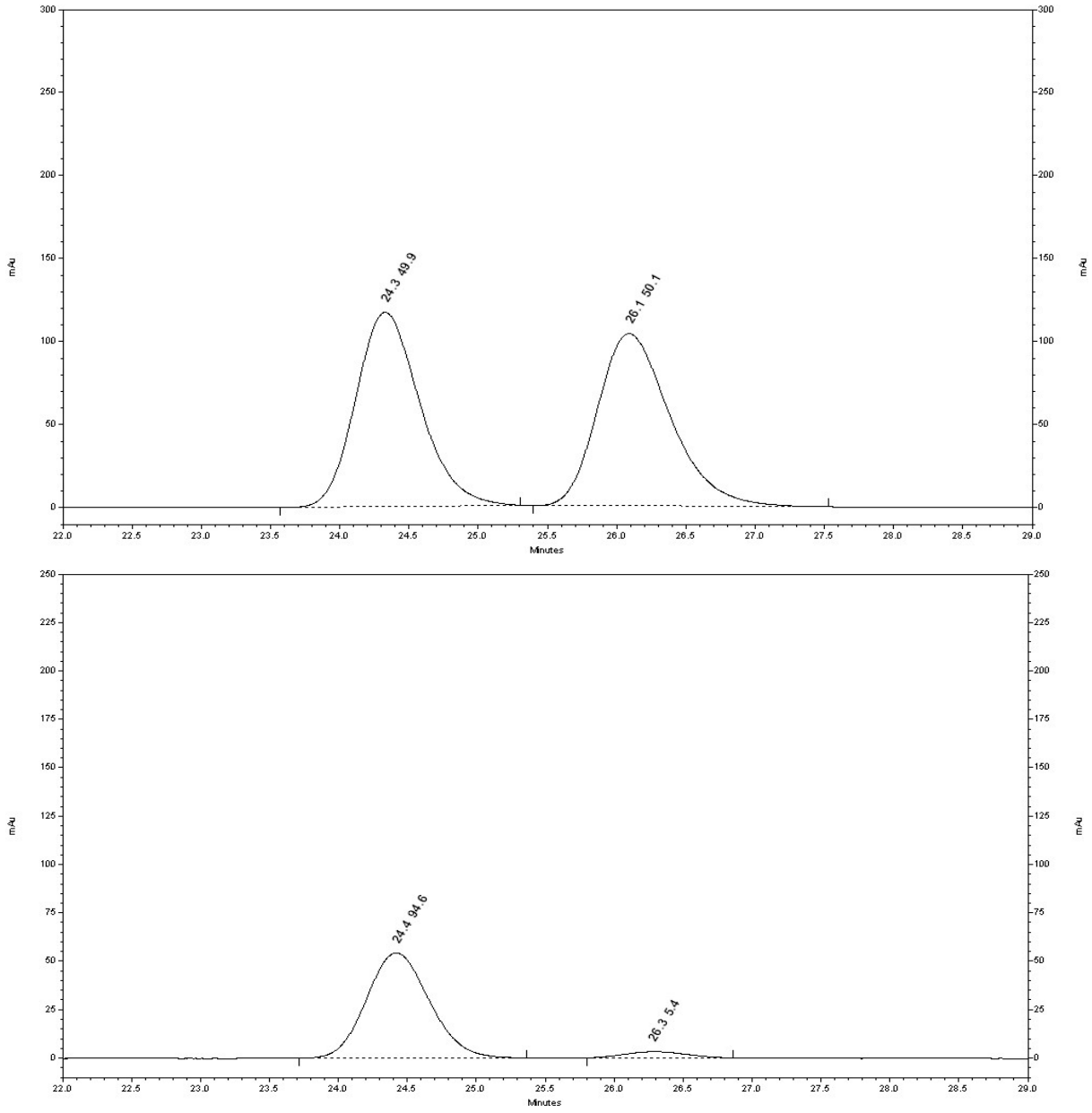

3-(4-methoxyphenyl)bicyclo[3.1.0]hex-2-ene (SI 17)

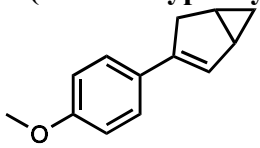

HPLC Chiralpak OJ column (99.5:0.5 hexanes:isopropanol, 1 mL/min, 300 nm); first enantiomer t_r = 12.4 min, second enantiomer t_r = 15.8 min.

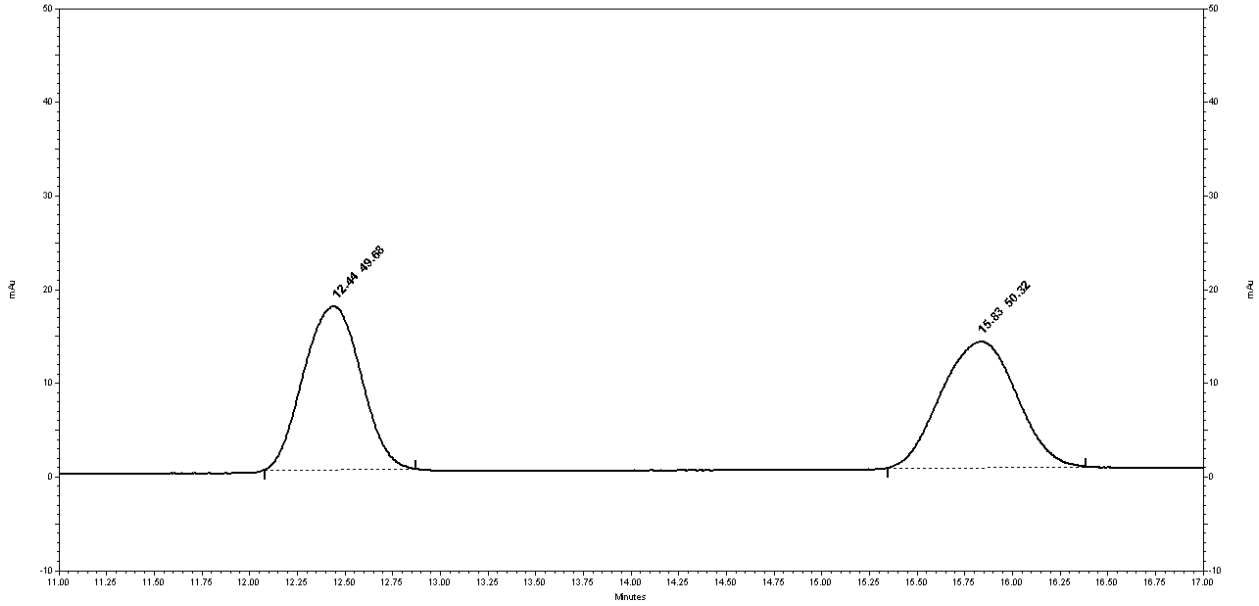

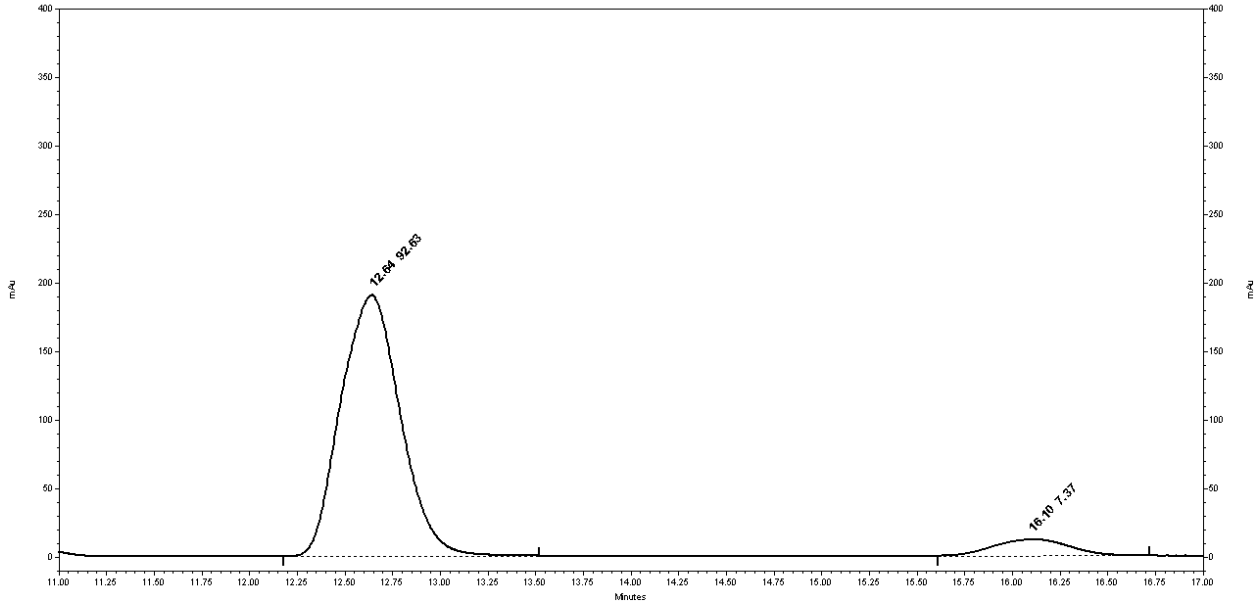

3-(4-iodophenyl)bicyclo[3.1.0]hex-2-ene (SI 18)

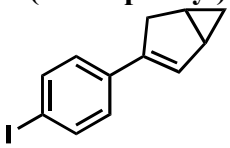

HPLC Chiralpak OJ column (99.5:0.5 hexanes:isopropanol, 1 mL/min, 270 nm); first enantiomer t_r = 16.8 min, second enantiomer t_r = 18.1 min.

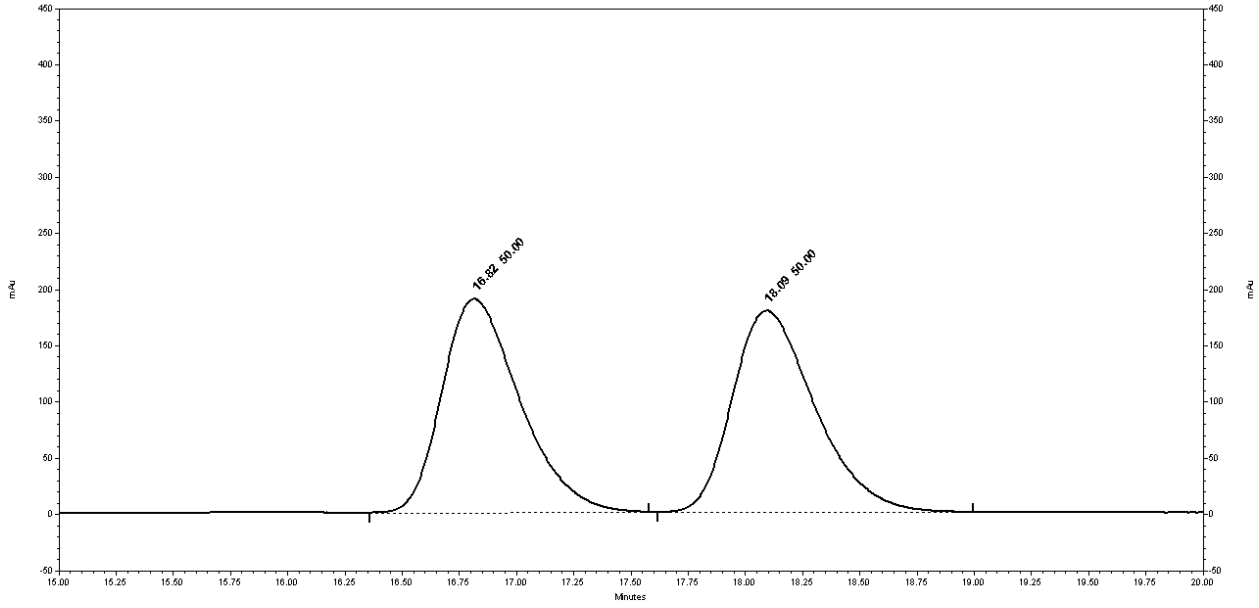

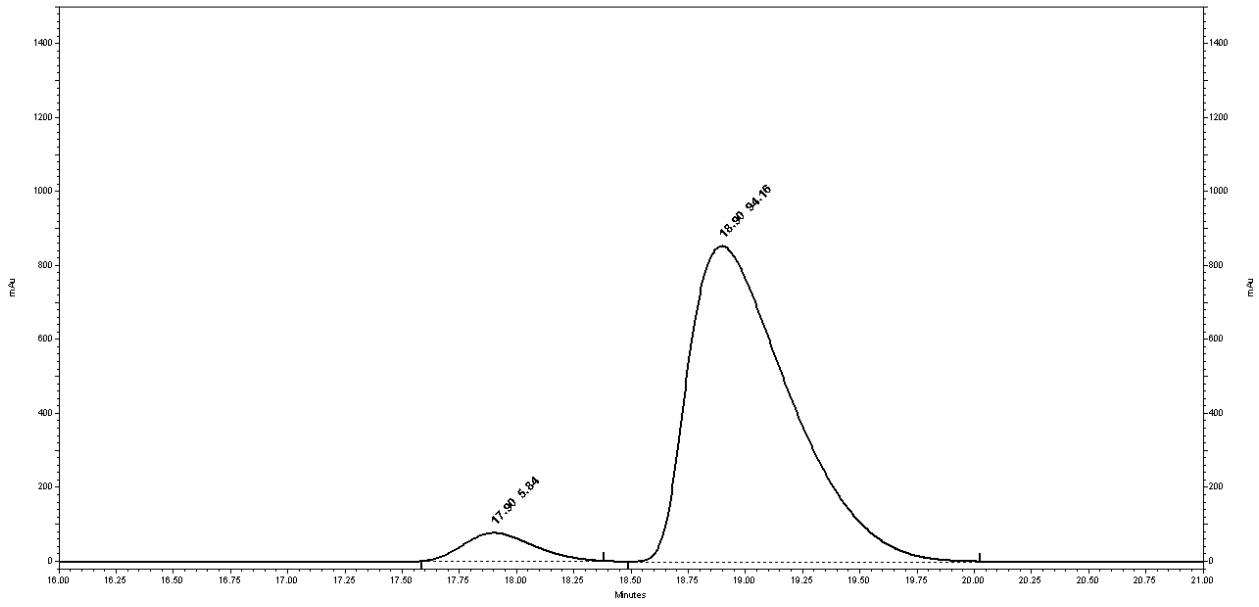

2-(bicyclo[3.1.0]hex-2-en-3-yl)benzofuran (SI 19)

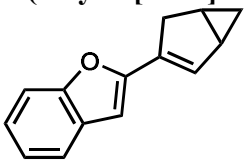

HPLC Chiralpak OD-H column (100:0 hexanes:isopropanol, 0.25 mL/min, 315 nm); first enantiomer t_r = 12.5 min, second enantiomer t_r = 14.6 min.

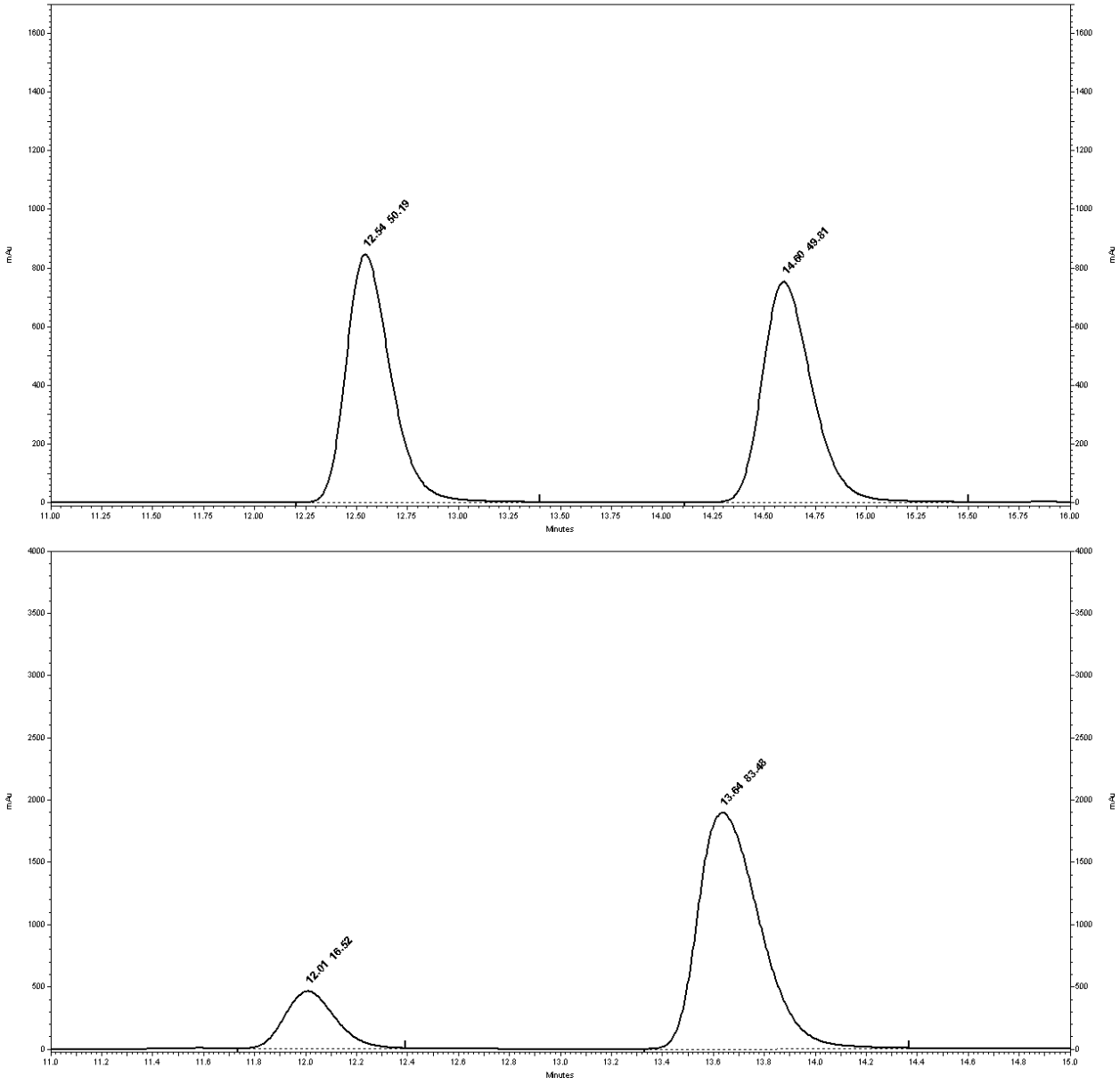

5-(bicyclo[3.1.0]hex-2-en-3-yl)-1-tosyl-1H-indole (SI 20)

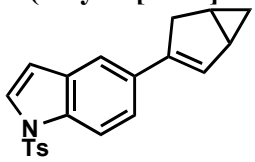

HPLC Chiralpak IA column (95:5 hexanes:isopropanol, 1 mL/min, 230 nm); first enantiomer t_r = 15.6 min, second enantiomer t_r = 20.9 min.

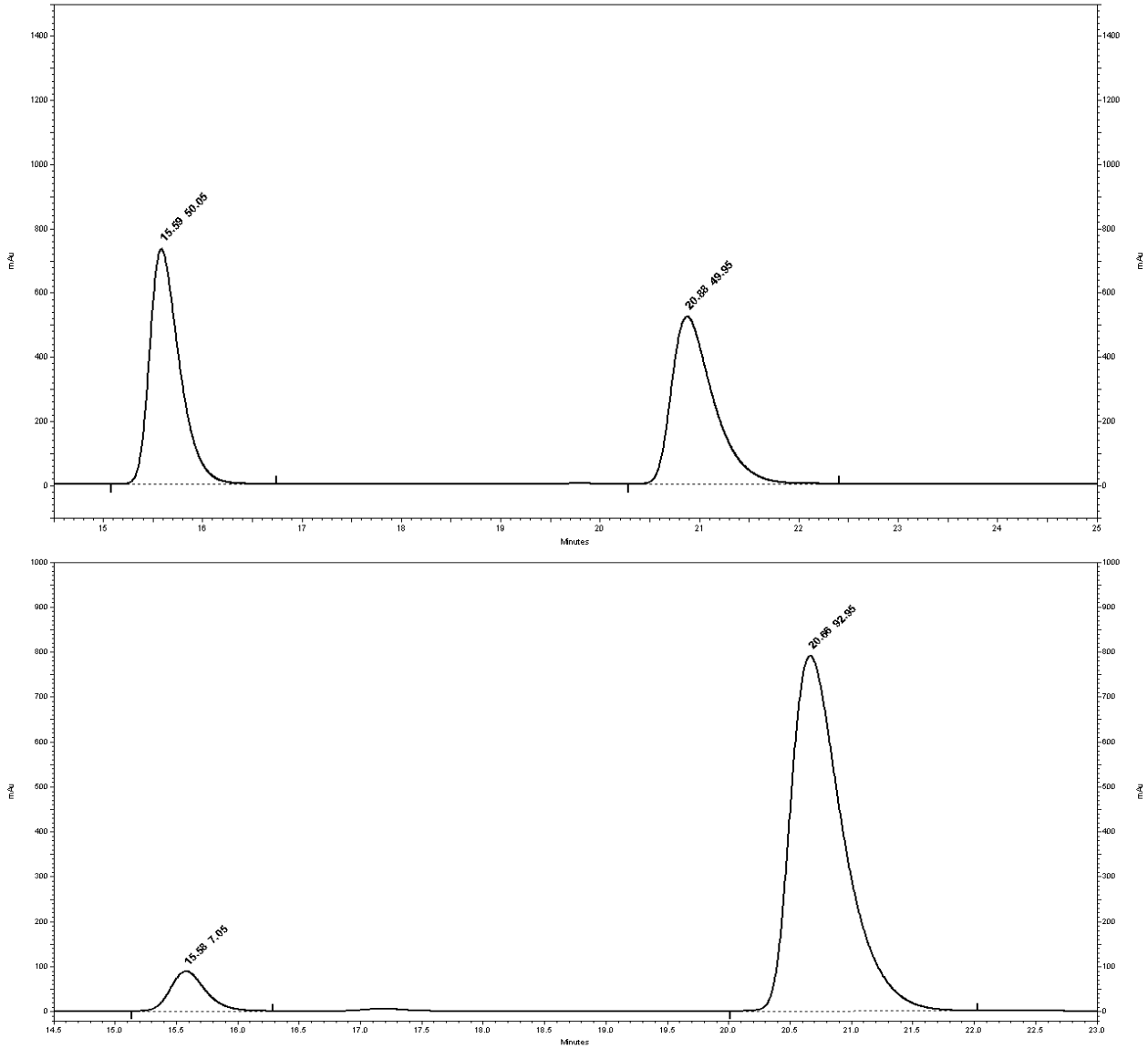

2-(bicyclo[3.1.0]hex-2-en-3-yl)thiophene (SI 21)

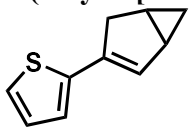

HPLC Chiralpak OD-H column (100:0 hexanes:isopropanol, 0.25 mL/min, 210 nm); first enantiomer t_r = 42.1 min, second enantiomer t_r = 44.3 min.

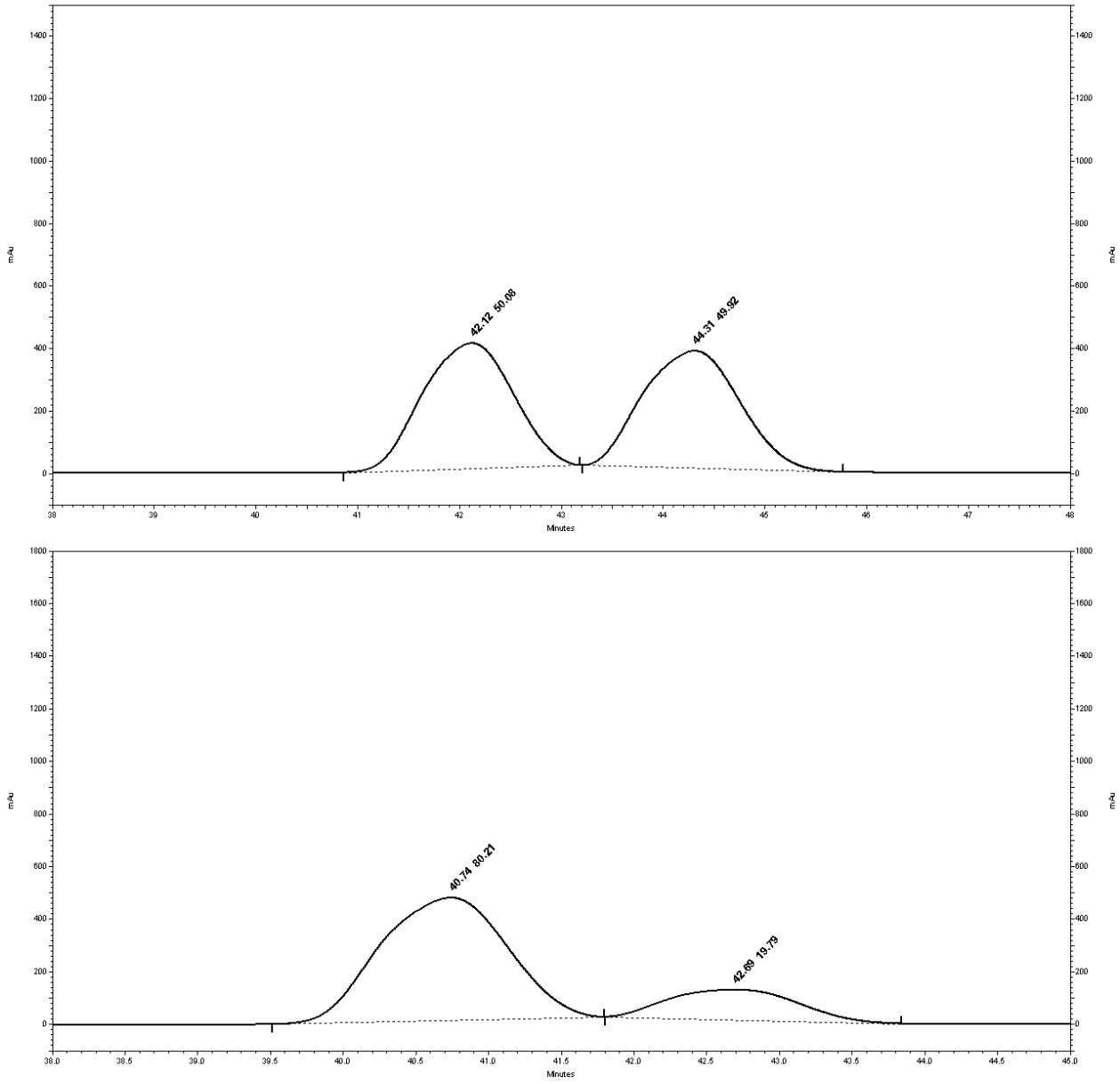

2.4.8 Crystallographic Data

Table 1. Crystal data and structure refinement for 3.

Identification code	rt002	
Empirical formula	C43 H40 Au Cl N4	
Formula weight	845.20	
Temperature	100(2) K	
Wavelength	0.71073 Å	
Crystal system	Monoclinic	
Space group	P 21	
Unit cell dimensions	a = 13.7541(10) Å	a= 90°.
	b = 16.5763(12) Å	b= 104.083(3)°.
	c = 16.6586(12) Å	g = 90°.
Volume	3683.9(5) $Å^3$	
Z	4	
Density (calculated)	1.524 Mg/m^3	
Absorption coefficient	4.102 mm^{-1}	
F(000)	1688	
Crystal size	0.180 x 0.120 x 0.100 mm^3	
Theta range for data collection	1.260 to 25.391°.	
Index ranges	-16<=h<=16, -19<=k<=19, -20<=l<=20	
Reflections collected	118416	
Independent reflections	13402 [R(int) = 0.0252]	
Completeness to theta = 25.000°	100.0 %	
Absorption correction	Semi-empirical from equivalents	
Max. and min. transmission	0.745 and 0.533	
Refinement method	Full-matrix least-squares on F^2	
Data / restraints / parameters	13402 / 1 / 887	
Goodness-of-fit on F^2	1.022	
Final R indices [I>2sigma(I)]	R1 = 0.0120, wR2 = 0.0269	
R indices (all data)	R1 = 0.0125, wR2 = 0.0270	
Absolute structure parameter	-0.0049(10)	
Extinction coefficient	n/a	
Largest diff. peak and hole	0.580 and -0.374 $e.Å^{-3}$	

Table 2. Atomic coordinates (x 10^4) and equivalent isotropic displacement parameters ($Å^2$x 10^3) for **3**. U(eq) is defined as one third of the trace of the orthogonalized U^{ij} tensor.

	x	y	z	U(eq)
C(1)	3198(2)	5725(2)	5684(2)	16(1)
C(2)	4010(2)	5257(2)	6039(2)	22(1)
C(3)	4797(2)	5123(2)	5648(2)	24(1)
C(4)	4762(2)	5453(2)	4906(2)	22(1)
C(5)	3942(2)	5944(2)	4502(2)	19(1)
C(6)	3896(3)	6293(2)	3721(2)	24(1)
C(7)	3106(2)	6758(2)	3333(2)	25(1)
C(8)	2307(2)	6887(2)	3712(2)	22(1)
C(9)	2326(2)	6553(2)	4460(2)	18(1)
C(10)	3138(2)	6078(2)	4893(2)	15(1)
C(11)	2380(2)	5867(2)	6142(2)	17(1)
C(12)	2206(3)	5153(2)	6672(2)	26(1)
C(13)	1935(2)	7072(2)	6875(2)	13(1)
C(14)	3617(2)	6733(2)	7194(2)	19(1)
C(15)	3489(2)	7520(2)	7620(2)	17(1)
C(16)	1893(2)	8266(2)	7781(2)	15(1)
C(17)	1670(2)	8948(2)	7158(2)	19(1)
C(18)	2522(2)	8520(2)	8624(2)	15(1)
C(19)	2494(2)	8057(2)	9342(2)	15(1)
C(20)	1920(2)	7347(2)	9313(2)	20(1)
C(21)	1926(2)	6922(2)	10021(2)	26(1)
C(22)	2499(3)	7186(2)	10794(2)	29(1)
C(23)	3056(3)	7872(2)	10843(2)	26(1)
C(24)	3086(2)	8324(2)	10128(2)	20(1)
C(25)	3714(2)	9000(2)	10170(2)	27(1)
C(26)	3752(2)	9414(2)	9472(2)	30(1)
C(27)	3144(2)	9179(2)	8700(2)	25(1)
C(28)	345(2)	7651(2)	5374(2)	15(1)
C(29)	1144(2)	8059(2)	5203(2)	18(1)
C(30)	1015(2)	8547(2)	4503(2)	23(1)

C(31)	69(3)	8616(2)	3969(2)	27(1)
C(32)	-730(3)	8202(2)	4132(2)	24(1)
C(33)	-610(2)	7718(2)	4833(2)	21(1)
C(34)	-1405(2)	7258(2)	5077(2)	21(1)
C(35)	-2409(2)	7227(2)	4629(2)	26(1)
C(36)	-3094(2)	6778(2)	4925(2)	35(1)
C(37)	-2791(2)	6364(3)	5662(2)	36(1)
C(38)	-1796(2)	6389(2)	6110(2)	31(1)
C(39)	-1101(2)	6836(2)	5826(2)	21(1)
C(40)	3004(2)	2097(2)	1340(2)	21(1)
C(41)	3806(2)	1853(2)	981(2)	23(1)
C(42)	4149(3)	2315(2)	395(2)	29(1)
C(43)	4941(3)	2063(3)	86(2)	39(1)
C(44)	5423(3)	1335(3)	357(2)	41(1)
C(45)	5114(3)	862(3)	913(2)	35(1)
C(46)	4300(3)	1107(2)	1249(2)	27(1)
C(47)	3995(3)	633(2)	1834(2)	31(1)
C(48)	3240(3)	879(2)	2178(2)	30(1)
C(49)	2758(2)	1629(2)	1933(2)	24(1)
C(50)	2450(3)	2881(2)	1059(2)	22(1)
C(51)	1680(3)	2784(2)	229(2)	33(1)
C(52)	2379(2)	3776(2)	2224(2)	15(1)
C(53)	918(2)	3045(2)	1704(2)	24(1)
C(54)	851(2)	3462(2)	2505(2)	25(1)
C(55)	1989(2)	4504(2)	3416(2)	16(1)
C(56)	2525(2)	4021(2)	4175(2)	20(1)
C(57)	1051(2)	4945(2)	3526(2)	15(1)
C(58)	682(2)	4817(2)	4208(2)	18(1)
C(59)	-117(2)	5274(2)	4356(2)	20(1)
C(60)	-542(2)	5865(2)	3828(2)	19(1)
C(61)	-205(2)	6018(2)	3098(2)	18(1)
C(62)	-618(2)	6649(2)	2548(2)	23(1)
C(63)	-294(2)	6795(2)	1854(2)	27(1)
C(64)	469(2)	6309(2)	1674(2)	24(1)
C(65)	904(2)	5709(2)	2198(2)	18(1)
C(66)	590(2)	5547(2)	2933(2)	16(1)

C(67)	4638(2)	3814(2)	3181(2)	17(1)
C(68)	4435(2)	3083(2)	3512(2)	21(1)
C(69)	5124(2)	2756(2)	4186(2)	25(1)
C(70)	6004(2)	3163(2)	4534(2)	27(1)
C(71)	6228(2)	3880(2)	4189(2)	22(1)
C(72)	5552(2)	4207(2)	3497(2)	17(1)
C(73)	5721(2)	4931(2)	3044(2)	18(1)
C(74)	6569(2)	5428(2)	3246(2)	21(1)
C(75)	6649(2)	6075(2)	2740(2)	25(1)
C(76)	5903(2)	6237(2)	2040(2)	26(1)
C(77)	5044(2)	5755(2)	1847(2)	20(1)
C(78)	4949(2)	5102(2)	2338(2)	16(1)
C(79)	1866(3)	4066(3)	8391(3)	49(1)
C(80)	2186(4)	4765(3)	8889(3)	68(2)
C(81)	4508(3)	3529(3)	7406(3)	45(1)
C(82)	4746(3)	3090(3)	6724(3)	62(1)
C(83)	7894(3)	3908(3)	7410(3)	46(1)
C(84)	8897(3)	3851(4)	7952(3)	78(2)
C(85)	9205(5)	4856(4)	10045(4)	89(2)
C(86)	8423(3)	5388(3)	10142(3)	65(1)
N(1)	2611(2)	6611(1)	6642(1)	13(1)
N(2)	2383(2)	7580(2)	7464(1)	14(1)
N(3)	1971(2)	3205(2)	1689(2)	18(1)
N(4)	1753(2)	3977(2)	2686(2)	16(1)
N(5)	1616(4)	3522(3)	7995(3)	88(2)
N(6)	4316(3)	3880(2)	7935(3)	61(1)
N(7)	7120(3)	3946(2)	6986(3)	63(1)
N(8)	9818(6)	4424(6)	9971(5)	191(4)
Cl(1)	289(1)	6187(1)	7570(1)	25(1)
Cl(2)	2740(1)	5090(1)	1059(1)	23(1)
Au(1)	395(1)	6954(1)	6387(1)	16(1)
Au(2)	3701(1)	4400(1)	2229(1)	14(1)

2.5 Notes and References

(17) Marinetti, A.; Jullien, H.; Voituriez, A. *Chem. Soc. Rev.* **2012**, *41*, 4884–4908.
(18) Hu, Y.; Bai, M.; Yang, Y.; Zhou, Q. *Org. Chem. Front.* **2017**, *4*, 2256–2275.
(19) Trost, B. M.; Krische, M. J. *Synlett* **1998**, 1–16.
(20) Trost, B. M. *Acc. Chem. Res.* **1990**, *23*, 34–42.
(21) Aubert, C.; Buisine, O.; Malacria, M. *Chem. Rev.* **2002**, *102*, 813–834.
(22) Ojima, I.; Tzamarioudaki, M.; Li, Z.; Donovan, R. J. *Chem. Rev.* **1996**, *96*, 635–662.
(23) Zhang, L.; Sun, J.; Kozmin, S. a. *Adv. Synth. Catal.* **2006**, *348*, 2271–2296.
(24) Lautens, M.; Klute, W.; Tam, W. *Chem. Rev.* **1996**, *96*, 49–92.
(25) Echavarren, A. M.; Nevado, C. *Chem. Soc. Rev.* **2004**, *33*, 431–436.
(26) Bruneau, C. *Angew. Chem. Int. Ed.* **2005**, *44*, 2328–2334.
(27) Michelet, V.; Toullec, P. Y.; Genêt, J. P. *Angew. Chem. Int. Ed.* **2008**, *47*, 4268–4315.
(28) Wang, S.; Zhang, L. *J. Am. Chem. Soc.* **2006**, *128*, 14274–14275.
(29) Fukamizu, K.; Miyake, Y.; Nishibayashi, Y. *Angew. Chem. Int. Ed.* **2009**, *48*, 2534–2537.
(30) Chen, G. Q.; Fang, W.; Wei, Y.; Tang, X. Y.; Shi, M. *Chem. Sci.* **2016**, *7*, 4318–4328.
(31) Mamane, V.; Gress, T.; Krause, H.; Fürstner, A. *J. Am. Chem. Soc.* **2004**, *126*, 8654–8655.
(32) Harrak, Y.; Blaszykowski, C.; Bernard, M.; Cariou, K.; Mainetti, E.; Mouriès, V.; Dhimane, A. L.; Fensterbank, L.; Malacria, M. *J. Am. Chem. Soc.* **2004**, *126*, 8656–8657.
(33) Luzung, M. R.; Markham, J. P.; Toste, F. D. *J. Am. Chem. Soc.* **2004**, *126*, 10858–10859.
(34) Wu, Z.; Retailleau, P.; Gandon, V.; Voituriez, A.; Marinetti, A. *Eur. J. Org. Chem.* **2016**, *2016*, 70–75.
(35) Brazeau, J. F.; Zhang, S.; Colomer, I.; Corkey, B. K.; Toste, F. D. *J. Am. Chem. Soc.* **2012**, *134*, 2742–2749.
(36) Patil, N. T. *Chem. - An Asian J.* **2012**, *7*, 2186–2194.
(37) Dorel, R.; Echavarren, A. M. *Chem. Rev.* **2015**, *115*, 9028–9072.
(38) Harris, R. J.; Widenhoefer, R. A. *Chem. Soc. Rev.* **2016**, *45*, 4533–4551.
(39) Bohan, P. T.; Dean Toste, F. *J. Am. Chem. Soc.* **2017**, *139*, 11016–11019.
(40) Nagao, I.; Shimizu, M.; Hiyama, T. *Angew. Chem. Int. Ed.* **2009**, *48*, 7573–7576.
(41) Fürstner, A.; Alcarazo, M.; César, V.; Lehmann, C. W. *Chem. Commun.* **2006**, No. 20, 2176–2178.
(42) Biasiolo, L.; Del Zotto, A.; Zuccaccia, D. *Organometallics* **2015**, *34*, 1759–1765.
(43) Jia, M.; Bandini, M. *ACS Catal.* **2015**, *5*, 1638–1652.
(44) Xia, Y.; Dudnik, A. S.; Gevorgyan, V.; Li, Y. *J. Am. Chem. Soc.* **2008**, *130*, 6940–6941.
(45) LaLonde, R. L.; Sherry, B. D.; Kang, E. J.; Toste, F. D. *J. Am. Chem. Soc.* **2007**, *129*, 2452–2453.
(46) Keith, J. M.; Larrow, J. F.; Jacobsen, E. N. *Adv. Synth. Catal.* **2001**, *343*, 5–26.
(47) Rachwalski, M.; Vermue, N.; Rutjes, F. P. J. T. *Chem. Soc. Rev.* **2013**, *42*, 9268–9282.
(48) Bhat, V.; Welin, E. R.; Guo, X.; Stoltz, B. M. *Chem. Rev.* **2017**, *117*, 4528–4561.
(49) Martin, V. S.; Woodard, S. S.; Katsuki, T.; Yamada, Y.; Ikeda, M.; Sharpless, K. B. *J. Am. Chem. Soc.* **1981**, *103*, 6237–6240.
(50) Ito, H.; Kunii, S.; Sawamura, M. *Nat. Chem.* **2010**, *2*, 972–976.
(51) Lundin, P.; Fu, G. *Synfacts* **2010**, 1277–1277.
(52) Chen, M.; Roush, W. R. *J. Am. Chem. Soc.* **2011**, *133*, 5744–5747.
(53) Langlois, J. B.; Emery, D.; Mareda, J.; Alexakis, A. *Chem. Sci.* **2012**, *3*, 1062–1069.
(54) Delvos, L. B.; Oestreich, M. *Synthesis* **2015**, *47*, 924–933.

(55) Mohr, J. T.; Moore, J. T.; Stoltz, B. M. *Beilstein J. Org. Chem.* **2016**, *12*, 2038–2045.
(56) Winn, C. L.; Guillen, F.; Pytkowicz, J.; Roland, S.; Mangeney, P.; Alexakis, A. *J. Organomet. Chem.* **2005**, *690*, 5672–5695.
(57) Campbell, C. D.; Concellón, C.; Smith, A. D. *Tetrahedron Asymmetry* **2011**, *22*, 797–811.
(58) Urban, S.; Ortega, N.; Glorius, F. *Angew. Chem. Int. Ed.* **2011**, *50*, 3803–3806.
(59) Katayev, D.; Jia, Y.; Sharma, A. K.; Banerjee, D.; Sunoj, R. B. *Chem. - A Eur. J.* **2013**, *19*, 11916–11927.
(60) Zhan, Z. P.; Yu, J. L.; Liu, H. J.; Cui, Y. Y.; Yang, R. F.; Yang, W. Z.; Li, J. P. *J. Org. Chem.* **2006**, *71*, 8298–8301.
(61) Ardolino, M. J.; Morken, J. P. *J. Am. Chem. Soc.* **2012**, *134*, 8770–8773.
(62) Ardolino, M. J.; Eno, M. S.; Morken, J. P. *Adv. Synth. Catal.* **2013**, *355*, 3413–3419.

Chapter 3

Highly Enantioselective Mukaiyama-Michael Addition Controlled by Chiral Phosphoramidite Gold(III) Catalysts

3.1 Introduction

Conjugate addition reactions to α,β-unsaturated carbonyl compounds are one of the most commonly used and powerful methods used to generate carbon-carbon bonds.[63,64] In 1974 Mukaiyama and coworkers reported the Lewis acid-catalyzed conjugate addition of a silyl enol ether to α,β-unsaturated carbonyl compounds, giving rise to the term Mukaiyama-Michael addition (Scheme 2.1).[65] Since this first report there have been extensive efforts made towards developing asymmetric Mukaiyama-Michael addition reactions due to their widespread use in organic synthesis.[66] While there has been significant progress for numerous classes of α,β-unsaturated carbonyl compounds, α,β-unsaturated aldehydes have only seen limited progress due to their propensity to undergo 1,2-addition when coordinated by Lewis acid.[67,68]

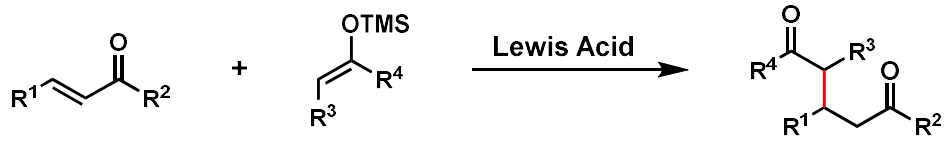

Scheme 3.1 General reaction scheme for a Mukaiyama-Michael Addition.

In 2003 MacMillan and coworkers reported the first enantioselective organocatalytic Mukaiyama-Michael reaction wherein they synthesized highly enantioenriched γ-butenolides via chiral iminium catalysis with α,β-unsaturated aldehydes.[66] At the time, the scope of the reaction was limited to siloxy-furans as the nucleophilic partner in the reaction. In 2005, Wang and coworkers developed an enantioselective organocatalytic Mukaiyama-Michael reaction with α,β-unsaturated aldehydes and silyl enol ethers by taking advantage of the iminium catalysis developed previously by MacMillan and coworkers.[69] This work was further expanded upon by MacMillan and coworkers in 2009 where they disclosed that silyl ketene thioacetals were competent nucleophiles in the asymmetric transformation (Scheme 3.2).[70] Importantly, they also noted that simple silyl ketene acetals were incompatible with their reaction conditions due to substrate hydrolysis from the acidic reaction conditions required for iminium catalysis.

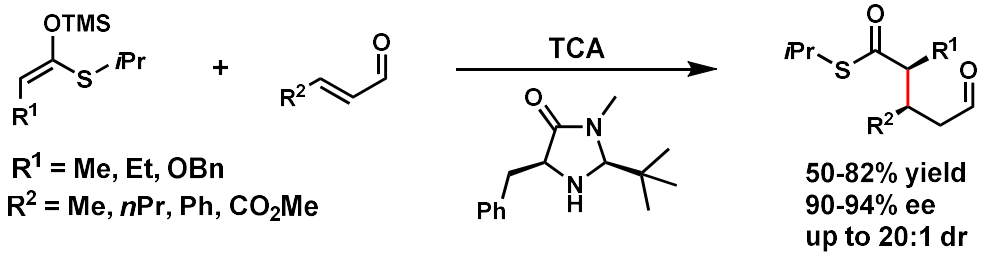

Scheme 3.2 Enantioselective Mukaiyama-Michael reaction with silyl ketene thioacetals.

In the publication from Toste and coworkers disclosing the new gold(III) scaffold discussed in Chapter 1, several reactions where the new complex was a competent catalyst were also described.[7] Among those reactions was a Mukaiyama-Michael addition of silyl ketene acetals with α,β-unsaturated aldehydes. When catalyzed by gold(I) complexes, the 1,2-adduct was found to be the exclusive product; however the gold(III) catalyst resulted in exclusively the 1,4-adduct (Scheme 3.3). Additionally, silyl ketene acetals were found to be competent nucleophiles because the reaction does not require acidic conditions like those previously reported by MacMillan and coworkers.[70] This unprecedented selectivity and substrate compatibility seen when using gold(III) as the Lewis acid catalyst presented us with the opportunity to develop the first enantioselective

Mukaiyama-Michael reaction between α,β-unsaturated aldehydes and silyl ketene acetals. As a result we would allow expedient access to an entire class of enantioenriched 1,5-dicarbonyl complexes, with the added potential for further chemical modification of the resultant ester, which is not present when silyl enol ethers are used as the nucleophile.

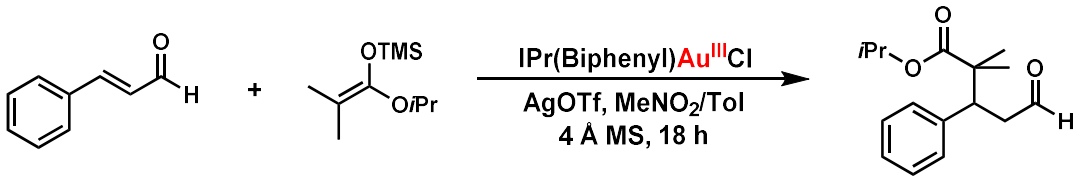

Scheme 3.3 Mukaiyama-Michael addition catalyzed by a gold(III) complex.

After successfully showing that chiral NHC gold(III) complexes were competent catalysts for asymmetric transformations, we wanted to probe whether phosphine gold(III) complexes would also be competent. We hoped to take advantage of the large library of existing work based on phosphine gold(I) complexes and apply that knowledge to gold(III) complexes. With this in mind we hypothesized that these chiral phosphine based ligands could be efficient sources for the introduction of chirality to develop an enantioselective Mukaiyama-Michael addition between α,β-unsaturated aldehydes and silyl ketene acetals.

3.2 Results and Discussion

3.2.1 Synthesis and Testing of Phosphine Based Gold(III) Complexes for the Mukaiyama-Michael Addition

Although Toste and coworkers discovered that some cationic NHC gold(I) complexes could undergo oxidative addition with biphenylene, the same was not true of phosphine gold(I) complexes. Therefore in order to synthesize gold(III) complexes with chiral phosphine based ligands, we needed to approach from the gold(III) dimer previously described. The phosphine ligands were able to be directly added to the gold(III) dimer to give the desired chiral gold(III) complexes (Scheme 3.4).

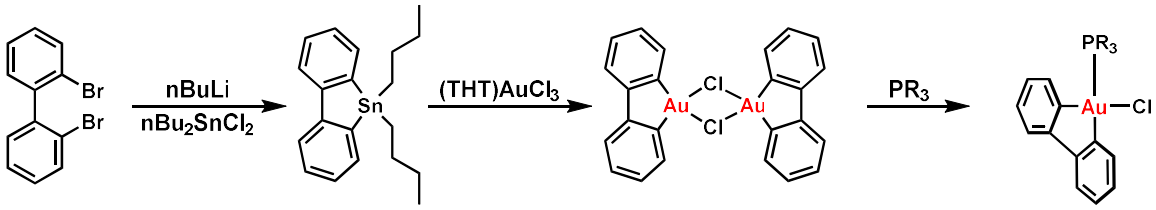

Scheme 3.4 Synthesis of chiral phosphine based gold(III) complexes.

Following this route we rapidly synthesized a library of chiral gold(III) complexes with phosphines and phosphoramidites ligands (Table 2.1). When testing these complexes as catalysts in the Mukaiyama-Michael addition reaction, we observed that gold(III) complexes with chiral phosphine ligands did not provide desired levels of reactivity or enantioselectivity (entry **3.1**). Due to the history of success in enantioselective gold(I) chemistry with phosphoramidite ligands, we next explored their effect on the system.[2,71,72] BINOL-based phosphoramidite ligands proved to be an ineffective ligand scaffold for the transformation (entries **3.2-3.4**). However, we did discover that a TADDOL-based phosphoramidite ligand on the gold(III) catalyst was successful at

promoting good reactivity and high enantioselectivity (entry **3.5**). Modification of the aryl substituents on the TADDOL-based ligand with 3,5-Me-Ph resulted in similar yield and an increased enantioselectivity up to 90% ee (entry **3.6**). Further increase of the steric bulk on the aryl substituents did not increase enantioselectivity, nor did the use of electron donating substituents (entries **3.7-3.8**). The addition of electron withdrawing substituents on the aryl rings produced an intractable mixture of gold(III) complex and ligand and were therefore not considered as suitable ligands for the transformation.

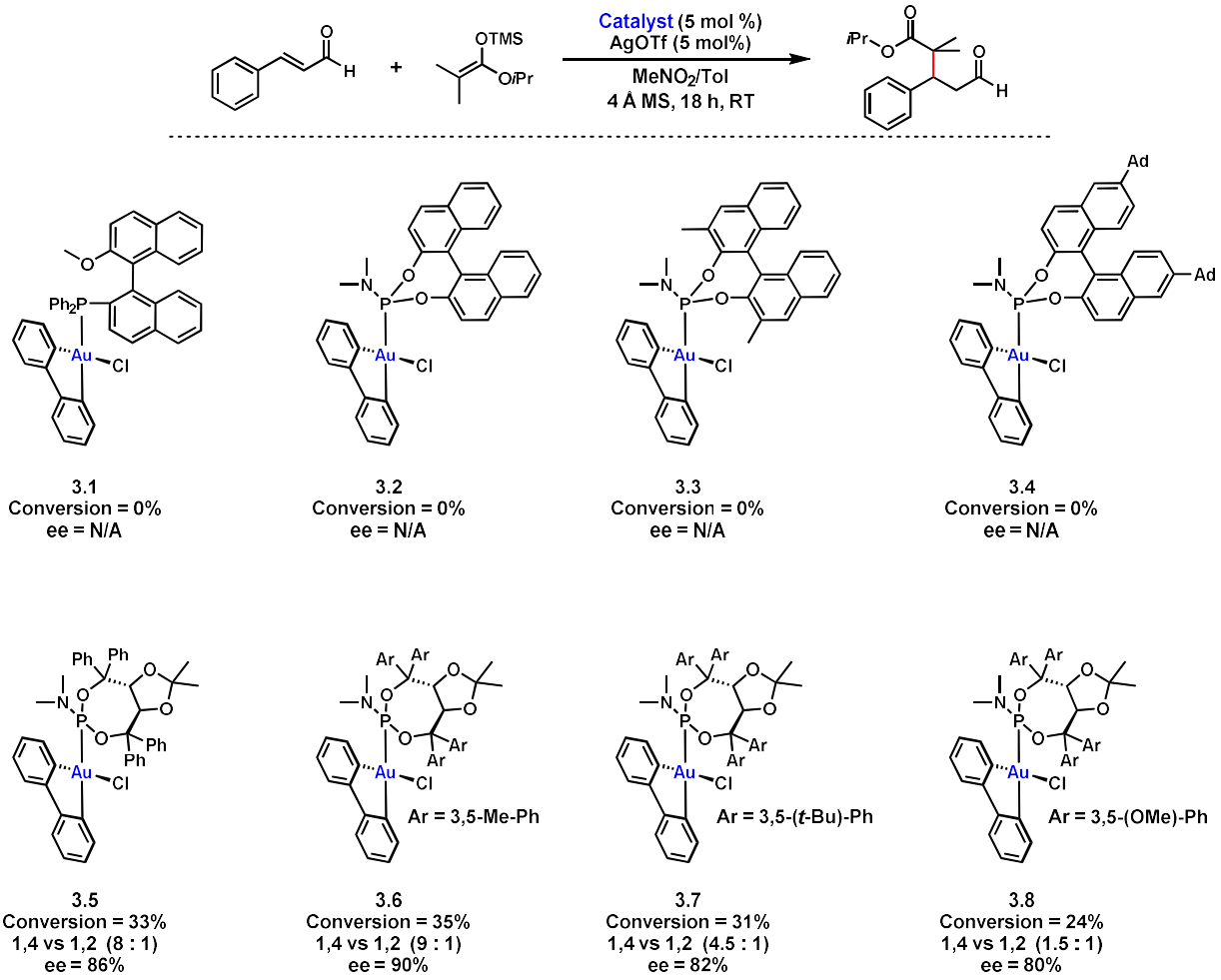

Table 3.1 Ligand optimization for the enantioselective Mukaiyama-Michael addition.

3.2.2 Optimization of Reaction Conditions for the Mukaiyama-Michael Addition

Attempts at further optimization next began with a solvent screen (Table 3.2). The original disclosure from Toste and coworkers reported that a mixture of toluene and nitromethane was the solvent system of choice.[7] We confirmed that neither toluene nor nitromethane on their own were compatible solvents with this reaction (entries 1-2). Acetonitrile was also found to not be compatible with the reaction, presumably due to tight coordination to the cationic gold(III) species (entry 3). Chloroform, DCM, and THF were also not optimal solvents due to their propensity to favor formation of a 1,2-adduct over the desired 1,4-adduct (entries 4-6). Swapping toluene for benzene or *o*-dichlorobenzene in the solvent mixture with nitromethane resulted in decreased conversion, but did maintain similar levels of selectivity for the 1,4-addition product (entries 7-8).

Because these modifications did not improve any desired metrics of our reaction, we continued forward using the original solvent mixture (entry 9).

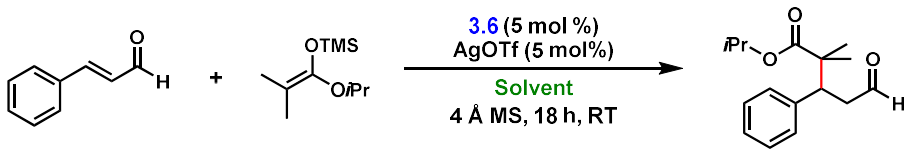

Entry	Solvent	Conversion	1,4 vs 1,2
1	Tol	0	-
2	$MeNO_2$	4	-
3	MeCN	0	-
4	$CHCl_3$	5	-
5	DCM	45	1 : 3
6	THF	65	0 : 1
7	Ph : $MeNO_2$	22	8 : 1
8	*o*-DCB : $MeNO_2$	13	10 : 1
9	Tol : $MeNO_2$	30	10 : 1

Table 3.2 Solvent optimization for the enantioselective Mukaiyama-Michael addition. Entries 7-9 run with 0.166 M benzene, *o*-dichlorobenzene, and toluene, respectively, with 1.2 M nitromethane.

The importance of the identity of the silver salt and therefore the counterion was covered thoroughly in Chapter 2, and following the same reasoning we also wanted to explore what effects the identity of the counterion would have in the Mukaiyama-Michael addition (Table 3.3). A number of counterions were found to be incompatible, presumably due to tight binding of the counterion to the cationic gold(III) center, blocking the active site (entries 1-3) Switching to less coordinating counterions gave increased reactivity, except in the case of tetrafluoroborate which resulted in no reactivity (entries 4-7). Ultimately, silver triflate was chosen to move forward with optimization because it provided good levels of selectivity for the 1,4-adduct while maintaining high enantioselectivity; however, it did result in lower conversion when compared to other silver salts (entry 8).

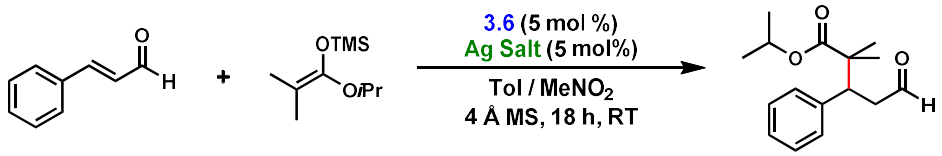

Entry	Silver Salt	Conversion (%)	Ratio (1,4 : 1,2)	ee (%)
1	AgOTRIP	0	-	-
2	AgOTs	0	-	-
3	AgOBz	0	-	-
4	$AgBF_4$	0	-	-
5	$AgPF_6$	21	1 : 1	-
6	$AgNTF_2$	81	1 : 1	56
7	$AgSbF_6$	74	2 : 1	61
8	AgOTf	35	8 : 1	90

Table 3.3 Counterion optimization for the enantioselective Mukaiyama-Michael addition.

Due to the increased solubility of silver salts in nitromethane, if more than one equivalent of salt was added, then the excess salt may not be removed during the filtration step of the reaction.

Because excess silver salt could potentially play a role in the reaction, we tested adding additional equivalents of silver salt to the reaction mixture (Table 3.4). We found that less than one equivalent of silver salt simply slowed down the reactivity as expected, and excess equivalents of silver salt did not have an impact on conversion, 1,4 vs 1,2 selectivity, or enantioselectivity (entries 1-4). In practice, this meant that an excess of silver salt could be used when generating the cationic gold(III) complex with no deleterious impact on the outcome of the reaction. This can be beneficial when handling silver salts which are highly hygroscopic and, as a result, they are difficult to accurately mass out.

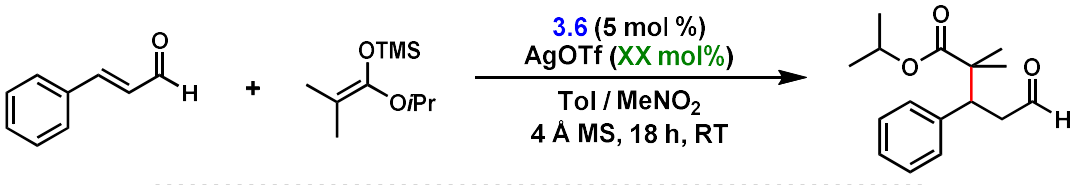

Entry	Equiv of AgOTf	Conversion (%)	1,4 vs 1,2
1	0.5	41	9 : 1
2	1	55	10 : 1
3	2	53	9 : 1
4	4	50	10 : 1

Table 3.4 Counterion equivalents effect on the enantioselective Mukaiyama-Michael addition.

Although the original report of the gold(III) catalyzed Mukaiyama-Michael reaction included the use of 4 Å molecular sieves (mol sieves), we wanted to confirm that this additive was necessary to achieve our desired outcome and to test if there were any better candidates (Table 3.5). When no additive was used, complete conversion was observed but with a 1:8 ratio of 1,4 vs 1,2-addition (entry 1). This indicated that perhaps the additive was necessary to achieve the desired levels of selectivity, and with that in mind we moved on to explore at other additives to control the amount of water present in the reaction. Magnesium sulfate and sodium sulfate showed much lower levels of conversion while maintaining poor levels of selectivity for the 1,4-adduct (entries 2-4). When testing mol sieves we employed both 3 Å and 4 Å varieties in bead and powder form (entries 5-8). Across all types of mol sieves, we found that optimal results were achieved when using powdered 4 Å mol sieves (entry 5). We also tested SBA 15 (mesoporous silica sieve with narrow pore size distribution), 13X mol sieves (10 Å pore size), type Y mol sieves (zeolite based), and FER HSZ-720 KOA (zeolite based) to see if they would produce better results than the 4 Å mol sieves; but, we observed significantly less reactivity and almost exclusive selectivity for the 1,2-adduct over the 1,4-adduct in all cases (entries 9-12).[73]

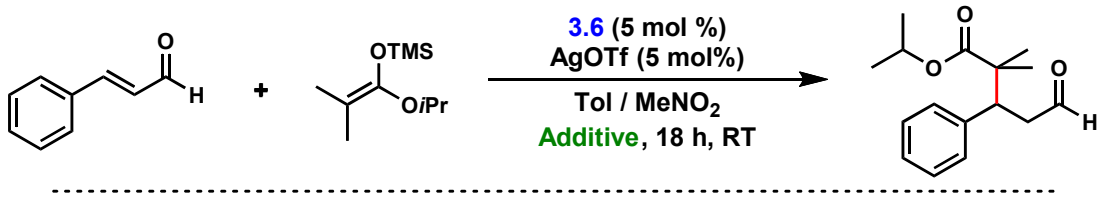

Entry	Additive	Conversion (%)	1,4 vs 1,2
1	None	100	1 : 8
2	$MgSO_4$	39	1 : 6
3	Na_2SO_4	49	1 : 3
4	$Na_2SO_4 \bullet 10\ H_2O$	48	1 : 8
5	4 Å MS, powdered	35	8 : 1
6	4 Å MS, beads	92	1 : 2
7	3 Å MS, powdered	55	1 : 1
8	3 Å MS, beads	21	1 : 1
9	SBA 15	0	-
10	FER HSZ-720 KOA	33	1 : 16
11	13x MS	8	1 : >20
12	Type Y MS	8	1 : >20

Table 3.5 Additive optimization for the enantioselective Mukaiyama-Michael addition.

In an effort to further increase the conversion of the reaction we also tested a number of modifications to the reaction conditions (Table 3.6). First, we observed that decreasing the equivalents of mol sieves was detrimental and increasing the equivalents of mol sieves had almost no effect on the extent to which the reaction went towards complete conversion (entries 1-3). Increased reaction time also did not further increase conversion of the reaction, indicating that perhaps the reaction was stalling out (entries 4-6). Further increasing catalyst loading did improve conversion, but only up to a maximum of 10 mol% catalyst loading (entries 7-9). We next hypothesized that the silyl ketene acetal might be decomposing during the course of the reaction. This hypothesis led us to try adding an additional 1.5 equivalents of the silyl ketene acetal after 24 hours of reaction time, which resulted in a slight increase in conversion up to 71% (entry 10). To test for catalyst deactivation or decomposition we added an additional 10 mol% of catalyst after 24 hours but did not observe any noticeable increase in conversion (entry 11). Lastly, we explored rate of addition of the silyl ketene acetal and optimal results were observed when the silyl ketene acetal was added in four portions over a period of 4 hours, resulting in 85% conversion and 91% ee, while maintaining high 1,4-addition selectivity (entries 12-13).

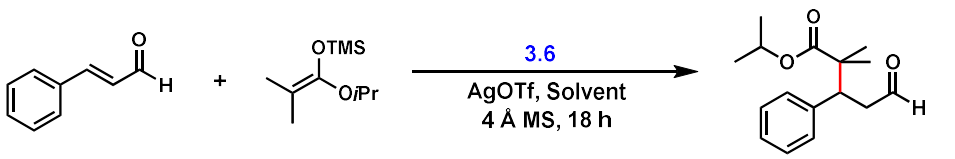

Entry	Modification	Conversion (%)	Ratio (1,4 : 1,2)	ee (%)
1	860 mg/mmol$_{SM}$ 4 Å MS	17	6 : 1	-
2	1720 mg/mmol$_{SM}$ 4 Å MS	36	7 : 1	90
3	3440 mg/mmol$_{SM}$ 4 Å MS	32	7 : 1	90
4	24 hr	35	8 : 1	90
5	48 hr	36	8 : 1	90
6	72 hr	36	8 : 1	90
7	5% Catalyst	35	8 : 1	90
8	10% Catalyst	60	8 : 1	90
9	15% Catalyst	53	7 : 1	87
10	1.5 equiv SKA	71	7 : 1	90
11	0.1 equiv Catalyst	60	7 : 1	90
12	4 x 0.375 equiv SKA	62	9 : 1	90
13	4 x 0.750 equiv SKA	85	10 : 1	91

Table 3.6 Reactivity optimization for the enantioselective Mukaiyama-Michael addition. SKA = Silyl Ketene Acetal

3.2.3 Scope of the Nucleophile for the Mukaiyama-Michael Addition

With the optimized conditions in hand we next looked towards expanding the scope of the reaction (Table 3.7). We first explored what silyl substituents were optimal for the silyl ketene acetal and found that the trimethylsilyl (TMS) substrate resulted in 65% conversion, 8:1 regioselectivity favoring the desired 1,4-addition product, and 90% ee (entry **3.9**). Changing to the triethylsilyl (TES) silyl ketene acetal resulted in only 35% conversion, a 1:1 ratio of 1,4-addition versus 1,2-addition, and the enantioselectivity was drastically lowered to 13% ee (entry **3.10**). The *tert*-butyldimethylsilyl (TBS) substrate was completely unreactive under our conditions (entry **3.11**). Moving forward with TMS silyl ketene acetals, we next tested alteration of the alkyl chain on the parent ester. Modification from isopropyl to ethyl or phenethyl improved conversion, enantioselectivity, and regioselectivity, but modification to phenyl resulted in only trace product formation (entries **3.12-3.14**). When testing disubstituted silyl ketene acetals we observed no product (entries **3.15-3.16**). Tri-substituted silyl ketene acetals introduce the possibility to generate an additional stereocenter due to the prochiral nature of the nucleophile, resulting in diastereomeric products. With this in mind, we tested a number of tri-substituted silyl ketene acetals in our reaction and observed no reactivity (entries **3.17-3.18**). However, when employing tetra-substituted prochiral silyl ketene we did observe reactivity, and in the case of **3.20** we observed moderate diastereoselectivity resulting in a 2:1 ratio of diastereomers (entries **3.19-3.20**).

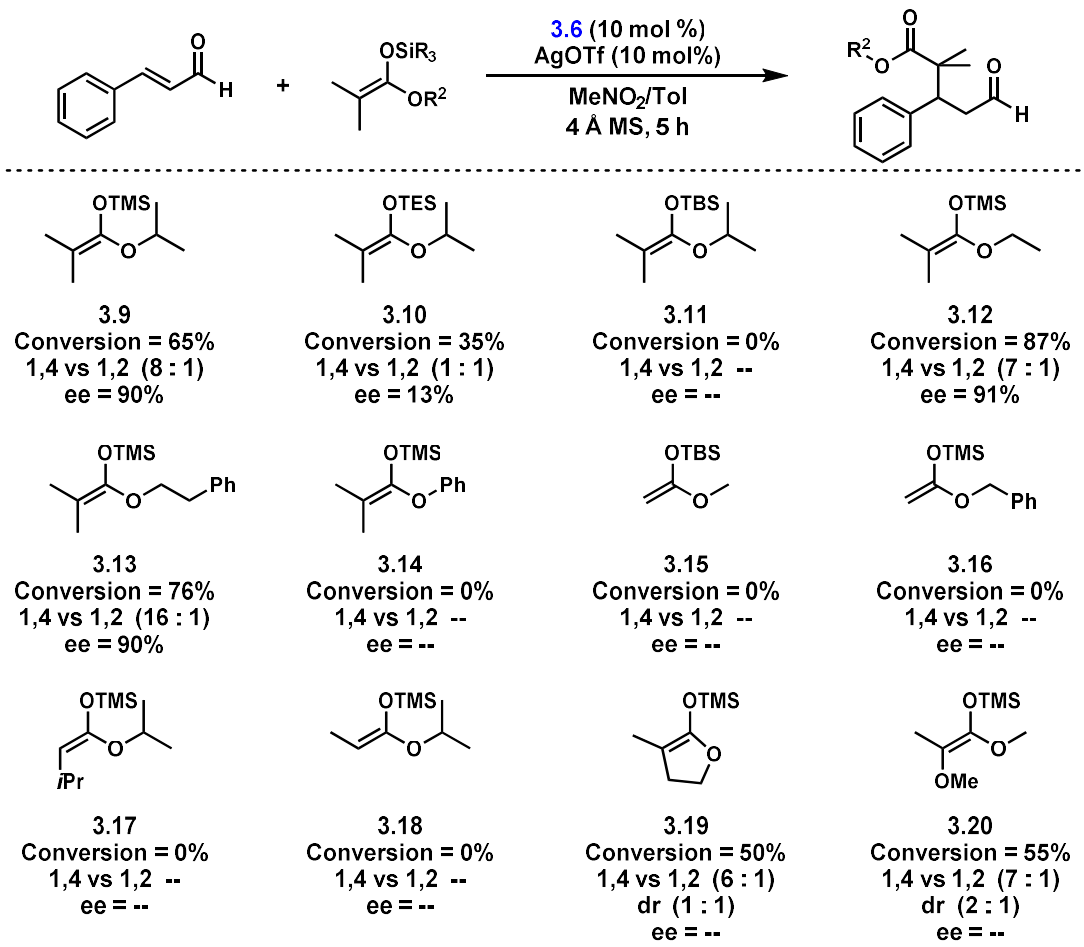

Table 3.7 Nucleophile substrate scope for the enantioselective Mukaiyama-Michael addition.

3.2.4 Scope of the Electrophile for the Mukaiyama-Michael Addition

Preliminary substrate scope of the electrophile component has also been explored (Table 3.8). Substituted cinnamaldehydes were widely compatible with the reaction conditions when using **3.9** as the nucleophilic silyl ketene acetal. The unsubstituted, *p*-methoxy, *p*-methyl, and *p*-chloro cinnamaldehydes all resulted in moderate conversion, high selectivity for the 1,4-adduct over the 1,2 adduct (≥6:1), as well as excellent enantioselectivity (≥90% ee) for the unsubstituted and *p*-methoxy variants (entries **3.20-3.24**). The significantly more electron donating *p*-diethylamino substituted cinnamaldehyde resulted in only 22% consumption of starting material, but only the 1,4-adduct was detected. Switching our silyl ketene acetal nucleophile to **3.12** or **3.13**, we observed that the unsubstituted, *p*-chloro, and *p*-methyl cinnamaldehydes were tolerated with high conversion (up to 87%), high regioselectivity (up to 9:1), and excellent enantioselectivity (up to 91% ee) (entries **3.25-3.28**). In addition to cinnamaldehydes, we also explored the scope of alkyl α,β-unsaturated aldehydes for this Mukaiyama-Michael reaction. When utilizing **3.13** as the nucleophile, we observed poor regioselectivity (1:1.2) for the 1,4-adduct, as well as only 30% ee (entry **3.29**). When **3.12** was used as the nucleophile with a similar alkyl α,β-unsaturated aldehyde, we observed almost complete conversion but limited regioselectivity (3:1) and enantioselectivity (23% ee) (entry **3.30**). When we replaced the aryl ring with cyclohexyl we observed no conversion (entry **3.31**). Further efforts are currently underway to explore the factors that are influencing the observed results for conversion, regioselectivity, and enantioselectivity.

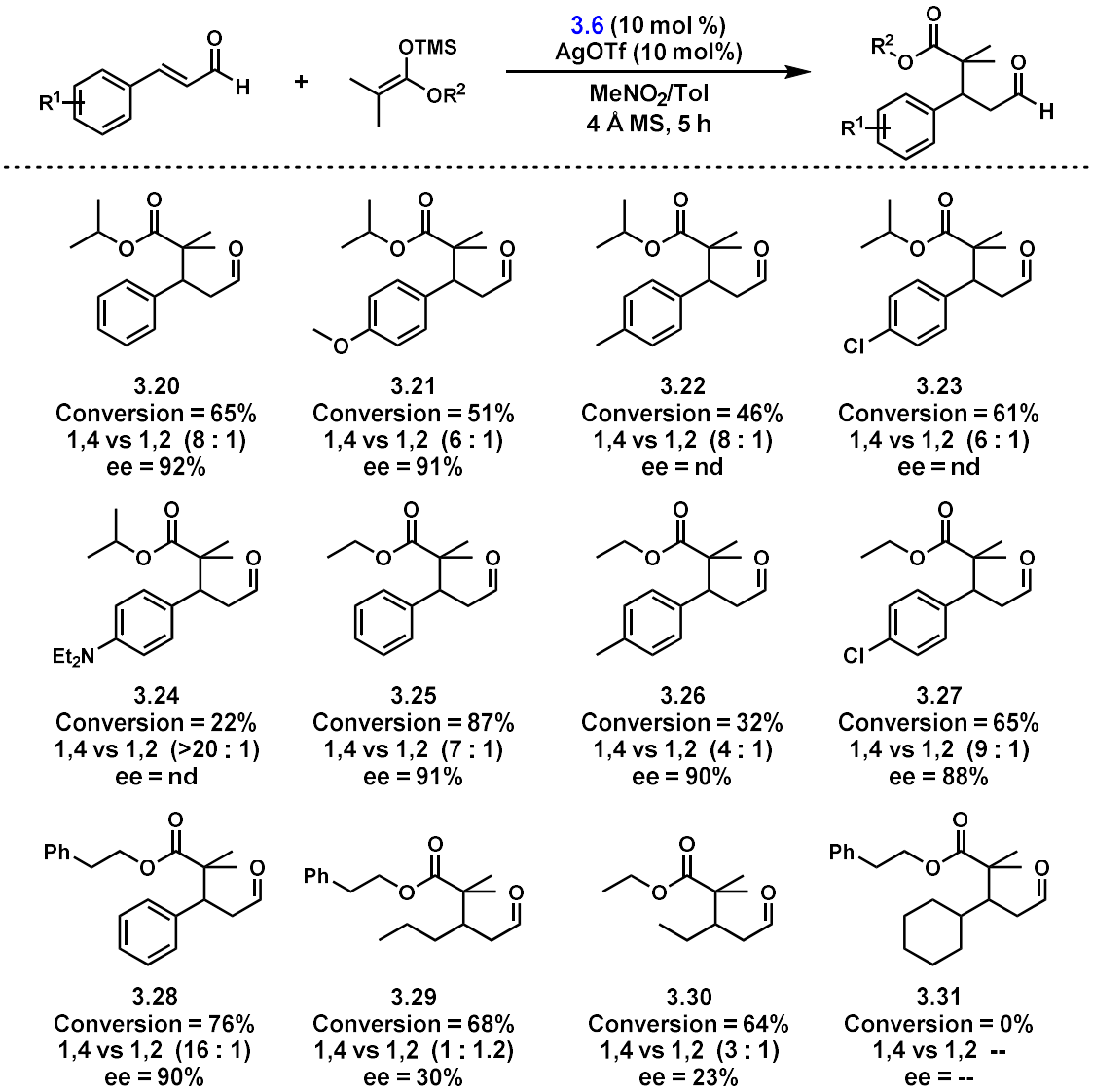

Table 3.8 Nucleophile substrate scope for the enantioselective Mukaiyama-Michael addition.

3.3 Conclusion

In summary, we have developed a new method for an enantioselective Mukaiyama-Michael addition in which the chirality is dictated by a phosphoramidite gold(III) catalyst. To the best of our knowledge, this is the first report of a highly enantioselective Mukaiyama-Michael addition wherein silyl ketene acetals are suitable nucleophiles for the transformation, as well as the first report exploiting chiral phosphoramidite gold(III) catalysts as the source of chirality. The successful realization of this catalytic system has also greatly increased the accessible chemical space available for our biphenyl-stabilized gold(III) complexes by showing that phosphines and phosphoramidites can be highly competent ligands. Additional work on this catalytic system is currently under way and focused on expanding the substrate scope of the transformation and control of the diastereoselectivity.

3.4 Supporting Information

3.4.1 General Methods

Unless stated otherwise, all reactions were performed in oven-dried glassware sealed with rubber septa under a nitrogen atmosphere and were stirred with Teflon-coated magnetic stir bars. Dry tetrahydrofuran (THF), acetonitrile (MeCN), dichloromethane (DCM), methanol (MeOH), and toluene (Tol) were obtained by passing these previously degassed solvents through activated alumina columns. All other reagents were used as received. Reactions were monitored by thin layer chromatography (TLC) on Silicycle Siliaplate^{TM} glass backed TLC plates (250 μm thickness, 60 Å porosity, F-254 indicator) and visualized by UV irradiation and iodine stain. Volatile solvents were removed under reduced pressure with a rotary evaporator and dried on high vacuum on a Schlenk line. ^{1}H-NMR and ^{13}C-NMR spectra were taken with Bruker AV-300, AVQ-400, AVB-400, AV-500, DRX-500, and AV-600 spectrometers. Chemical shifts are reported relative to the residual solvent signal. NMR data are reported as follows: chemical shift (multiplicity, coupling constants where applicable, number of hydrogens). Splitting is reported with the following symbols: s = singlet, d = doublet, t = triplet, dd = doublet of doublets, dt = doublet of triplets, m = multiplet, dq = doublet of quartets, ddd = doublet of doublets of doublets, ddt = doublet of doublets of triplets. Chiral phase high performance liquid chromatography (HPLC) was performed on Shimadzu VP and Shimadzu prominence series instruments using the specified column (5μm, 4.6 mm x 250 mm). Chiral GC analysis was performed on an Agilent system. Racemic traces were obtained by substituting IPr(Biphenyl)Au(III)Cl in place of the chiral Au(III) catalyst (**3.6**). High-resolution mass spectra (HRMS) were obtained from the Micro-Mass/Analytical Facility operated by the College of Chemistry, University of California, Berkeley. Previously reported compounds were synthesized according to literature procedures. The following compounds were prepared according to previously published procedures and their spectra match those reported in literature: ((1-isopropoxy-2-methylprop-1-en-1-yl)oxy)trimethylsilane,[74] ((1-ethoxy-2-methylprop-1-en-1-yl)oxy)trimethylsilane,[75] trimethyl((2-methyl-1-phenoxyprop-1-en-1-yl)oxy)silane,[74] *tert*-butyl((1-methoxyvinyl)oxy)dimethylsilane,[76] ((1-(benzyloxy)vinyl)oxy)trimethylsilane,[77] (*E*)-((1-isopropoxy-3-methylbut-1-en-1-yl)oxy)tri-methylsilane,[78] (*Z*)-((1-isopropoxyprop-1-en-1-yl)oxy)trimethylsilane,[79] trimethyl((3-methyl-4,5-dihydrofuran-2-yl)oxy)silane,[75] and (*E*)-((1,2-dimethoxyprop-1-en-1-yl)oxy)trimethylsilane.[80]

3.4.2 Preparation and Characterization of Phosphine and Phosphoramidite Gold(III) Complexes

Scheme 3.5 General preparation for chiral phosphine based gold(III) complexes.

To a suspension of Au(III)(biphenyl) chloride (1 equiv) in DCM was added the corresponding phosphine or phosphoramidite (2 equiv) under atmospheric conditions. The reaction mixture was stirred for 1 h at 22 °C until the solution became homogeneous, and then

passed through silica and dried under vacuum to give the crude product. The pure product was isolated by column chromatography (DCM:hexanes 1:1).

Catalyst 3.1

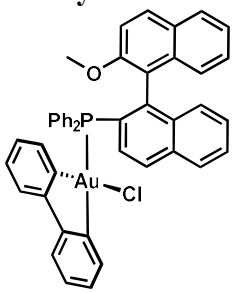

Prepared according to the general procedure with the corresponding phosphine. **^{1}H NMR** (400 MHz, $CDCl_3$) δ 8.21 – 8.14 (m, 1H), 7.99 (d, J = 8.0 Hz, 2H), 7.97 – 7.94 (m, 1H), 7.68 – 7.62 (m, 2H), 7.59 (d, J = 9.1 Hz, 1H), 7.57 – 7.52 (m, 1H), 7.40 – 7.29 (m, 4H), 7.22 (td, J = 8.3, 1.8 Hz, 6H), 7.16 – 7.10 (m, 3H), 7.07 – 7.01 (m, 2H), 6.98 (d, J = 8.0 Hz, 1H), 6.97 – 6.92 (m, 1H), 6.90 (td, J = 7.5, 1.1 Hz, 1H), 6.74 (dd, J = 7.4, 3.6 Hz, 2H), 6.67 (d, J = 8.5 Hz, 1H), 6.22 (td, J = 7.6, 1.6 Hz, 1H), 3.42 (s, 3H).; **^{13}C NMR** (101 MHz, $CDCl_3$) δ 166.53, 165.22, 155.07, 154.97, 154.90, 153.98, 153.93, 152.22, 142.99, 142.90, 137.39, 137.27, 135.63, 135.53, 135.44, 135.33, 134.51, 134.00, 133.91, 133.84, 133.02, 131.64, 131.52, 131.19, 130.98, 130.39, 130.36, 128.85, 128.63, 128.40, 128.20, 128.09, 127.44, 127.36, 127.32, 127.17, 127.06, 127.02, 126.76, 126.69, 126.40, 125.98, 125.61, 125.48, 123.21, 121.26, 120.88, 120.81, 118.23, 118.18, 112.30, 54.93.; **^{31}P NMR** (162 MHz, $CDCl_3$) δ 40.84.

Catalyst 3.2

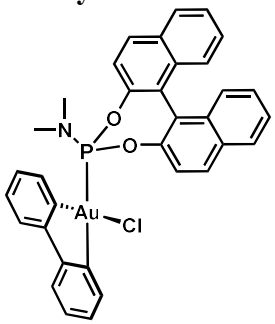

Prepared according to the general procedure with the corresponding phosphoramidite. **^{1}H NMR** (400 MHz, CD_2Cl_2, mixture of atropisomers) δ 8.23 – 8.09 (m, 3H), 8.04 (d, J = 8.3 Hz, 1H), 7.99 (d, J = 8.5 Hz, 1H), 7.93 (d, J = 8.2 Hz, 1H), 7.66 (dd, J = 8.8, 1.1 Hz, 1H), 7.55 (ddd, J = 8.1, 6.6, 1.3 Hz, 1H), 7.50 – 7.39 (m, 4H), 7.39 – 7.28 (m, 4H), 7.26 – 7.15 (m, 2H), 7.10 (tdd, J = 7.4, 6.2, 3.4 Hz, 1H), 7.02 (t, J = 7.7 Hz, 1H), 2.81 (s, 3H), 2.78 (s, 3H).; **^{13}C NMR** (101 MHz, CD_2Cl_2, mixture of atropisomers) δ 164.58, 162.70, 154.69, 154.58, 154.03, 153.96, 152.74, 147.81, 147.68, 147.44, 147.38, 134.55, 132.48, 132.45, 132.33, 132.18, 131.96, 131.77, 131.36, 131.22, 128.57, 128.51, 128.23, 128.06, 127.78, 127.75, 127.27, 126.94, 126.81, 126.78, 126.63, 125.92, 125.80, 122.49, 122.38, 122.13, 121.38, 121.24, 121.14, 120.36, 53.98, 53.71, 53.64, 53.44, 53.17, 52.90, 37.41, 37.31, 29.70.; **^{31}P NMR** (162 MHz, CD_2Cl_2) δ 148.85.

Catalyst 3.3

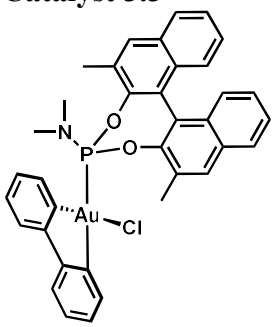

Prepared according to the general procedure with the corresponding phosphoramidite. **^{1}H NMR** (400 MHz, $CDCl_3$, mixture of atropisomers) δ 8.36 – 8.27 (m, 1H), 7.96 – 7.85 (m, 3H), 7.84 – 7.74 (m, 2H), 7.53 – 7.46 (m, 1H), 7.45 – 7.35 (m, 3H), 7.34 – 7.25 (m, 3H), 7.24 – 7.08 (m, 5H), 6.80 (t, J = 7.6 Hz, 1H), 2.77 – 2.54 (m, 12H).; **^{13}C NMR** (151 MHz, $CDCl_3$, mixture of atropisomers) δ 164.63, 163.37, 155.16, 155.09, 154.05, 154.00, 152.67, 152.66, 146.99, 146.95, 146.86, 133.60, 132.97, 132.94, 131.73, 131.68, 131.37, 131.36, 131.22, 131.20, 130.70, 129.61, 129.09, 128.31, 128.09, 127.75, 127.60, 127.40, 127.38, 127.12, 127.03, 126.91, 126.88, 125.97, 125.94, 125.71, 125.63, 123.13, 123.11, 122.45, 122.43, 122.11, 121.28, 121.22, 37.35, 29.71, 19.31, 17.18.; **^{31}P NMR** (162 MHz, $CDCl_3$) δ 147.97.

Catalyst 3.4

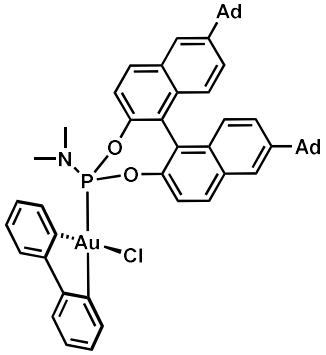

Prepared according to the general procedure with the corresponding phosphoramidite. **^{1}H NMR** (400 MHz, $CDCl_3$, mixture of atropisomers) δ 8.27 (dd, J = 13.4, 7.7 Hz, 1H), 8.13 – 8.06 (m, 1H), 8.02 (d, J = 8.8 Hz, 1H), 7.89 (d, J = 8.1 Hz, 1H), 7.86 – 7.82 (m, 1H), 7.74 (s, 1H), 7.56 (d, J = 8.8 Hz, 1H), 7.45 (s, 2H), 7.41 (d, J = 7.4 Hz, 1H), 7.38 – 7.32 (m, 2H), 7.29 (m, 2H), 7.23 – 7.14 (m, 2H), 7.14 – 7.07 (m, 1H), 7.01 – 6.93 (m, 1H), 2.80 (s, 3H), 2.77 (s, 3H), 2.13 (d, J = 21.7 Hz, 6H), 2.06 – 2.00 (m, 6H), 2.00 – 1.93 (m, 6H), 1.89 – 1.70 (m, 12H).; **^{13}C NMR** (151 MHz, $CDCl_3$, mixture of atropisomers) δ 164.53, 163.27, 154.81, 154.74, 154.21, 152.59, 152.58, 148.81, 148.64, 146.83, 134.38, 132.68, 132.66, 132.04, 131.77, 131.24, 130.93, 130.56, 130.40, 128.16, 127.98, 127.55, 127.53, 127.09, 126.99, 126.88, 126.69, 125.22, 124.86, 123.43, 123.39, 122.48, 122.15, 122.08, 121.17, 121.10, 120.11, 42.99, 42.92, 37.63, 37.57, 36.75, 36.74, 36.31, 36.20, 28.86, 28.84.; **^{31}P NMR** (162 MHz, $CDCl_3$) δ 148.57.

Catalyst 3.5

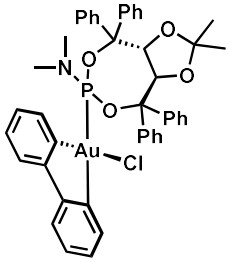

Prepared according to the general procedure with the corresponding phosphoramidite. **^{1}H NMR** (400 MHz, $CDCl_3$, mixture of atropisomers) δ 8.11 (ddd, *J* = 13.6, 7.8, 1.3 Hz, 1H), 7.86 (d, *J* = 7.7 Hz, 2H), 7.72 – 7.64 (m, 2H), 7.47 (dd, *J* = 8.2, 6.8 Hz, 2H), 7.40 – 7.29 (m, 12H), 7.28 – 7.23 (m, 2H), 7.14 – 7.06 (m, 2H), 7.03 (tdd, *J* = 7.4, 5.7, 1.6 Hz, 1H), 6.97 – 6.90 (m, 2H), 6.90 – 6.84 (m, 1H), 6.79 (td, *J* = 7.6, 1.6 Hz, 1H), 5.84 (d, *J* = 7.9 Hz, 1H), 5.47 (d, *J* = 7.9 Hz, 1H), 2.32 (s, 3H), 2.30 (s, 3H), 0.56 (s, 3H), 0.48 (s, 3H).; **^{13}C NMR** (101 MHz, $CDCl_3$, mixture of atropisomers) δ 164.45, 163.13, 155.39, 155.31, 153.95, 153.91, 152.23, 152.22, 144.03, 140.68, 140.64, 140.10, 140.05, 139.53, 132.62, 132.59, 131.31, 131.25, 129.32, 129.19, 129.11, 128.65, 128.51, 128.37, 128.33, 127.70, 127.51, 127.38, 127.27, 127.22, 127.02, 127.00, 126.84, 126.82, 126.48, 126.38, 121.50, 120.69, 120.62, 115.61, 91.26, 91.12, 89.08, 79.38, 79.37, 77.64, 77.62, 36.81, 36.74, 29.67, 26.59, 26.16.; **^{31}P NMR** (162 MHz, $CDCl_3$) δ 123.08.

Catalyst 3.6

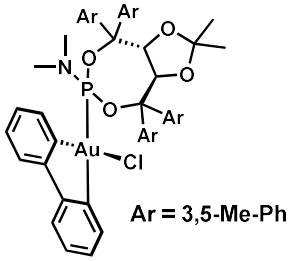

Prepared according to the general procedure with the corresponding phosphoramidite. **^{1}H NMR** (300 MHz, $CDCl_3$, mixture of atropisomers) δ 8.27 – 8.14 (m, 1H), 7.58 (s, 2H), 7.35 – 7.21 (m, 5H), 7.18 – 7.06 (m, 1H), 7.10 – 6.99 (m, 2H), 6.98 (d, J = 8.1 Hz, 6H), 6.90 (s, 1H), 6.84 – 6.73 (m, 1H), 6.43 (s, 1H), 5.88 (d, J = 7.8 Hz, 1H), 5.37 (d, J = 7.8 Hz, 1H), 2.38 (s, 6H), 2.35 (s, 6H), 2.32 (s, 6H), 2.29 (s, 3H), 2.25 (s, 3H), 0.61 (s, 3H), 0.55 (s, 3H).; **^{13}C NMR** (101 MHz, $CDCl_3$, mixture of atropisomers) δ 165.24, 163.24, 154.77, 154.66, 154.30, 154.24, 152.39, 152.37, 144.09, 140.62, 140.55, 140.24, 140.15, 139.01, 138.68, 137.74, 136.42, 136.14, 132.78, 132.75, 131.85, 131.76, 131.13, 130.03, 129.26, 129.08, 127.39, 127.21, 127.08, 126.86, 126.84, 126.79, 126.53, 126.38, 125.15, 121.40, 120.61, 120.51, 115.34, 91.65, 91.44, 89.09, 79.59, 79.57, 77.40, 77.38, 36.86, 36.75, 26.77, 26.46, 21.71, 21.64, 21.48, 21.24.; **^{31}P NMR** (162 MHz, $CDCl_3$) δ 121.33.

Catalyst 3.7

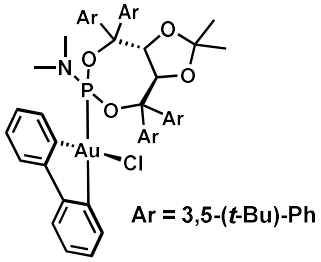

Prepared according to the general procedure with the corresponding phosphoramidite. **^{1}H NMR** (600 MHz, $CDCl_3$, mixture of atropisomers) δ 8.06 (dd, J = 13.7, 7.7 Hz, 1H), 7.57 – 7.52 (m, 1H), 7.47 (s, 2H), 7.38 (t, J = 1.7 Hz, 1H), 7.29 – 7.23 (m, 5H), 7.19 (dd, J = 4.4, 2.8 Hz, 2H), 7.15 (t, J = 1.6 Hz, 1H), 7.08 (d, J = 1.7 Hz, 2H), 7.06 – 7.00 (m, 2H), 6.97 (tdd, J = 7.4, 5.7, 1.4 Hz, 2H), 6.76 – 6.70 (m, 1H), 5.99 (d, J = 7.7 Hz, 1H), 5.66 (d, J = 7.6 Hz, 1H), 2.30 (s, 3H), 2.28 (s, 3H), 1.31 (s, 18H), 1.25 (s, 18H), 1.23 (s, 18H), 0.98 (s, 18H), 0.45 (s, 3H), 0.32 (s, 3H).; **^{13}C NMR** (151 MHz, $CDCl_3$, mixture of atropisomers) δ 164.64, 163.29, 155.25, 155.18, 154.75, 154.70, 152.75, 152.74, 150.57, 150.31, 148.73, 143.93, 141.23, 141.18, 140.49, 140.44, 139.73, 133.16, 133.14, 131.97, 131.90, 127.32, 127.28, 126.92, 126.40, 126.30, 124.10, 123.66, 123.16, 122.11, 121.90, 121.63, 120.71, 120.57, 120.50, 120.25, 115.17, 92.74, 92.61, 90.84, 79.84, 79.83, 78.45, 78.44, 37.44, 37.37, 35.12, 35.08, 34.92, 34.72, 31.76, 31.65, 31.62, 31.19, 27.01, 26.20.; **^{31}P NMR** (162 MHz, $CDCl_3$) δ 122.47.

Catalyst 3.8

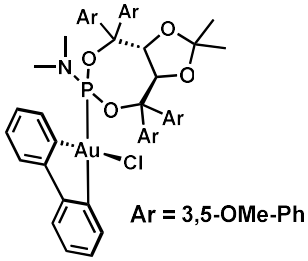

Prepared according to the general procedure with the corresponding phosphoramidite. **^{1}H NMR** (300 MHz, $CDCl_3$, mixture of atropisomers) δ 8.15 (ddd, J = 13.8, 7.7, 1.3 Hz, 1H), 7.31 – 7.24 (m, 3H), 7.16 – 7.00 (m, 4H), 6.88 (d, J = 2.3 Hz, 2H), 6.79 (td, J = 7.6, 1.6 Hz, 1H), 6.76 – 6.60 (m, 1H), 6.54 (d, J = 2.3 Hz, 2H), 6.51 (d, J = 2.1 Hz, 2H), 6.42 (dt, J = 5.7, 2.3 Hz, 3H), 5.83 (t, J = 2.1 Hz, 1H), 5.75 (d, J = 7.9 Hz, 1H), 5.31 (d, J = 7.8 Hz, 1H), 3.88 (s, 6H), 3.79 (s, 6H), 3.72 (s, 6H), 3.27 (s, 6H), 2.43 (s, 3H), 2.40 (s, 3H), 0.70 (s, 3H), 0.65 (s, 3H).; **^{13}C NMR** (101 MHz, $CDCl_3$, mixture of atropisomers) δ 165.01, 163.02, 160.90, 160.77, 159.92, 159.47, 154.30, 154.17, 154.10, 152.64, 152.62, 146.17, 142.19, 142.11, 141.90, 141.82, 140.76, 132.83, 132.79, 131.89, 131.80, 127.57, 127.24, 126.99, 126.96, 126.55, 126.40, 121.40, 120.72, 120.62, 115.46, 108.50, 108.08, 107.92, 105.83, 100.51, 99.93, 99.75, 99.47, 91.74, 91.53, 88.75, 79.61, 77.84, 77.36, 56.17, 55.63, 55.51, 54.96, 37.38, 37.27, 26.88, 26.69.; **^{31}P NMR** (162 MHz, $CDCl_3$) δ 122.24.

3.4.3 Preparation and Characterization of Mukaiyama-Michael Products

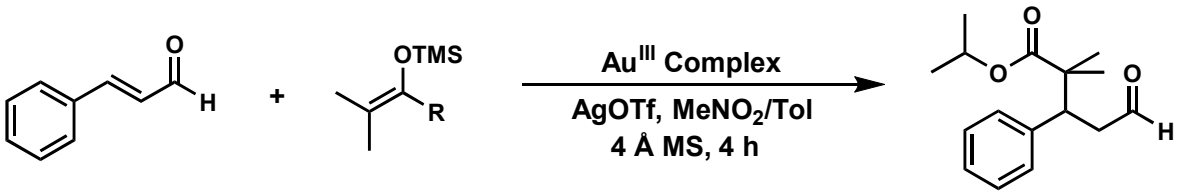

Scheme 3.6 General preparation for Mukaiyama-Michael products.

To the gold(III) complex (0.1 equiv) in nitromethane (1.2 M) and toluene (0.166 M) was added the silver salt (0.1 equiv) in a 1 dram vial. The resultant reaction mixture was sonicated for 15 minutes and then passed through a glass fiber filter in to a 1 dram vial with 4 Å mol sieves (1720 mg / mmol of aldehyde). To this vial was then added aldehyde (1 equiv) and silyl ketene acetal (3 equiv). The silyl ketene acetal was added in four portions spaced 1 hour apart. After the final addition of the silyl ketene acetal the reaction mixture was stirred for 1 hour and the filtered over a glass fiber filter in to a 1 dram vial. To this vial containing the reaction mixture was then added trifluoroacetic acid and subsequently stirred for 1 hr. The reaction mixture was then concentrated under reduced pressure and purified by column chromatography.

isopropyl 2,2-dimethyl-5-oxo-3-phenylpentanoate

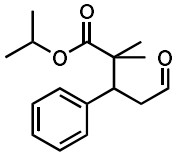

Prepared according to the general procedure. Purified by column chromatography (9:1 hexanes:ethyl acetate). Characterization matches previously reported data.[7] **HPLC** Chiralpak IC column (98:2 hexanes:isopropanol, 1 mL/min, 206 nm); first enantiomer tr = 14.3 min, second enantiomer tr = 15.9 min.

isopropyl 3-(4-methoxyphenyl)-2,2-dimethyl-5-oxopentanoate

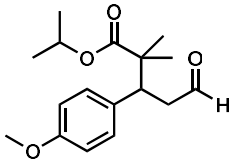

Prepared according to the general procedure. Purified by column chromatography (9:1 hexanes:ethyl acetate). **^{1}H NMR** (500 MHz, $CDCl_3$) δ 9.51 (dd, *J* = 3.0, 1.3 Hz, 1H), 7.13 – 7.09 (m, 2H), 6.84 – 6.80 (m, 2H), 4.98 (hept, *J* = 6.3 Hz, 1H), 3.57 (dd, *J* = 11.6, 3.7 Hz, 1H), 2.92 (ddd, *J* = 16.6, 11.6, 3.0 Hz, 1H), 2.62 (ddd, *J* = 16.6, 3.7, 1.3 Hz, 1H), 1.24 (d, *J* = 6.2 Hz, 3H), 1.20 (d, *J* = 6.3 Hz, 3H), 1.11 (s, 3H), 1.05 (s, 3H).; **^{13}C NMR** (151 MHz, $CDCl_3$) δ 201.70, 176.64, 158.85, 131.04, 130.73, 113.71, 77.16, 68.18, 55.35, 46.12, 46.01, 45.10, 24.64, 21.90, 21.83, 21.11.; **HPLC** Chiralpak IA column (98:2 hexanes:isopropanol, 1 mL/min, 230 nm); first enantiomer tr = 9.3 min, second enantiomer tr = 9.8 min.

isopropyl 2,2-dimethyl-5-oxo-3-(p-tolyl)pentanoate

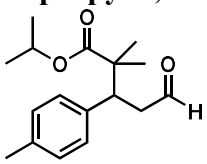

Prepared according to the general procedure. Purified by column chromatography (9:1 hexanes:ethyl acetate). **^{1}H NMR** (300 MHz, $CDCl_3$) δ 9.51 (dd, *J* = 2.9, 1.4 Hz, 1H), 7.08 (m, 4H), 4.98 (hept, *J* = 6.2 Hz, 1H), 3.58 (dd, *J* = 11.4, 3.8 Hz, 1H), 2.94 (ddd, *J* = 16.6, 11.5, 2.9 Hz, 1H), 2.62 (ddd, *J* = 16.6, 3.8, 1.4 Hz, 1H), 2.31 (s, 3H), 1.24 (d, *J* = 6.3 Hz, 3H), 1.20 (d, *J* = 6.3 Hz, 3H), 1.11 (s, 3H), 1.06 (s, 3H).; **^{13}C NMR** (126 MHz, $CDCl_3$) δ 201.69, 176.64, 136.98, 135.99, 129.65, 129.01, 77.16, 68.19, 46.38, 46.03, 45.05, 24.73, 21.90, 21.82, 21.07, 2.09.

isopropyl 3-(4-chlorophenyl)-2,2-dimethyl-5-oxopentanoate

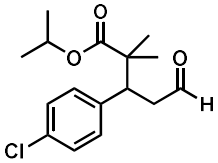

Prepared according to the general procedure. Purified by column chromatography (9:1 hexanes:ethyl acetate). **^{1}H NMR** (300 MHz, $CDCl_3$) δ 9.54 (d, *J* = 2.5 Hz, 1H), 7.30 – 7.24 (m, 2H), 7.13 (d, *J* = 8.6 Hz, 2H), 4.98 (hept, *J* = 6.2 Hz, 1H), 3.61 (dd, *J* = 11.3, 3.6 Hz, 1H), 2.94 (ddd, *J* = 17.1, 11.4, 2.6 Hz, 1H), 2.69 (dd, *J* = 17.0, 3.7 Hz, 1H), 1.23 (d, *J* = 6.3 Hz, 3H), 1.19 (d, *J* = 6.2 Hz, 3H), 1.11 (s, 3H), 1.06 (s, 3H).; **^{13}C NMR** (151 MHz, $CDCl_3$) δ 200.83, 176.26, 137.88, 133.26, 131.00, 128.50, 77.16, 68.39, 46.03, 45.91, 45.09, 24.56, 21.88, 21.81, 21.34.

ethyl 2,2-dimethyl-5-oxo-3-phenylpentanoate

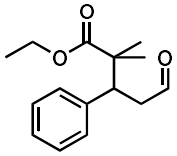

Prepared according to the general procedure. Purified by column chromatography (9:1 hexanes:ethyl acetate). **^{1}H NMR** (600 MHz, $CDCl_3$) δ 9.53 (dd, J = 2.6, 1.3 Hz, 1H), 7.29 (dd, J = 8.3, 6.7 Hz, 2H), 7.25 – 7.21 (m, 1H), 7.21 – 7.15 (m, 2H), 4.11 (qd, J = 7.2, 2.4 Hz, 2H), 3.62 (dd, J = 11.1, 4.0 Hz, 1H), 2.97 (ddd, J = 16.8, 11.2, 2.7 Hz, 1H), 2.69 (ddd, J = 16.8, 4.0, 1.4 Hz, 1H), 1.24 (t, J = 7.2 Hz, 3H), 1.15 (s, 3H), 1.09 (s, 3H).; **^{13}C NMR** (151 MHz, CDCl3) δ 201.25, 176.84, 139.02, 129.50, 128.14, 127.22, 60.71, 46.67, 45.90, 44.82, 24.39, 21.16, 14.07.; **HPLC** Chiralpak IC column (98:2 hexanes:isopropanol, 1 mL/min, 192 nm); first enantiomer tr = 15.2 min, second enantiomer tr = 17.9 min.

ethyl 3-(4-chlorophenyl)-2,2-dimethyl-5-oxopentanoate

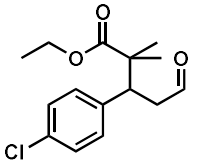

Prepared according to the general procedure. Purified by column chromatography (9:1 hexanes:ethyl acetate). **^{1}H NMR** (600 MHz, $CDCl_3$) δ 9.55 – 9.54 (m, 1H), 7.28 – 7.25 (m, 2H),

7.14 – 7.10 (m, 2H), 4.16 – 4.06 (m, 2H), 3.61 (dd, J = 11.1, 3.8 Hz, 1H), 2.99 – 2.89 (m, 1H), 2.71 (ddt, J = 17.2, 4.0, 1.2 Hz, 1H), 1.24 (t, J = 7.1 Hz, 3H), 1.13 (s, 3H), 1.08 (s, 3H).; **HPLC** Chiralpak OD-H column (99:1 hexanes:isopropanol, 1 mL/min, 232 nm); first enantiomer tr = 19.6 min, second enantiomer tr = 25.6 min.

ethyl 2,2-dimethyl-5-oxo-3-(p-tolyl)pentanoate

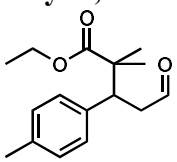

Prepared according to the general procedure. Purified by column chromatography (9:1 hexanes:ethyl acetate). **^{1}H NMR** (400 MHz, CDCl3) δ 9.51 (s, 1H), 7.15 – 7.02 (m, 4H), 4.28 – 3.98 (m, 2H), 3.59 (dd, J = 11.2, 3.9 Hz, 1H), 3.11 – 2.80 (m, 1H), 2.65 (dd, J = 16.3, 3.9 Hz, 1H), 2.31 (s, 3H), 1.24 (t, J = 7.1 Hz, 3H), 1.13 (s, 3H), 1.08 (s, 3H).; **HPLC** Chiralpak OD-H column (99:1 hexanes:isopropanol, 1 mL/min, 232 nm); first enantiomer tr = 14.6 min, second enantiomer tr = 22.2 min.

phenethyl 2,2-dimethyl-5-oxo-3-phenylpentanoate

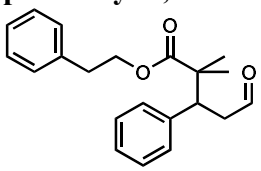

Prepared according to the general procedure. Purified by column chromatography (9:1 hexanes:ethyl acetate). **^{1}H NMR** (300 MHz, $CDCl_3$) δ 9.43 (dd, J = 2.8, 1.3 Hz, 1H), 7.39 – 7.32 (m, 2H), 7.29-7.22 (m, 6H) 7.17 – 7.13 (m, 2H), 4.33 (td, J = 6.8, 3.3 Hz, 2H), 3.58 (dd, J = 11.2, 4.0 Hz, 1H), 2.97 (t, J = 6.7 Hz, 2H), 2.94 – 2.84 (m, 1H), 2.56 (ddd, J = 16.8, 4.0, 1.3 Hz, 1H), 1.15 (s, 3H), 1.08 (s, 3H).; **^{13}C NMR** (151 MHz, $CDCl_3$) δ 201.34, 176.92, 139.04, 137.96, 129.63, 129.06, 128.66, 128.31, 127.40, 126.78, 65.35, 46.78, 46.17, 44.83, 35.12, 24.54, 21.27.; **HPLC** Chiralpak OD-H column (95:5 hexanes:isopropanol, 1 mL/min, 223 nm); first enantiomer tr = 15.8 min, second enantiomer tr = 17.8 min.

phenethyl 2,2-dimethyl-3-(2-oxoethyl)hexanoate

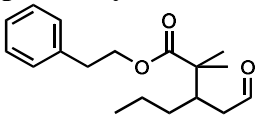

Prepared according to the general procedure. Purified by column chromatography (9:1 hexanes:ethyl acetate). **^{1}H NMR** (600 MHz, $CDCl_3$) δ 9.64 (dd, J = 2.5, 1.6 Hz, 1H), 7.32 – 7.28 (m, 2H), 7.24 – 7.20 (m, 3H), 4.28 (td, J = 6.9, 1.0 Hz, 2H), 2.94 (t, J = 6.9 Hz, 2H), 2.37 (ddd, J = 16.9, 4.6, 1.7 Hz, 1H), 2.34 – 2.29 (m, 1H), 2.17 (ddd, J = 16.9, 6.3, 2.5 Hz, 1H), 1.32 – 1.23 (m, 2H), 1.13 – 1.00 (m, 8), 0.84 (t, J = 7.0 Hz, 3H).; **^{13}C NMR** (151 MHz, $CDCl_3$) δ 202.23, 177.35, 137.78, 128.88, 128.44, 126.55, 64.99, 45.93, 45.93, 39.30, 34.98, 33.68, 22.62, 22.19, 21.27, 14.17.; **HPLC** Chiralpak OJ-H column (99:1 hexanes:isopropanol, 1 mL/min, 218 nm); first enantiomer tr = 16.6 min, second enantiomer tr = 18.1 min.

ethyl 3-ethyl-2,2-dimethyl-5-oxopentanoate

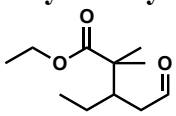

Prepared according to the general procedure. Purified by column chromatography (9:1 hexanes:ethyl acetate). **^{1}H NMR** (300 MHz, $CDCl_3$) δ 9.82 (t, J = 2.0 Hz, 1H), 4.16 (qd, J = 7.2, 1.2 Hz, 2H), 2.56 – 2.46 (m, 1H), 2.42 – 2.25 (m, 2H), 1.57 – 1.47 (m, 1H), 1.30 (t, J = 7.1 Hz, 3H), 1.24 – 1.08 (m, 8H), 0.93 (t, J = 7.4 Hz, 3H).; **GC** Cyclodex-B Column (30 m x 0.25 mm ID x 0.25 µm film). 160 °C, FID detector, first enantiomer tr = 8.65 min, second enantiomer 8.67 min.

3.4.4 Mol Sieve Characterization

To further understand the effect that the mol sieves have on the reaction we did further characterization first using BET (Brunauer, Emmett and Teller) to determine the specific surface area of the mol sieves. Using this method, we were able to discern that the 4 Å molecular sieves had a BET surface area of 2.1072 m^2/g. This measurement is quite low, therefore indicating that surface adsorption is likely not a significant contributing factor for the selectivity exhibited. We next tested the mol sieves using Diffuse Reflectance for Infrared Fourier Transform Spectroscopy (DRIFTS) to look at the composition of the mol sieves. To test for the presence of Brønsted and Lewis-Acid sites on the 4 Å mol sieves pyridine was added to the system and then monitored over a period of 11 minutes at 50 °C (Figure 3.1). The pyridine related peaks were found to rapidly diminish, indicating that there was no chemisorbed pyridine on the surface and therefore no strong Lewis-acid sites on the mol sieves. Additionally, a clear change in the DRIFTS signal is observed when the mol sieves are pretreated, demonstrating that water is adsorbed on the mol sieves from the manufacturer.

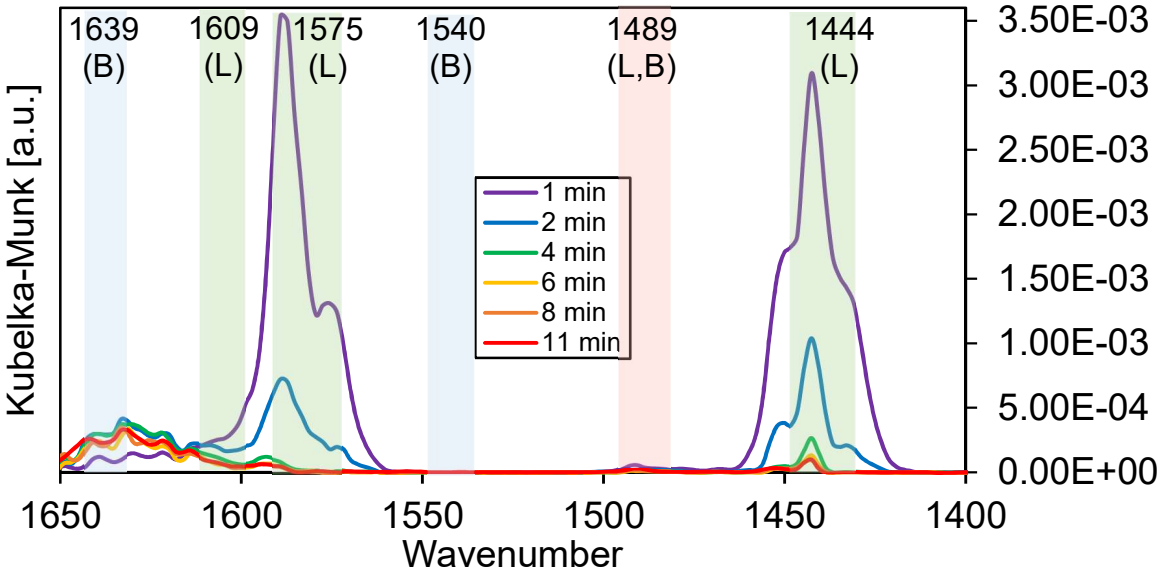

Figure 3.1 DRIFTS spectrum of the 4 Å mol sieves after addition of pyridine.

3.4.5 NMR Spectra

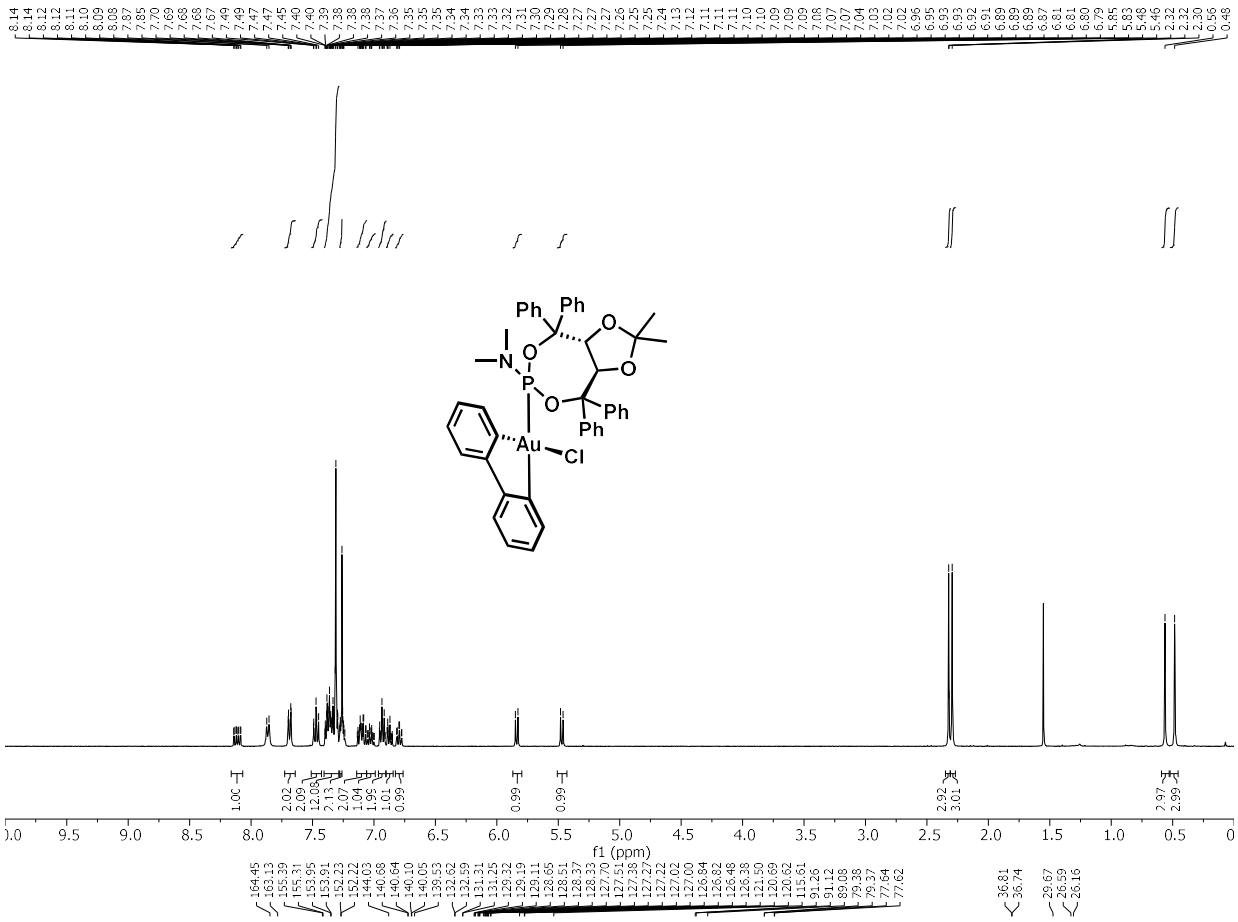
Ph
Ph
O
O
N
O
P
O
O
Ph
Ph
Au
Cl
f1 (ppm)

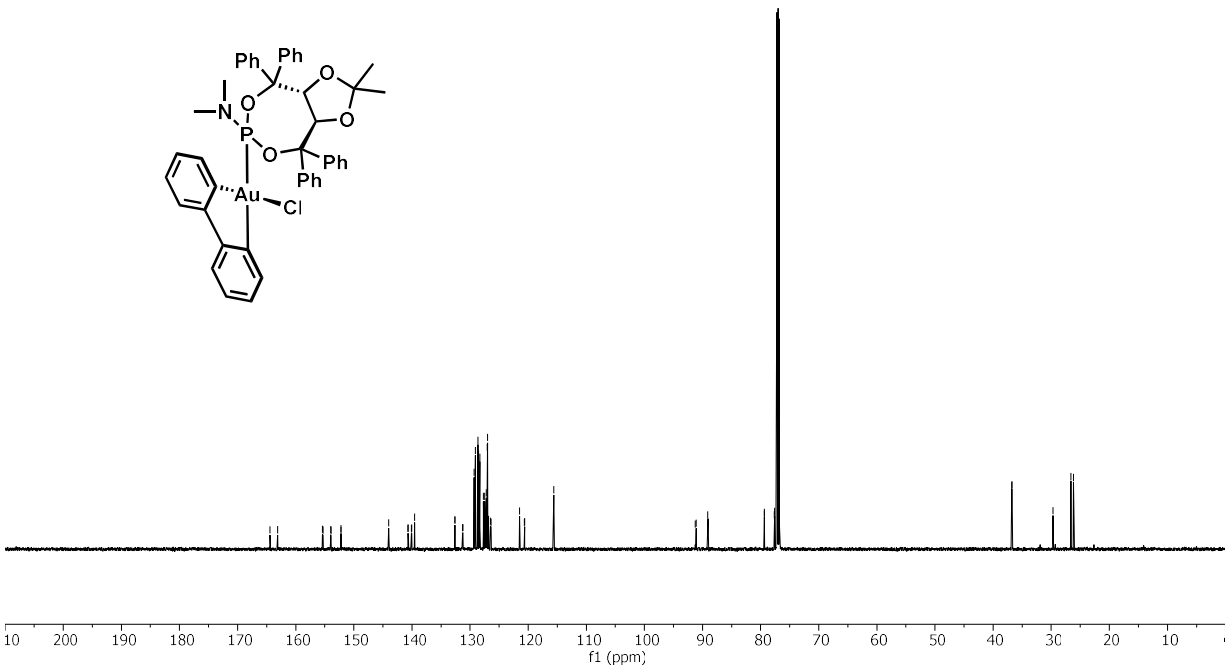
Ph
Ph
O
O
N
O
P
O
O
Ph
Ph
Au
Cl
f1 (ppm)

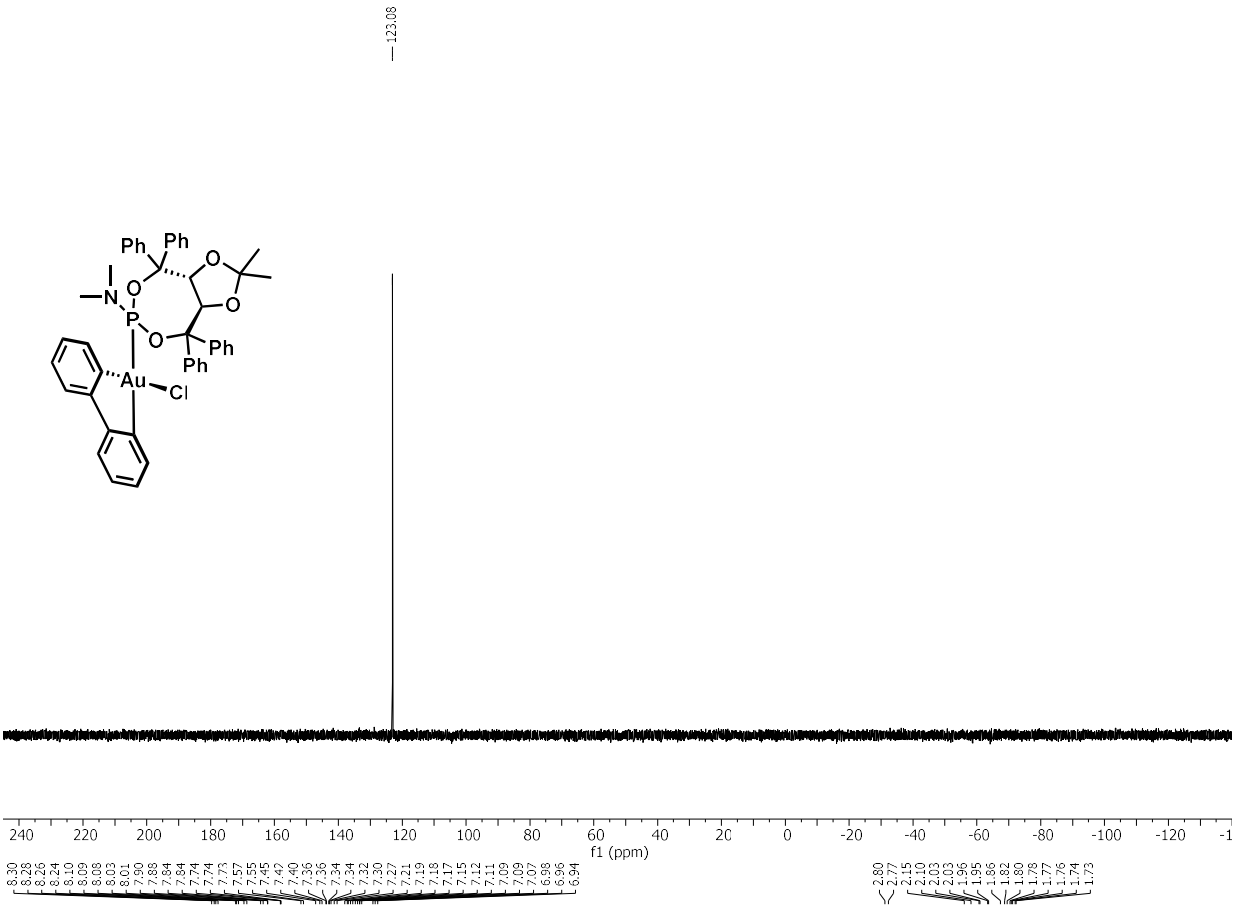
123.08
Ph
Ph
O
O
N
O
P
O
O
Ph
Ph
Au
Cl
f1 (ppm)

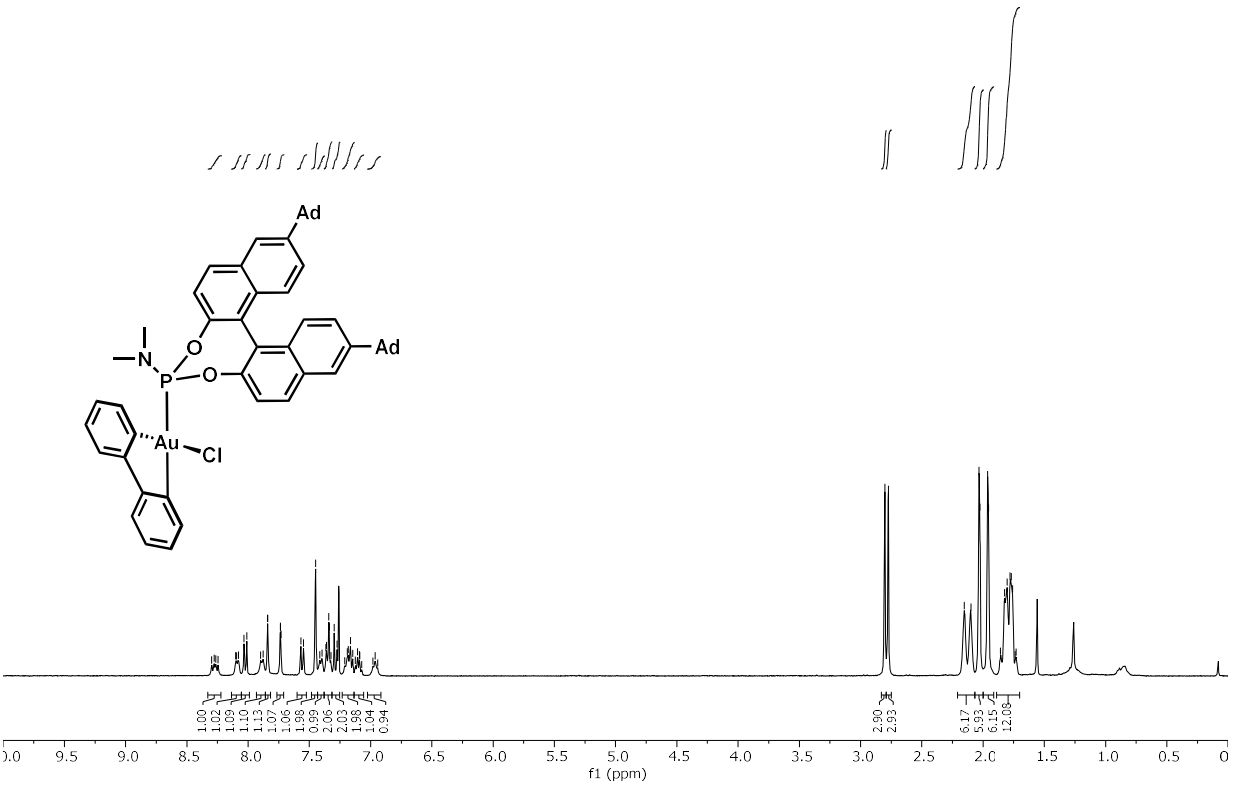
Ad
Ad
N
O
P
O
O
Au
Cl
f1 (ppm)

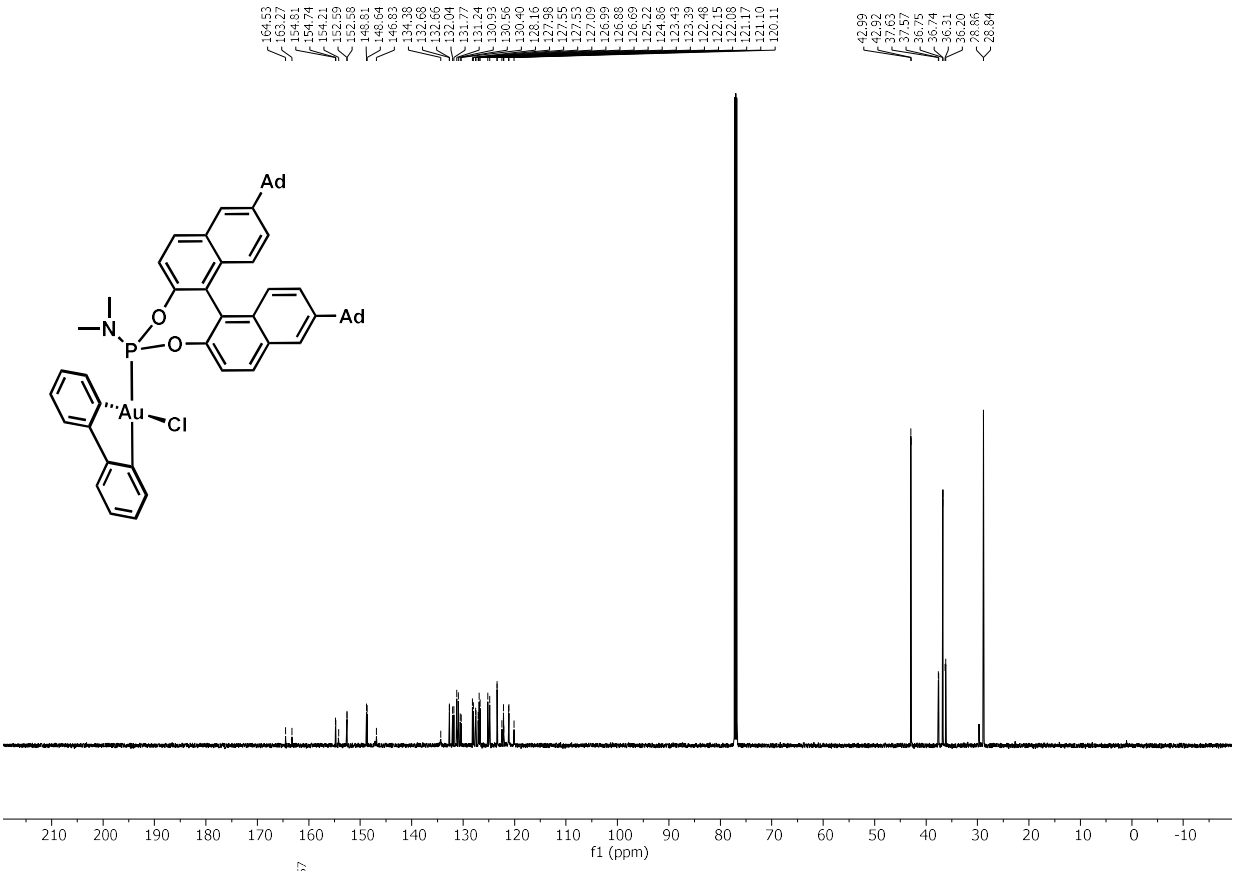
164.53
163.27
154.81
154.74
154.21
152.59
152.58
148.81
148.64
146.83
134.38
132.68
132.66
132.04
131.77
131.24
130.93
130.56
130.40
128.16
127.98
127.55
127.53
127.09
126.99
126.88
126.69
125.22
124.86
123.43
123.39
122.48
122.15
122.08
121.17
121.10
120.11
42.99
42.92
37.63
37.57
36.75
36.74
36.31
36.20
28.86
28.84
Ad
Ad
N
O
P
O
Au
Cl
210 200 190 180 170 160 150 140 130 120 110 100 90 80 70 60 50 40 30 20 10 0 -10
f1 (ppm)

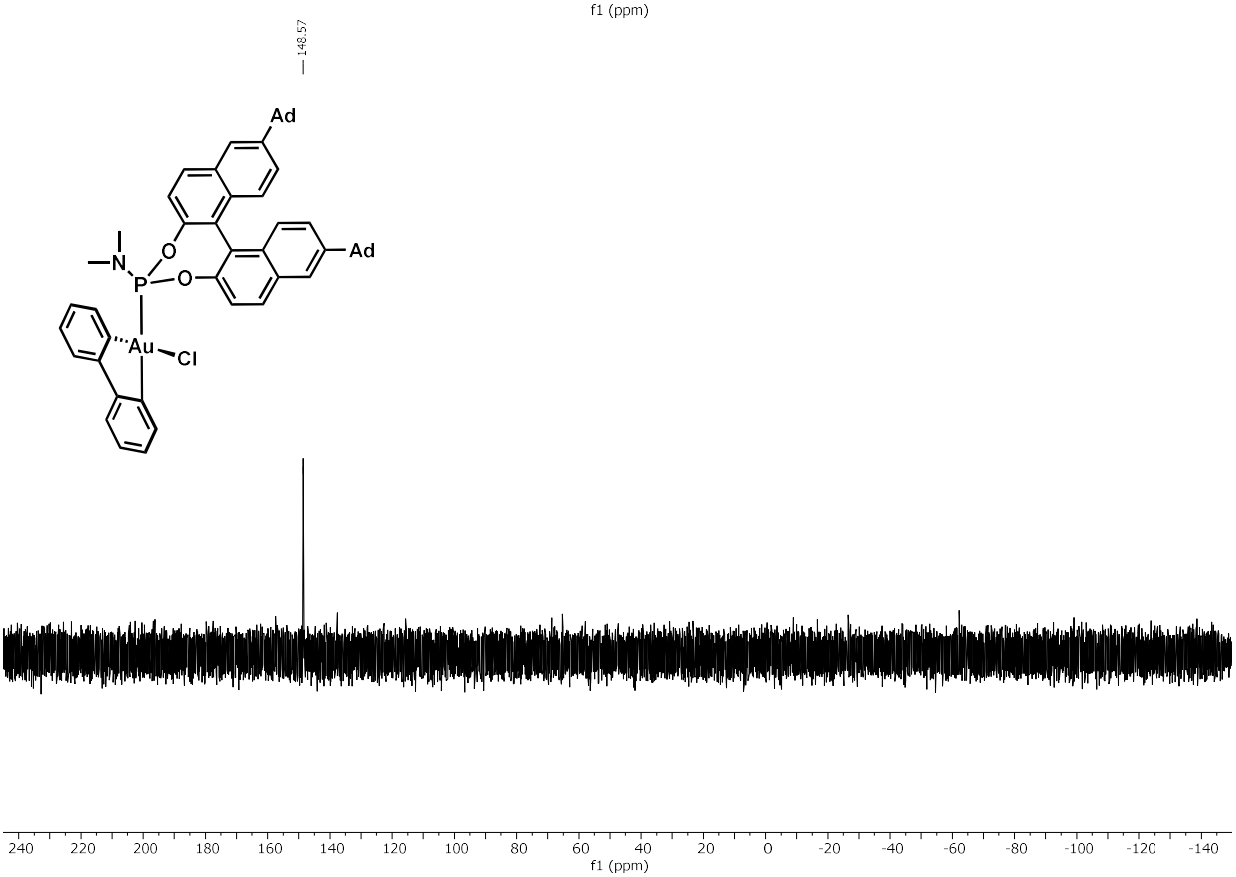
148.57
Ad
Ad
N
O
P
O
Au
Cl
240 220 200 180 160 140 120 100 80 60 40 20 0 -20 -40 -60 -80 -100 -120 -140
f1 (ppm)

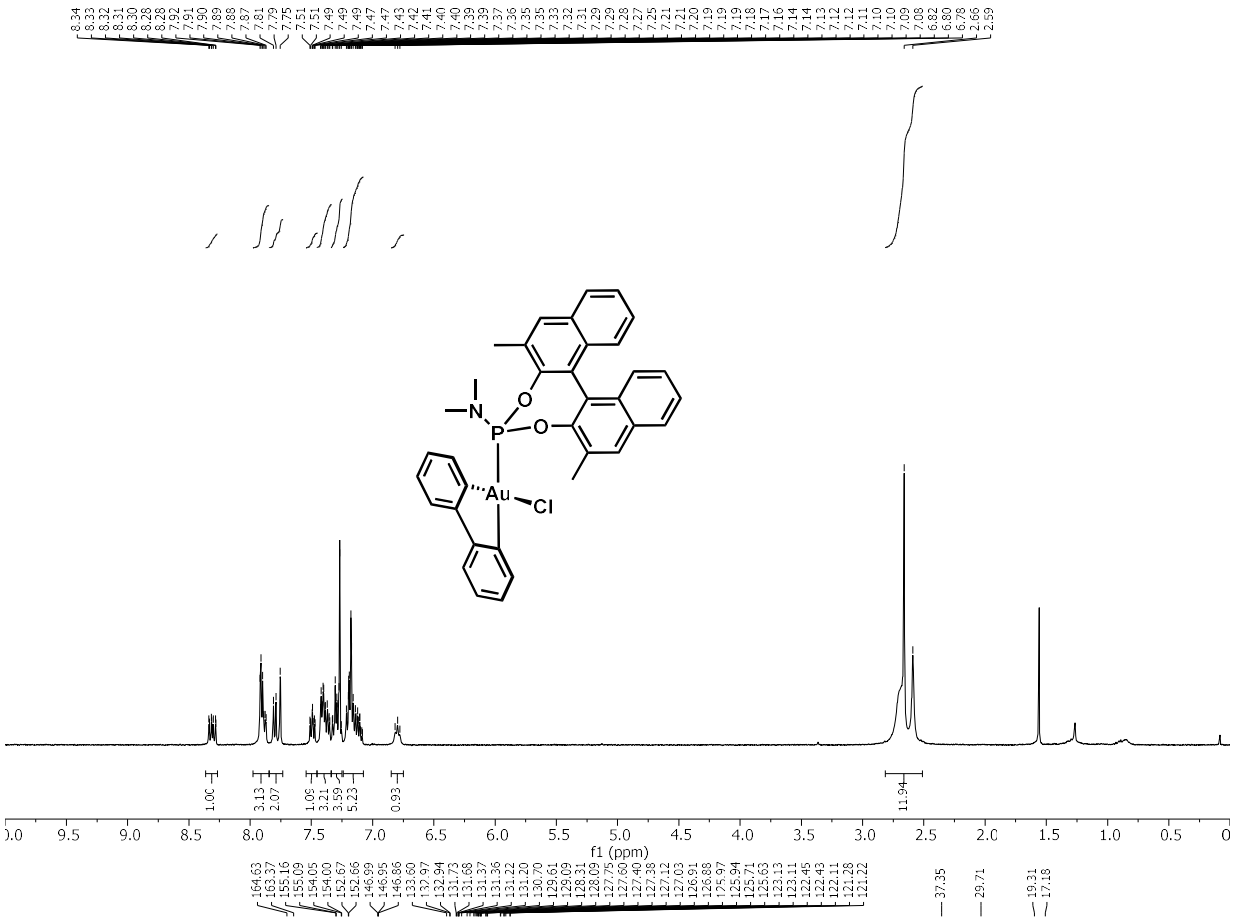
f1 (ppm)

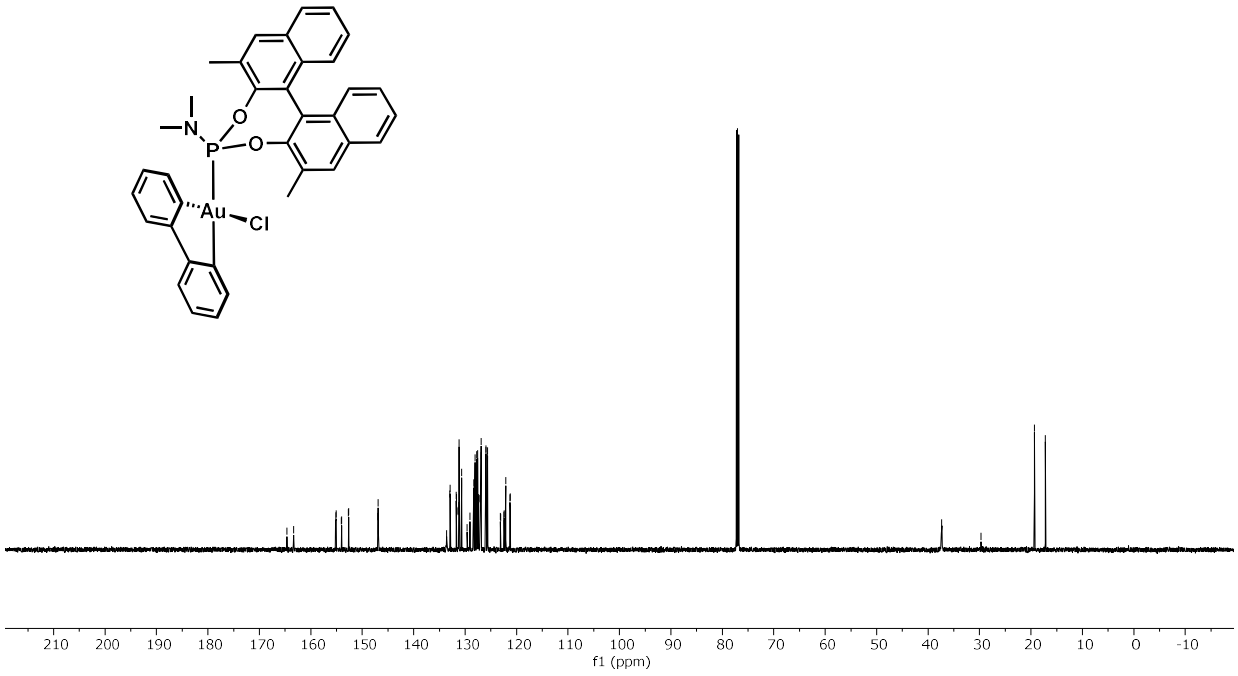
f1 (ppm)

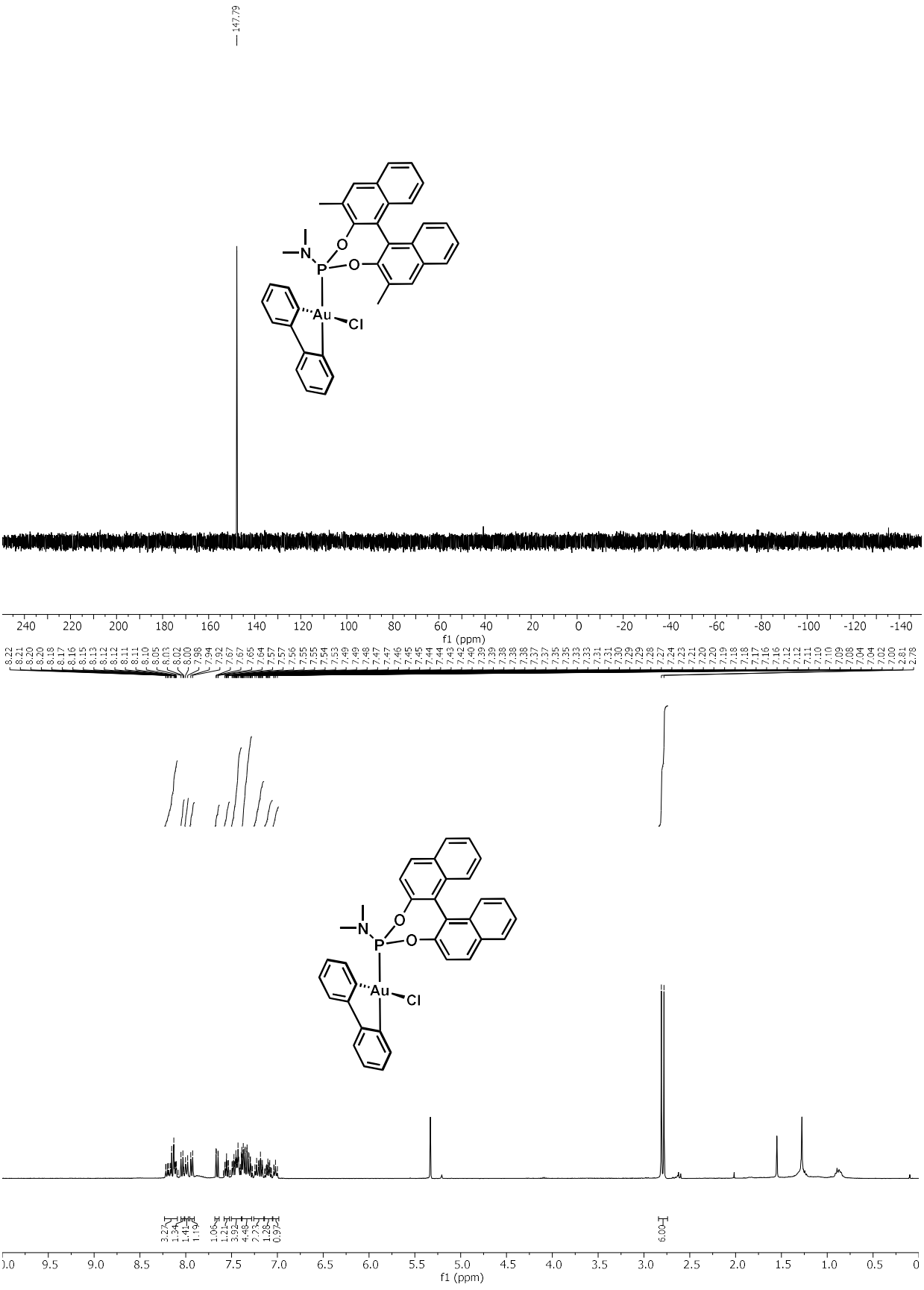
147.79
N
O
P
O
Au
Cl
f1 (ppm)
6.00
f1 (ppm)

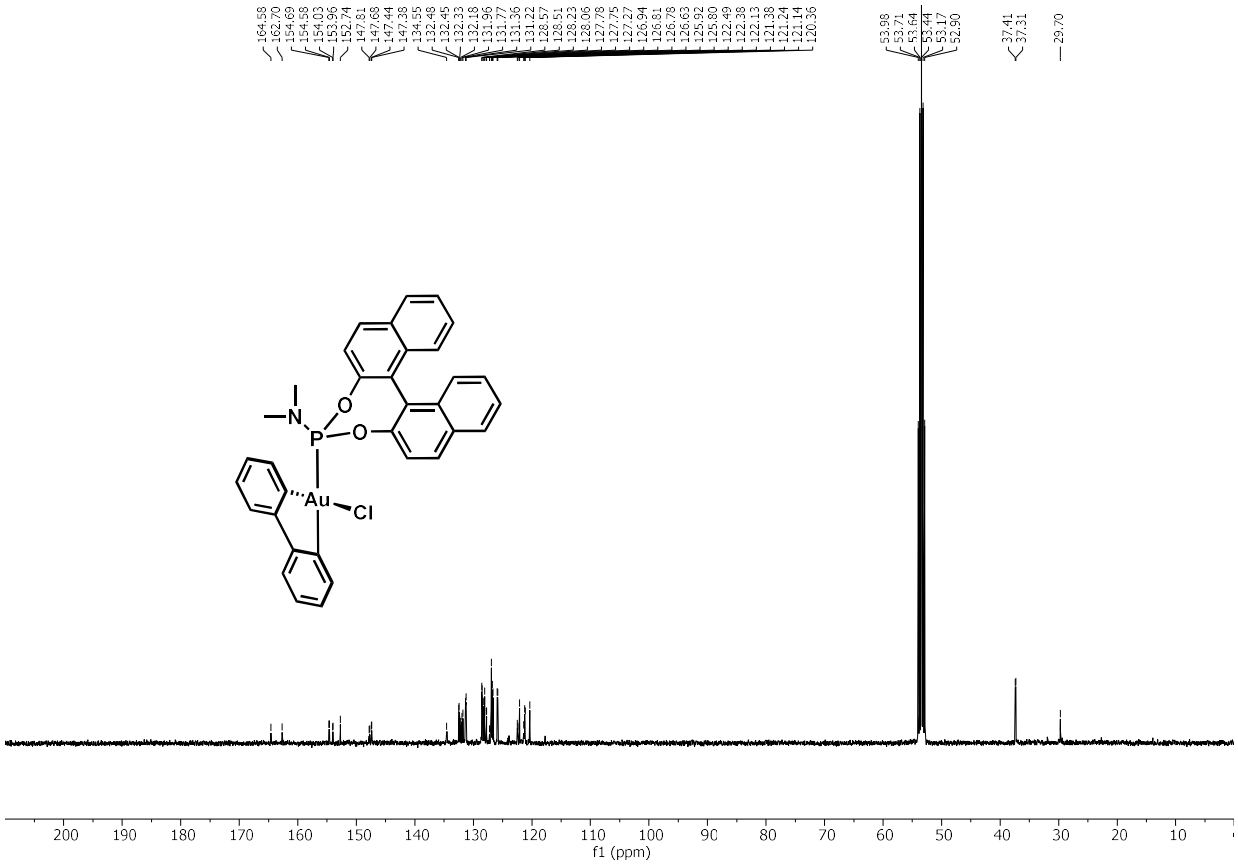
164.58
162.70
154.69
154.58
154.03
153.96
152.74
147.81
147.68
147.44
147.38
134.55
132.48
132.45
132.33
132.18
131.96
131.77
131.36
131.22
128.57
128.51
128.23
128.06
127.78
127.75
127.27
126.94
126.81
126.78
126.63
125.92
125.80
122.49
122.38
122.13
121.38
121.24
121.14
120.36
53.98
53.71
53.64
53.44
53.17
52.90
37.41
37.31
29.70
N
P
O
O
O
Au
Cl
200 190 180 170 160 150 140 130 120 110 100 90 80 70 60 50 40 30 20 10
f1 (ppm)

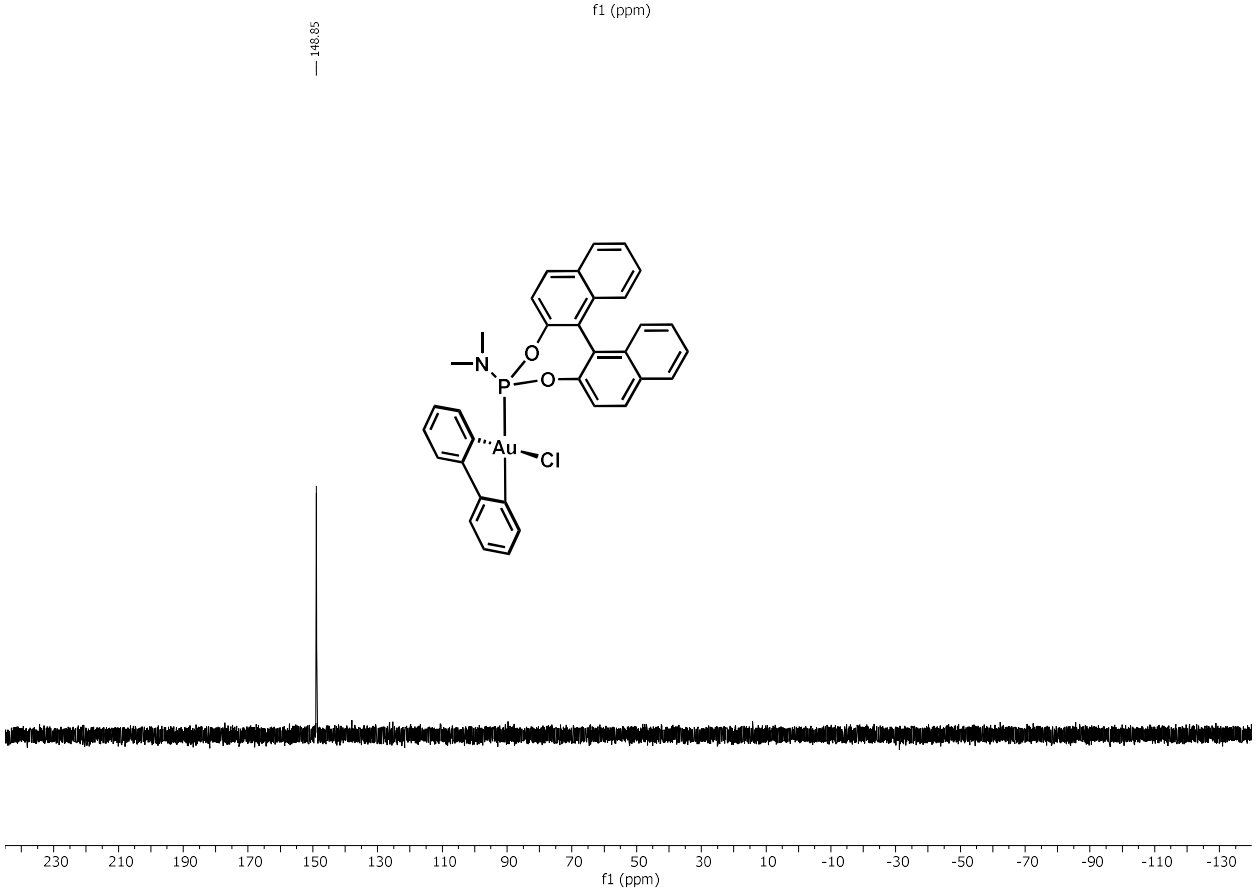
148.85
N
P
O
O
O
Au
Cl
230 210 190 170 150 130 110 90 70 50 30 10 -10 -30 -50 -70 -90 -110 -130
f1 (ppm)

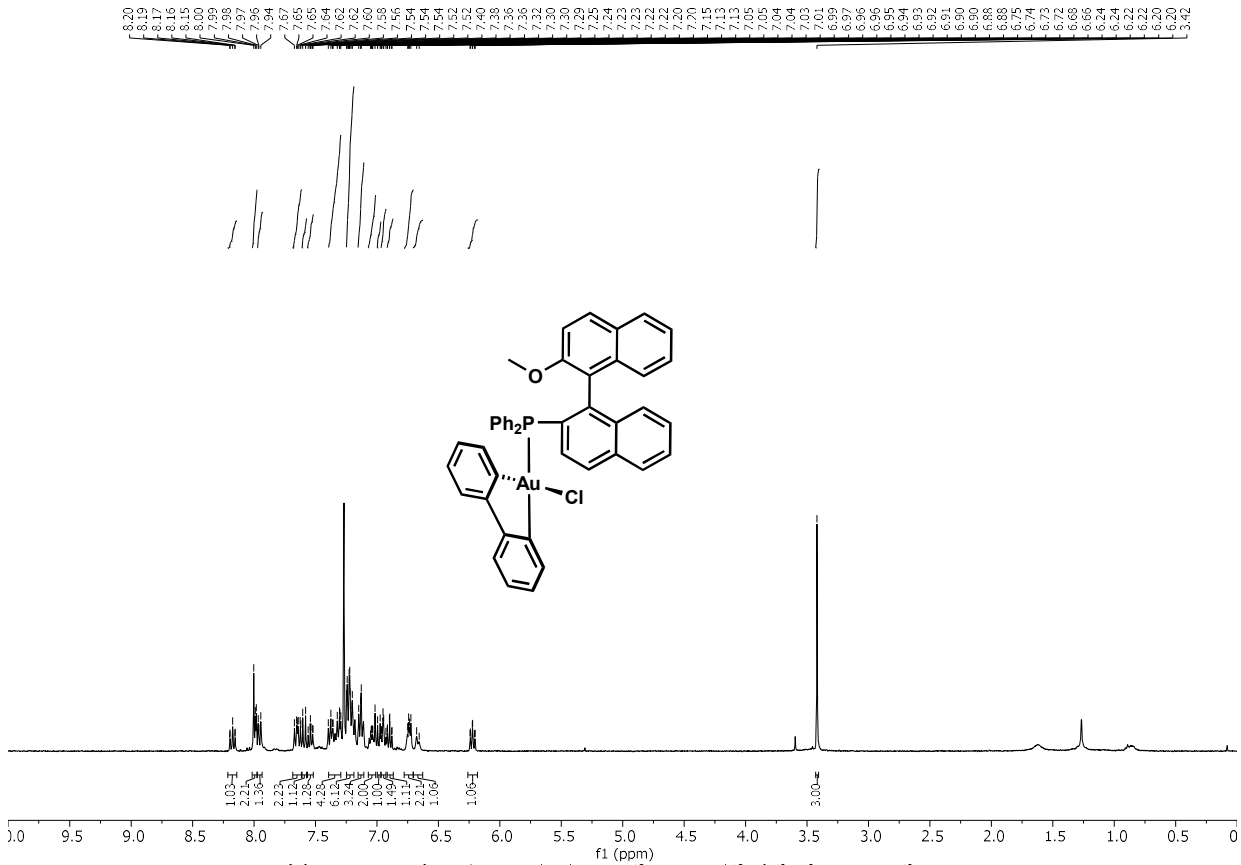
8.20 8.19 8.17 8.16 8.15 8.00 7.99 7.98 7.97 7.96 7.94 7.67 7.65 7.64 7.62 7.60 7.58 7.56 7.54 7.54 7.54 7.52 7.52 7.40 7.38 7.36 7.32 7.30 7.30 7.29 7.25 7.24 7.23 7.23 7.22 7.22 7.20 7.20 7.15 7.13 7.05 7.05 7.04 7.04 7.03 7.01 6.99 6.97 6.96 6.96 6.95 6.94 6.93 6.92 6.91 6.90 6.90 6.88 6.88 6.75 6.74 6.73 6.72 6.68 6.66 6.24 6.24 6.22 6.22 6.20 6.20 3.42
O
Ph2P
Au
Cl
1.03 2.25 1.36 2.23 1.12 1.28 4.28 6.12 3.24 2.00 1.00 1.49 1.11 2.21 1.06 1.06 3.00
f1 (ppm)

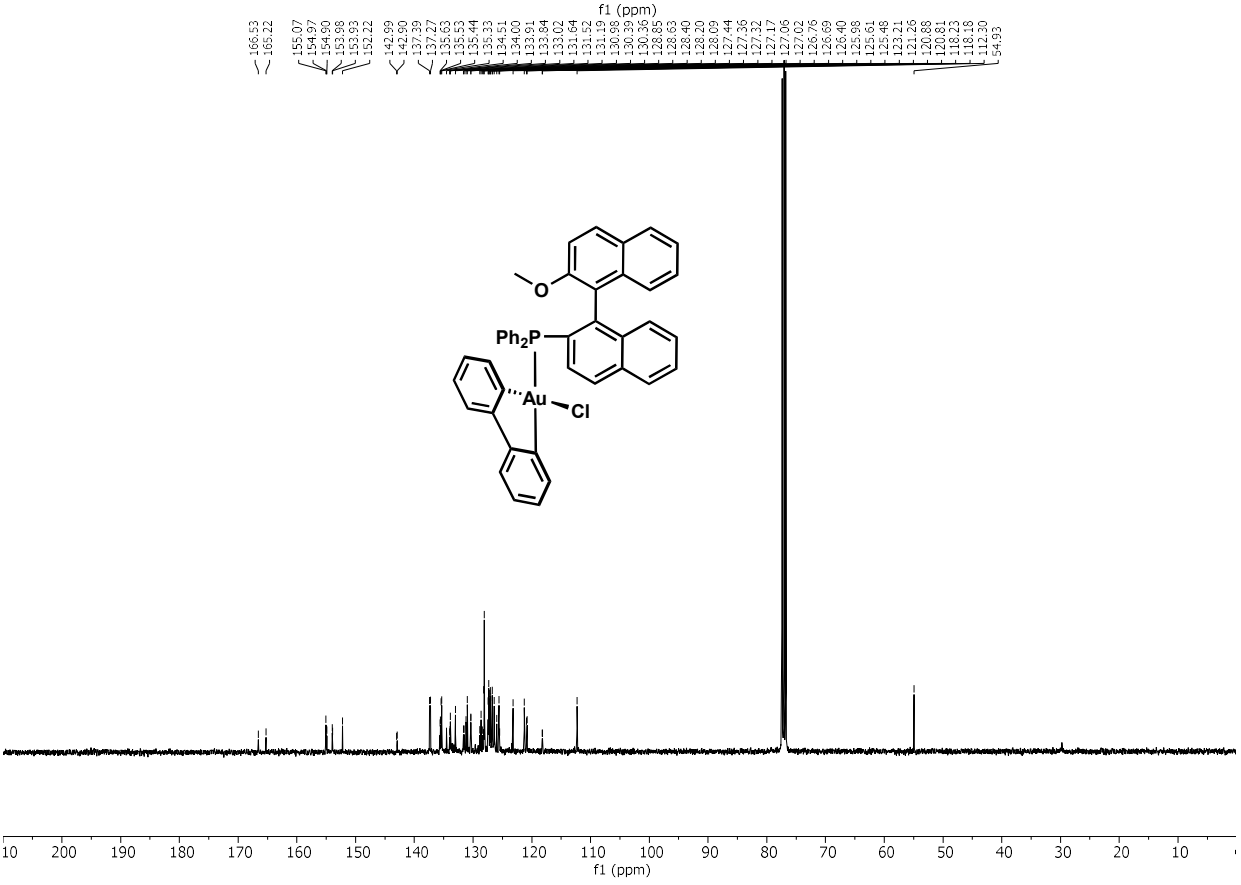
166.53 165.22 155.07 154.97 154.90 153.98 153.93 152.22 142.99 142.90 137.39 137.27 135.63 135.53 135.44 135.33 134.51 134.00 133.91 133.84 133.02 131.64 131.52 131.19 130.98 130.39 130.36 128.85 128.63 128.40 128.20 128.09 127.44 127.36 127.32 127.17 127.06 127.02 126.76 126.69 126.40 125.98 125.61 125.48 123.21 121.26 120.88 120.81 118.23 118.18 112.30 54.93
O
Ph2P
Au
Cl
f1 (ppm)

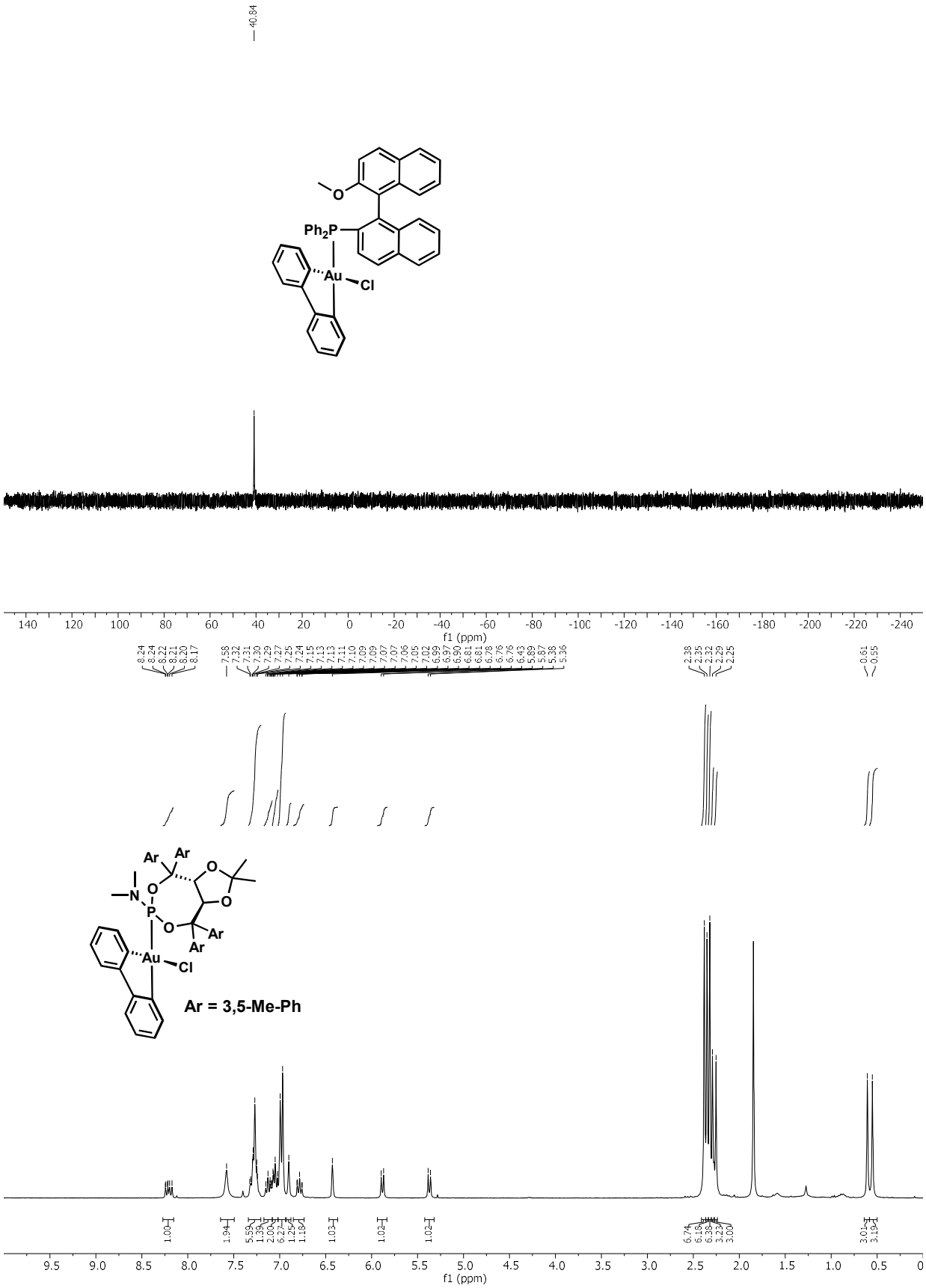
40.84
O
Ph2P
Au
Cl
f1 (ppm)
Ar
Ar
O
N
O
P
O
O
O
Ar
Ar
Au
Cl
Ar = 3,5-Me-Ph
f1 (ppm)

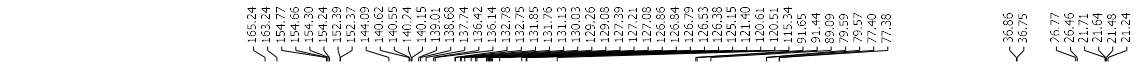

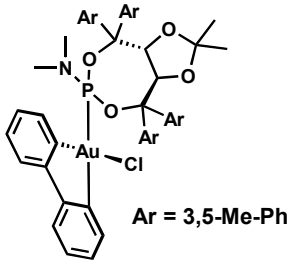

Ar = 3,5-Me-Ph

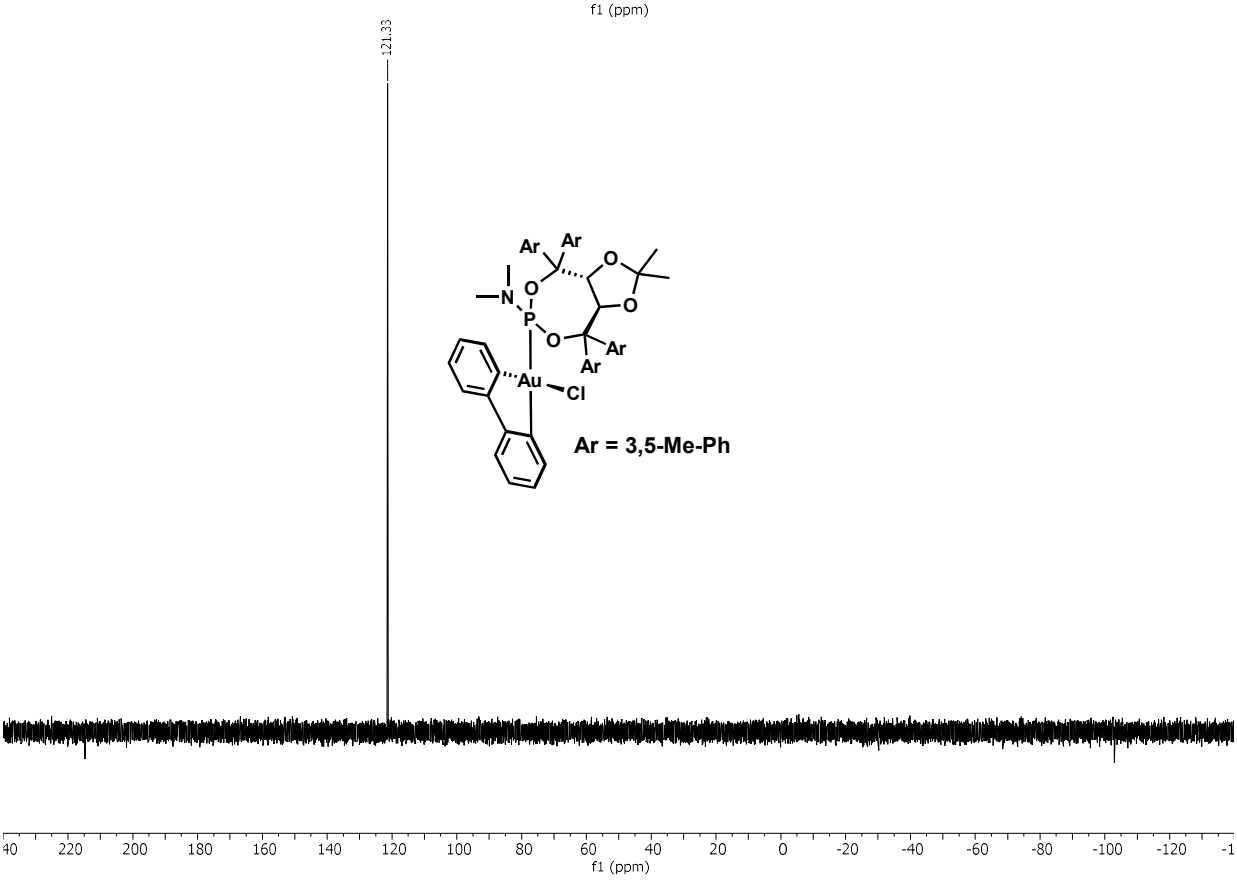

Ar = 3,5-Me-Ph

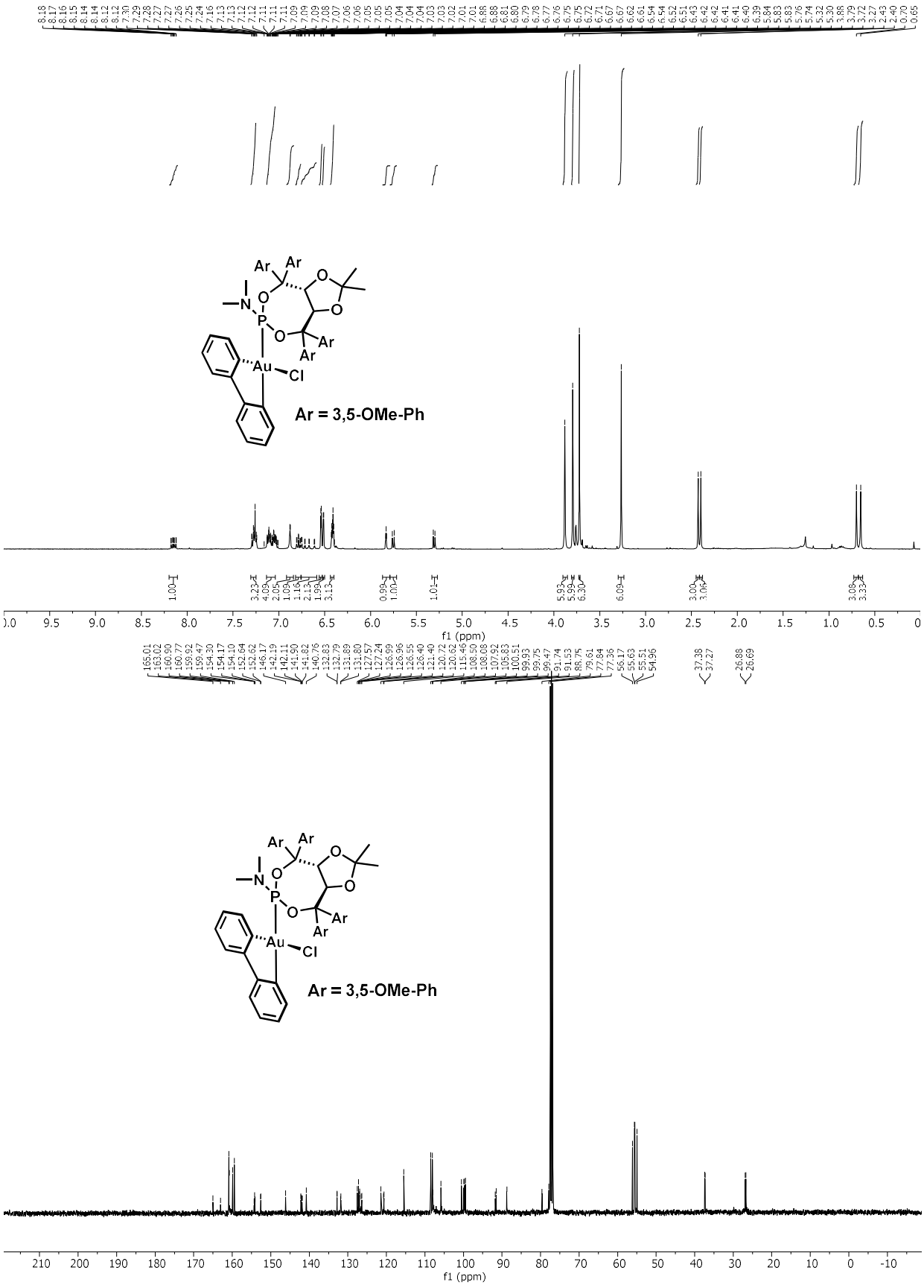
Ar = 3,5-OMe-Ph
f1 (ppm)
Ar = 3,5-OMe-Ph
f1 (ppm)

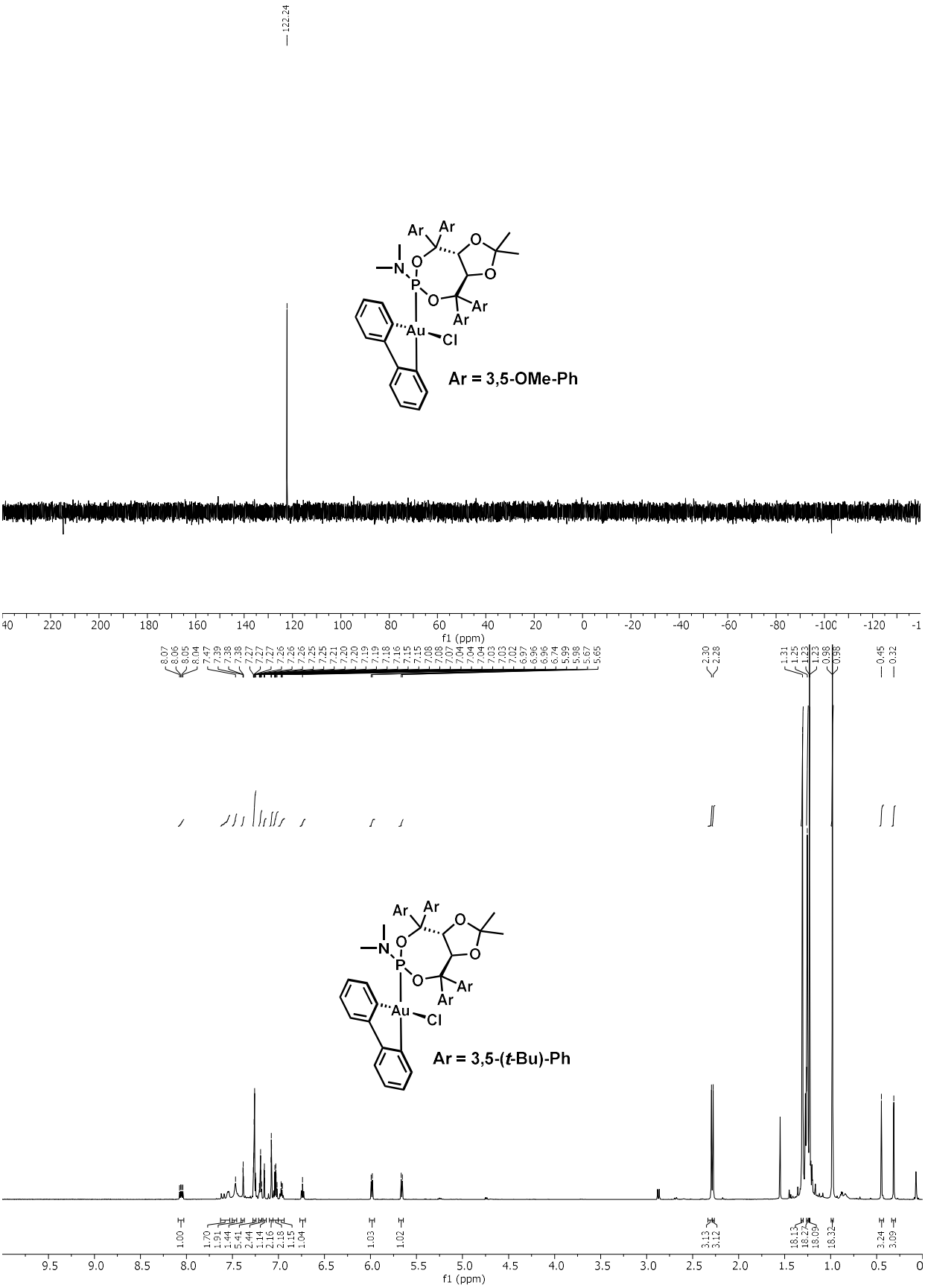
122.24
Ar = 3,5-OMe-Ph
f1 (ppm)
Ar = 3,5-(t-Bu)-Ph
f1 (ppm)

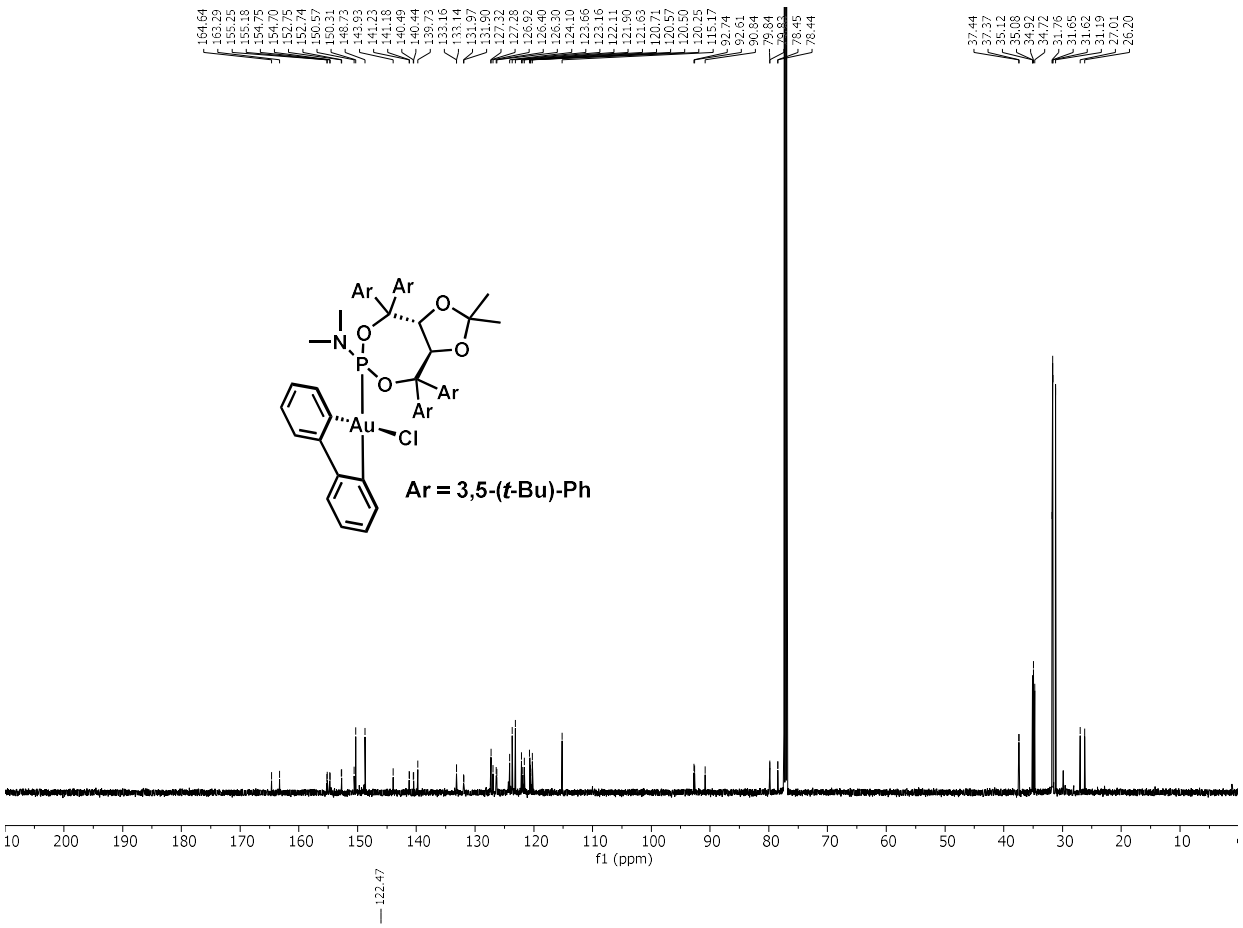
Ar = 3,5-(t-Bu)-Ph
f1 (ppm)

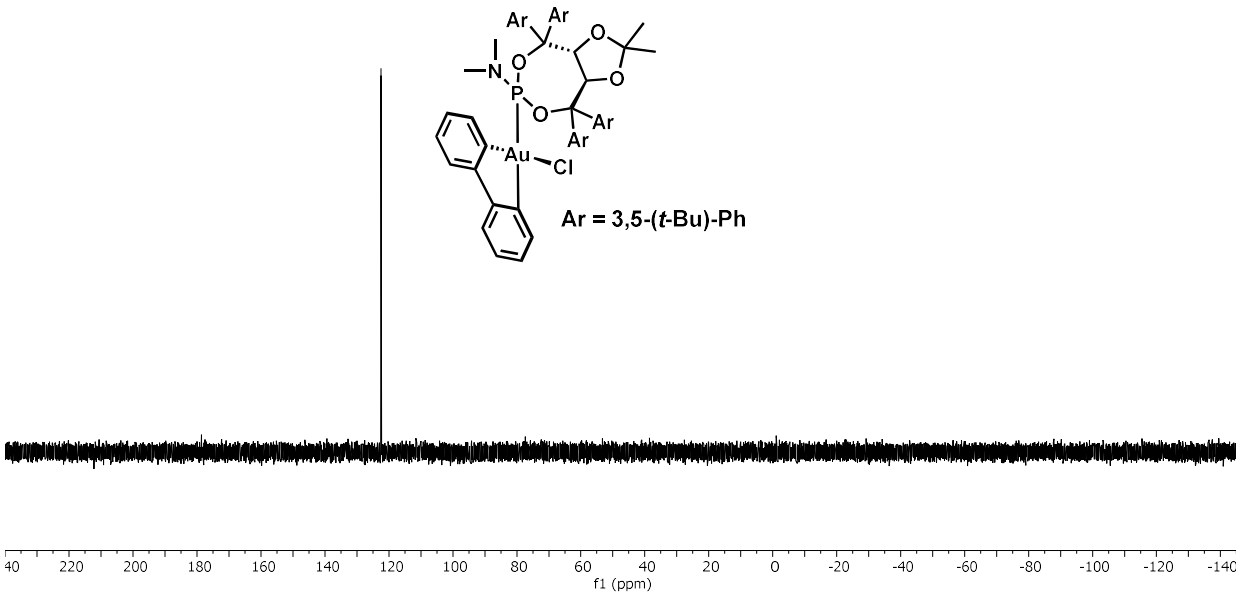
Ar = 3,5-(t-Bu)-Ph
f1 (ppm)

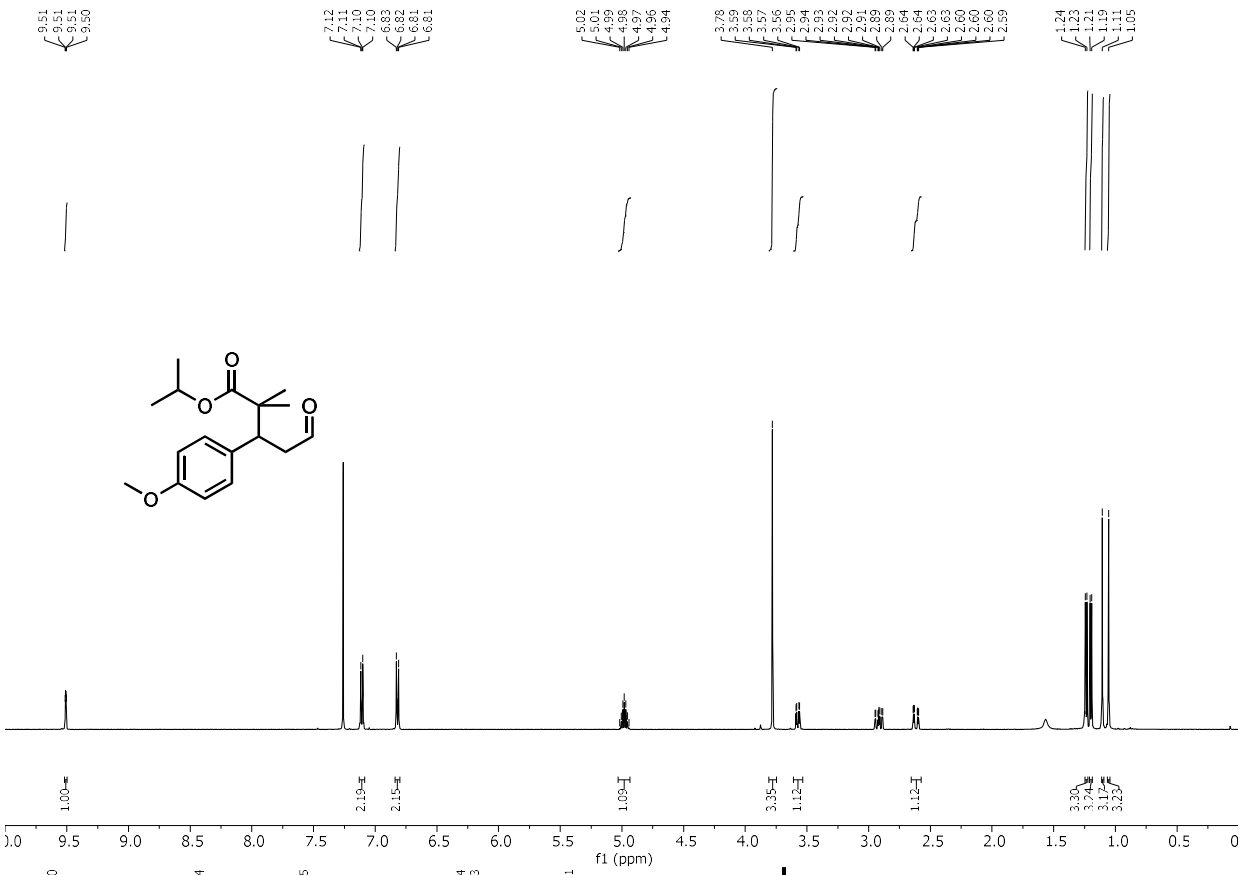
9.51
9.51
9.51
9.50
7.12
7.11
7.10
7.10
6.83
6.82
6.81
6.81
5.02
5.01
4.99
4.98
4.97
4.96
4.94
3.78
3.59
3.58
3.57
3.56
2.95
2.94
2.93
2.92
2.92
2.91
2.89
2.89
2.64
2.64
2.63
2.63
2.60
2.60
2.60
2.59
1.24
1.23
1.21
1.19
1.11
1.05
1.00
2.19
2.15
1.09
3.35
1.12
1.12
3.30
3.24
3.17
3.23
f1 (ppm)

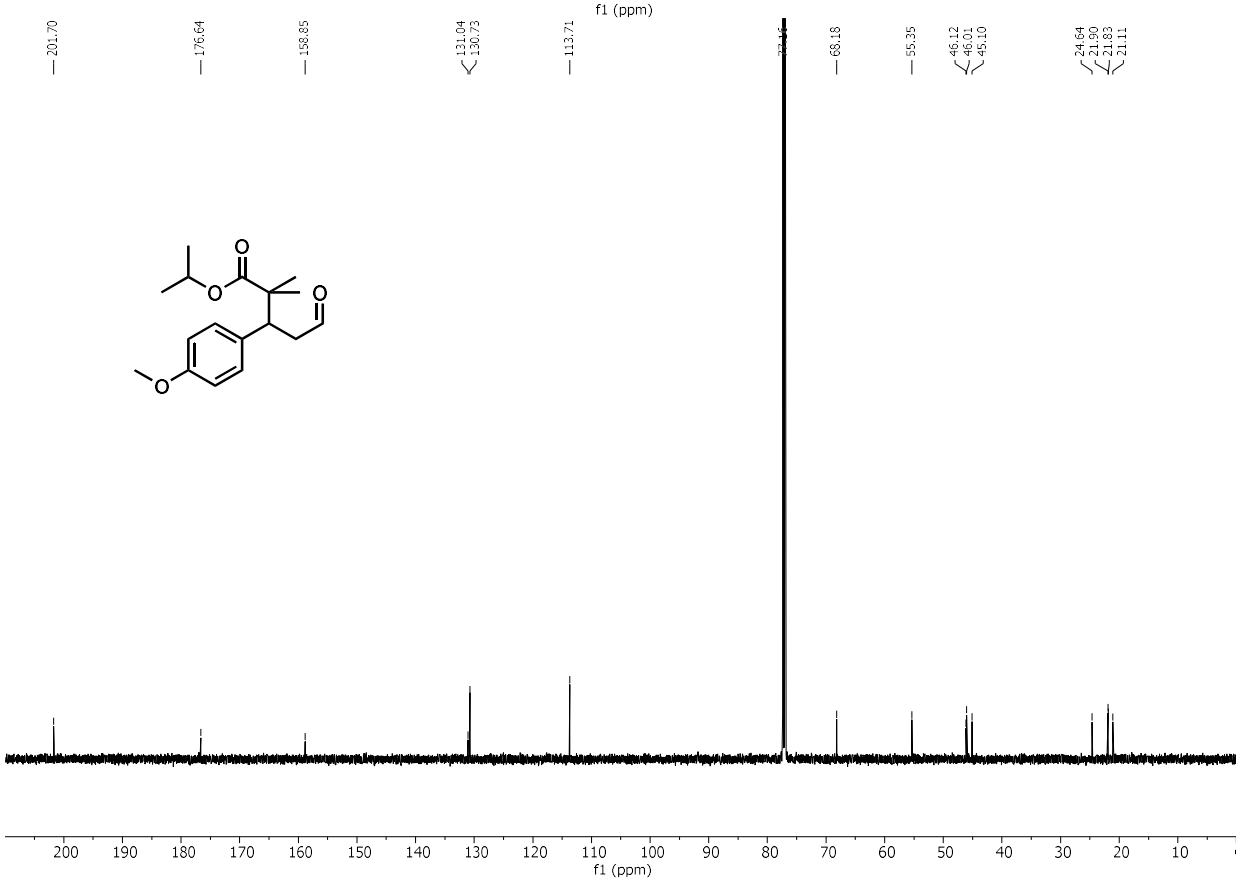
201.70
176.64
158.85
131.04
130.73
113.71
77.41
68.18
55.35
46.12
46.01
45.10
24.64
21.90
21.83
21.11
f1 (ppm)

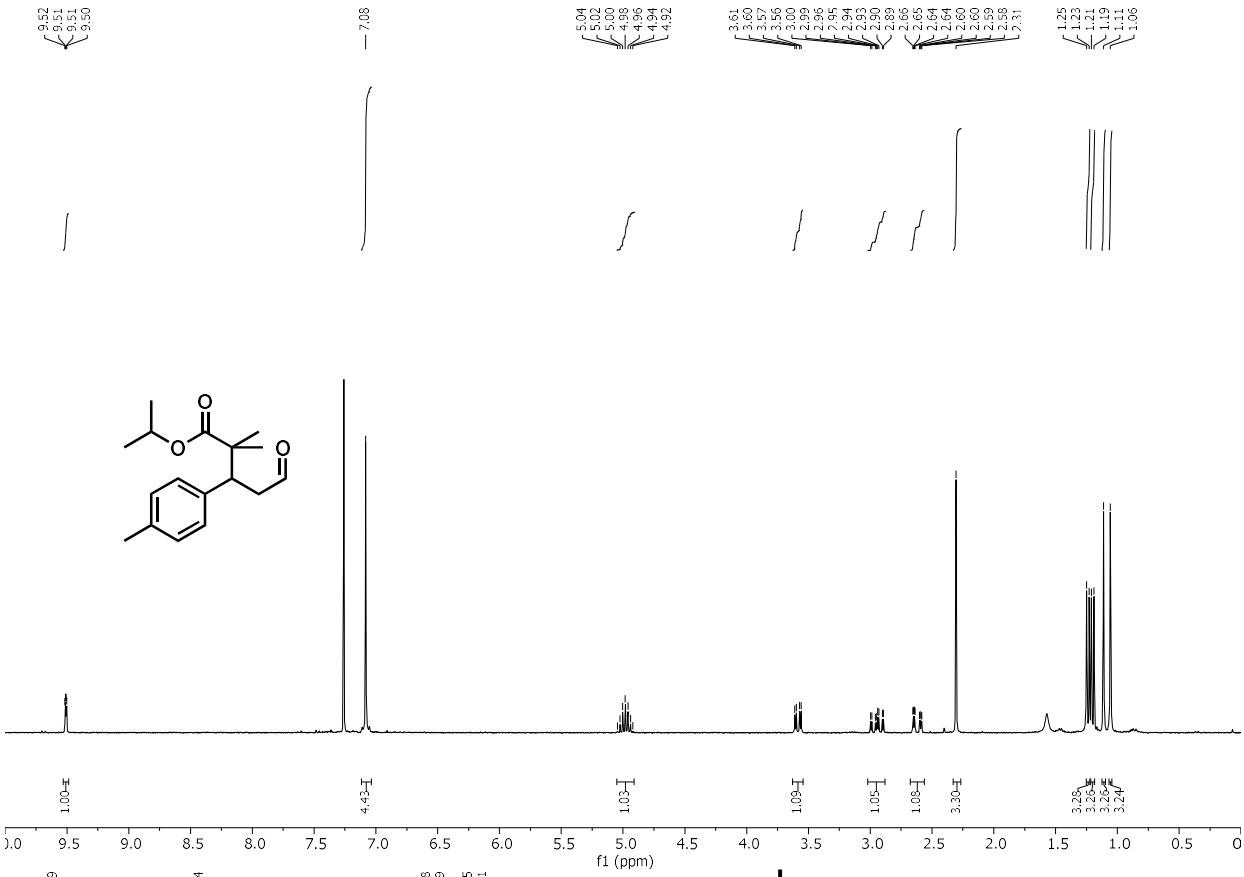
9.52
9.51
9.51
9.50
7.08
5.04
5.02
5.00
4.98
4.96
4.94
4.92
3.61
3.60
3.57
3.56
3.00
2.99
2.96
2.95
2.94
2.93
2.90
2.89
2.66
2.65
2.64
2.64
2.60
2.59
2.58
2.31
1.25
1.23
1.21
1.19
1.11
1.06
1.00
4.43
1.03
1.09
1.05
1.08
3.30
3.25
3.25
3.25
3.24
f1 (ppm)

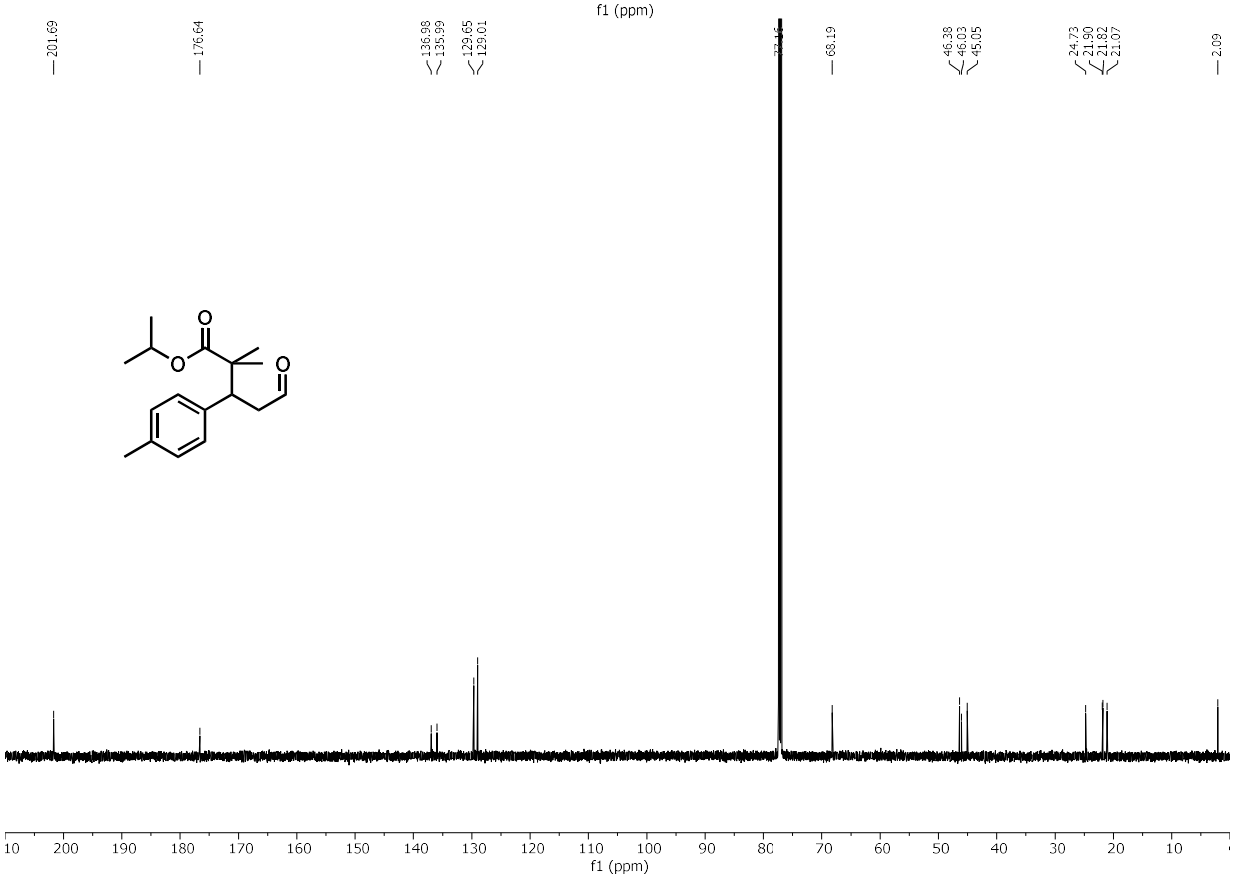
201.69
176.64
136.98
135.99
129.65
129.01
77.16
68.19
46.38
46.03
45.05
24.73
21.90
21.82
21.07
2.09
f1 (ppm)

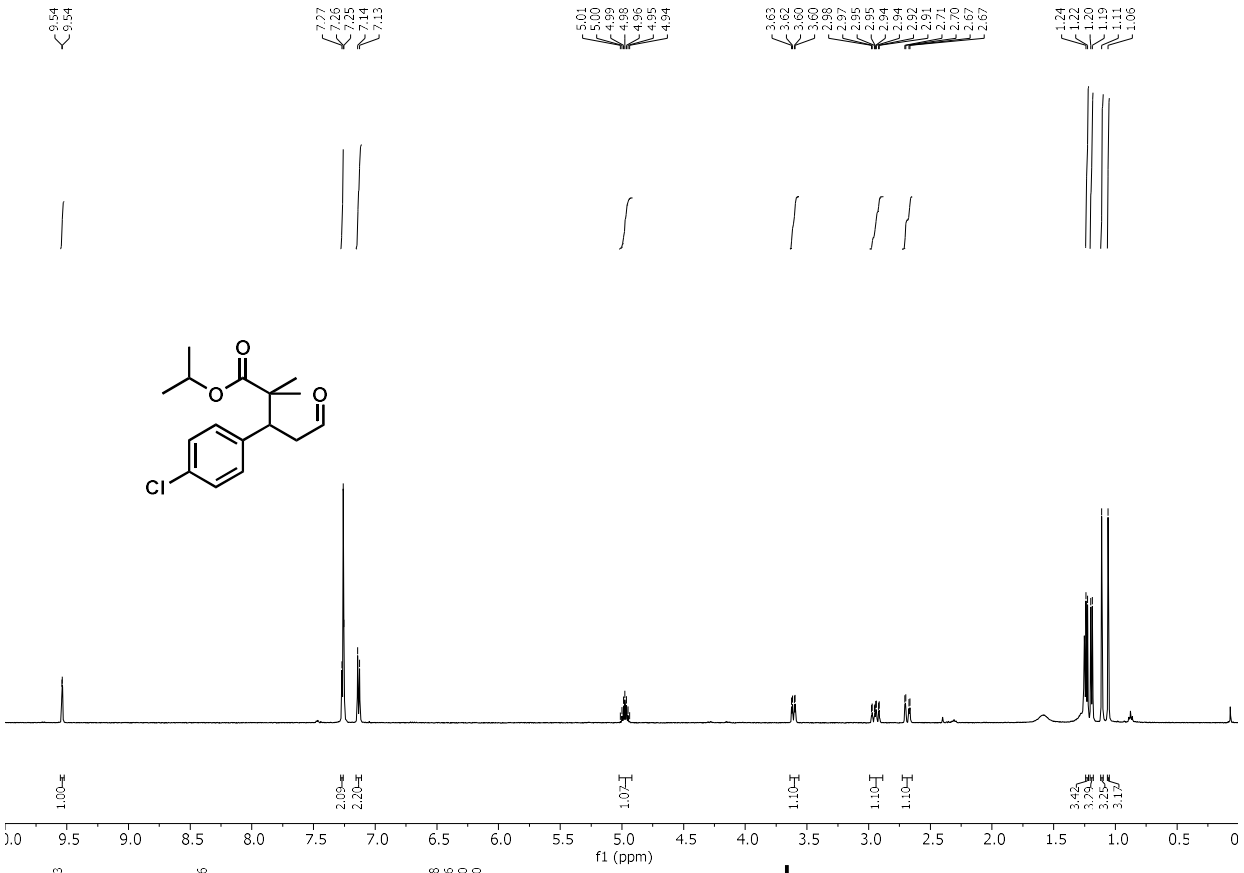
9.54
9.54
7.77
7.26
7.25
7.14
7.13
5.01
5.00
4.99
4.98
4.96
4.95
4.94
3.63
3.62
3.60
3.60
2.98
2.97
2.95
2.95
2.94
2.94
2.92
2.91
2.71
2.70
2.67
2.67
1.24
1.22
1.20
1.19
1.11
1.06
O
O
O
Cl
1.00
2.09
2.20
1.07
1.10
1.10
1.10
3.42
3.25
3.17
f1 (ppm)

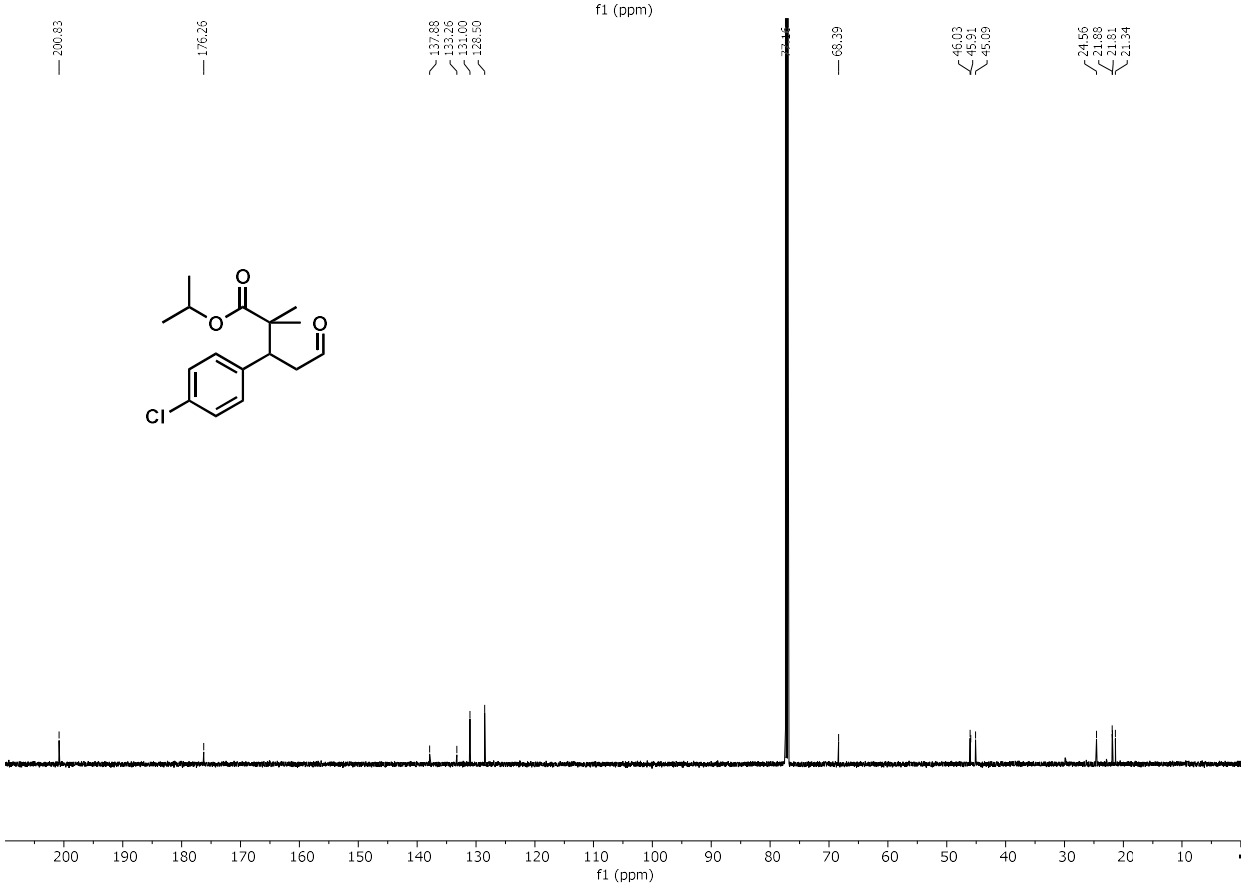
200.83
176.26
137.88
133.26
131.00
128.50
68.39
46.03
45.91
45.09
24.56
21.88
21.81
21.34
O
O
O
Cl
f1 (ppm)

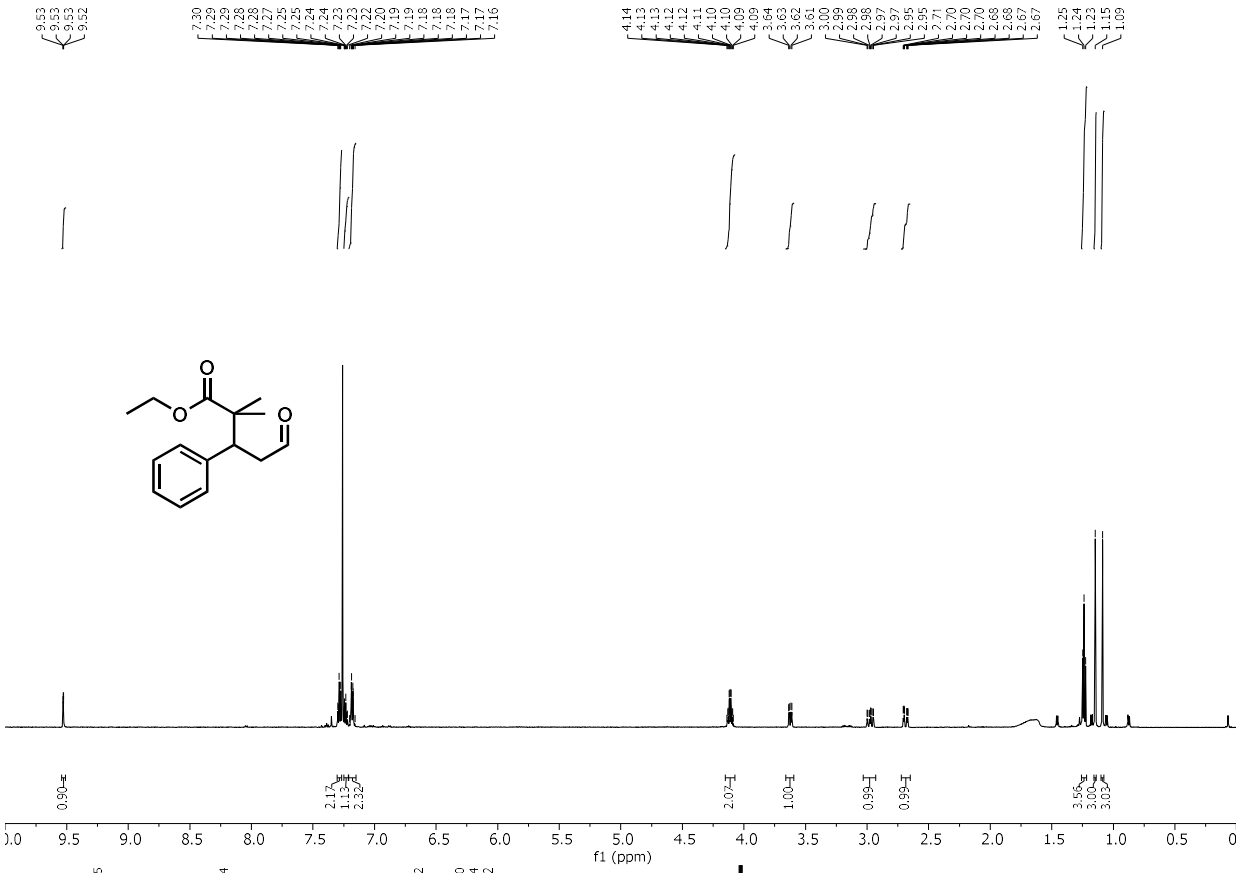
9.53
9.53
9.53
9.52
7.30
7.29
7.29
7.29
7.28
7.28
7.27
7.25
7.25
7.24
7.24
7.23
7.23
7.22
7.20
7.19
7.19
7.18
7.18
7.18
7.17
7.17
7.16
4.14
4.13
4.13
4.12
4.12
4.11
4.10
4.10
4.09
4.09
3.64
3.63
3.62
3.61
3.00
2.99
2.98
2.98
2.97
2.97
2.95
2.95
2.71
2.70
2.70
2.70
2.68
2.68
2.67
2.67
1.25
1.24
1.23
1.15
1.09
O
O
O
0.90
2.17
1.13
2.32
2.07
1.00
0.99
0.99
3.56
3.00
3.03
f1 (ppm)

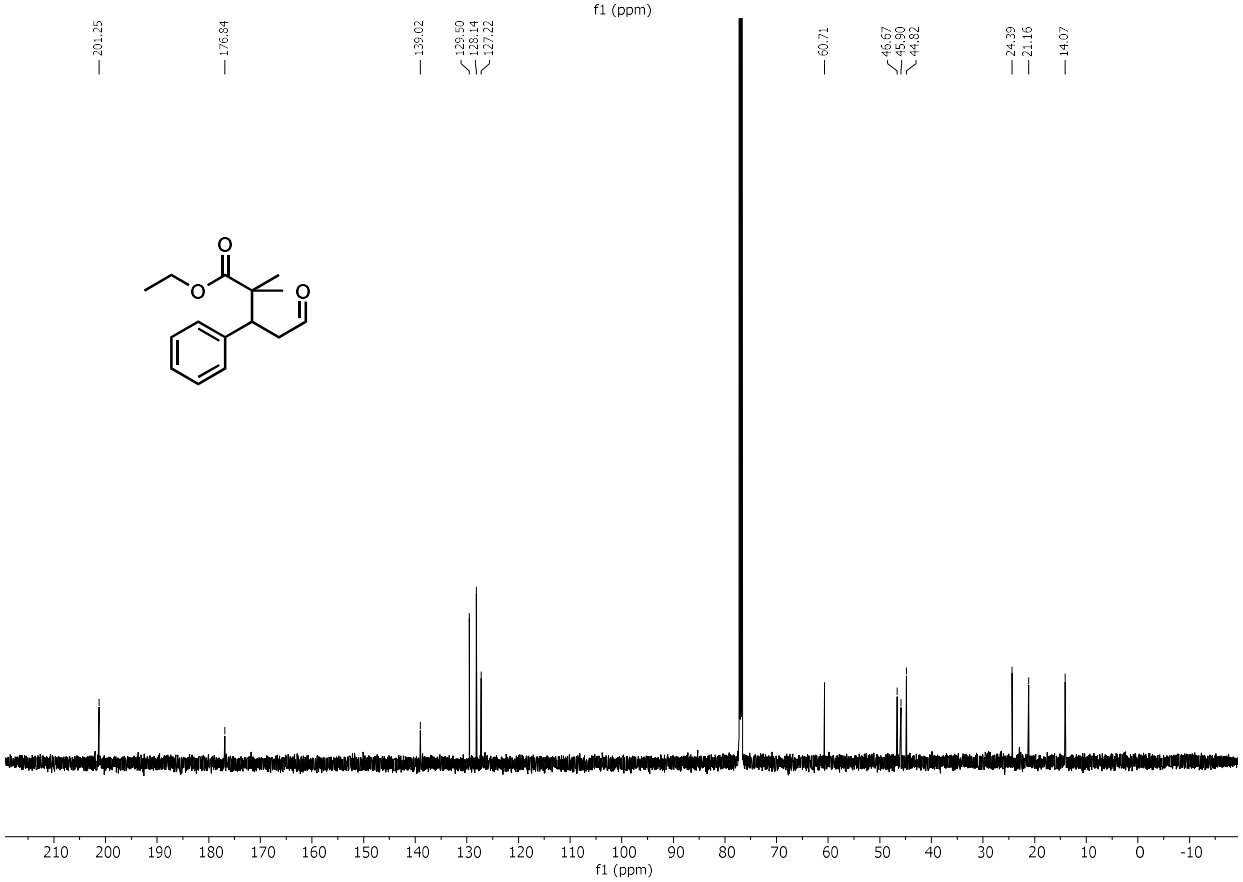
201.25
176.84
139.02
129.50
128.14
127.22
60.71
46.67
45.90
44.82
24.39
21.16
14.07
O
O
O
f1 (ppm)

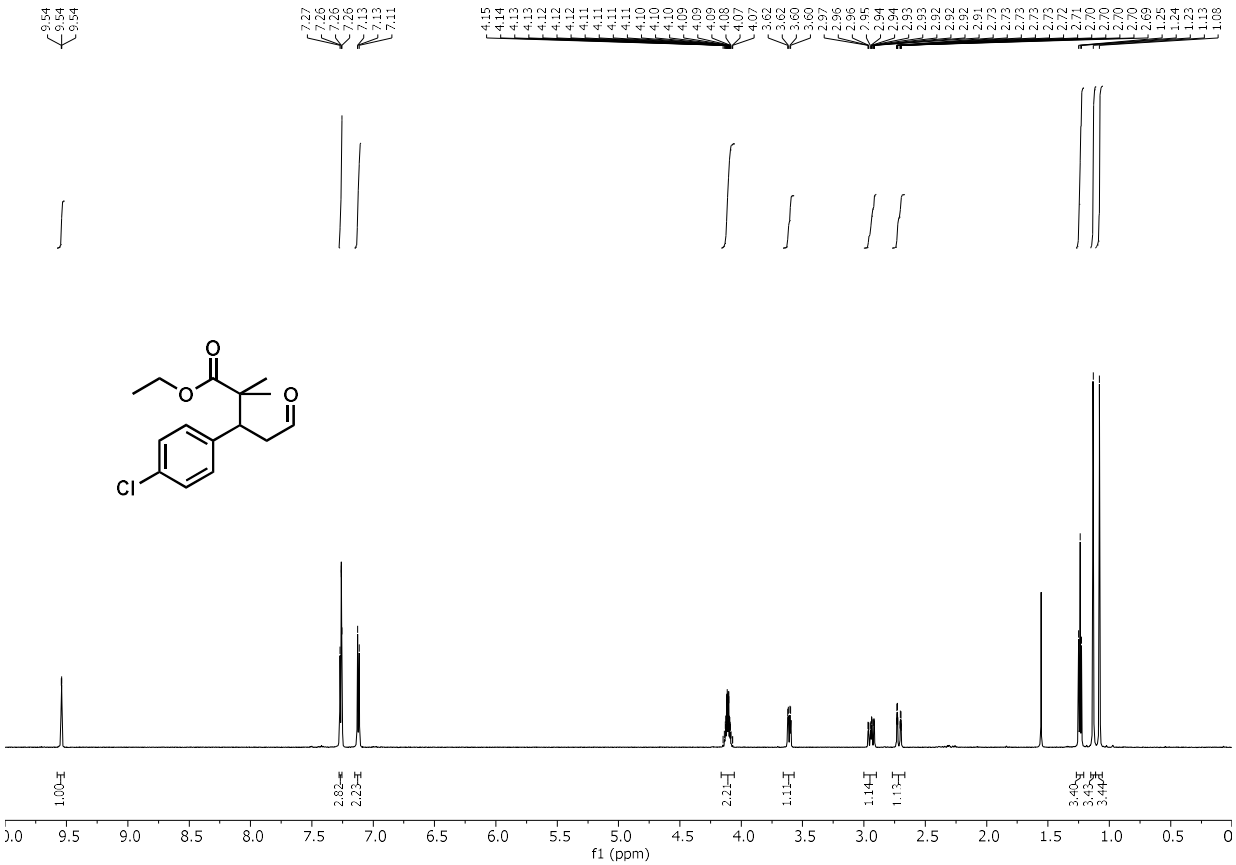
f1 (ppm)

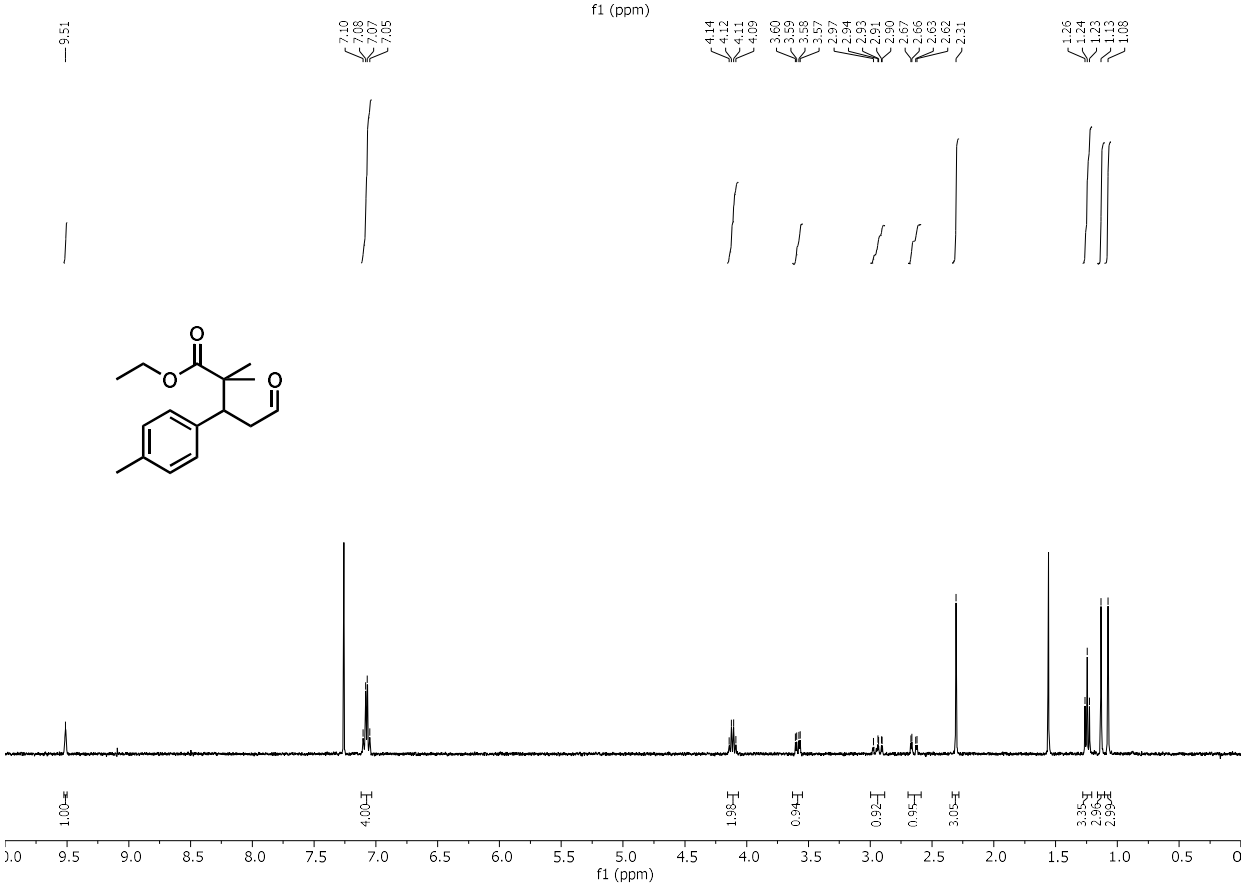
f1 (ppm)

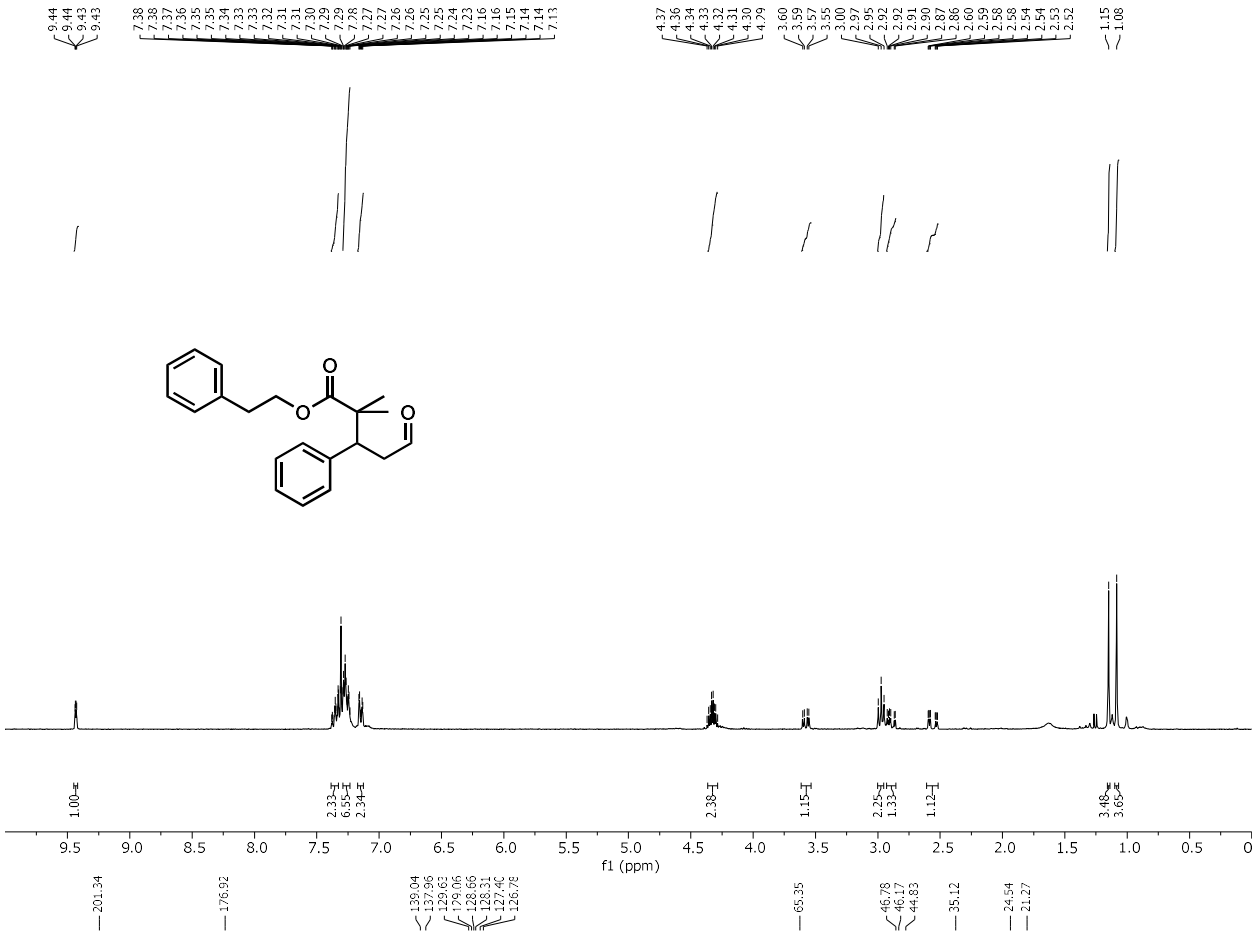
9.44
9.44
9.43
9.43
7.38
7.38
7.37
7.36
7.35
7.35
7.34
7.33
7.33
7.32
7.31
7.31
7.30
7.29
7.29
7.28
7.27
7.27
7.26
7.26
7.25
7.25
7.24
7.23
7.16
7.16
7.15
7.14
7.14
7.13
4.37
4.36
4.34
4.33
4.32
4.31
4.30
4.29
3.60
3.59
3.57
3.55
3.00
2.97
2.95
2.92
2.92
2.91
2.90
2.87
2.86
2.60
2.59
2.58
2.58
2.54
2.54
2.53
2.52
1.15
1.08
O
O
O
1.00
2.33
6.55
2.34
2.38
1.15
2.25
1.33
1.12
3.48
3.65
9.5
9.0
8.5
8.0
7.5
7.0
6.5
6.0
5.5
5.0
4.5
4.0
3.5
3.0
2.5
2.0
1.5
1.0
0.5
0
f1 (ppm)

201.34
176.92
139.04
137.96
129.62
129.06
128.65
128.31
127.46
126.78
65.35
46.78
46.17
44.83
35.12
24.54
21.27

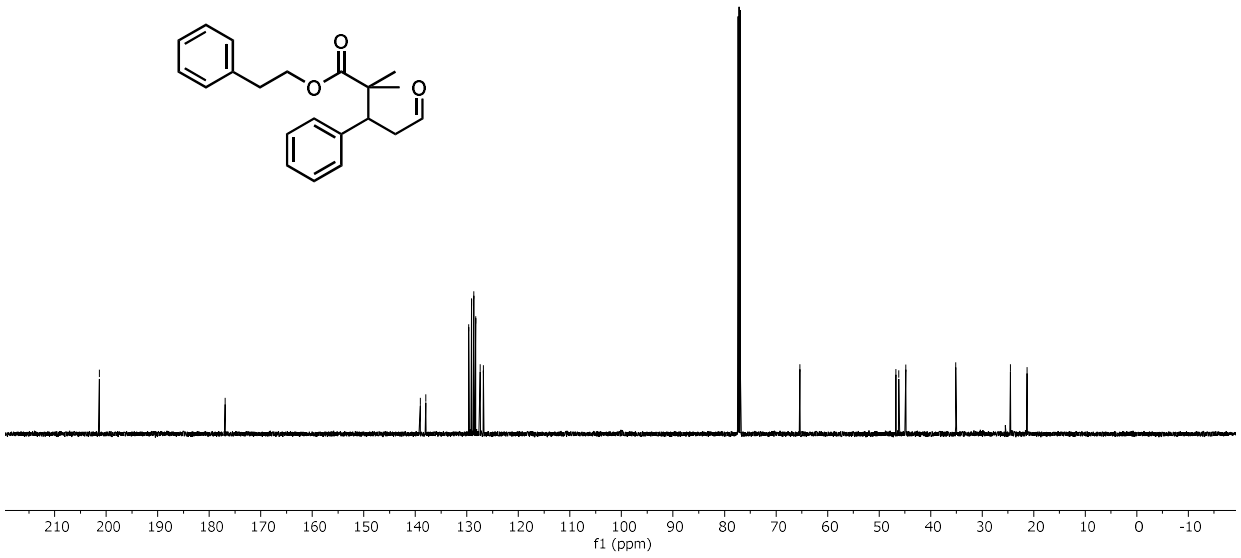
O
O
O
210
200
190
180
170
160
150
140
130
120
110
100
90
80
70
60
50
40
30
20
10
0
-10
f1 (ppm)

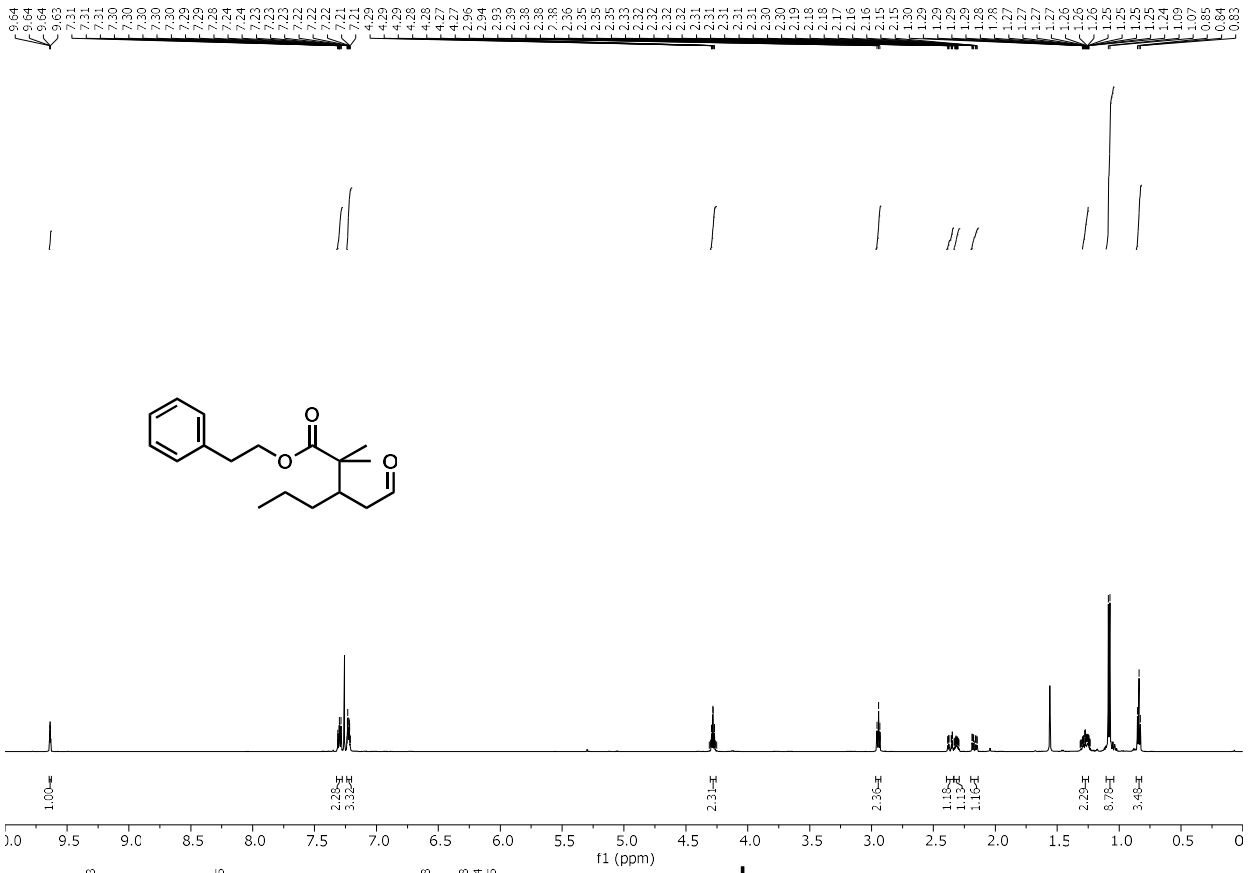
f1 (ppm)


f1 (ppm)

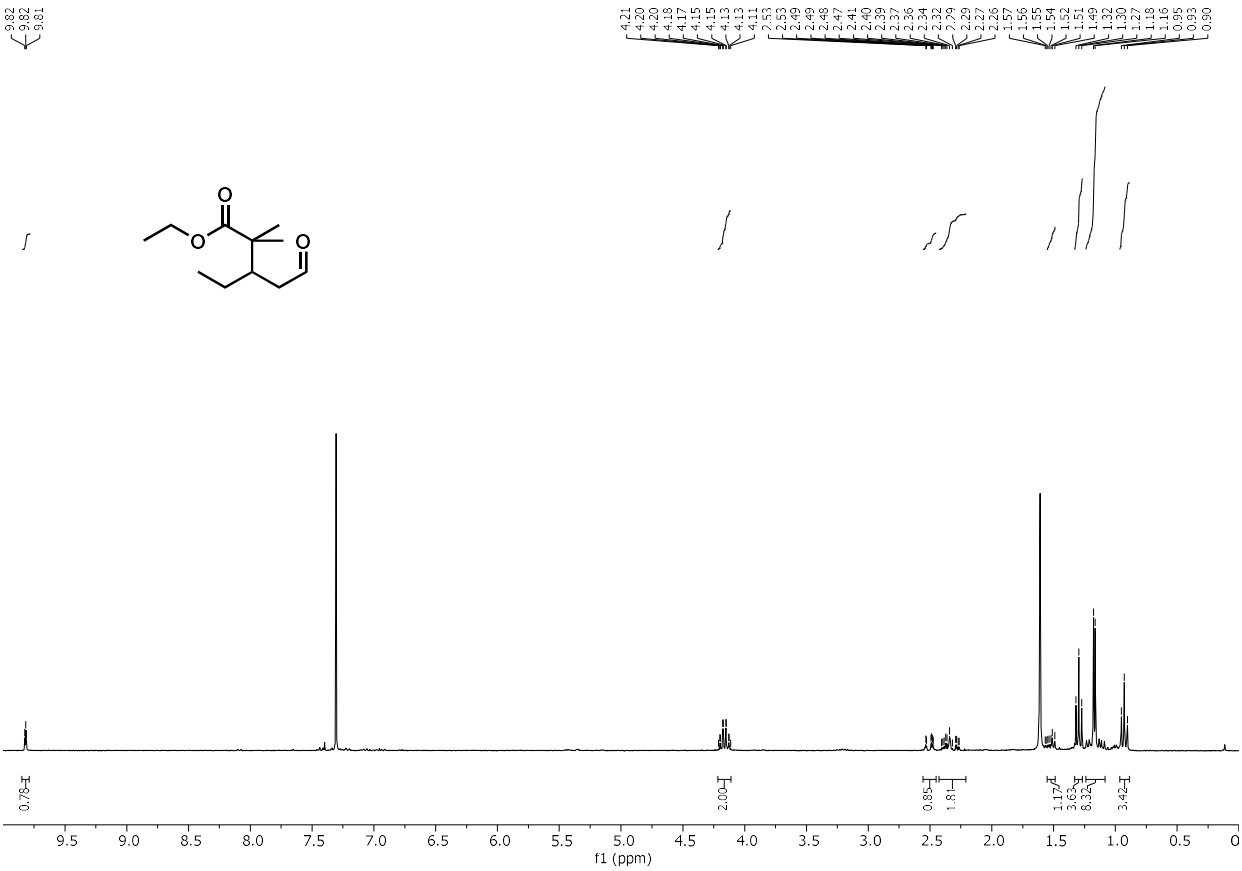
9.82
9.82
9.81
4.21
4.20
4.20
4.18
4.17
4.15
4.15
4.13
4.13
4.11
2.53
2.53
2.49
2.49
2.48
2.47
2.41
2.40
2.39
2.37
2.36
2.34
2.32
2.29
2.29
2.27
2.26
1.57
1.56
1.55
1.54
1.52
1.51
1.49
1.32
1.30
1.27
1.18
1.16
0.95
0.93
0.90
O
O
O
0.78
2.00
0.85
1.81
1.17
3.65
8.32
3.42
9.5
9.0
8.5
8.0
7.5
7.0
6.5
6.0
5.5
5.0
4.5
4.0
3.5
3.0
2.5
2.0
1.5
1.0
0.5
0
f1 (ppm)

3.4.6 HPLC Traces

isopropyl 2,2-dimethyl-5-oxo-3-phenylpentanoate

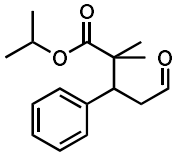

HPLC Chiralpak IC column (98:2 hexanes:isopropanol, 1 mL/min, 206 nm); first enantiomer tr = 14.3 min, second enantiomer tr = 15.9 min. Primary trace obtained from a mixture of purified enantioenriched runs due to difficulty of separation and coelution of the achiral catalyst IPr(Biphenyl)AuCl with the second enantiomer of product.

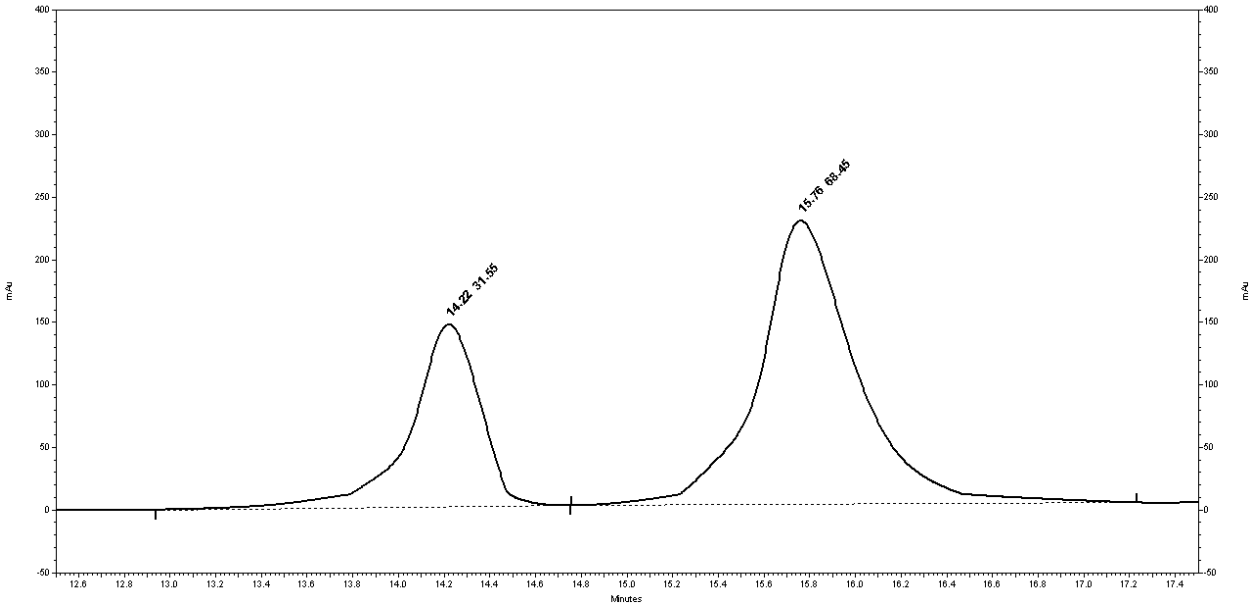

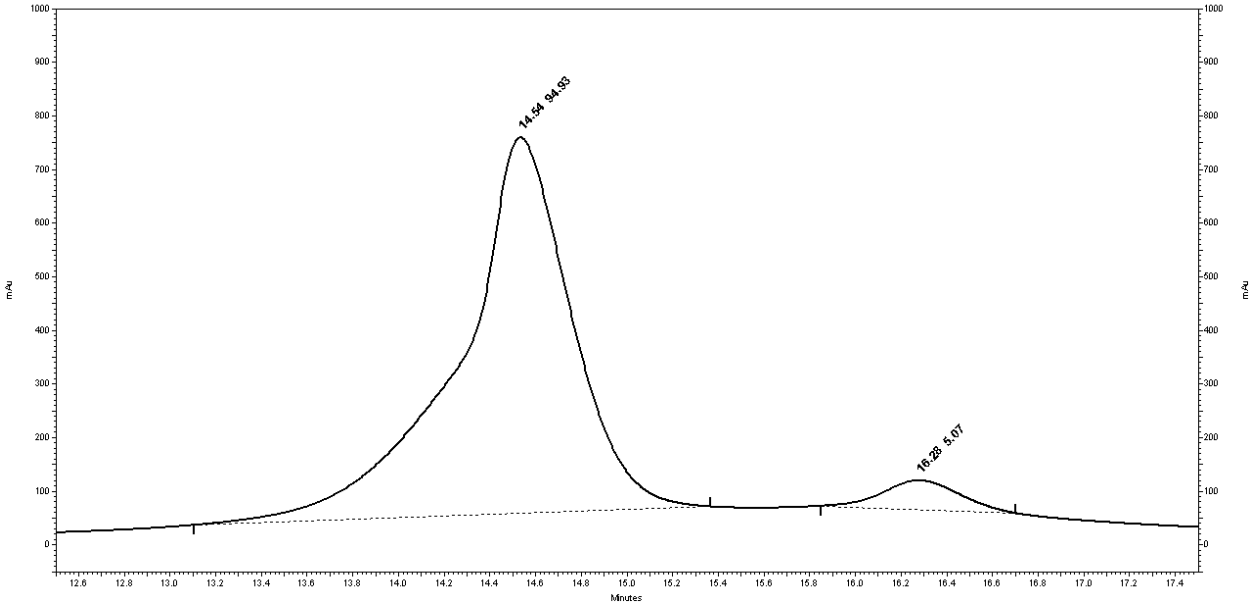

isopropyl 3-(4-methoxyphenyl)-2,2-dimethyl-5-oxopentanoate

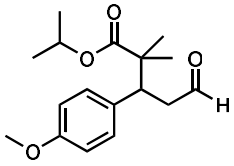

HPLC Chiralpak IA column (98:2 hexanes:isopropanol, 1 mL/min, 230 nm); first enantiomer tr = 9.3 min, second enantiomer tr = 9.8 min.

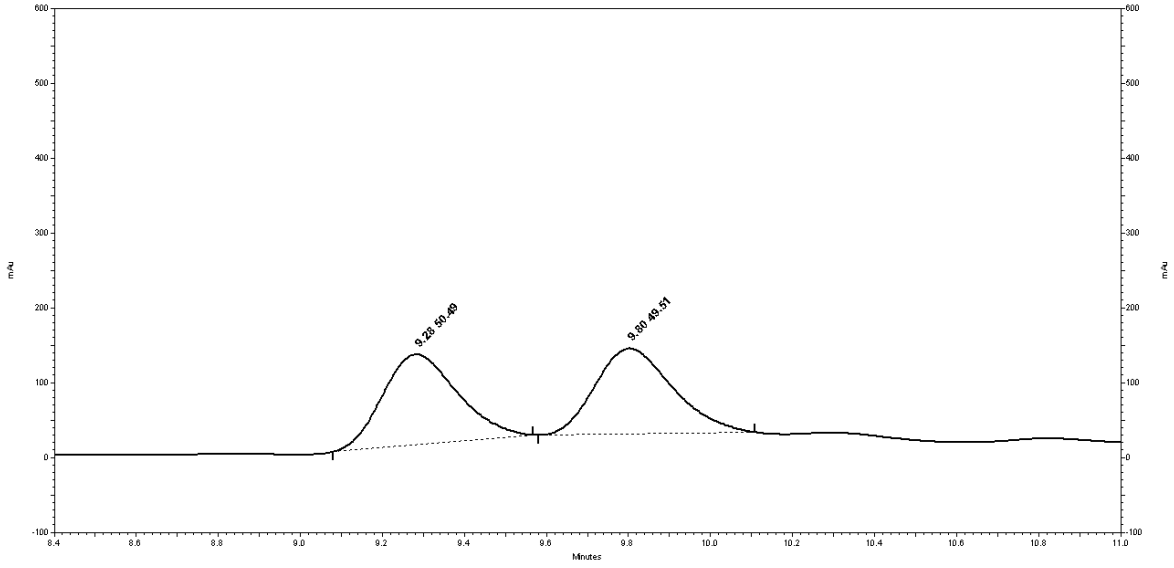

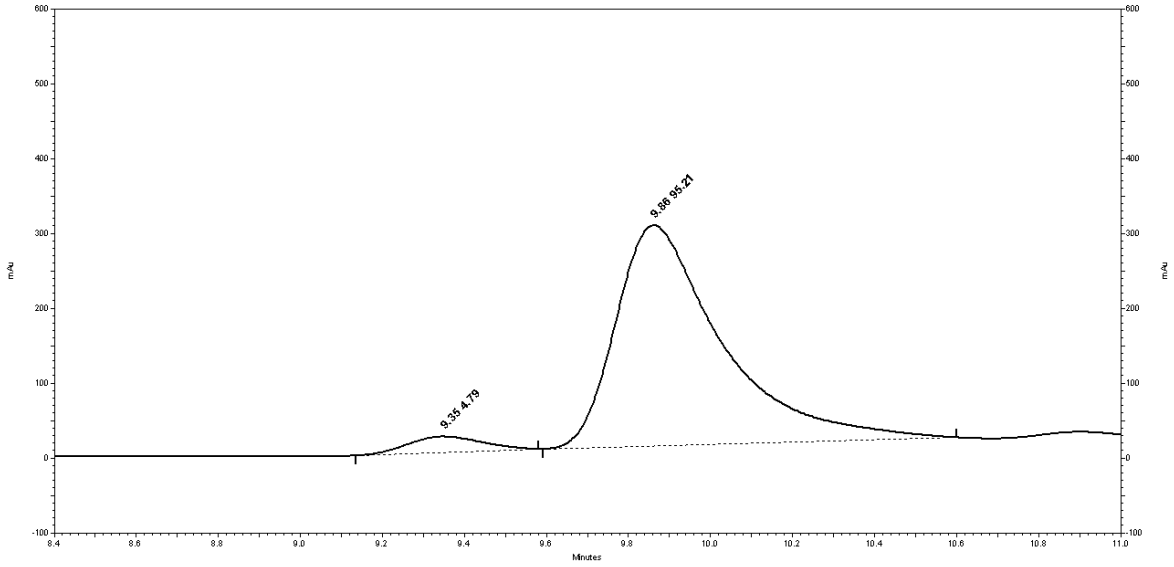

ethyl 2,2-dimethyl-5-oxo-3-phenylpentanoate

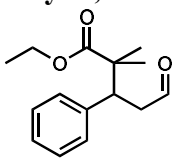

HPLC Chiralpak IC column (98:2 hexanes:isopropanol, 1 mL/min, 192 nm); first enantiomer tr = 15.2 min, second enantiomer tr = 17.9 min.

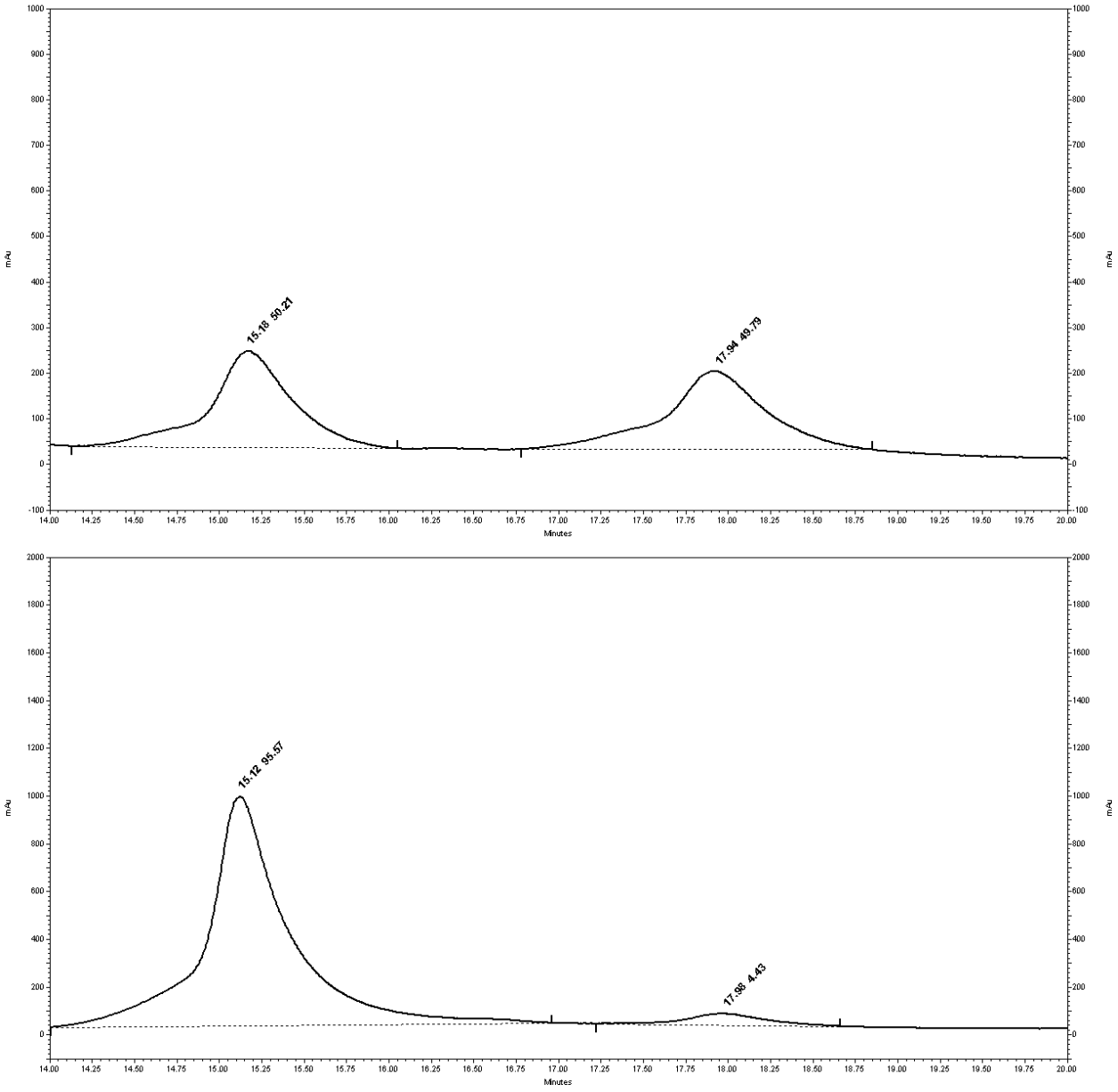

ethyl 3-(4-chlorophenyl)-2,2-dimethyl-5-oxopentanoate

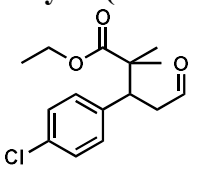

HPLC Chiralpak OD-H column (99:1 hexanes:isopropanol, 1 mL/min, 232 nm); first enantiomer tr = 19.6 min, second enantiomer tr = 25.6 min.

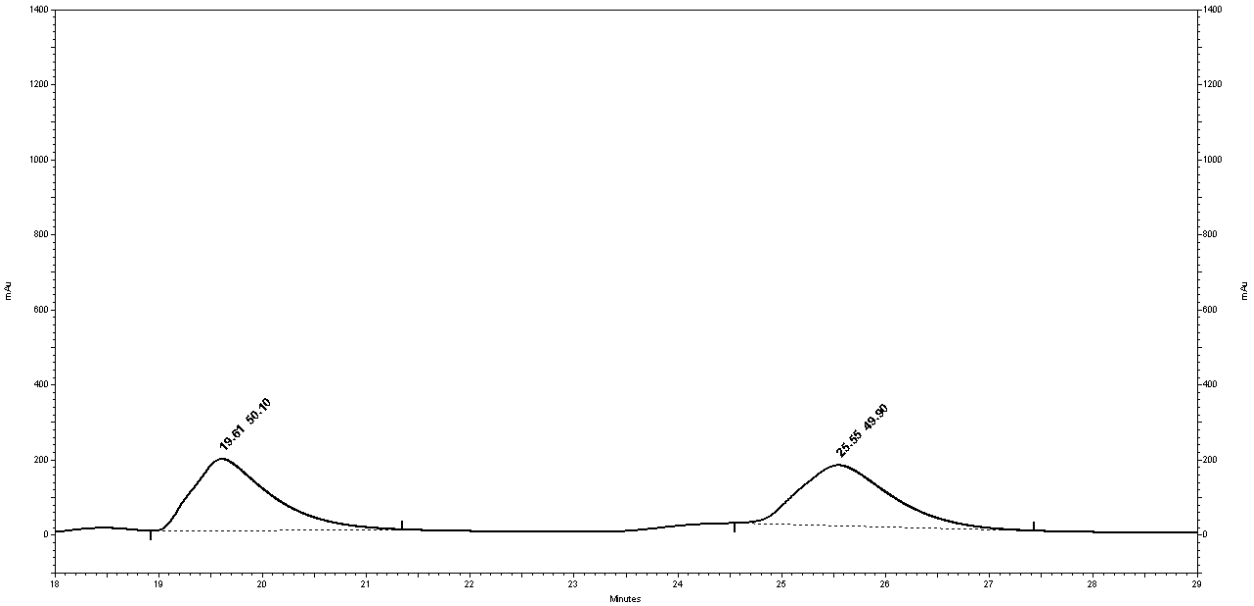

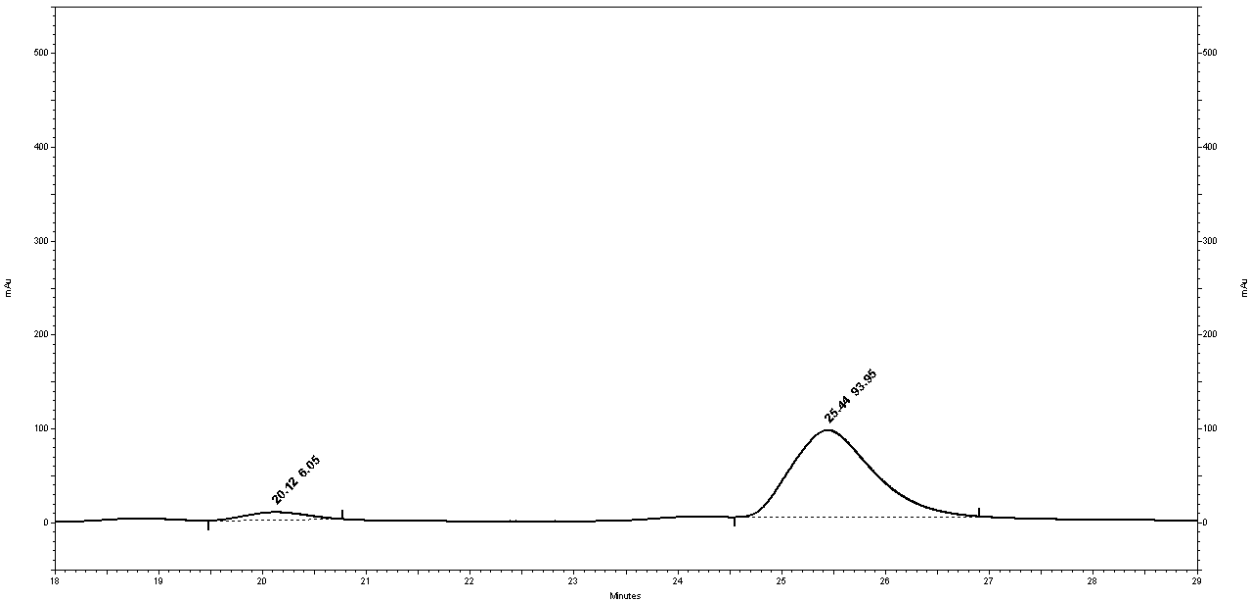

ethyl 2,2-dimethyl-5-oxo-3-(p-tolyl)pentanoate

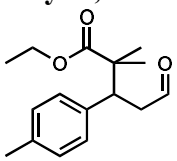

HPLC Chiralpak OD-H column (99:1 hexanes:isopropanol, 1 mL/min, 230 nm); first enantiomer tr = 14.6 min, second enantiomer tr = 22.2 min.

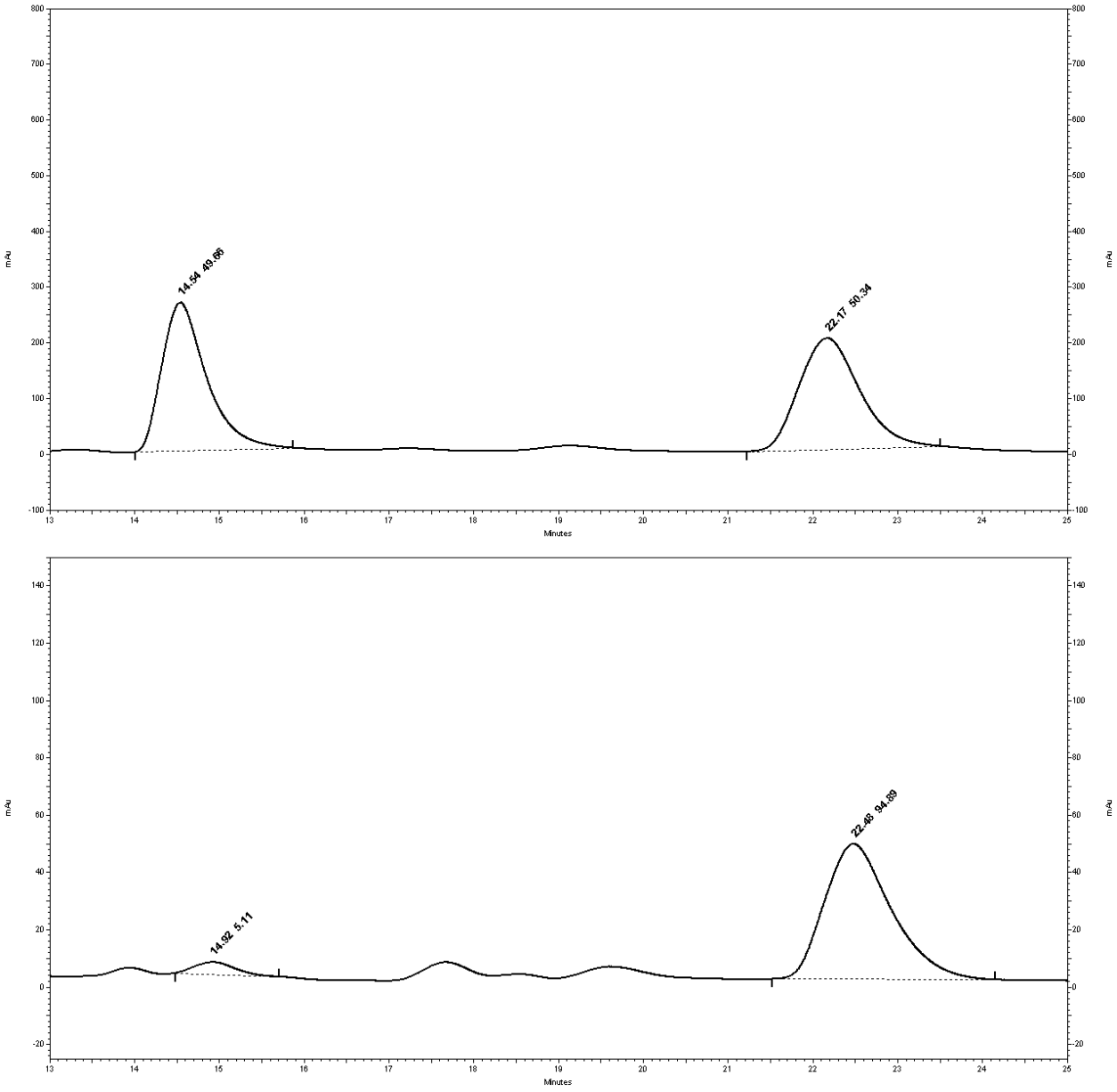

phenethyl 2,2-dimethyl-5-oxo-3-phenylpentanoate

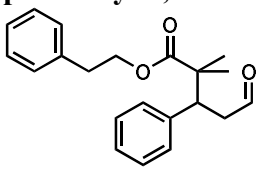

HPLC Chiralpak OD-H column (95:5 hexanes:isopropanol, 1 mL/min, 223 nm); first enantiomer tr = 15.8 min, second enantiomer tr = 17.8 min.

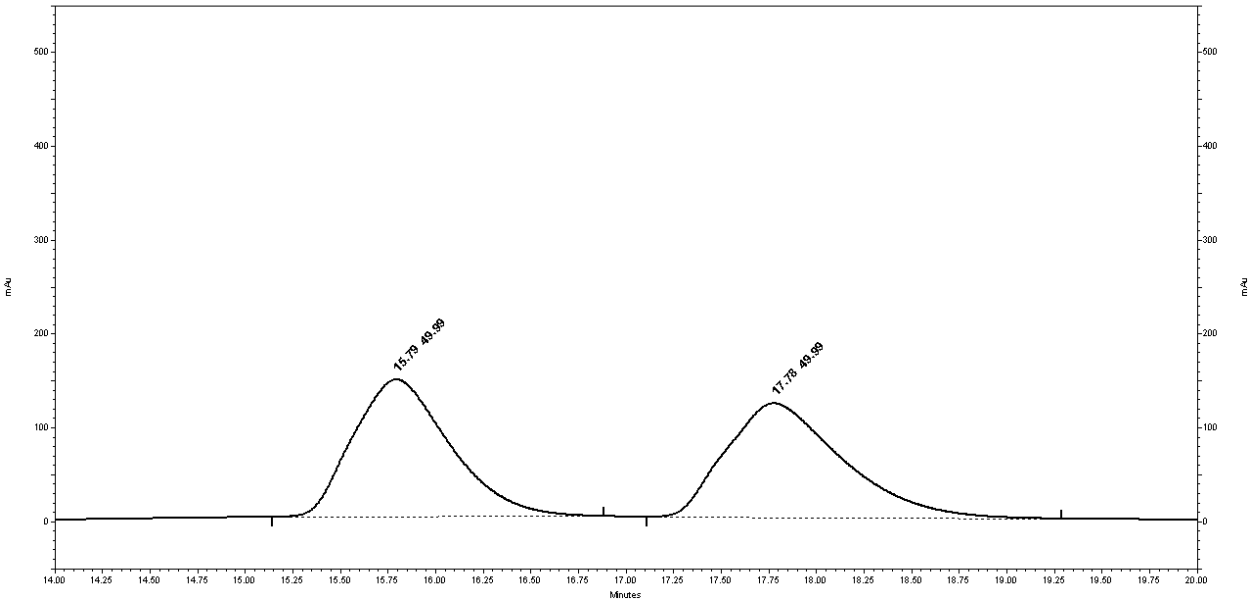

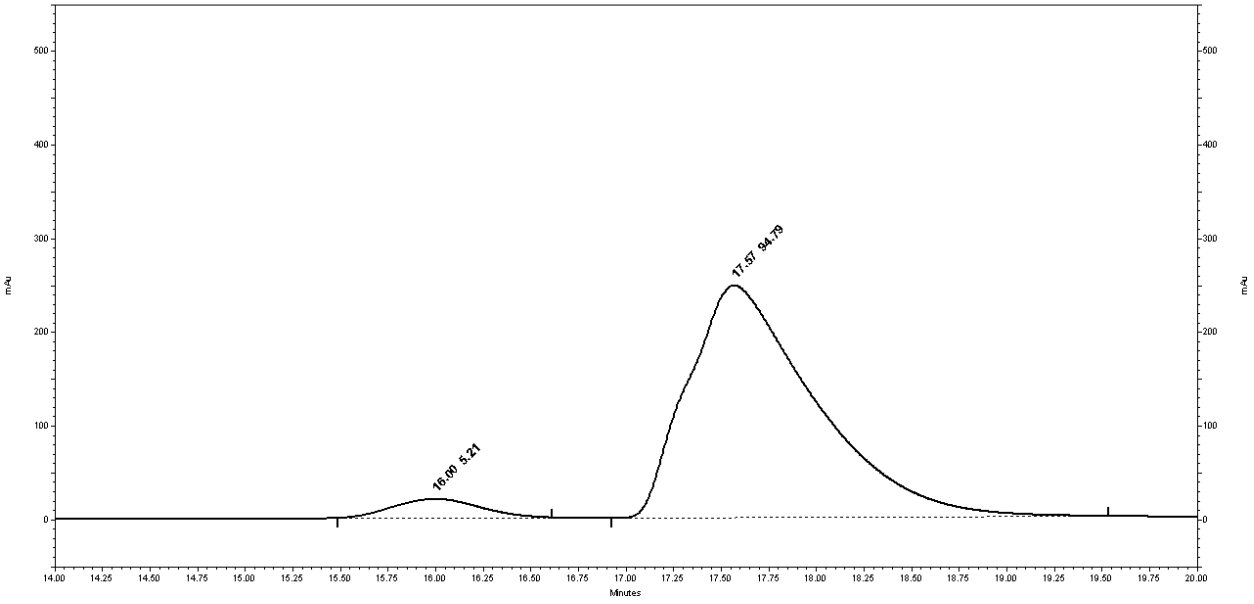

phenethyl 2,2-dimethyl-3-(2-oxoethyl)hexanoate

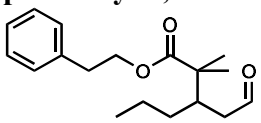

HPLC Chiralpak OJ-H column (99:1 hexanes:isopropanol, 1 mL/min, 218 nm); first enantiomer tr = 16.6 min, second enantiomer tr = 18.1 min.

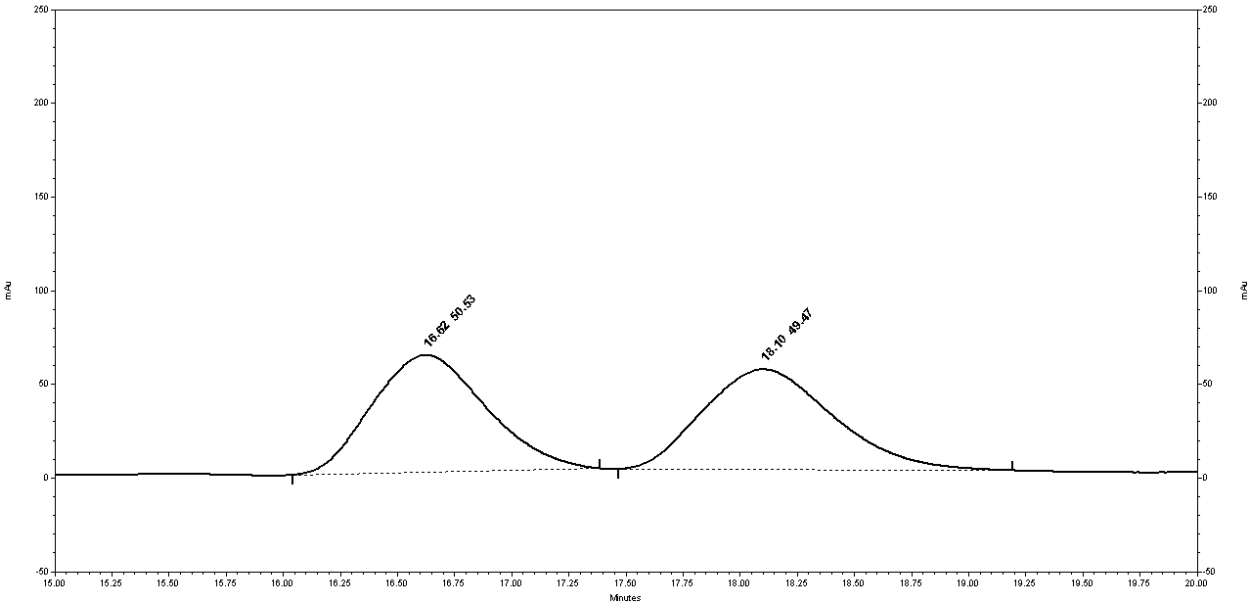

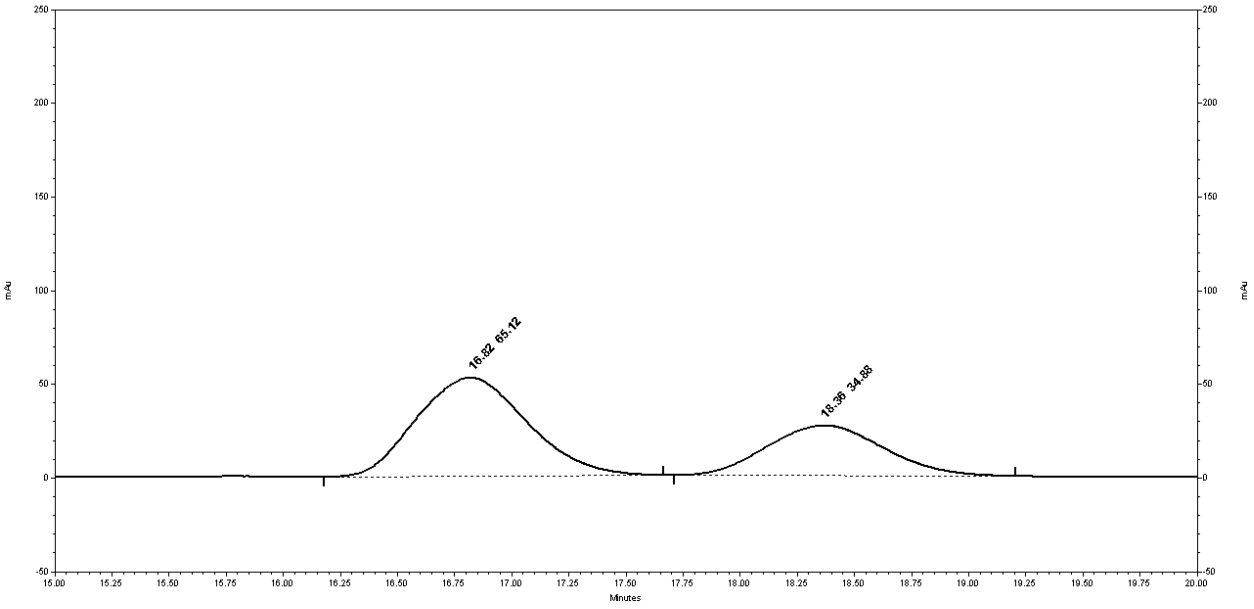

ethyl 3-ethyl-2,2-dimethyl-5-oxopentanoate

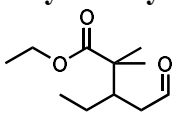

GC CP-Chirasil-Dex CB (30 m x 0.25 mm ID x 0.25 µm film). 160 °C, FID detector, first enantiomer tr = 8.65 min, second enantiomer 8.67 min.

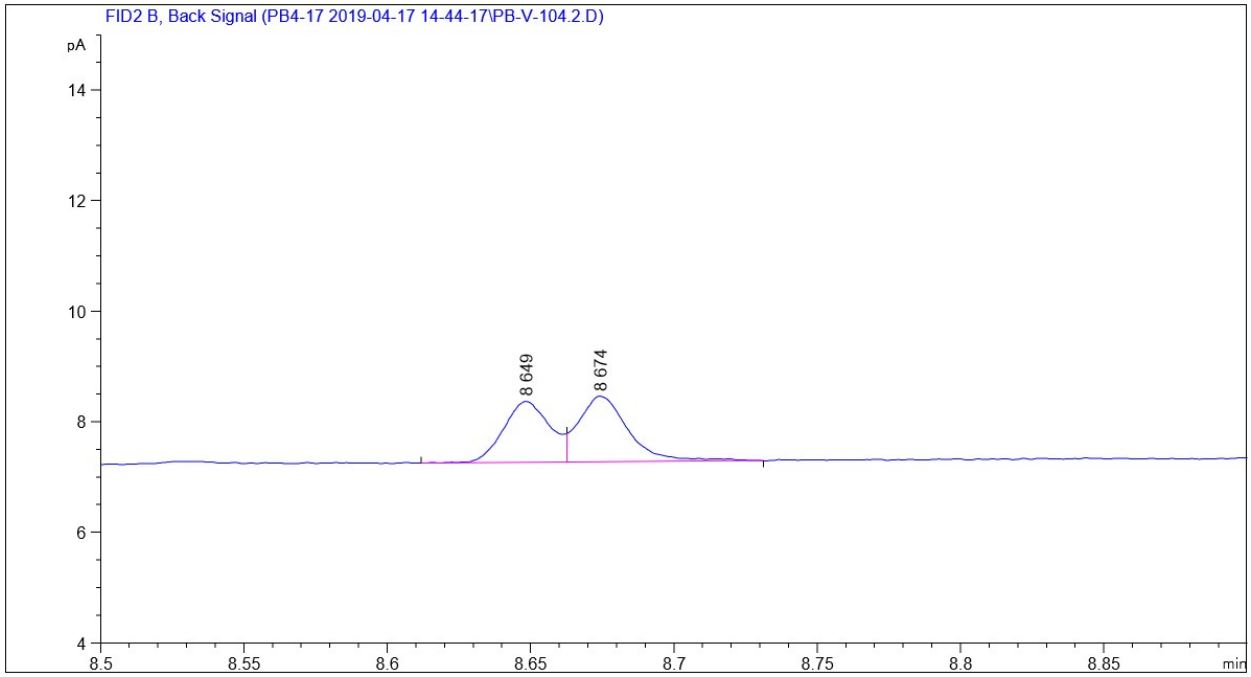

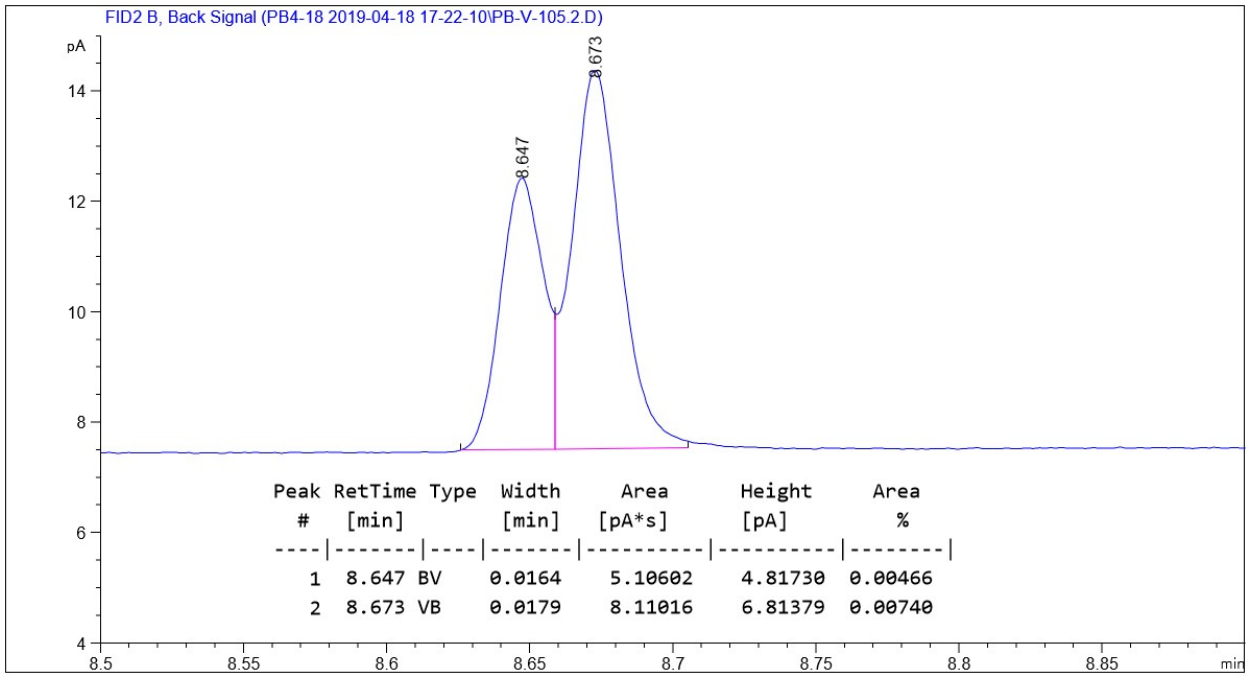

Peak #	RetTime [min]	Type	Width [min]	Area [pA*s]	Height [pA]	Area %
1	8.647	BV	0.0164	5.10602	4.81730	0.00466
2	8.673	VB	0.0179	8.11016	6.81379	0.00740

3.5 Notes and References

(63) Zhang, Y.; Wang, W. *Catal. Sci. Technol.* **2012**, *2*, 42–53.
(64) Hui, C.; Pu, F.; Xu, J. *Chem. - A Eur. J.* **2017**, *23*, 4023–4036.
(65) Narasaka, K.; Soai, K.; Mukaiyama, T. *Chem. Lett.* **2006**, *3*, 1223–1224.
(66) Brown, S. P.; Goodwin, N. C.; MacMillan, D. W. C. *J. Am. Chem. Soc.* **2003**, *125*, 1192–1194.
(67) Yamaguchi, M.; Shiraishi, T.; Hirama, M. *Angew. Chem. Int. Ed. Engl.* **1993**, *32*, 1176–1178.
(68) Saito, M.; Nakajima, M.; Hashimoto, S. *Chem. Commun.* **2000**, No. 19, 1851–1852.
(69) Wang, W.; Li, H.; Wang, J. *Org. Lett.* **2005**, *7*, 1637–1639.
(70) Borths, C. J.; Carrera, D. E.; MacMillan, D. W. C. *Tetrahedron* **2009**, *65*, 6746–6753.
(71) Teller, H.; Corbet, M.; Mantilli, L.; Gopakumar, G.; Goddard, R.; Thiel, W.; Fürstner, A. *J. Am. Chem. Soc.* **2012**, *134*, 15331–15342.
(72) González, A. Z.; Benitez, D.; Tkatchouk, E.; Goddard, W. A.; Toste, F. D. *J. Am. Chem. Soc.* **2011**, *133*, 5500–5507.
(73) Thielemann, J. P.; Girgsdies, F.; Schlögl, R.; Hess, C. *Beilstein J. Nanotechnol.* **2011**, *2*, 110–118.
(74) Hatano, M.; Takagi, E.; Ishihara, K. *Org. Lett.* **2007**, *9*, 4527–4530.
(75) Lei, W.-L.; Feng, K.-W.; Wang, T.; Wu, L.-Z.; Liu, Q. *Org. Lett.* **2018**, *20*, 7220–7224.
(76) Bae, H. Y.; List, B. *Chem. - A Eur. J.* **2018**, *24*, 13767–13772.
(77) Kiyooka, S.; Matsumoto, S.; Shibata, T.; Shinozaki, K. *Tetrahedron* **2010**, *66*, 1806–1816.
(78) Peifer, M.; Berger, R.; Shurtleff, V. W.; Conrad, J. C.; MacMillan, D. W. C. *J. Am. Chem. Soc.* **2014**, *136*, 5900–5903.
(79) Zhou, F.; Yamamoto, H. *Angew. Chem. Int. Ed.* **2016**, *55*, 8970–8974.
(80) Zhou, F.; Yamamoto, H. *Org. Lett.* **2016**, *18*, 4974–4977.

Chapter 4

Efforts Towards Enantioselective Photocatalysis Enabled by Chiral Gold(III) Complexes

4.1 Introduction

Photocatalysis has rapidly become a widely investigated field over the past decade as it has enabled access to unique activation modes that are not thermodynamically favorable under traditional catalytic systems. Photocatalysis is typically defined by a mechanism, such as energy transfer or single electron transfer, in which photonic energy is converted in to chemical energy.[81] Recent forays in to this field have proven to be a largely fruitful endeavor, particularly with respect to photoredox transformations.[82–84]

While there are an almost countless number of catalytic systems that are competent for the promotion of enantioselective thermal transformations, there are strikingly few methods for enantioselective photochemical transformations. These limited enantioselective photochemical transformations are an extremely valuable asset by providing access to a number of structural motifs that are traditionally challenging to synthesize under thermal conditions, such as cyclobutanes from [2+2] cycloadditions.[85,86]

There is an inherent difficulty associated with controlling the background reactivity of a photochemical transformation; direct excitation of a substrate not bound to a chiral reagent resulting in a racemic transformation. This has traditionally been addressed through the use of a stoichiometric chiral reagent or additive, enforcing the enantioinducing information to be present in each reactive species.[87] An example of this strategy was reported by Bach and coworkers where they took advantage of hydrogen bonding interactions to facilitate the binding of the substrate to their chiral host (Scheme 4.1).[88,89] They hypothesized that the prochiral lactam would coordinate to a chiral amide, derived from Kemp's triacid, and undergo a stereoselective transformation. Through this strategy, they successfully obtained up to 93% ee with 2.6 equivalents of the chiral host sensitizer.

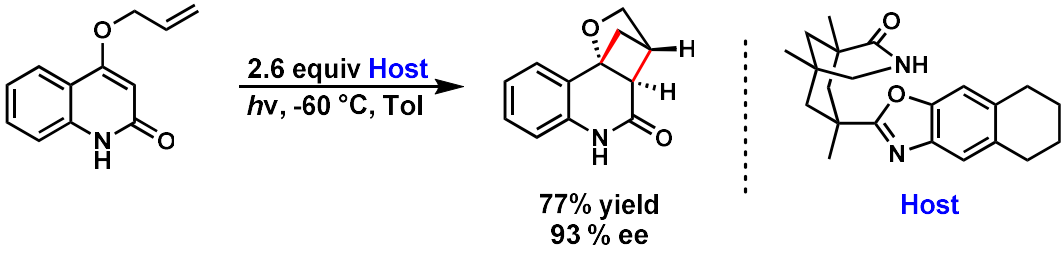

Scheme 4.1 Enantioselective intramolecular [2+2] photocycloaddition of prochiral lactams with a hydrogen-bonding host.

Bach and coworkers have further expanded upon this work by developing several catalytic variants of this reaction, with catalyst loading as low as 5 mol %.[90,91] They accomplished this through judicious choice of sensitizer, substrate, and light source. By ensuring that the sensitizer-substrate complex absorbs light at a longer wavelength than the unbound substrate, they selectively excited the sensitizer-substrate complex, thereby avoiding background reactivity due to direct excitation of the substrate. Unfortunately, this scaffold is very limited in terms of applicability to other reactions and substrates due to the required hydrogen bonding association between the substrate and sensitizer, severely limiting the scope and functionality of compatible substrates.[92] Additionally, this transformation requires careful irradiation with a monochromatic light source, and the background reactivity still remains problematic. Nevertheless, Bach and coworkers have also shown that chiral oxazaborolidines can be used in the asymmetric [2+2] photocycloaddition of enones (Scheme 4.2). However, success for this transformation again relies on the catalyst-

substrate complex being excited preferentially over the substrate to minimize background reactivity, which restricts the substrate scope to cyclic enones.[93,94]

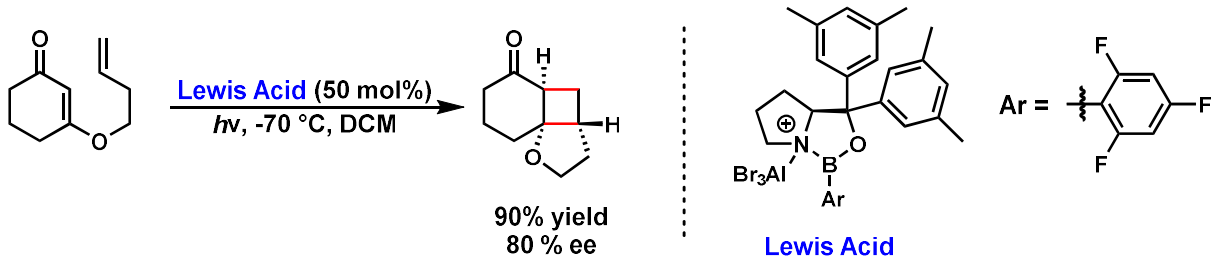

Scheme 4.2 Enantioselective intramolecular [2+2] photocycloaddition using a chiral oxazaborolidine catalyst.

With these limitations in mind, Yoon and coworkers proposed their visible light-induced photocatalytic [2+2] cycloaddition as an excellent starting point for the development of an enantioselective photocatalytic reaction where racemic background reactivity is non-existent.[85] They hypothesized that if Lewis acid coordination could induce a bathochromic shift in the energy of the singlet excited state, then perhaps a similar effect on the triplet excited state energy would also occur. Using a dual-catalytic system with an achiral transition-metal photocatalyst and a chiral Lewis acid cocatalyst they showed that this was indeed possible (Scheme 4.3).[86] The triplet energy of unbound chalcone was experimentally determined to be ~51 kcal/mol, and once bound to the scandium Lewis acid the excited triplet energy was lowered to ~33 kcal/mol. Triplet energy transfer from the photocatalyst was therefore only able to generate the excited state triplet of the Lewis acid bound substrate, eliminating achiral background reactivity.

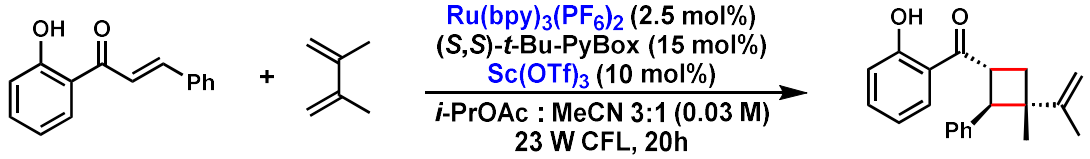

Scheme 4.3 Enantioselective intramolecular [2+2] photocycloaddition through Lewis acid-catalyzed triplet energy transfer.

With the observation that Lewis acid-bound organic substrates can have markedly different triplet energy levels from the unbound substrate, we began to wonder if this phenomenon could be applied to a transformation where a gold complex could act as both the Lewis acid and photosensitizer simultaneously. While there exists some precedent in the literature for gold acting as a photosensitizer, all reported reactions employ a neutral gold(III) complex as the photosensitizer.[6,95–97] We hypothesized that we could harness the power of the Lewis acidic nature of gold(III) in addition to its potential photocatalytic properties to develop a singular Lewis acid-photocatalyst that would operate under the same principles as the dual catalytic system from Yoon and coworkers.[7]

4.2 Results and Discussion

4.2.1 Photophysical Properties of Gold(III) Complexes

We first set out to explore some of the photophysical properties of the gold(III) complexes that we had previously synthesized in order to examine the feasibility of our proposal of using gold(III) as a dual Lewis acid-photocatalyst. The absorbance spectrum of **4.1** shows that absorption begins at a wavelength of ~340 nm, in the ultraviolet (UV) region (Figure 4.1). When the complex was treated with silver hexafluoroantimonate to generate the cationic and catalytically active species (**4.1a**), the absorbance spectrum shifted to absorb closer to 380 nm and included new small features at 360 nm and 340 nm. This indicated that while visible light (400–700 nm) is not absorbed by our catalyst, UV light is absorbed and can still be used to excite our complex.

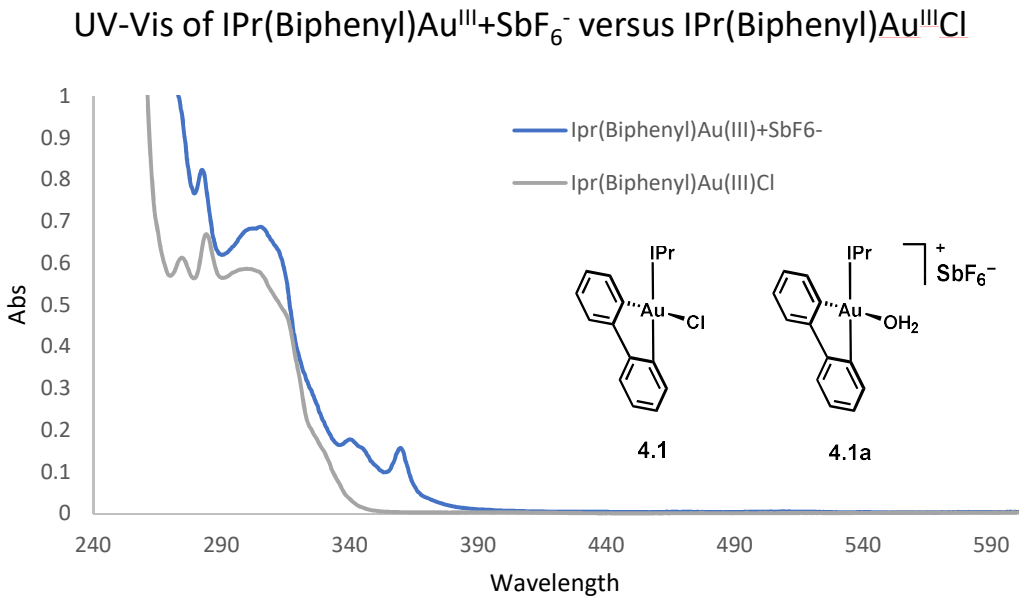

Figure 4.1 Absorbance spectrum of IPr(Biphenyl)AuCl and IPr(Biphenyl)Au$^+$SbF$_6^-$.

Once we determined the wavelength ranges that our complexes were absorbing, we began to examine their emission spectra. From the emission spectrum, specifically focusing on the phosphorescence, we could determine the triplet energy of the gold(III) complexes. Furthermore, under an energy transfer mechanism, this measurement provides an upper bound for the energy that could be used to generate the corresponding excited triplet state in the bound substrate. We first looked at the time-resolved emission spectrum of IPr(Biphenyl)AuCl in chloroform at room temperature (Figure 4.2). From this spectrum we observed the short-lived singlet excitation fluorescence around 400 nm and the longer-lived triplet excitation phosphorescence centered around 510 nm. The emission maximum at 510 nm corresponds to an excited triplet energy of 56 kcal/mol. Transient-absorption spectroscopy was also utilized to determine the excited singlet and triplet lifetimes (Figure 4.3). From this data it was determined that the excited singlet state undergoes a $S_1 \rightarrow S_0$ transition resulting in a fluorescence emission and has a lifetime of 44.6 ns. The excited triplet state undergoes phosphorescence with a $T_1 \rightarrow T_0$ transition and has a lifetime of 4.9 μs.

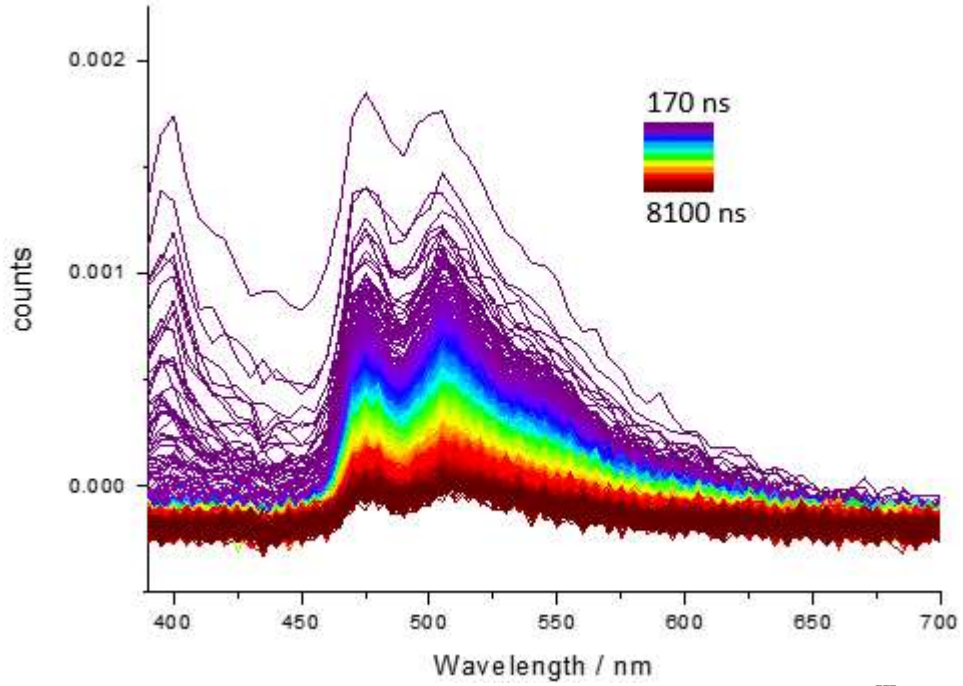

Figure 4.2 Time-resolved emission spectrum of IPr(Biphenyl)Au^{III}Cl

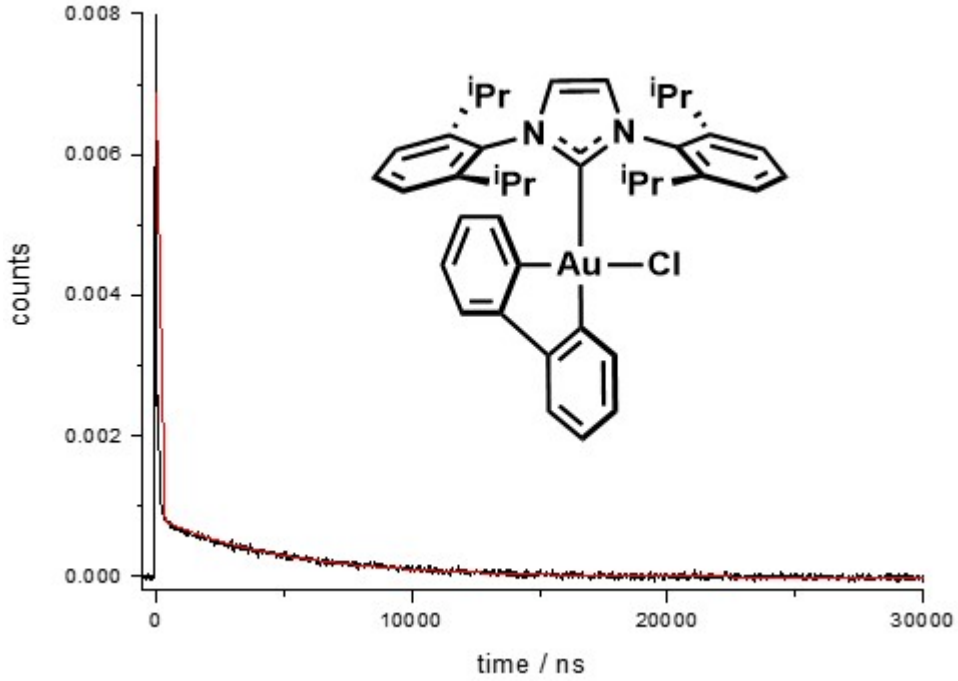

Figure 4.3 Transient-absorption spectrum of IPr(Biphenyl)Au^{III}Cl

We then examined the spectroscopic properties of the cationic gold(III) complex, which would more closely resemble the active species that would be present during catalysis with our system. In the time-resolved emission spectrum of **4.1a**, we interestingly observed a single fluorescence peak corresponding to the $S_1 \rightarrow S_0$ transition with no phosphorescence peak (Figure

4.4). Intrigued by the possibility that we were no longer accessing the excited triplet state of the gold(III) complex, we again probed the complex using transient-absorption spectroscopy (Figure 4.5). From this data it was immediately apparent that complex was still accessing both the excited singlet and triplet states, with a lifetime of 18.6 ns and 4.3 μs respectively. Due to the absence of phosphorescence from our excited triplet state, we hypothesized that there must be some other non-radiative decay operative, such as through heat in solution. Additionally, an excited triplet state lifetime of 4.3 μs is sufficiently long-lived enough to allow for energy transfer to take place, considering that the excited state triplet lifetime of a known photocatalyst, $[Ru(bpy)_3]Cl_2$, is a much shorter 0.9 μs.[98]

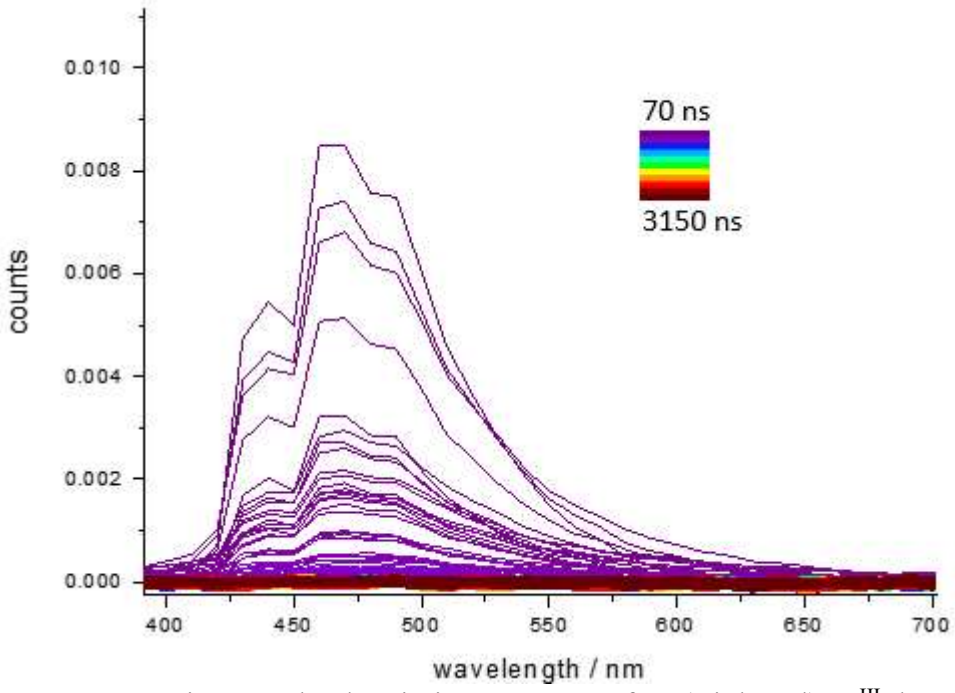

Figure 4.4 Time-resolved emission spectrum of IPr(Biphenyl)$Au^{III}SbF_6$

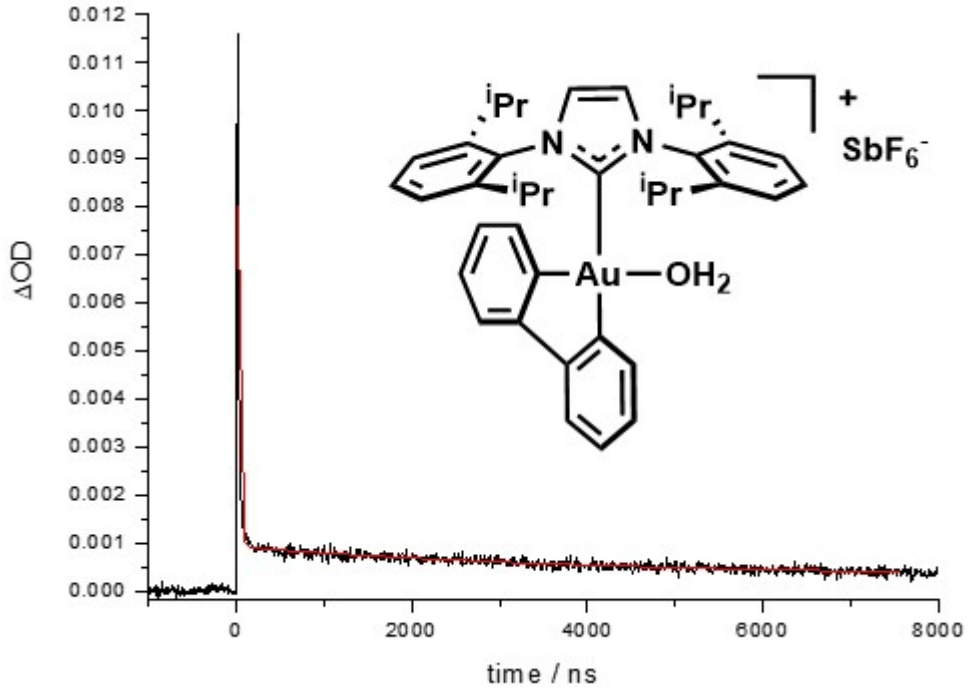

Figure 4.5 Transient-absorption spectrum of IPr(Biphenyl)$Au^{III}SbF_6$

Although there was no detected phosphorescence emission from **4.1a**, we concluded from the transient-absorption spectroscopy that we were still accessing the desired excited triplet state. When comparing the two gold(III) complexes, we observed red-shifted fluorescence of **4.1a** by 50 nm relative to **4.1**. If we make a similar assumption for the phosphorescence peak shift, then we can assume that the cationic gold(III) complex has a triplet state energy of around 51 kcal/mol.

4.2.2 Tuning the Photophysical Properties of Gold(III) Complexes

With our baseline photophysical properties established, we next explored the manipulation of these properties. Time-dependent density functional theory (TDDFT) calculations at the B3LYP level to determine excitation and emission from the first excited state of **4.1** in the gas phase suggested that modification to the biphenyl substituent would have the largest impact on perturbing the energy level of the lowest unoccupied molecular orbital (LUMO), and we therefore focused our efforts on modifying the biphenyl ligand.

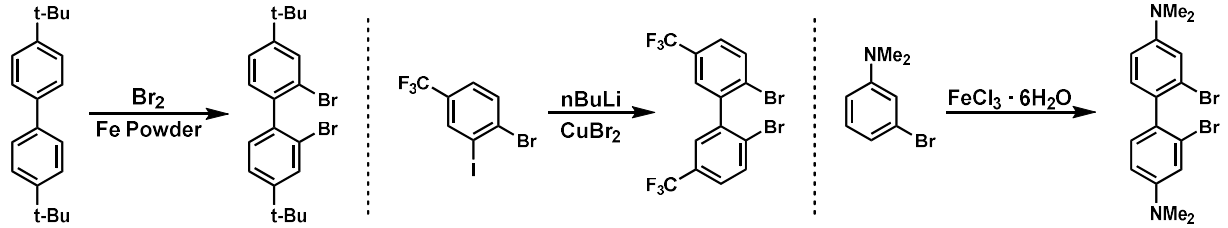

Scheme 4.4 Synthesis of substituted dibromobiphenyl coumpounds

We began with the synthesis of a number of substituted biphenyl bromides with varying electronics (Scheme 3.4). With these dibromobiphenyl compounds in hand we then synthesized the corresponding gold(III) complexes so that we could begin to test their photophysical properties

(Scheme 4.5). We found that the electron withdrawing trifluoromethyl groups of **4.2** resulted in a blueshift of 5 nm which corresponds to a triplet state energy level of around 57 kcal/mol. Complex **4.3** exhibited a redshift of 15 nm when compared to **4.1**, resulting in a triplet energy level of 54 kcal/mol. When attempting to characterize complex **4.4**, we found that the complex rapidly decomposed to yield IPrAuCl (*vide infra*). Although we were able to attenuate the photophysical properties of the gold(III) complexes through modifications of the biphenyl substituent, the overall effect on the triplet energy was negligible. Thus, we proceeded with the more easily accessed unsubstituted biphenyl ligand for our work.

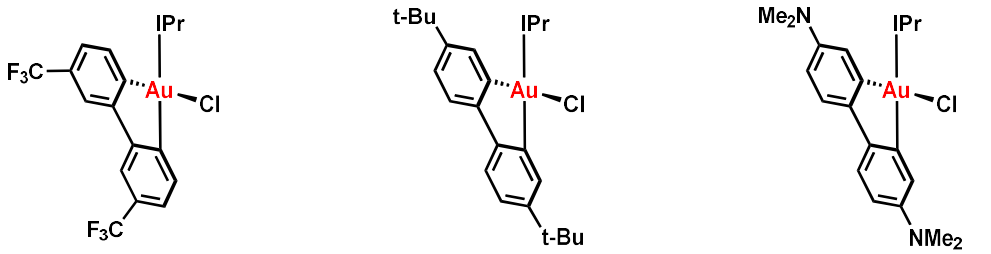

T_1 = 57 kcal/mol — **4.2**

T_1 = 54 kcal/mol — **4.3**

Decomposition — **4.4**

Scheme 4.5 Substituted biphenyl gold(III) complexes

4.2.3 Testing for Dual Lewis Acid-Photocatalysis

We began our search for a suitable reaction to test our hypothesis by exploring a variety of α,β-unsaturated carbonyl compounds that we could potentially excite to their triplet energy state and trap the resulting intermediate with dimethyl acetylenedicarboxylate (DMAD) (Scheme 4.6). Beginning with 2-pyridone, which Bach and coworkers had previously shown to be the ideal substrate for their system, we did not see any reactivity.[92] Cyclic and acyclic enones were also tested, and did not result in the desired trapping of the excited substrate with DMAD. Because we observed no gold-catalyzed reactivity with the substrates, we hypothesized that we were not generating the excited triplet state of the α,β-unsaturated carbonyl compounds, and wanted to take a step back to test our catalyst in a more well-defined system, one originally reported by Yoon and coworkers.[86]

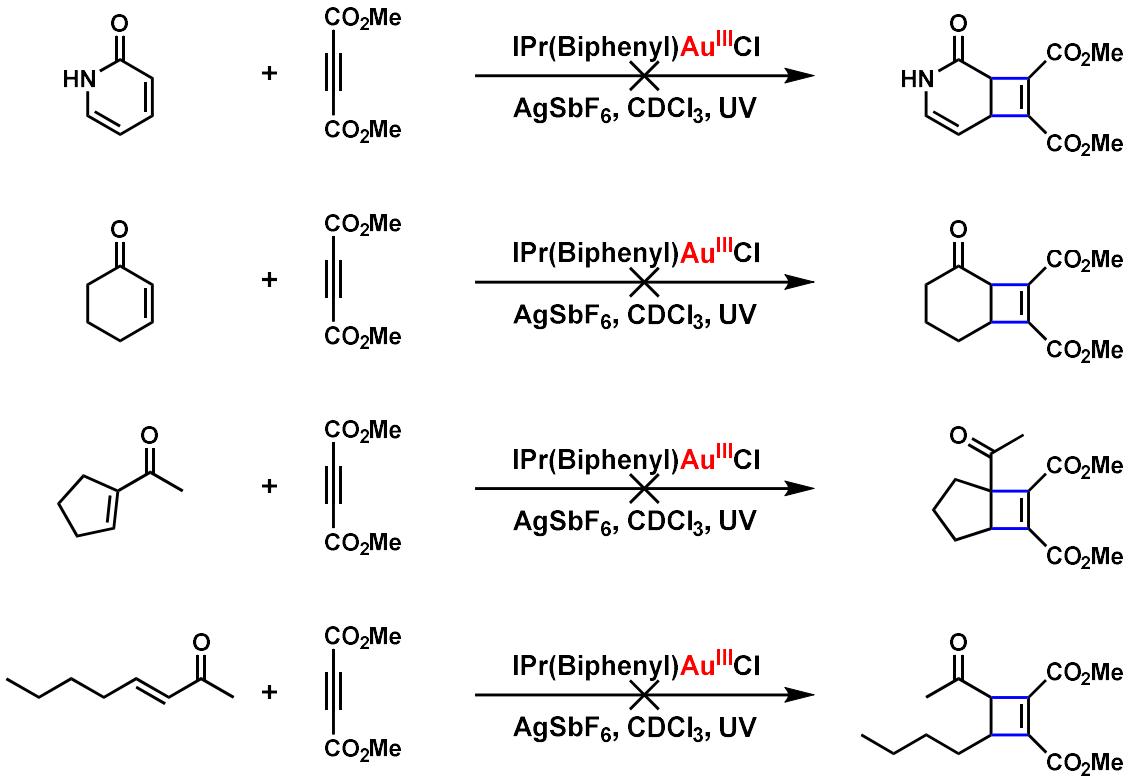

Scheme 4.6 Attempted trapping of reactive intermediates with DMAD.

Based on the work done in the Yoon lab, we knew that chalcone has an excited triplet energy level of 54 kcal/mol, and the scandium-bound chalcone has an excited triplet energy level of 33 kcal/mol. Under our previous assumption that complex **4.1a** has an excited state triplet energy level around 51 kcal/mol, the corresponding substrate-catalyst adduct could absorb in the proper energy range to undergo an energy transfer mechanism with the bound chalcone, which should have a lower energy excited triplet state. This energy transfer could generate the desired excited state triplet species, which could be further trapped in a [2+2] photocycloaddition. A catalyst screen of the reaction system did not result in desired product formation from any of the sampled catalysts (Table 2.1). Both NHC and phosphine based gold(III) complexes were tested; however, no desired reactivity was observed with any of the complexes. To mitigate potential issues with steric congestion at the gold(III) center that may interfere with substrate coordination, we also evaluated **4.5** as a catalyst, but again observed no gold-catalyzed reactivity.

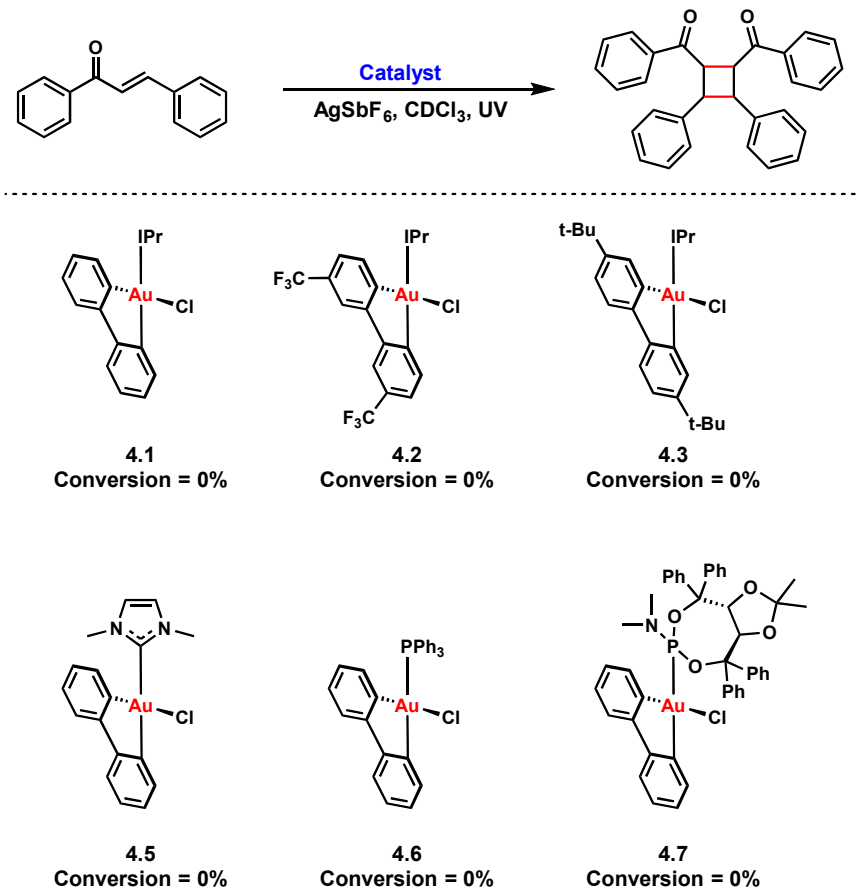

Table 4.1 Catalyst screen for a [2+2] photocycloaddition of chalcone.

Complex **4.5** was further tested in the [2+2] photocycloaddition reaction of chalcone to determine whether our choice of solvent or silver salt were not optimal (Table 4.2). Testing a variety of silver salts where the resulting counterion ranged from coordinating to non-coordinating yielded no conversion of the chalcone to the desired cycloadduct (entries 1-8). Another screen of a wide range of solvents yielded no conversion of the chalcone to the desired [2+2] dimer (entries 9-16). As we evaluated other substrates for the gold-catalyzed [2+2] photocycloaddition reaction, we observed a common issue: the α,β-unsaturated carbonyl compounds were absorbing in the UV region and undergoing background reactivity. This is a difficult obstacle to overcome in this system because the gold(III) complexes absorb exclusively in the UV region. Therefore, the UV irradiation required to generate the excited gold(III) species could, instead, excite the substrate. This issue could be circumvented by shifting the absorption of the gold(III) complex to the visible region.

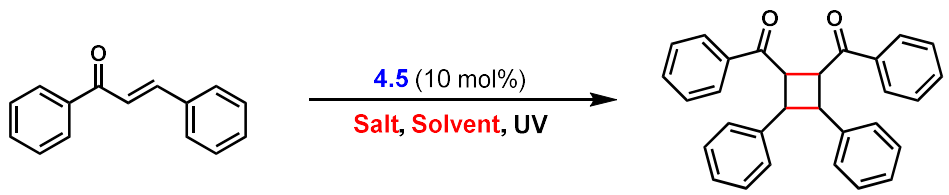

Entry	Ag Salt	Conversion (%)	Entry	Solvent	Conversion (%)
1	$AgSbF_6$	0	9	MeCN	0
2	AgOTf	0	10	Tol	0
3	$AgBF_4$	0	11	DMSO	0
4	$AgPF_6$	0	12	MeOH	0
5	AgOBz	0	13	Acetone	0
6	AgOMs	0	14	Ph	0
7	AgOTs	0	15	$CHCl_3$	0
8	$AgNTF_2$	0	16	DCM	0

Table 4.2 Solvent and silver salt optimization for a [2+2] photocycloaddition of chalcone.

4.2.4 Singlet Oxygen Sensitization using Gold(III) Complexes

Based on the photophysical data gathered from complexes **4.1**, **4.2**, and **4.3**, we hypothesized that electron donating substituents on the biphenyl backbone would shift the absorbance towards the visible spectrum. Thus, we attempted to synthesize complex **4.4** and evaluate its properties because it could allow for exclusive excitation of the substrate-catalyst adduct. Upon synthesis and isolation however, we found that the complex rapidly decomposed to IPrAuCl with no biphenyl decomposition byproducts observed in solution. Additionally, while evaluating our gold(III) complexes as dual Lewis acid-photocatalysts, we observed an interesting phenomenon when the reactions were performed open to air rather than under a N_2 atmosphere. When complex **4.1** was irradiated open to the atmosphere, we again saw complete decomposition to IPrAuCl, loss of biphenylene, and formation of a precipitate. If the gold complex were decomposing *via* reductive elimination, we would expect biphenylene in the resulting reaction mixture. Additionally, if complex **4.1** were decomposition *via* protodeauration, biphenyl would be an expected byproduct. However, neither biphenylene nor biphenyl were observed in the corresponding reaction mixture. Additionally, we found that if the reaction with **4.1** had O_2 bubbled through it for 5 minutes before exposing it to UV irradiation, the reaction would proceed to completion significantly more rapidly. This led us to hypothesize that **4.1** and **4.4** were acting as a singlet oxygen ($^1O_2$) sensitizers when irradiated (under UV and visible light, respectively) in the presence of triplet oxygen ($^3O_2$), resulting in decomposition of the gold(III) species from the generated $^1O_2$.

Singlet oxygen sensitization occurs when an excited triplet state compound transfers its energy to $^3O_2$, which generates the excited state species, $^1O_2$ (Figure 4.6). The energy of $^1O_2$ is ~22 kcal/mol higher than that of $^3O_2$, which suggests that we have ample energy with our system to generate the excited singlet state of O_2 based on our previous emission studies.

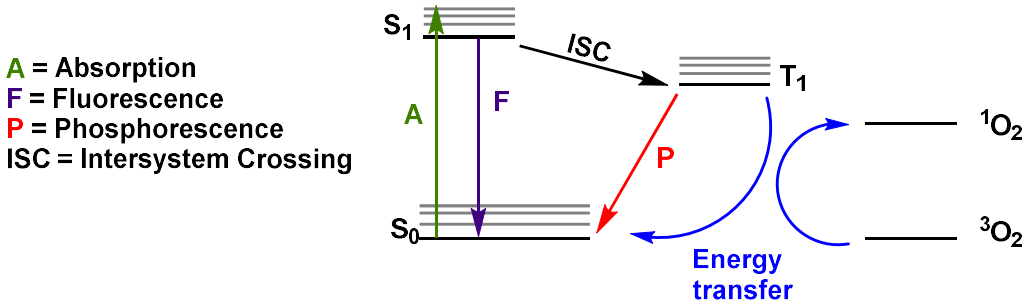

Figure 4.6 Jablonski diagram for the generation of singlet oxygen.

In an attempt to further confirm the presence of $^1O_2$ in the system, we studied a known $^1O_2$ reaction, a Diels-Alder reaction of 9,10-dimethylanthracene with $^1O_2$. This reaction results in the formation of an endoperoxide product. When we attempted this reaction using **4.1** as the $^1O_2$ sensitizer, we observed trace formation of the desired product after one hour (Scheme 4.7).

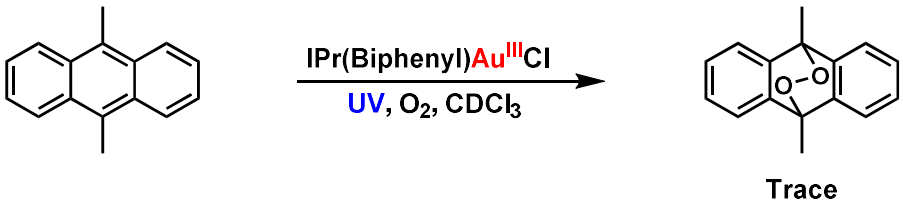

Scheme 4.7 Diels-Alder reaction between 9,10-dimethylanthracene and $^1O_2$.

This promising result led us to consider another reaction with $^1O_2$, the oxidation of benzylic amines.[96] We began testing our system with the oxidation of dibenzyl amine (Table 4.3). We found that both the chloride bound and cationic gold(III) complex (**4.1** and **4.1a**) were competent catalysts for this transformation, with the cationic complex providing slightly higher conversions under otherwise equivalent conditions (entries 1-2). When performing the necessary control reactions, we did not observe any the silver salt-mediated reactivity (entry 3). Additionally, no background reactivity was observed in the absence of the gold(III) complex (entry 4). We then probed whether a gold(I) species generated from potential *in-situ* reductive elimination or decomposition could be responsible for the observed oxidation of dibenzyl amine. No conversion was observed when IPrAuCl was employed as the catalyst, suggesting that gold(III) is required for the observed reactivity (entry 5). Lastly, when the reaction was run in the absence of irradiation, no conversion was observed (entry 6). These results therefore support the assumption that we are indeed generating $^1O_2$ from our excited state gold(III) species.

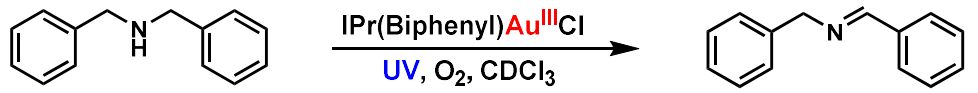

Entry	Modifications	Conversion (%)
1	None	40
2	AgOTf	45
3	Only AgOTf	Trace
4	No Au(III)	Trace
5	Au(I)	Trace
6	No Light	0

Table 4.3 Control reactions for a gold(III)-photocatalyzed oxidation of dibenzylamine.

These promising results led us to continue further optimization of the conditions for this $^1O_2$ oxidation of benzylic amines. Because our ultimate goal is to perform an enantioselective transformation, it is important that we screen potential counterions that would influence how tightly a substrate may bind to the cationic gold(III) center. Thus, we tested various silver salts under our reaction conditions and found that all resulting complexes yielded conversion to the desired imine product (Table 4.4). The best result was obtained when silver mesylate was employed to generate the cationic gold(III) complex, where after 2 hours of irradiation we obtained 60% conversion to the desired imine (entry 6).

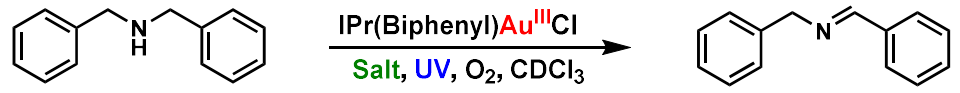

Entry	Silver Salt	Conversion (%)
1	$AgBF_4$	41
2	$AgSbF_6$	35
3	$AgPF_6$	42
4	$AgNTf_2$	54
5	AgOTf	45
6	AgOMs	60
7	AgOBz	48
8	AgOTs	53

Table 4.4 Counterion optimization for a gold(III)-photocatalyzed oxidation of dibenzylamine.

After probing various counterions for this gold(III)-photocatalyzed oxidation, we evaluated the feasibility of an enantioselective oxidation of a chiral benzylic amine in the presence of a chiral gold(III) complex. We hypothesized that if one enantiomer of amine was preferentially bound to the chiral gold(III) complex, generation of $^1O_2$ in close proximity could kinetically favor conversion of the bound enantiomer of amine (Scheme 4.8). Subsequent reduction of the reaction mixture could then be employed deracemization of chiral benzylic amines.

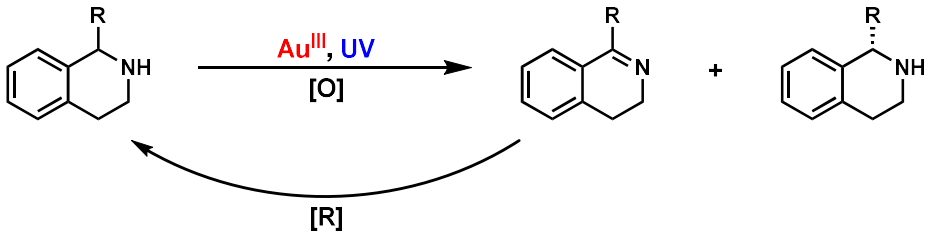

Scheme 4.8 Proposed gold(III)-photocatalyzed deracemization of benzylic amines *via* $^1O_2$ oxidation.

To test our hypothesis we evaluated a variety of chiral gold(III) complexes to use as photosensitizers for the oxidation reaction (Table 4.5). Unfortunately we found that all chiral gold(III) complexes bearing phosphine, phosphoramidite, or NHC ligands did not yield enantioenriched recovered amine.

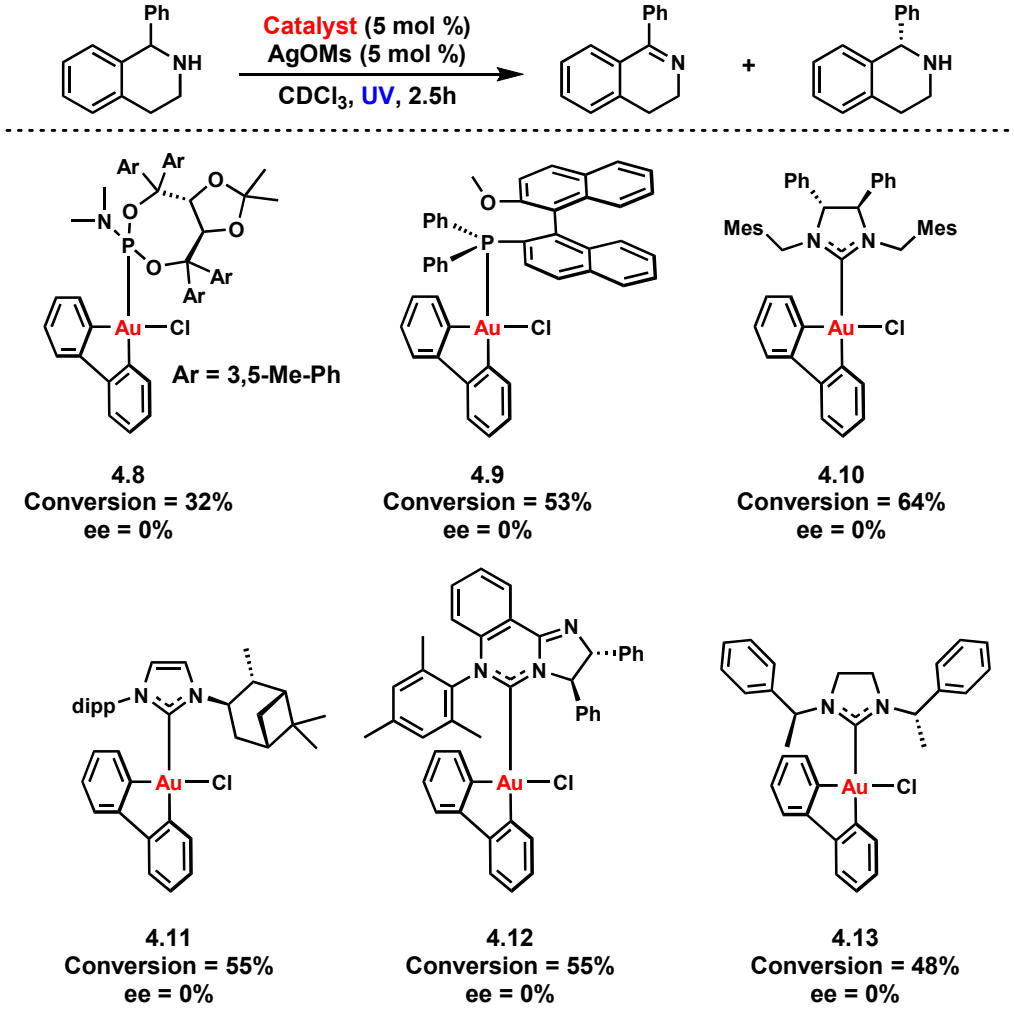

Table 4.5 Chiral gold(III) complexes used in the deracemization dibenzylamine.

We then examined the scope of this transformation to determine whether there might be interesting chemo- or regioselectivity imparted by the gold(III) complexes. We found that secondary benzylic amines were competent substrates for the transformation, yielding 55-65%

product after 2.5 hours of irradiation (substrates **4.8**-**4.10**). We observed sluggish oxidation of **4.11** relative to substrates **4.8**-**4.10**, but the pendant primary amine did not appear to influence the reaction selectivity. We then studied substrate **4.12** to probe the possibility for a chemoselective gold(III)-catalyzed reaction. We observed selective oxidation of the benzylic amine by $^1O_2$ and no oxidation of the pendent alkene. Primary benzylic amines and silylated benzylic amines were also not oxidized with our catalytic system (entries **4.13**-**4.15**). Benzylic amines bearing amide and aniline functionality were also inert under our catalytic conditions (entries **4.16**-**4.17**). These results are extremely promising for the development of a chemoselective oxidation using $^1O_2$, which is generally considered to be a very reactive species that typically reacts indiscriminately.

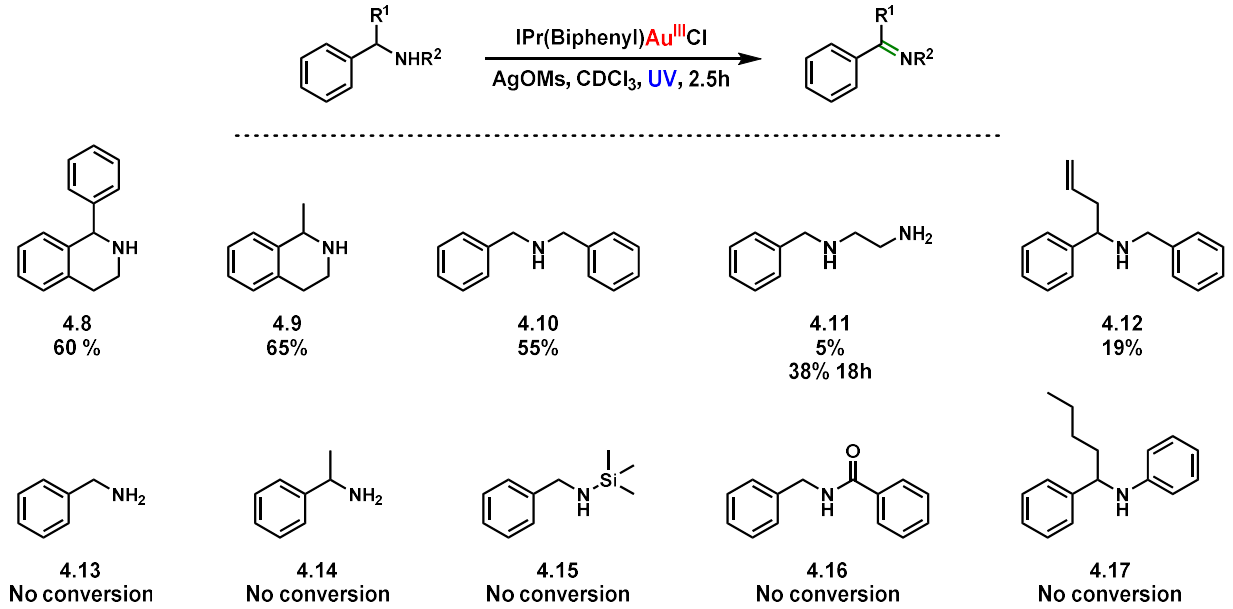

Table 4.6 Scope of a gold(III)-photocatalyzed $^1O_2$ oxidation of benzylic amines to imines.

4.3 Conclusion

In summary, we have explored the photophysical properties of our gold(III) complexes and found that they have triplet state energies around 56 kcal/mol for the chloride-bound complex and 51 kcal/mol for the cationic species. We have attempted to use these complexes as dual Lewis acid-photocatalysts for [2+2] photocycloadditions but have thus far been unsuccessful. Additional work is currently ongoing in the lab towards achieving this goal. We have successfully utilized these gold(III) complexes as photosensitizers for the generation of $^1O_2$ and applied this towards the oxidation of benzylic amines. A preliminary substrate scope has been explored and we have seen promising results for a chemoselective oxidation of amines that could be further applied as a late stage functionalization technique.

4.4 Supporting Information

4.4.1 General Methods

Unless stated otherwise, all reactions were performed in oven-dried glassware sealed with rubber septa under a nitrogen atmosphere and were stirred with Teflon-coated magnetic stir bars. Dry tetrahydrofuran (THF), acetonitrile (MeCN), dichloromethane (DCM), methanol (MeOH), and toluene (Tol) were obtained by passing these previously degassed solvents through activated

alumina columns. All other reagents were used as received. Reactions were monitored by thin layer chromatography (TLC) on Silicycle Siliaplate^{TM} glass backed TLC plates (250 µm thickness, 60 Å porosity, F-254 indicator) and visualized by UV irradiation and iodine stain. Volatile solvents were removed under reduced pressure with a rotary evaporator and dried on high vacuum on a Schlenk line. ^{1}H-NMR and ^{13}C-NMR spectra were taken with Bruker AV-300, AVQ-400, AVB-400, AV-500, DRX-500, and AV-600 spectrometers. Chemical shifts are reported relative to the residual solvent signal. NMR data are reported as follows: chemical shift (multiplicity, coupling constants where applicable, number of hydrogens). Splitting is reported with the following symbols: s = singlet, d = doublet, t = triplet, dd = doublet of doublets, dt = doublet of triplets, m = multiplet, dq = doublet of quartets, ddd = doublet of doublets of doublets, ddt = doublet of doublets of triplets. Chiral phase high performance liquid chromatography (HPLC) was performed on Shimadzu VP and Shimadzu prominence series instruments using the specified column (5µm, 4.6 mm x 250 mm). High-resolution mass spectra (HRMS) were obtained from the Micro-Mass/Analytical Facility operated by the College of Chemistry, University of California, Berkeley. Previously reported compounds were synthesized according to literature procedures. The following compounds were prepared according to previously published procedures and their spectra match those reported in literature: 2,2'-dibromo-4,4'-di-tert-butyl-1,1'-biphenyl,[99] 2,2'-dibromo-5,5'-bis(trifluoromethyl)-1,1'-biphenyl,[100] and 2,2'-dibromo-*N*^{4},*N*^{4},*N*$^{4'}$,*N*$^{4'}$-tetramethyl-[1,1'-biphenyl]-4,4'-diamine.[101] The spectra of the following imines were found to match those reported in literature: 1-phenyl-3,4-dihydroisoquinoline,[102] 1-methyl-3,4-dihydroisoquinoline,[103] benzyl-1-phenylmethanimine,[104] (*E*)-2-(benzylideneamino)ethan-1-amine,[105] and (*E*)-*N*-benzyl-1-phenylbut-3-en-1-imine.[106]

4.4.2 Methodology for the [2+2] of α,β-unsaturated ketones with DMAD

To a 1 dram vial was added the Au(III) catalyst (0.05 equiv), silver salt (0.05 equiv), and solvent (0.3 M). The vial was capped and sonicated for 5 minutes. The reaction mixture was passed through a glass fiber filter and collected in a 1 dram vial. To the vial was added the α,β-unsaturated aldehyde (1 equiv) and DMAD (5 equiv). The subsequent reaction mixture underwent 3 cycles of freeze, pump, thaw and filled with N_2. The reaction mixture was then irradiated with a UV lamp for 18 hours. The progress of the reaction was then monitored by ^{1}H NMR spectroscopy.

4.4.3 Methodology for the [2+2] Photocycloaddition Reactions of Chalcone

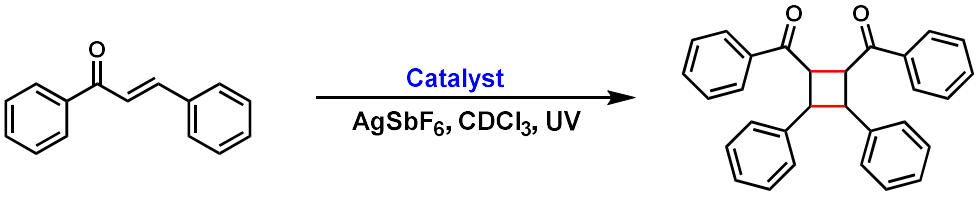

Scheme 4.9 General methodology for the [2+2] photocycloaddition of chalcone.

To a 1 dram vial was added the Au(III) catalyst (0.05 equiv), silver salt (0.05 equiv), and solvent (0.3 M). The vial was capped and sonicated for 5 minutes. The reaction mixture was passed through a glass fiber filter and collected in a 1 dram vial. To the vial was added the chalcone (2 equiv) and the subsequent reaction mixture underwent 3 cycles of freeze, pump, thaw and filled with N_2. The reaction mixture was then irradiated with a UV lamp for 18 hours. The progress of the reaction was then monitored by ^{1}H NMR spectroscopy.

4.4.4 Methodology for the $^1O_2$ Oxidation of Benzylic Amines

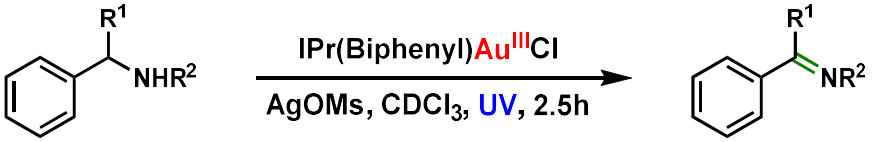

Scheme 4.10 General preparation of imine products.

To a 1 dram vial was added the Au(III) catalyst (0.05 equiv), silver salt (0.05 equiv), and solvent (0.3 M). The vial was capped and sonicated for 5 minutes. The reaction mixture was passed through a glass fiber filter and collected in a 1 dram vial. To the vial was added the benzyl amine (1 equiv) and then was bubbled through with O_2 for 15 minutes and subsequently irradiated with a UV lamp for 2.5 hours. The starting material and product were then isolated by column chromatography (5:1 hexanes : ethyl acetate).

4.4.5 Preparation and Characterization of Gold(III) Complexes

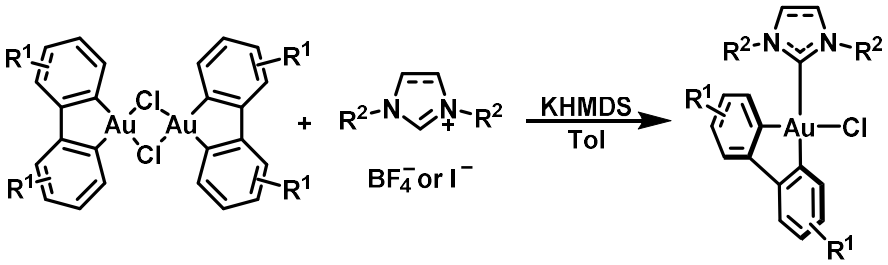

Scheme 4.11 Synthesis of gold(III)-NHC complexes with substituted biphenyl ligands.

In a glovebox, to the corresponding imidazolium salt (2 equiv) in toluene (0.1 M) was added KHMDS (2.4 equiv) in one portion at 22 °C. The reaction mixture was stirred for 5 h and then [Au(III)(biphenyl) chloride]$_2$ (1 equiv) was added in one portion. The reaction mixture was stirred for 16 h and then the reaction vessel was removed from the glovebox. The reaction mixture was then passed through Celite and dried under vacuum to give the crude product. The pure product was isolated by column chromatography (DCM:hexanes 1:1).

Catalyst 4.2

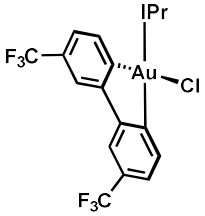

Prepared according to the general procedure with the corresponding imidazolium salt. **^{1}H NMR** (600 MHz, $CDCl_3$) δ 8.05 (d, J = 8.1 Hz, 1H), 7.37 (s, 1H), 7.31 (d, J = 2.0 Hz, 1H), 7.29 – 7.23 (m, 1H), 7.15 (dt, J = 7.7, 1.7 Hz, 2H), 7.12 – 7.06 (m, 1H), 7.02 (dt, J = 7.7, 1.7 Hz, 2H), 6.96 – 6.88 (m, 2H), 2.99 (hept, J = 7.6, 7.2 Hz, 2H), 2.90 (hept, J = 6.8 Hz, 2H), 1.30 (d, J = 6.4 Hz, 6H), 1.05 (d, J = 6.6 Hz, 6H), 0.93 (d, J = 6.6 Hz, 6H), 0.71 (d, J = 6.3 Hz, 6H).; **^{13}C NMR** (151

MHz, $CDCl_3$) δ 185.25, 161.74, 154.63, 153.83, 151.87, 147.06, 144.42, 133.70, 133.68, 133.49, 130.98, 129.38, 129.17, 125.66, 125.28, 125.05, 124.75, 124.35, 123.61, 123.59, 123.56, 123.48, 123.24, 117.87, 117.84, 117.02, 117.00, 29.02, 28.74, 26.66, 26.53, 22.91, 22.67.; **^{19}F NMR** (565 MHz, $CDCl_3$) δ -62.62, -62.80.

Catalyst 4.3

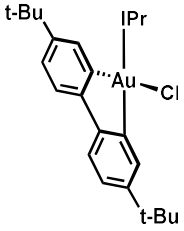

Prepared according to the general procedure with the corresponding imidazolium salt. **^{1}H NMR** (600 MHz, $CDCl_3$) δ 8.02 (d, J = 2.0 Hz, 1H), 7.35 (t, J = 7.7 Hz, 2H), 7.21 (d, J = 7.7 Hz, 2H), 7.17 – 7.08 (m, 5H), 7.05 (d, J = 8.0 Hz, 1H), 6.97 (d, J = 8.1 Hz, 1H), 6.72 (s, 1H), 3.33 – 3.25 (m, 2H), 2.78 – 2.71 (m, 2H), 1.42 (d, J = 6.6 Hz, 6H), 1.22 (s, 9H), 1.16 (s, 9H), 1.11 (d, J = 6.8 Hz, 6H), 0.98 (d, J = 6.9 Hz, 6H), 0.55 (d, J = 6.6 Hz, 6H).; **^{13}C NMR** (151 MHz, $CDCl_3$) δ 190.08, 159.29, 159.27, 152.43, 151.95, 151.90, 150.56, 150.53, 150.50, 148.54, 148.51, 147.67, 146.71, 145.03, 134.26, 134.23, 134.20, 131.20, 130.48, 130.23, 130.20, 130.08, 129.15, 129.12, 129.08, 126.85, 126.79, 126.42, 125.45, 125.40, 125.23, 124.93, 124.80, 124.34, 123.34, 121.69, 121.11, 119.54, 119.52, 119.09, 35.14, 34.48, 31.50, 31.43, 29.48, 29.35, 29.20, 28.79, 22.86, 22.74, 22.50, 21.93.

Catalyst 4.5

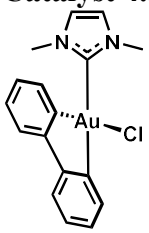

Prepared according to the general procedure with the corresponding imidazolinium salt. 1H NMR (300 MHz, $CDCl_3$) δ 8.23 – 8.14 (m, 1H), 7.48 – 7.36 (m, 2H), 7.23 – 7.12 (m, 3H), 7.10 (s, 2H), 6.80 – 6.71 (m, 1H), 6.38 (d, J = 7.7 Hz, 1H), 3.88 (s, 6H).

Catalyst 4.10

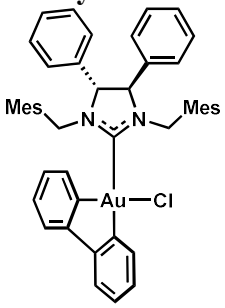

Prepared according to the general procedure with the corresponding imidazolinium salt. **^{1}H NMR** (600 MHz, $CDCl_3$) δ 8.29 – 8.25 (m, 1H), 7.72 (d, J = 7.6 Hz, 1H), 7.50 (dd, J = 7.7, 1.6 Hz, 1H), 7.45 – 7.32 (m, 8H), 7.26 – 7.24 (m, 4H), 7.18 (td, J = 7.4, 6.5, 3.7 Hz, 2H), 7.02 (td, J

= 7.5, 1.5 Hz, 1H), 6.87 (d, J = 7.0 Hz, 2H), 6.58 (d, J = 4.1 Hz, 4H), 5.22 (dd, J = 30.7, 14.5 Hz, 2H), 4.88 (d, J = 14.8 Hz, 1H), 4.60 (d, J = 14.3 Hz, 1H), 4.28 (d, J = 6.1 Hz, 1H), 4.06 (d, J = 6.1 Hz, 1H), 1.83 (d, J = 5.9 Hz, 12H).

4.4.6 NMR Spectra

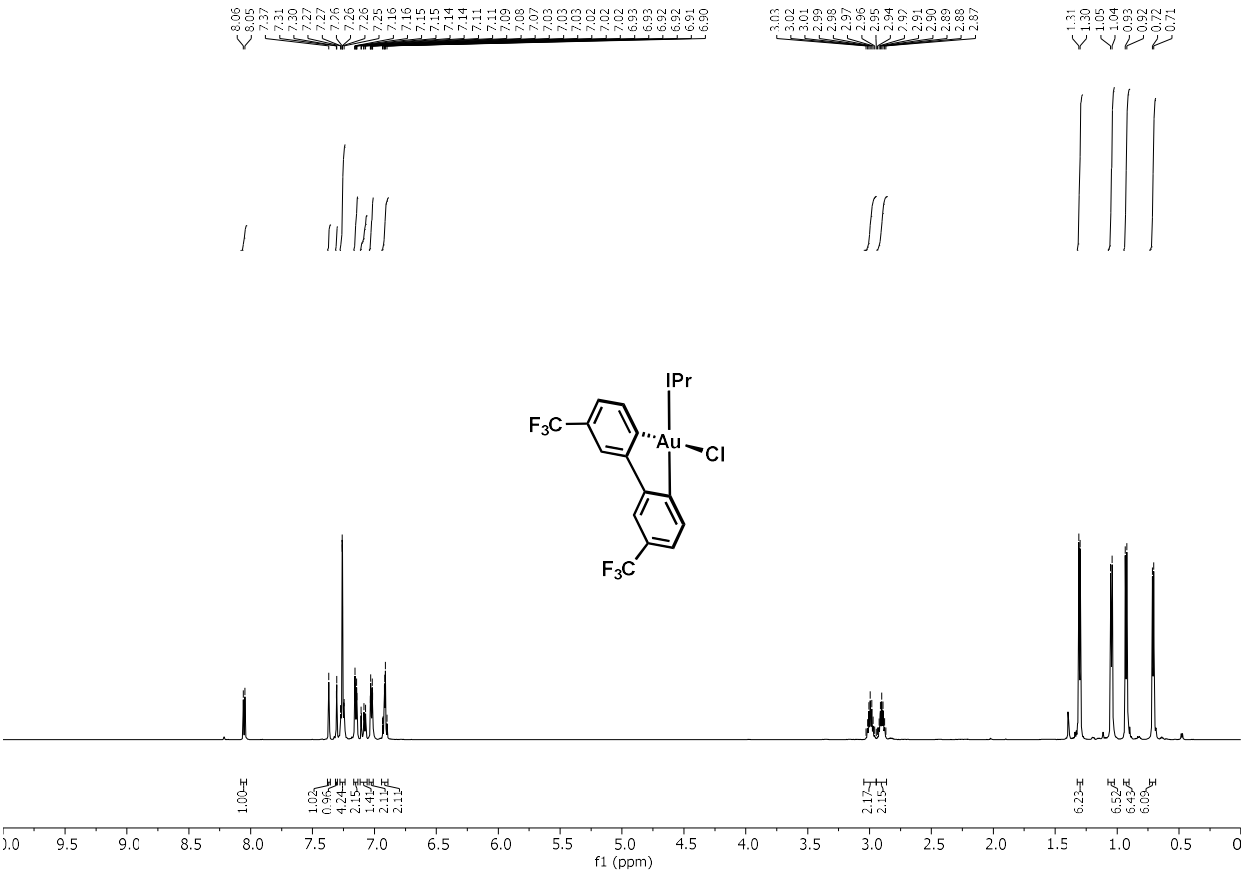

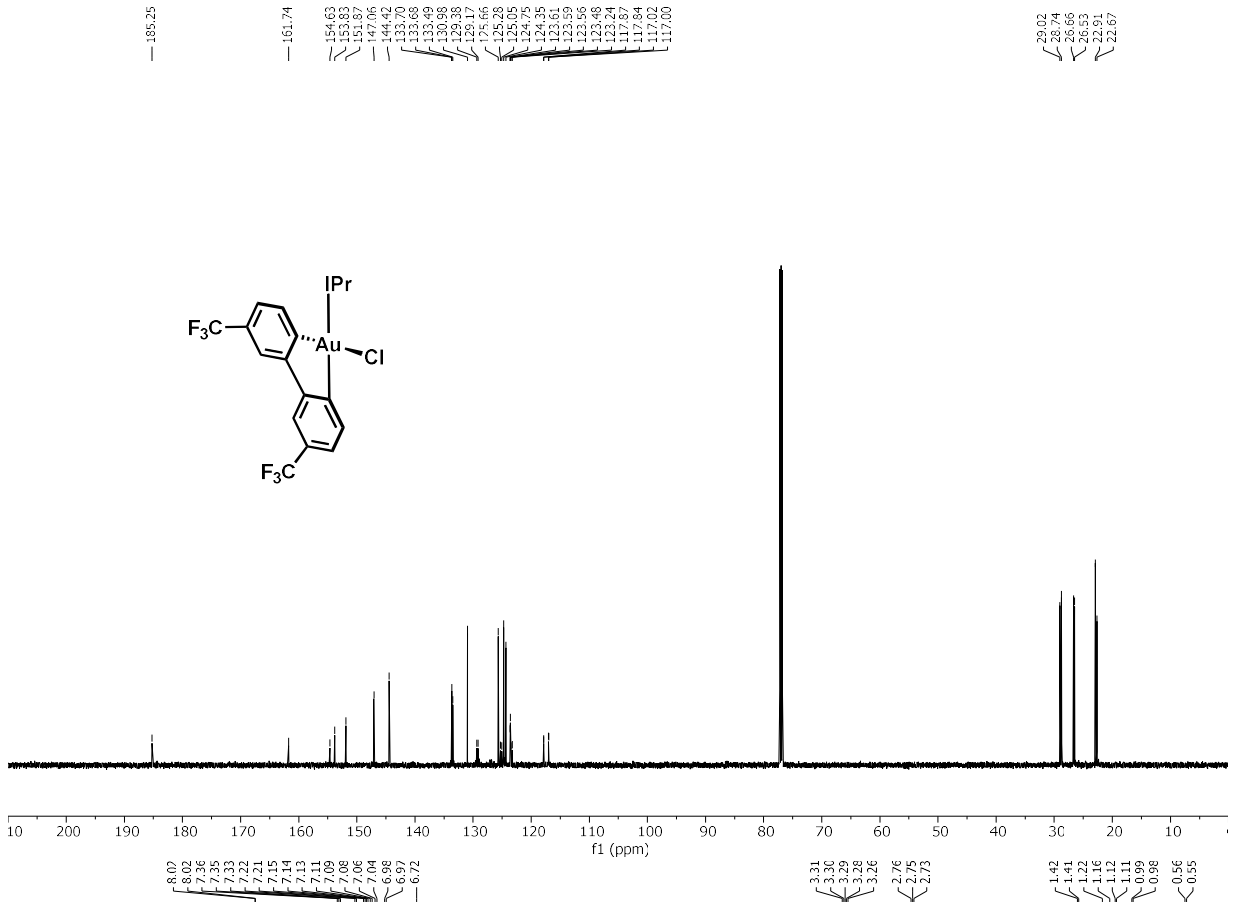
185.25
161.74
154.63
153.83
151.87
147.06
144.42
133.70
133.68
133.49
130.98
129.38
126.17
125.66
125.28
125.05
124.75
124.35
123.61
123.59
123.56
123.48
123.24
117.87
117.84
117.02
117.00
29.02
28.74
26.66
26.53
22.91
22.67
IPr
F3C
Au
Cl
F3C
f1 (ppm)

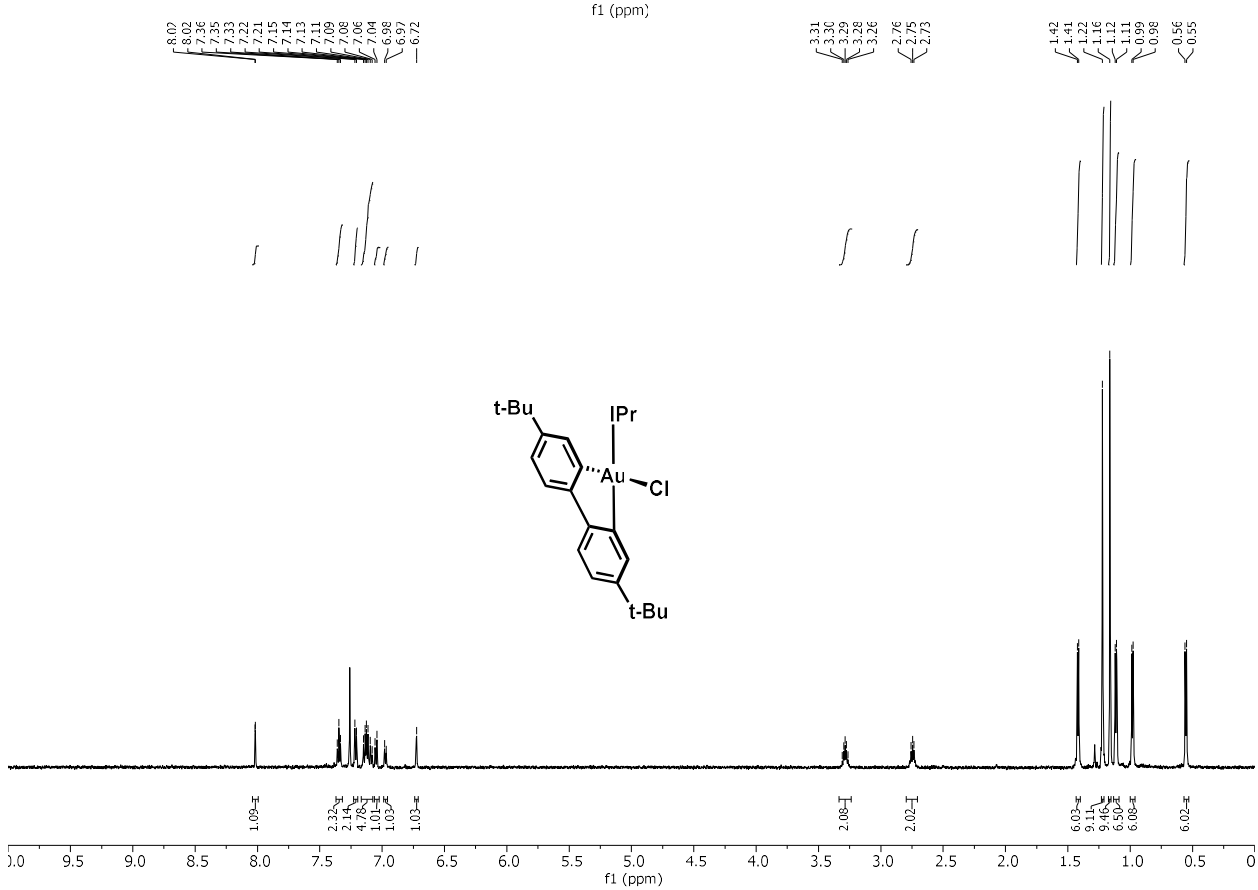
8.02
8.02
7.36
7.35
7.33
7.22
7.21
7.15
7.14
7.13
7.11
7.09
7.08
7.06
7.04
6.98
6.97
6.72
3.31
3.30
3.29
3.28
3.26
2.76
2.75
2.73
1.42
1.41
1.22
1.16
1.12
1.11
0.99
0.98
0.56
0.55
t-Bu
IPr
Au
Cl
t-Bu
1.09
2.33
2.14
4.78
1.01
1.03
1.03
2.08
2.02
6.03
9.11
9.46
6.50
6.08
6.02
f1 (ppm)

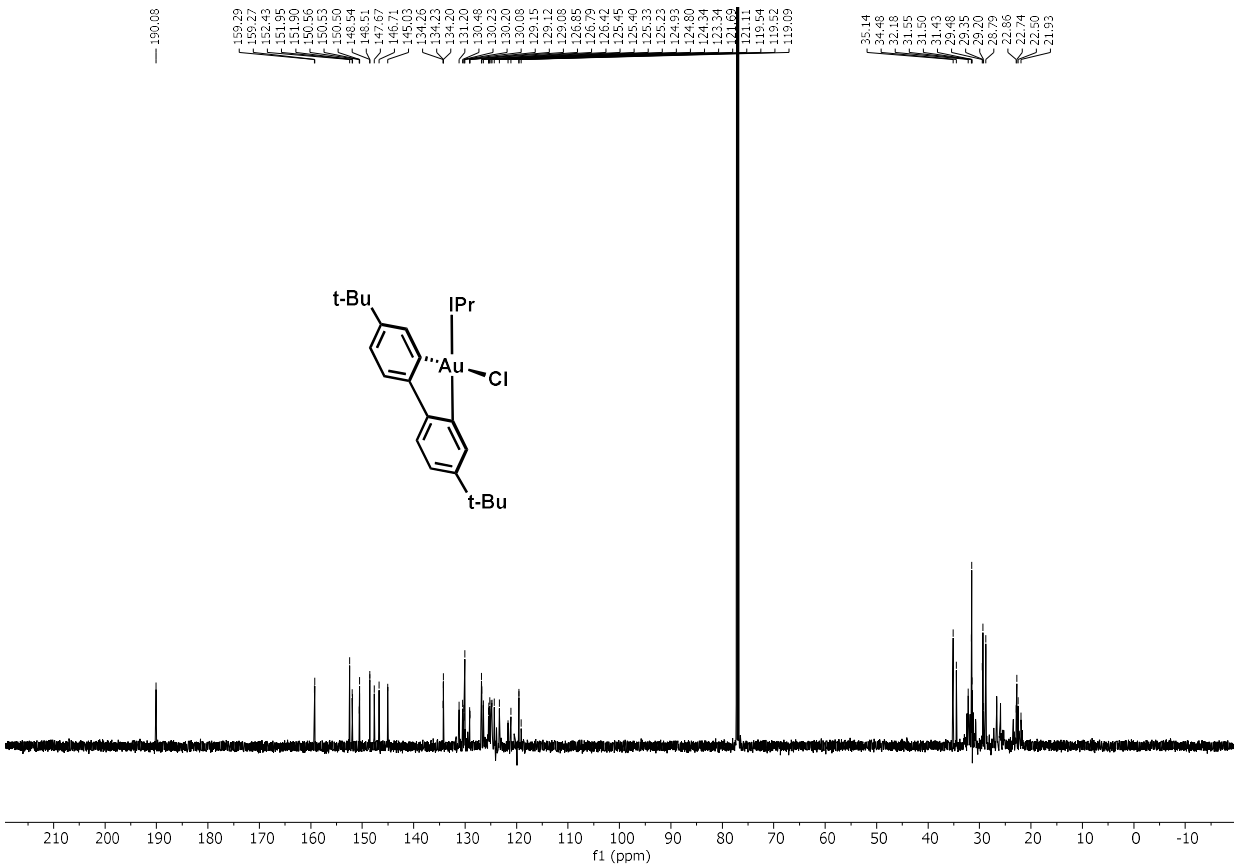
190.08
159.29
159.27
152.43
151.95
151.90
150.56
150.53
150.50
148.54
148.51
147.67
146.71
145.03
134.26
134.23
134.20
131.20
130.48
130.23
130.20
130.08
129.15
129.12
129.08
126.85
126.79
126.42
125.45
125.40
125.33
125.23
124.93
124.80
124.34
123.34
121.69
121.11
119.54
119.52
119.09
35.14
34.48
32.18
31.55
31.50
31.43
29.48
29.35
29.20
28.79
22.86
22.74
22.50
21.93
t-Bu
IPr
Au
Cl
t-Bu
210 200 190 180 170 160 150 140 130 120 110 100 90 80 70 60 50 40 30 20 10 0 -10
f1 (ppm)

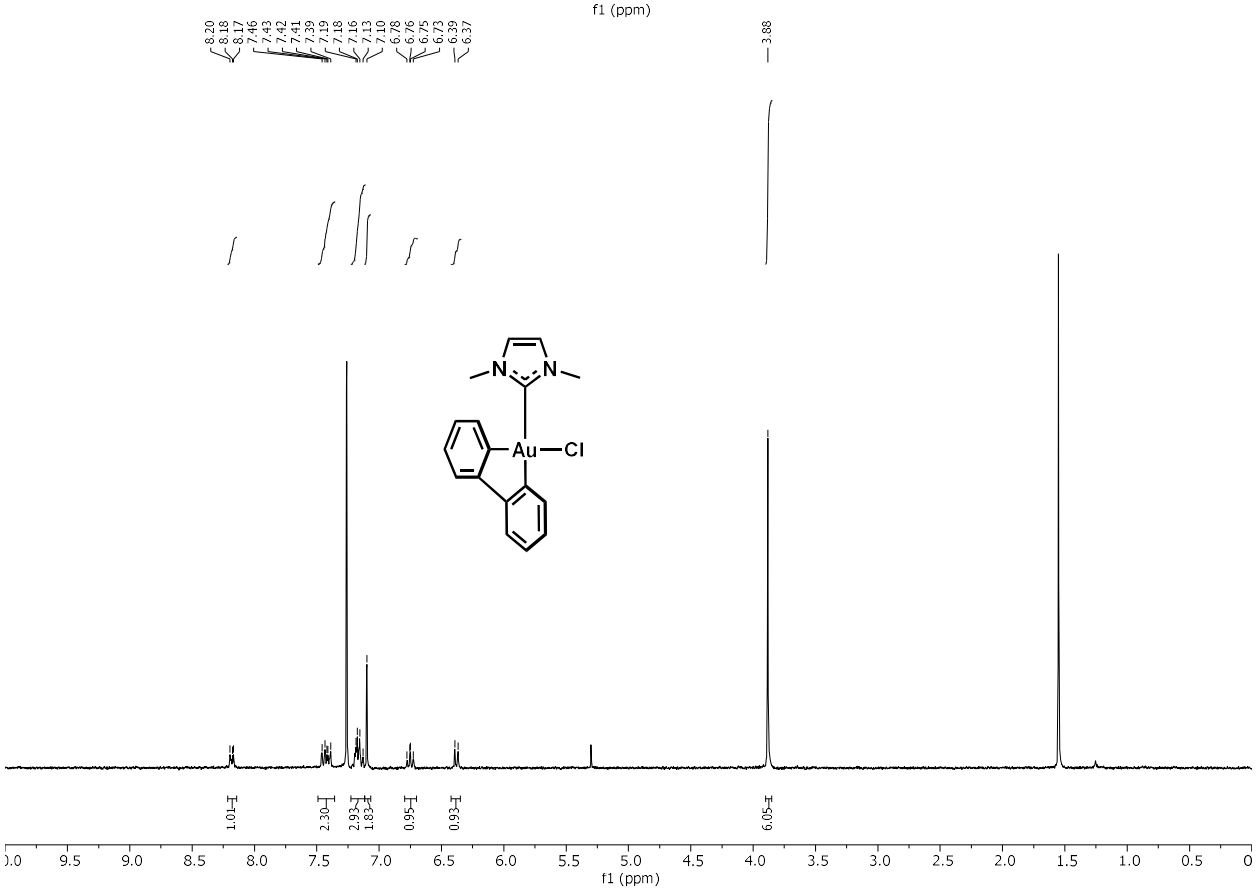
8.20
8.18
8.17
7.46
7.43
7.42
7.41
7.39
7.19
7.18
7.16
7.13
7.10
6.78
6.76
6.75
6.73
6.39
6.37
3.88
N
N
Au
Cl
1.01
2.30
2.93
1.83
0.95
0.93
6.05
0.0 9.5 9.0 8.5 8.0 7.5 7.0 6.5 6.0 5.5 5.0 4.5 4.0 3.5 3.0 2.5 2.0 1.5 1.0 0.5 0
f1 (ppm)

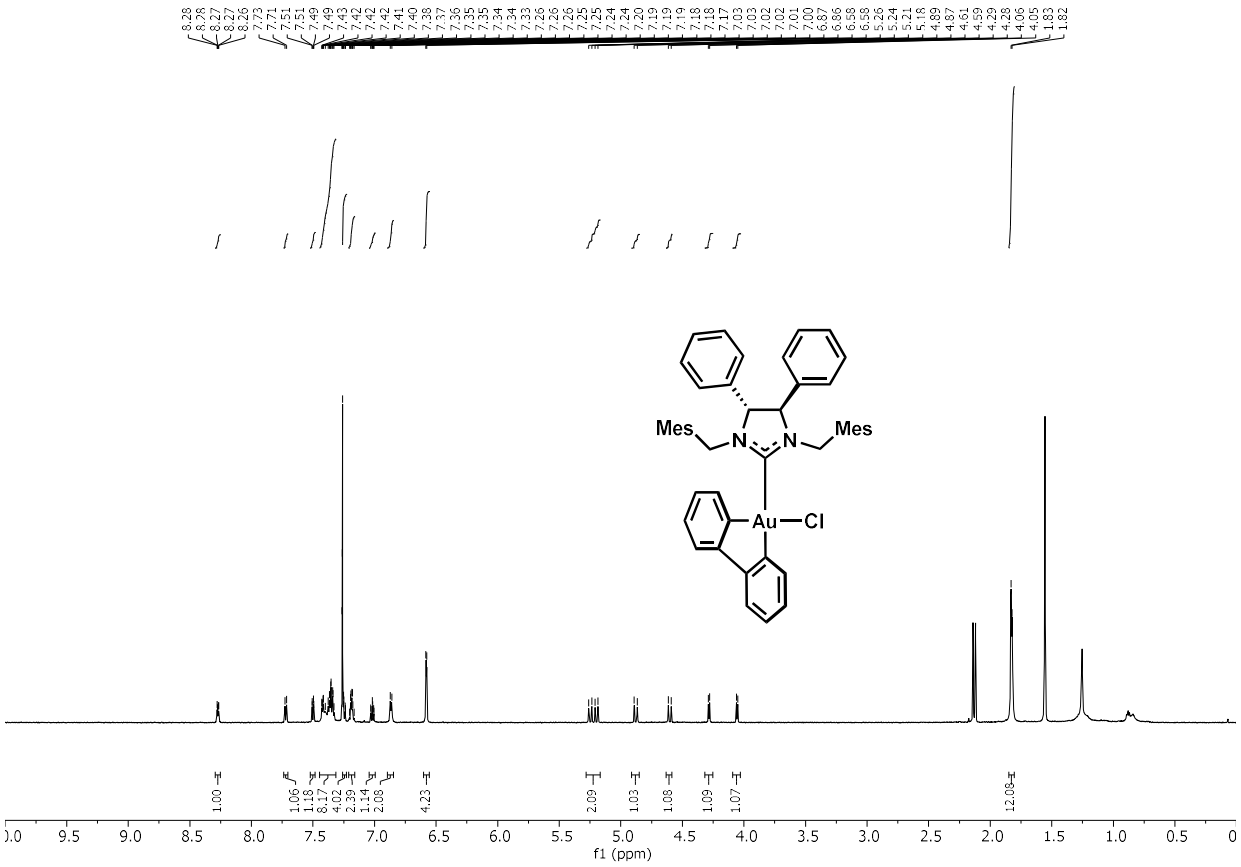

4.5 Notes and References

(79) Zhou, F.; Yamamoto, H. *Angew. Chem. Int. Ed.* **2016**, *55*, 8970–8974.
(80) Zhou, F.; Yamamoto, H. *Org. Lett.* **2016**, *18*, 4974–4977.
(81) Twilton, J.; MacMillan, D. W. C.; Le, C.; Zhang, P.; Shaw, M. H.; Evans, R. W. *Nat. Rev. Chem.* **2017**, *1*, 0052.
(82) Shaw, M. H.; Twilton, J.; MacMillan, D. W. C. *J. Org. Chem.* **2016**, *81*, 6898–6926.
(83) Wang, C. S.; Dixneuf, P. H.; Soulé, J. F. *Chem. Rev.* **2018**, *118*, 7532–7585.
(84) Prier, C. K.; Rankic, D. A.; MacMillan, D. W. C. *Chem. Rev.* **2013**, *113*, 5322–5363.
(85) Du, J.; Skubi, K. L.; Schultz, D. M.; Yoon, T. P. *Science* **2014**, *344*, 392–396.
(86) Blum, T. R.; Miller, Z. D.; Bates, D. M.; Guzei, I. A.; Yoon, T. P. *Science* **2016**, *354*, 1391–1395.
(87) Cauble, D. F.; Lynch, V.; Krische, M. J. *J. Org. Chem.* **2003**, *68*, 15–21.
(88) Bach, T.; Bergmann, H.; Harms, K. *Angew. Chem. Int. Ed.* **2000**, *39*, 2302–2304.
(89) Bach, T.; Bergmann, H.; Grosch, B.; Harms, K. *J. Am. Chem. Soc.* **2002**, *124*, 7982–7990.
(90) Grimme, S.; Bach, T.; Bauer, A.; Westka, F. *Nature* **2005**, *436*, 1139–1140.
(91) Müller, C.; Bauer, A.; Bach, T. *Angew. Chem. Int. Ed.* **2009**, *48*, 6640–6642.
(92) Tröster, A.; Alonso, R.; Bauer, A.; Bach, T. *J. Am. Chem. Soc.* **2016**, *138*, 7808–7811.
(93) Brimioulle, R.; Bach, T. *Science* **2013**, *342*, 840–843.
(94) Brimioulle, R.; Bach, T. *Angew. Chem. Int. Ed.* **2014**, *53*, 12921–12924.
(95) To, W. P.; Tong, G. S. M.; Cheung, C. W.; Yang, C.; Zhou, D.; Che, C. M. *Inorg. Chem.*

2017, *56*, 5046–5059.
(96) Zehnder, T. N.; Blacque, O.; Venkatesan, K. *Dalt. Trans.* **2014**, *43*, 11959–11972.
(97) To, W.-P.; Chan, K. T.; Tong, G. S. M.; Ma, C.; Kwok, W.-M.; Guan, X.; Low, K.-H.; Che, C.-M. *Angew. Chem. Int. Ed.* **2013**, *52*, 6648–6652.
(98) Abdel-Shafi, A. A.; Ward, M. D.; Schmidt, R. *Dalt. Trans.* **2007**, No. 24, 2517–2527.
(99) Liu, F.; Shen, X.; Wu, Y.; Bai, L.; Zhao, H.; Ba, X. *Tetrahedron Lett.* **2016**, *57*, 4157–4161.
(100) van Kalkeren, H. A.; Leenders, S. H. A. M.; Hommersom, C. R. A.; Rutjes, F. P. J. T.; van Delft, F. L. *Chem. - A Eur. J.* **2011**, *17*, 11290–11295.
(101) Pan, J.; Li, J.; Huang, R.; Zhang, X.; Shen, H.; Xiong, Y.; Zhu, X. *Tetrahedron* **2015**, *71*, 5341–5346.
(102) Movassaghi, M.; Hill, M. D. *Org. Lett.* **2008**, *10*, 3485–3488.
(103) Liu, D.; Venhuis, B. J.; Wikström, H. V.; Dijkstra, D. *Tetrahedron* **2007**, *63*, 7264–7270.
(104) Marinescu, L. G.; Pedersen, C. M.; Bols, M. *Tetrahedron* **2005**, *61*, 123–127.
(105) Xiao, Z.; Chen, C.; Brisson, E. R. L.; Collins, J.; Ng, W. S.; Connal, L. A. *J. Polym. Sci. Part A Polym. Chem.* **2016**, *54*, 3407–3410.
(106) Feula, A.; Fossey, J. S. *RSC Adv.* **2013**, *3*, 5370.